Testing Protocol Development for a Proton Exchange Membrane Fuel Cell

Shannon Page

A thesis presented for the degree of
Doctor of Philosophy
in
Mechanical Engineering
at the
University of Canterbury
Christchurch, New Zealand
27 April 2007

ABSTRACT

Fuel cell technology has undergone significant development in the past 15 years, spurred in part by its unique energy conversion characteristics; directly converting chemical energy to electrical energy. As fuel cell technology has past through the prototype/pre-commercialisation development, there is increasing interest in manufacturing and application issues. Of the six different fuel cell types pursued commercially, the Proton Exchange Membrane (PEM) fuel cell has received the greatest amount of research and development investment due to its suitability in a variety of applications. A particular application, to which state-of-the art PEMFC technology is suited, is backup/uninterruptible power supply (UPS) systems, or stand-by power systems.

The most important feature of any backup/UPS system is reliability. Traditional backup power systems, such as those utilising valve regulated lead acid (VRLA) batteries, employ remote testing protocols that acquire battery state-of-health and state-of-charge information. This information plays a critical role in system management and reliability assurance. A similar testing protocol developed for a PEM fuel cell would be a valuable contribution to the commercialization of these systems for backup/UPS applications.

This thesis presents a novel testing and analysis procedure, specifically designed for a PEM fuel cell in a backup power application. The test procedure electronically probes the fuel cell in the absence of hydrogen. Thus, the fuel cell is in an inactive, or passive, state throughout the testing process. The procedure is referred to as the passive state dynamic behaviour (PSDB) test. Analysis and interpretation of the passive test results is achieved by determining the circuit parameter values of an equivalent circuit model (ECM). A novel ECM of a fuel cell in a passive state is proposed, in which physical properties of the fuel cell are attributed to the circuit model components. Therefore, insight into the physical state of the fuel cell is achieved by determining the values of the circuit model parameters. A method for determining the circuit parameter values of many series connected cells (a stack) using the results from a single stack test is also presented. The PSDB test enables each cell in a fuel cell stack to be tested and analysed using a simple procedure that can be incorporated into a fuel cell system designed for backup power applications.

An experimental system for implementing the PSDB test and evaluating the active performance of three different PEM fuel cells was developed. Each fuel cell exhibited the same characteristic voltage transient when subjected to the PSDB test. The proposed ECM was shown to accurately model the observed transient voltage behaviour of a single cell and many series connected cells. An example of how the PSDB test can provide information on the active functionality of a fuel cell is developed. This method consists of establishing baseline performance of the fuel cell in an active state, in conjunction with a PSDB test and identification of model parameter values. A subsequent PSDB test is used to detect changes in the state of the fuel cell that correspond to performance changes when the stack is active. An explicit example is provided, where certain cells in a stack were purposefully humidified. The change in state of the cells was identified by the PSDB test, and the performance change of the effected cells was successfully predicted. The experimental test results verify the theory presented in relation to the PSDB test and equivalent circuit model.

ACKNOWLEDGEMENTS

I have been lucky to have the guidance of two supervisors throughout my Ph.D. studies, Professor Adnan Anbuky and Dr. Susan Krumdieck.

I am very thankful to Susan Krumdieck for the time she spent helping me with my thesis, but most of all, for the times when the discussion moved into other areas of engineering. I greatly appreciate the knowledge and skills I have gained from her.

To Adnan Anbuky who without, this project would never have started. I am very grateful to his advice, not only pertaining to the project, but particularly the encouraging words, and wisdom on how to accomplish a Ph.D.

To Dr. Jack Brouwer, Professor Scott Samuelsen, and all the fantastic students and staff of the National Fuel Cell Research Centre, University of California, Irvine. Thank-you for accommodating and teaching me so much in my time there. Most of all, thank-you for making me feel like one of the crew from day one, I simply had the greatest time in the US. I would also like to thank the Education Abroad Program, and the international staff at the University of Canterbury and the University of California, for their considerable efforts in making this happen.

I would like to thank Technology New Zealand for financial support, and Eaton New Zealand for their support.

To my office mates, and fellow research students, particularly those whom have worked directly with me on fuel cell research. I have greatly appreciated their help, and the numerous discussions about research.

To my friends, I very much appreciated the talks we had about work, particularly the ones that occurred over a beer or two.

To the University of Canterbury technical support staff, particularly Ron Tinker and Paul Southward, who were always happy to help me out when needed.

And finally, to my wonderful parents, who have helped and supported me over all these years.

TABLE OF CONTENTS

TABLE OF FIGURES

TABLE OF TABLES

1 INTRODUCTION

1.1 FUEL CELL TECHNOLOGY

A fuel cell is an electrochemical device that converts chemical energy directly into electrical energy. Fundamentally, a fuel cell works in the same manner as a battery. However, the chemical reactants (typically hydrogen and oxygen) are continuously fed to the fuel cell, with the product (water) continuously removed. Thus, a fuel cell is sometimes referred to as a continuous battery; as long as fuel and oxygen are supplied, the fuel cell will continue to produce electrical power.

Fuel cells have undergone significant development in the last 15 years, spurred in part by their unique energy conversion characteristics, including high efficiency and minimal environmental impact at the point of use compared with combustion engines. There are six types of fuel cells actively being researched and developed. The materials, construction, operating conditions and other system components required for each fuel cell type vary greatly, thus the suitable applications for each fuel cell type ranges widely. The name of each fuel cell type originates from the electrolyte employed. Table 1.1 lists each alongside its main characteristics. In general, fuel cell technology has passed through pre-commercialisation development, with increasing interest in manufacturing and application issues.

Table 1.1 Fuel Cell Types Currently Under Development

Fuel Cell Type	Temperature	Power Range	Applications
Solid Oxide Fuel cell (SOFC)	750 – 1000^{o}C	200kW – 2MW	Stationary Base load generation
Molten Carbonate Fuel Cell (MCFC)	~650^{o}C	200kW	Stationary Base load generation
Phosphoric Acid Fuel Cell (PAFC)	~220^{o}C	200kW – 1MW	Stationary Base load generation
Alkaline Fuel Cell (AFC)	80 – 140^{o}C	Few W – 200kW	Space, Distributed Generation
Proton Exchange Membrane Fuel Cell (PEMFC)	30 – 90^{o}C	10W – 100kW	Automotive, Distributed Generation, Back-up Power
Direct Methanol Fuel Cell (DMFC)	20 – 50^{o}C	mW – fewW	Portable Electronics

The proton exchange membrane (PEM) fuel cell has arguably received the greatest amount of research and development in recent years. PEM fuel cells operate at low temperatures, possess a quick start-up time and are comparatively simple in their construction (i.e. an all solid device compared with fuel cells using liquid electrolytes). PEM fuel cells are suited to a number of applications, thus providing a number of market opportunities. These include portable power (~10W), backup and residential (~5kW), and automotive applications (~80kW). Numerous prototype and demonstration systems have been developed for each application. Issues such as cost, hydrogen storage, lifetime and reliability remain barriers that must be overcome before PEM fuel cells are competitive with traditional technology. The technical development required before PEM fuel cells can compete commercially depends on the application. For instance, significant improvements in cost and hydrogen storage are required before PEM fuel cells can compete with the internal combustion engine for transportation. However, significant improvements in cost and other technical areas are not required for certain applications. Existing state-of-the art PEMFC technology closely matches the requirements of backup/UPS, or stand-by power systems [1], [2]. Therefore, these applications are a near term possibility for PEM fuel cell market penetration [3]. Existing backup power technology is described in the next section, focusing on telecommunications backup power systems.

1.2 BACKUP POWER TECHNOLOGY

Figure 1.1 shows a typical telecommunications backup power installation [4].

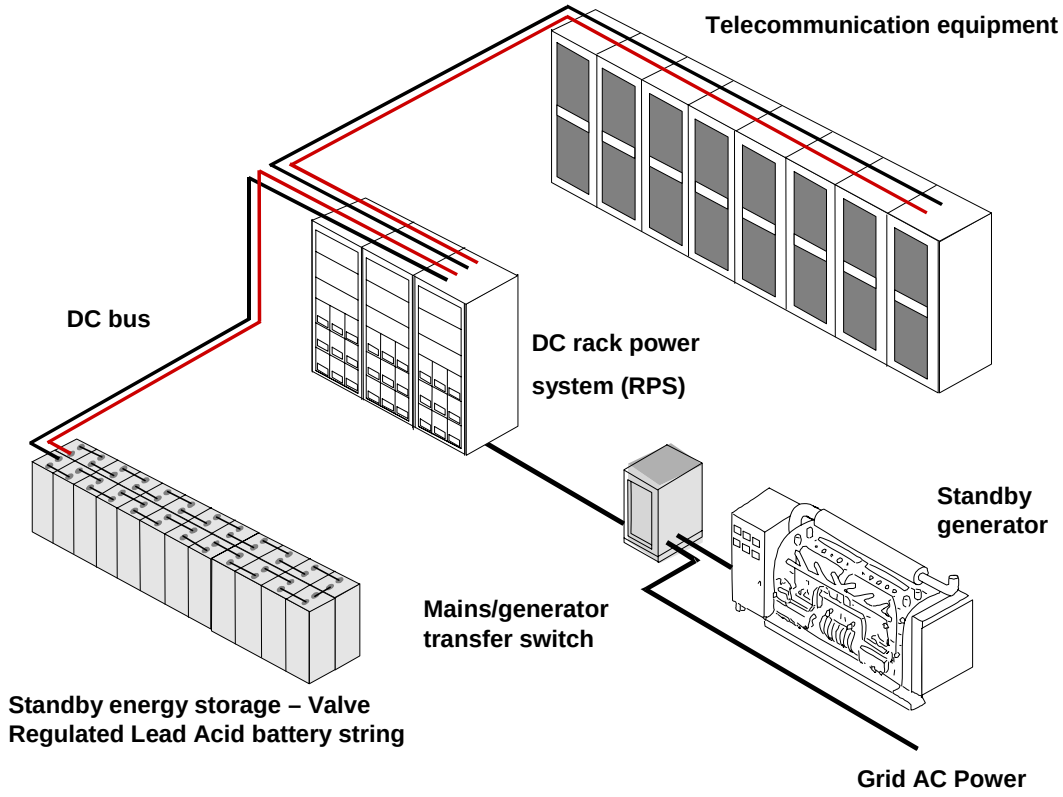

Figure 1.1 Standard Telecommunication Back-Up Power System

Under normal operating conditions, the telecommunications load is powered through a rack power system (RPS) that converts grid AC power to the required DC voltage (12, 24, or most commonly 48V) using a number of rectifying units. In the event of AC power failure, a bank of batteries that are tied to the DC bus through the RPS, continue to supply DC power to the load. The battery of choice for backup power is the valve regulated lead acid (VRLA) battery. They differ from the common flooded lead acid used in automotive applications, as the VLRA is a completely sealed unit (maintenance free) and incorporates a one way valve to release the build up of any gasses accumulated during charging. A standby diesel generator may also be included in the system as shown in the Figure 1.1. However, it is common for the VRLA battery to be the only backup power source. Installations provide up to 8hrs of backup power, and are located in roadside cabinets or office basements [5].

The most important requirement of any backup power system is reliability. Telecommunications data includes voice, internet traffic, electronic transactions etc, and the cost of service disruptions can be extremely high [6]. The required availability for telecommunications is currently 0.99999 (5 nines) which equates to an allowable down time of 315 seconds per year [3]. However, a required availability of 6 – 7 nines or higher may be needed for new digital loads [6]. To achieve this level of reliability, a backup power system is designed with redundancies, i.e.

multiple battery strings and rectifying units. This allows the system to function in the event of any one (or more) units failing. In addition to system redundancy, management and monitoring of the system is also a critical component in assuring functionality, and hence reliability of the system [7]. By testing the system (particularly the VLRA battery) a problem can be detected and rectified before it affects the functionality of the system in the event of a AC Power failure. Research and development of backup power management and monitoring strategies has been active for several years [4], [8]-[11]. Techniques include partial discharge of the VRLA battery to acquire state of health (SOH) and state of charge (SOC) information. Such testing methods are integrated into the backup power system, allowing testing and assessment of the system to be conducted remotely. Commercially available VRLA based backup power systems meet the 5 nines required.

Disadvantages with traditional VRLA batteries and generators have encouraged research into alternative energy systems for backup power. The VRLA battery is expensive, particularly as the lifetime can be in the order of 3 – 5 years [12], which also raises environmental concerns. VRLA banks are heavy, and take up a considerable floor space. If the required backup service time extends beyond 8hrs, the VRLA becomes impractical based on cost, volume and mass, thus a generator is usually used. The main draw back of a generator stems from environmental issues, with noise and emissions limiting possible locations. A number of alternative energy systems have been proposed that may overcome the disadvantages of traditional technology, with fuel cell technology a prominent contender.

1.3 PEM FUEL CELLS IN BACKUP POWER APPLICATIONS

A number of fuel cell types have been investigated for telecommunications, not only for providing standby power, but using the fuel cell as the primary power source [13]. Telecommunications power systems using 200kW phosphoric acid fuel cells have been presented [14]-[16]. In addition to electrical power generation, waste heat from the fuel cell system is utilized for absorption cooling of the telecommunications equipment. The system supplies primary power using the mains power as backup. Solid oxide fuel cell systems have also been suggested for telecommunications as a primary power or even as a stand-by power system [17], [18]. The Zinc-Air and Aluminium-Air “fuel cells” have also been advocated for

use in back-up power applications [19]. However, these are not true fuel cells. Even though oxygen from the air is delivered to the cathode, the metal anode is consumed during power generation and must be replaced along with the electrolyte in order to recharge the Metal-Air fuel cell. By far the most popular fuel cell type aimed at telecommunications and back-up power systems is the PEM [2], [20]-[23]. Table 1.2 lists four of the most advanced systems along with their basic specifications.

Table 1.2 PEM Backup Power Systems

				
	Idatech® ElectraGen™5	**Palcan®** PalPac500 - UPS	**PlugPower®** GenCore® 5T48	**ReliOn™** Independence-1000™
Power	0-5000 W	500W	0 – 5000W	0 – 1000W
Voltage	Nominal -48 VDC (optional +48 VDC). Limit -48 VDC to -52 VDC	110-120 VAC	46 – 56 VDC (48) adjustable 42 – 60 VDC operating	24 or 48VDC Nominal
Fuel	Commercial grade 99.95% dry H_2	H_2 gas from metal hydride	99.95% dry H_2	Industrial grade H_2 99.95%
Fuel consumption @ rated power	75 slpm	5 hrs @ 500W with H2 stored in system (1800l)	62 slpm	15 slpm
Dimensions w×d×h (cm)	60×60×120	53×47×50	66×61×112	44.5×69×51 19” rack mountable
Weight (kg)	226	N/A	227	66
Operating Temperature	-40 to +50^{o}C	+5 to +40^{o}C	-40 to +46^{o}C	0 to 46^{o}C
Other Notes	N/A	Size includes hydrogen storage (metal Hydride)	$15 000, cost	Contains 6 hot swappable fuel cell cartridges
Reference	[24]	[25]	[26]	[27]

A common feature of these systems is that they operate on pure hydrogen; therefore, the system must be actively serviced to be refuelled. Although there was initial interest in regenerative systems [21], they are not being pursued in a commercial capacity at this time [28]. The systems shown in Table 1.2 do not eliminate the need for a battery, as power is required to start the fuel cell system (to operate solenoid valves, fans etc). In addition, batteries will supply power to the load until the fuel cell is up to full power (in the range of a few minutes). Although the required battery capacity can be integrated into a fuel cell system [25] it will usually be another component of the backup power system. A fuel cell system incorporating a super capacitor has been proposed, thus eliminating the battery completely [29].

A PEM fuel cell system may offer advantages over traditional backup power technology. Primarily, the benefits of PEM technology arise in the reduction or elimination of VRLA battery strings. The exact benefits depend on the PEM fuel cell configuration and the required service time of the backup power system. For example, Smith *et al.* compared a 10kW prototype regenerative fuel cell system, which includes the fuel cell, compressed hydrogen storage (7hr supply) and an electrolyser, to a battery system of equal power and run time. A 75% savings in floor space was calculated and a 25% cost savings compared to batteries was projected, ignoring battery replacement costs [21]. A simple fuel cell system with compressed hydrogen storage is predicted to be cost effective when the service time is greater than 4 hours, as increasing the stored hydrogen capacity is cheaper, requires less volume and is lighter than adding the equivalent energy in batteries. For a service time of 12 hours, the fuel cell system is expected to have cost savings of 25-50% over 10 years, assuming battery replacement is carried out every 4 years [12], [22]. Lin *et al.* [23] compared a 2kW fuel cell system (including a methanol reformer for H_2 production) with a battery backup system of equal power. The systems were compared on cost, weight and volume for different required service times, up to 24 hours. The fuel cell system out performed the battery system in all respects as the required service time increased.

PEM fuel cells are also being considered as an alternative to the diesel generator, which would most likely be employed when long service times are required. Although a fuel cell system offers no advantage in size or cost over a diesel generator, noise and emissions are significantly reduced.

Despite advantages of fuel cell systems over traditional backup power technology, fuel cells have not been widely employed on a commercial level. Due to reliability requirements, end users must select incumbent technology. Remote testing and monitoring of incumbent VRLA based backup power systems is an integral part in assuring system functionality, thus achieving the required 5 or more nines of availability. Currently, no such testing or monitoring strategies exist for fuel cells in a backup power application. An important advancement in the commercialization of PEM technology would be the development of testing methods that could be incorporated into the monitoring and management of a PEM fuel cell, thus increasing the reliability of the system.

1.4 PURPOSE OF THESIS

The primary objective of this thesis is to develop a testing method for a Proton Exchange Membrane Fuel Cell in an application setting, such as telecommunications backup power. The testing method and subsequent analysis is designed to provide information on the operational status of the fuel cell, which will be used as part of a monitoring and management strategy. The novel testing process developed for this research has been named the passive state dynamic behaviour (PSDB) test.

The PSDB is based on electronically probing the fuel cell while in a passive, non-functioning state. While in a passive state, the fuel cell is claimed to act as an RC circuit, and by obtaining the parameter values of an equivalent circuit model, information about the active performance of the cells can be determined.

There are significant differences between the PSDB test and exting fuel cell testing methods. Therefore, certain aspects of the fuel cell analysis presented in the thesis are unique. Traditionally, fuel cells are tested while operating, and the resulting analysis is similar to that conducted on other electrochemical devices such as batteries and electrolysis cells. As the PSDB test is based on electrically probing the fuel cell in the absence of hydrogen, a similarity between a passive fuel cell and a double layer capacitor (DLC) is explored in this thesis. A circuit model of the fuel cell in a passive state is also derived, and a novel method for determining parameter values is described. The PSDB test provides insight into fuel cell properties that cannot be observed when using traditional testing techniques.

1.5 THESIS STRUCTURE

Chapter 2 describes the Proton Exchange Membrane Fuel Cell, concentrating on the cell structure and typical stack construction. The ideal and real steady state performance of a PEM fuel cell is described. The loss mechanisms, which cause the fuel cell to perform at a level less than ideal are also explained. The final section describes the physical construction of a DLC and compares it to the PEM fuel cell.

Chapter 3 reviews traditional testing techniques used for analysing individual cells and stacks. A review of fuel cell equivalent circuit models (ECM) is provided, as these are commonly used to model and interpret the results of fuel cell tests. A review of double layer capacitor (DLC) testing and modelling is also provided. This chapter provides information on the dynamic characteristics of both the fuel cell and the DLC.

Chapter 4 describes the PSDB test method. A new ECM is proposed, based on the physical structure of a passive PEM fuel cell as detailed in Chapter 3. A comparison with exiting fuel cell and DLC models is provided, with additional discussion on model uniqueness. Based on the model, the voltage response of a fuel cell subjected to the PSDB test is predicted.

Chapter 5 describes the experimental test system used for implementing the PSDB test. The specifications of the three fuel cells tested in this research are described, together with details of their active operation.

Chapter 6 provides a qualitative explanation of the results produced when the PSDB test is implemented on a fuel cell. Reference is given to the physical properties of the fuel cell and a double layer capacitor (DLC) described in Chapter 2 and 3. Results are presented for individual cells and stacks.

Chapter 7 details the numerical technique employed for acquiring the ECM parameter values. Sample results are provided, demonstrating convergence and the propagation of experimental measurement error.

Chapter 8 relates the PSDB test results with the functionality of the fuel cell. A direct correlation between passive and active testing is demonstrated. A method in which the ECM parameter values are used to predict changes in the active functionality of cells within a fuel cell stack is also detailed.

Chapter 9 summarises the thesis, list the achievements and proposes future work.

1.6 REFERENCES

[1] Barbir F, Tombaugh P, Maloney T, Molter T, “Fuel Cell Stack and System Development: Matching Markets to Technology”, Fuel Cell Seminar Abstracts, Palm Springs California, pp. 948-951, Nov. 18-21, 2002

[2] Lehman, P.A, Chamberlin, C.E, Zoellick, J.I, Engel, R.A, “A photovoltaic/fuel cell power system for a remote telecommunications station” Photovoltaic Specialists Conference, Conference Record of the Twenty-Eighth IEEE, pp. 1552-1555, Sep. 15-22, 2000

[3] Anbuky A, “Potential of Fuel Cells for the Standby Power Industry”, Fuel Cell Seminar Abstracts, Palm Springs California, pp. 486-489, Nov. 18-21, 2002

[4] Pascoe P.E, “Standby VRLA battery behavioural prediction : a thesis submitted for the fulfilment of the requirement for the degree of Doctor of Philosophy of Engineering (Electrical and Electronic)”, University of Canterbury, Electrical and Electronic Engineering Department, New Zealand, 2002

[5] Osifchin, N. “A telecommunications buildings/power infrastructure in a new era of public networking” INTELEC 2000, Twenty-second International Telecommunications Energy Conference, pp. 1-7, Sep. 2000

[6] Roy S, “Reliability considerations for data centers power architectures” INTELEC 2001, Twenty-Third International Telecommunications Energy Conference, pp. 406-411, Oct. 2001

[7] Gruenstern R, Reher M, Gerner S, Shaffer D, Improved systems reliability through improved battery monitoring techniques Telecommunications Energy Conference, 1993. INTELEC '93. 15th International Volume 1, 27-30 Sept. 1993 Page(s):63 - 66 vol.1

[8] Hunter P.M “VRLA battery float charge : analysis and optimisation : a thesis submitted for the fulfilment of the requirement for the degree of Doctor of Philosophy of

Engineering (Electrical and Electronic)", Electrical and Electronic Engineering Department, University of Canterbury, New Zealand, 2003

[9] Kutluay K, Cadirci Y, Ozkazanc Y.S, Cadirci I, "A New Online State-of-Charge Estimation and Monitoring System for Sealed Lead–Acid Batteries in Telecommunication Power Supplies" IEEE Transactions on Industrial Electronics, Vol. 52, pp. 1315-1327, Oct. 2005

[10] Pascoe P.E, Anbuky A.H, "VRLA battery discharge reserve time estimation" IEEE Transactions on Power Electronics, Vol. 19, pp. 1515-1522, Nov. 2004

[11] Tsujikawa T, Kiyokawa I, Matsushima T, Muroyama S, "VRLA battery remote management system" INTELEC 2004, 26th Annual International Telecommunications Energy Conference, pp. 419–424, Sep. 19-23, 2004

[12] Billings R, Saathoff S, "Fuel cells as backup power for digital loop carrier systems", INTELEC 2004, 26th Annual International Telecommunications Energy Conference, pp. 88-91 Sep. 2004

[13] Lei X, Bentley J, "Fuel cell power systems for Telecommunications, INTELEC 2001, Twenty-Third International Energy Conference, pp. 677-682, Oct. 2001

[14] Ishizawa M, Okada S, Yamashita T, "Highly efficient heat recovery system for phosphoric acid fuel cells used for cooling telecommunication equipment", Journal of Power Sources, Vol. 86, pp. 294-297, Mar. 2000

[15] Kuwata Y, Take T, Aoki T, Ogata T, "Multifuel fuel-cell energy system for telecommunications cogeneration system", IEICE Transactions on Communications, E81B (11): pp. 2176-2182, Nov. 1998

[16] Koyashiki T, Yotsumoto K, "Advanced fuel cell energy system for telecommunications use" INTELEC '92, 14th International Telecommunications Energy Conference, pp. 4-11, Oct. 1992

[17] LeSage B.C, “Solid oxide fuel cell products for telecom applications Telecommunications”, INTELEC 2001 Twenty-Third International Telecommunications Energy Conference, pp. 667–670, Oct. 2001

[18] Krumdieck S, Page S, Round S, “Solid oxide fuel cell architecture and system design for secure power on an unstable grid”, Journal of Power Sources Vol. 125, pp. 189-198, Jan. 2004

[19] Colborn J, Smedley S, **“**Ultra-long duration backup for telecommunications applications using ZINC/AIR regenerative fuel cells”, INTELEC 2001 Twenty-Third International Telecommunications Energy Conference, pp. 576-581, 2001

[20] Varkaraki E, Lymberopoulos N, Zachariou A, “Hydrogen based emergency back-up system for telecommunication applications” Journal of Power Sources, Vol. 118, pp. 14-22, May 2003

[21] Smith W.F, Giancaterino J, “Telecom back-up power systems based upon PEM regenerative fuel cell technology” INTELEC 2001, Twenty-Third International Telecommunications Energy Conference, pp. 657 –661, 2001

[22] Saathoff S, “Fuel cells as backup power for state government communications sites” Fuel Cells Bulletin, pp. 10-12, Mar. 2004

[23] Lin M, Cheng Y, Lin M, Yen S, “Evaluation of PEMFC power systems for UPS base station applications”, Journal of Power Sources, Vol. 140, pp 346-349, Feb. 2005

[24] IdaTech, ElectraGen™5 Product specifications, http://www.idatech.com/media/pdf/ElectraGenFamily_Final.pdf

[25] Palcan Fuel Cells Ltd. Palcan's *PalPac® 500 - UPS* Product Specifications, http://www.palcan.com/s/Products.asp

[26] Plug Power GenCore® 5T48 Product Specifcations, http://www.plugpower.com/products/pdf/GenCore_Telecom_Datasheet.pdf

[27] ReliOn Independence-1000™ Product Specifications, http://www.relion-inc.com/pdf/ReliOnI1000J64Spec0706.pdf

[28] Proton Energy Systems, Inc. Current Product Listing, http://www.protonenergy.com/

[29] Perry M.L, Kotso S.A, “A back-up power solution with no batteries”, INTELEC 2004, 26th Annual International Telecommunications Energy Conference, pp. 210-217, Sep. 2004

2 THE PROTON EXCHANGE MEMBRANE FUEL CELL

This chapter describes the PEM fuel cell. The fundamental operating principles are described in Section 2.1 and cover the electrochemical reactions, relationship between fuel consumption and the operating current, and ideal voltage base on thermodynamic principles. A detailed description of the PEM fuel cell follows in Section 2.2, describing the cell materials, structure and typical stack and system configurations. This section also describes the loss mechanisms, which reduce the fuel cell operating voltage from the ideal maximum. Section 2.3 describes the steady state performance of a PEM fuel cell, including a quantitative (mathematical) treatment of the loss mechanisms. The dynamic performance of a PEM fuel cell is described in the following chapter, where testing and dynamic modelling of a PEM fuel cell is detailed. Section 2.4 describes the main degradation mechanisms of a PEM fuel cell.

This chapter also details the construction of a double layer capacitor (DLC). The similarity between a DLC and a PEM fuel cell is discussed and basic properties of the DLC are provided. The following chapter describes the quantitative performance of a DLC, in the context of testing and modelling.

2.1 ELECTROCHEMISTRY AND THEORETICAL PERFORMANCE OF A PEM FUEL CELL

Figure 2.1 shows how a PEM fuel cell, generates electric current by reacting hydrogen and oxygen (usually from in the air). The fundamental components of a fuel cell required to carry out this process, are two electrodes (anode and cathode), separated by an electrolyte. At the anode (negative terminal), the hydrogen molecules give up their electrons, which travel through an external circuit. The remaining hydrogen ions (H^+) travel through the membrane towards the cathode. At the cathode (positive terminal), hydrogen ions from the membrane, combine with electrons and oxygen, forming product water.

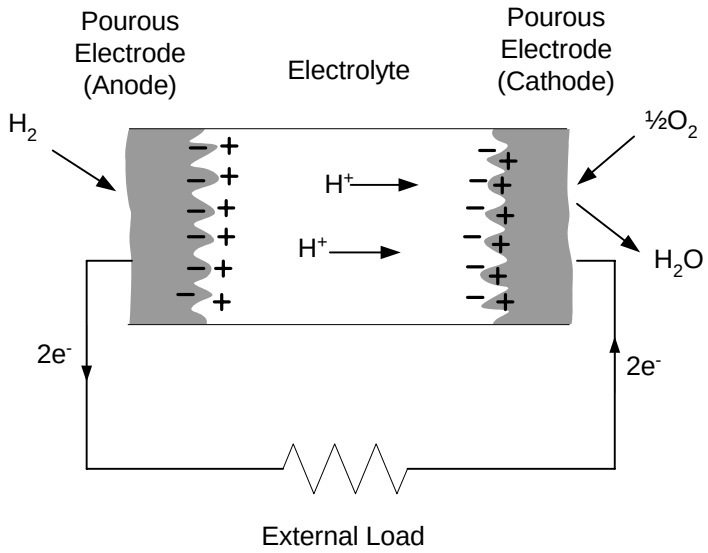

Figure 2.1 Essential Elements of an Operating PEM Fuel Cell

Formally written, the two half-cell reactions occurring at the anode and cathode are

$$H_2 \rightarrow 2H^+ + 2e^- \quad \text{and} \quad \tfrac{1}{2}O_2 + 2H^+ + 2e^- \rightarrow H_2O \qquad [2.1]$$

Thus, the overall reaction is simply

$$\tfrac{1}{2}O_2 + H_2 \rightarrow H_2O \qquad [2.2]$$

From equation 2.1, it can be seen that for every molecule of H_2 reacted, 2 electrons flow around the external circuit. Therefore, the current, i [A] for a single cell can be related to H_2 consumption, n [mole/s], by

$$n = \frac{i}{\mu_f 2F} \qquad [2.3]$$

where F is the Faraday constant, 96485 C/mole, and μ_f is the fuel utilization factor (between 0 and 1), as in practice not all of the hydrogen is electrochemically reacted by the fuel cell. For a PEM fuel cell operating on pure hydrogen, μ_f tends to be high.

The chemical energy that can be converted into electrical energy using a fuel cell is given by the change in Gibbs free energy of formation, Δg_f [J/mole] as applied to equation 2.2. Thus, at standard state (25°C, 1bar) Δg_f^0 for equation 2 is given by

$$\Delta g_f{}^0 = \Delta g_{f,H_2O}{}^0 - \Delta g_{f,H_2}{}^0 - ½\Delta g_{f,O_2}{}^0 = -237141 - 0 - 0 = -237141 \text{ J/mol} \quad [2.4]$$

Equation 2.4 is calculated using the higher heating value (HHV) of H_2O (liquid product). Instead of expressing the energy per mol of H_2 reacted, the energy can be given per unit of charge (Coulomb) flowing through the circuit, i.e. J/C, or voltage, V;

$$E = \frac{-\Delta g_f{}^0}{2F} = \frac{237141}{2 \times 96485} = 1.2289 \text{ V} \quad [2.5]$$

As Δg_f^0 decreases with increasing temperature, the ideal voltage of a fuel cell also reduces with increasing temperature. For example, the voltage of a hydrogen fuel cell operating at 1bar and 80°C using Equation 2.5 is 1.183V (HHV).

The enthalpy of formation, Δh_f for the reaction shown in equation 2.2, is 285 830 J/mol (HHV) [1]. If the fuel cell were able to convert all of this energy into work, the voltage would be equivalent to that given by equation 2.6.

$$E = \frac{-\Delta h_f{}^0}{2F} = \frac{285830}{2 \times 96485} = 1.481 \text{ V} \quad [2.6]$$

Therefore, the efficiency limit of a fuel cell operating under standard conditions is given by equation 2.7

$$Eff = 100\% \times \frac{\Delta g_f{}^0}{\Delta h_f{}^0} = 100\% \frac{237141}{285830} = 83.0\% \quad [2.7]$$

As Δh_f^0 is relatively constant with temperature (compared to Δg_f^0) the efficiency limit decreases with increasing fuel cell operating temperature.

As the reactants and products will be at states other than standard, an alternative to equation 2.5 is required. Using thermodynamic considerations [2], the pressures of reactants and products can be taken into account in the voltage expected of a fuel cell.

Starting with the definition of Gibbs free energy

$$g = h - Ts \qquad [2.8]$$

As applied to the change in Gibbs energy of formation

$$\Delta g_f = \Delta h_f - T\Delta s \qquad [2.9]$$

The entropy of gas species A, in an ideal gas mixture is given by [2]

$$s = s_A{}^0 - R\ln\left(\frac{P_A}{P^0}\right) \qquad [2.10]$$

Where P_A is the partial pressure of species A, P^0 is the standard pressure (1 bar) and $s_A{}^0$ is the entropy of A at standard conditions. The change in entropy as applied to reaction 2.2 is given by

$$\Delta s = s_{prod} - s_{react}$$

$$\Delta s = s_{H_2O} - \left[\tfrac{1}{2}s_{O_2} + s_{H_2}\right]$$

$$= s_{H_2O}{}^0 - R\,ln\left(\frac{P_{H_2O}}{P^0}\right) - \tfrac{1}{2}\left[s_{O_2}{}^0 - R\,ln\left(\frac{P_{O_2}}{P^0}\right)\right] - \left[s_{H_2}{}^0 - R\,ln\left(\frac{P_{H_2}}{P^0}\right)\right]$$

$$= s_{H_2O}{}^0 - \tfrac{1}{2}s_{O_2}{}^0 - s_{H_2}{}^0 + \left[\tfrac{1}{2}R\,ln\left(\frac{P_{O_2}}{P^0}\right) + R\,ln\left(\frac{P_{H_2}}{P^0}\right) - R\,ln\left(\frac{P_{H_2O}}{P^0}\right)\right]$$

$$\Delta s = \Delta s^0 + R\,ln\left(\frac{\left[P_{O_2}\right]^{\frac{1}{2}}\left[P_{H_2}\right]}{\left[P_{H_2O}\right]}\right) \qquad [2.11]$$

The pressures in equation 2.11 are all expressed in bar, thus the P^0 values are equal 1 and are not explicitly written in.

Substituting equation 2.11 into equation 2.9, the change in Gibbs energy for reactants and products not in their standard state is

$$\Delta g_f = \Delta h_f - T\Delta s$$

$$= \Delta h_f - T\left[\Delta s^o + R\,ln\left(\frac{\left[P_{O_2}\right]^{½}\left[P_{H_2}\right]}{\left[P_{H_2O}\right]}\right)\right]$$

$$\Delta g_f = \Delta g_f{}^0 - R\,ln\left(\frac{\left[P_{O_2}\right]^{½}\left[P_{H_2}\right]}{\left[P_{H_2O}\right]}\right) \qquad [2.12]$$

Dividing equation 2.12 by -2*F*, the commonly used Nernst equation is

$$E_0 = \frac{-\Delta g_f{}^0}{2F} + \frac{RT}{2F}\ln\left(\frac{\left[P_{O_2}\right]^{½}\left[P_{H_2}\right]}{\left[P_{H_2O}\right]}\right) \qquad [2.13]$$

E_0 is the expected voltage from a fuel cell operating at a given pressure and temperature. E_0 is often referred to as the thermodynamically reversible voltage, reversible open circuit voltage (OCV), or no-loss voltage. For the remainder of this thesis, E_0 will be called the "reversible voltage". In practice, the operating voltage of a PEM fuel cell will be substantially less than the reversible voltage due to a number of loss mechanisms. For example, the hydrogen ions moving through the electrolyte are subject to ohmic resistance. The typical operating voltage of a PEM fuel cell is around 0.7V. The difference between the reversible voltage and the operating voltage of a fuel cell has been called the over voltage, polarization, irreversibility, loss, and voltage drop [3]. For the remainder of this thesis, the term "voltage loss" will be used, with the term "loss mechanism" referring to the specific process giving rise to the voltage loss. The following Section describes the loss mechanisms qualitatively, with a quantitative treatment of voltage loss provided in Section 2.3.

2.2 MATERIALS AND CONSTRUCTION

A functional schematic of a PEM fuel cell system and stack is shown in Figure 2.2. A fuel cell system contains the fuel cell stack, along with auxiliary equipment such as fans/pumps, solenoid valves, cooling systems, controls etc, often referred to as the balance of plant. The fuel cell stack contains many individual cells, each consisting of an electrolyte, two electrodes (anode and cathode), and two gas diffusion layers. The cells are usually connected together using bipolar plates, thus forming a stack. Subsequent subsections provide detailed descriptions of the electrolyte, electrodes, gas diffusion layers, bipolar plates and common stack and system designs.

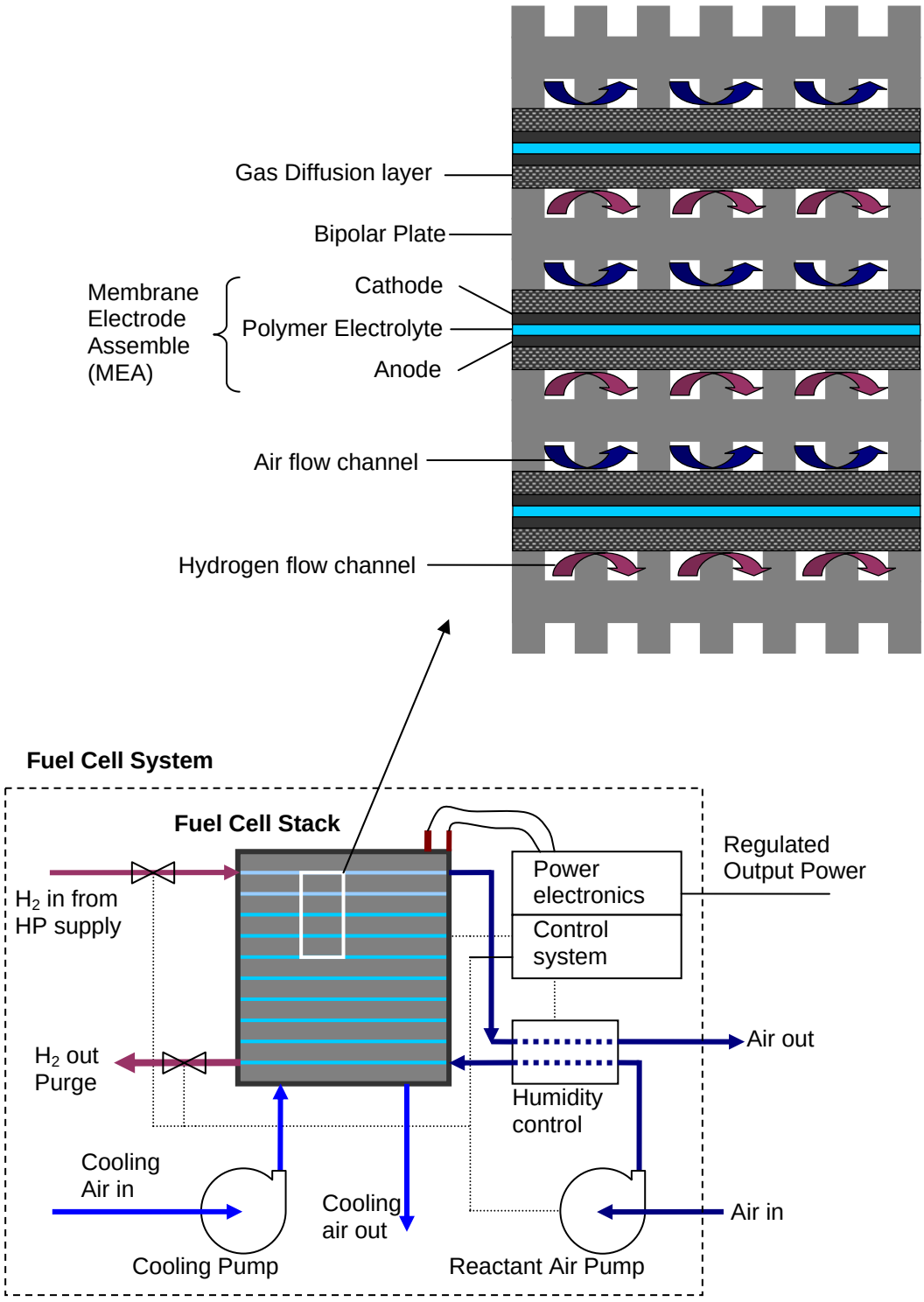

Figure 2.2 Schematic of a PEM Fuel Cell System, and Stack

2.2.1 ELECTROLYTE

A PEM fuel cell utilises a hydrated polymer sheet as the electrolyte, which has the required properties of being gas impermeable, electrically insulative and conductive to hydrogen ions. The polymer is composed of polytetrafluoroethylene (PTFT, more commonly know as Teflon),

with side chains of perfluorinated-vinyl-polyether that terminate in a sulfonic acid group, $-SO_3H$ [3]. A simplified diagram of a hydrated polymer is shown in Figure 2.3. The exact length and frequency of the side chains varies from polymer to polymer, giving rise to membranes with different equivalent weights (EW) defined as gram of polymer per mole of sulfonate sites. Membranes with an EW of 1100 are common, but 900 – 1400 can be manufactured [4].

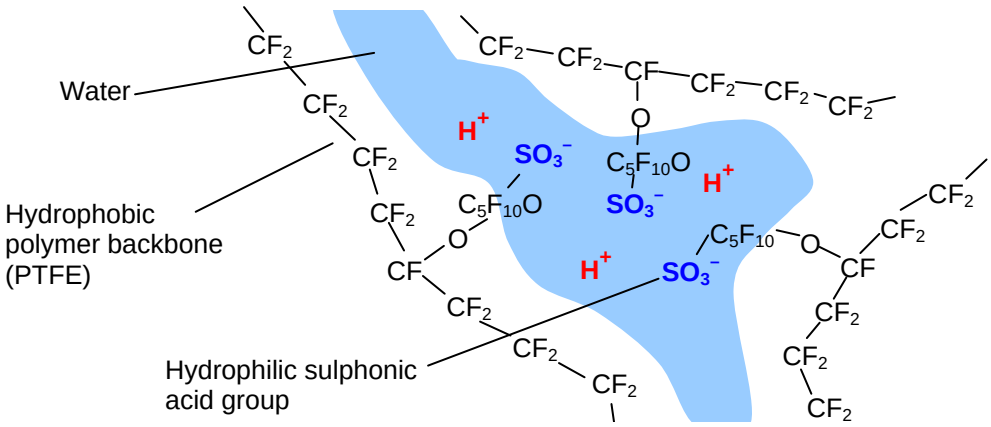

Figure 2.3 Polymer Membrane

When the membrane is hydrated, the weakly (ionicly) bound hydrogen ions are disassociated from the sulfonate group, which remains covalently fixed to the polymer. The hydrogen ions are coupled with a water molecule forming hydronium ions, H_3O^+ [5], and are free to move in the water throughout the hydrated polymer. As the PTFT back-bone is strongly hydrophobic, water tends to cluster around the hydrophilic sulfonic acid sites, forming discrete water channels within the polymer. As the water channels are continuous throughout the membrane, hydrogen ions can cross from one side of the membrane to the other. As with the movement of any charge through a conducting medium, the hydrogen ions are subject to resistance, resulting in a voltage loss. The ionic resistance is one of three predominate loss mechanisms in a fuel cell. The water content in the membrane directly determines the ionic resistance, and is perhaps the most important parameter for fuel cell performance. Essentially, the lower the water content, the smaller the water channels will be (and fewer of them) thus the ionic resistance increases [6]. The ionic resistance has been shown to be directly proportional to the hydration of the membrane [7]. When measuring the ability of a membrane to transport hydrogen ions, the ionic conductivity, S cm^{-1}, is most commonly used, which is the inverse of resistance, Ω cm.

The polymer membrane is not completely gas impermeable. Some hydrogen molecules will cross directly from the anode to the cathode, a processes known as fuel crossover. Fuel crossover is often neglected as it does not result in a major performance loss, except in the

extreme case of membrane perforation. A thinner membrane will have a lower resistance but at the cost of increased fuel crossover, together with lower mechanical strength. Table 2.1 lists a variety of commercially manufactured membranes used as PEM electrolytes.

Table 2.1 Commercially Available PEM Fuel Cell Membranes

Manufacturer	Product	Typical thickness* (mm)	Equivalent weight (EW) $\left(\frac{\text{gm of polymer}}{\text{mole of sulphonate sites}}\right)$
DuPont	Nafion 112	0.0508 (0.002 in)	1100
DuPont	Nafion 1035	0.0889 (0.0035 in)	1000
DuPont	Nafion 1135	0.0889 (0.0035 in)	1100
DuPont	Nafion 115	0.127 (0.005 in)	1100
DuPont	Nafion 105	0.127 (0.005 in)	1000
DuPont	Nafion 117	0.178 (0.007 in)	1100
Asahi Chemical Industry	Aciplex 1002	0.050	1000
Asahi Chemical Industry	Aciplex 1004	0.100	1000
Asahi Chemical Industry	Aciplex 1104	0.100	1100
Asahi glass Co.	Flemion SH80	0.080	909
Asahi glass Co.	Flemion SH150	0.160	909

* Thickness given for a dry membrane, the membrane will swell upon hydration.
Data from [8], [9], [10]

The most commonly used membrane, and that to which most others are compared is Nafion® from DuPont™. It is widely available with a number of distributors selling direct to the public. Gore™ has developed membranes specifically for PEM fuel cells under the trade name Gore–SELECT®. However, these are only sold as membrane electrode assemblies (MEA), where the anode and cathode are attached to the membrane, under the trade name Gore-PRIMEA® [11].

The exact chemical composition of different membranes results in differing conductance values and mechanical properties, such as strength. However, general membrane characteristics such as hydration sensitive performance will be similar for all membranes as the same transport mechanism is present. For example, Sumner *et al.* [6] compared the performance of Nafion 117 with a sulfonyl imide membrane, which has a $–SO_2NHSO_2CF_3$ group instead of the common sulfonic acid group, $–S_3H$. The conductivity of the two membranes as a function of hydration and temperature was found to be very similar. Therefore, the same ion transport mechanism, hydronium ions moving through liquid water channels, was concluded for both membranes.

2.2.2 ELECTRODES (ANODE & CATHODE)

The anode and cathode of a PEM fuel cell are physically very similar, and in many cases identical. The electrodes consist of a porous, high surface area carbon, which supports finely distributed catalyst particles where the electrochemical reactions take place. Figure 2.4 shows a schematic diagram of the electrolyte–electrode interface.

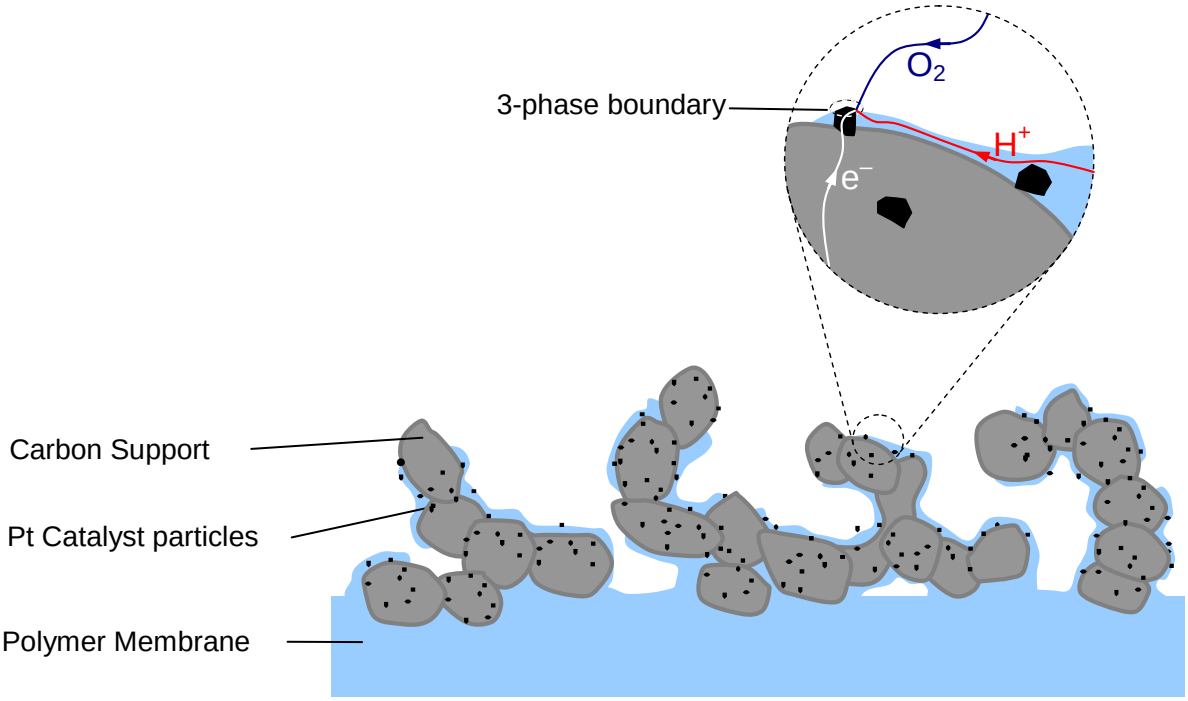

Figure 2.4 Electrode Stucture of a PEM Fuel Cell

The use of a catalyst is essential in a PEM fuel cell. At low operating temperature, the catalyst is required to promote the electrochemical reactions occurring at the anode and cathode. Even with the catalyst, there is a large voltage loss associated with the electrochemical reaction step. This loss mechanism is called the activation loss, and will be discussed in greater detail in Section 2.3.1. The electrochemical reactions only occur at the interface between the electrolyte, the catalyst surface and the gaseous phase, as it is only at this "three phase boundary" that the delivery or removal of ions, reactants, products and electrons can take place. An optimal electrode contains many three-phase boundaries, providing many sites where electrochemical reactions can take place. Essentially, the higher the total electrode surface area, the greater the number of three phase boundaries, and the higher the voltage performance.

The porosity of the electrode structure is also important as it facilitates the mass transport of reactant and product gases. The maximum rate that mass transport can occur defines the

maximum current obtainable from a fuel cell, often referred to as the limiting current i_l. In practice, fuel cells are not operated anywhere near i_l, as a large voltage loss will be incurred. This voltage loss is commonly referred to as the mass transport loss, which is the third major loss mechanism in a fuel cell. In the extreme case of operating a fuel cell at i_l, the mass transport loss results in the voltage of the fuel cell reducing to zero. Section 2.3.3 further discusses the mass transport loss, detailing the specific species thought to be responsible for the limiting current and how approaching this limit results in a voltage loss.

An important aspect of the electrode–electrolyte interface is the formation of an electric double layer, commonly referred to as the double layer. At the negatively changed anode where hydrogen ions are being generated, a layer of electrons on the electrode is attracted to a layer of hydrogen ions in the electrolyte. Figure 2.5a shows a simple representation of the double layer, where the ionic charge in the membrane equals the electronic charge on the electrode. A simple parallel plate capacitor is often used to model the double layer at the electrode–electrolyte interface. A similar double layer is formed at the cathode. The presence of the double layer gives the fuel cell a very high capacitance, a property explored in this research. In fact, the double layer phenomenon is exploited for manufacturing capacitors with very high capacitance values. These capacitors are discuses in detail in Section 2.5. The spatial distribution of the ionic charges in the electrolyte is not as simple as shown in Figure 2.5a. A more accurate representation of an electrolyte–electrode interface is shown in Figure 2.5b [12]. The inner most region, known as the inner Helmholtz layer consists predominantly of water molecules with their hydrogen ends (positive) orientated towards the negatively charged electrode. Depending on the electrode/electrolyte materials, positive or negative ions may be specifically adsorbed onto the electrode surface (not shown in Figure 2.5b). Further out into the electrolyte, a layer consisting of positive ions surrounded by water molecules defines the outer Helmholtz plane. The ionic charge in the outer Helmholtz plan may not equal the charge on the electrode. Therefore, a higher density of positive ionic charge will be found in the area just beyond the outer Helmholtz layer compared with the bulk electrolyte phase. In summary, the double layer results in a fuel cell possessing a high capacitance. Due to the complicated nature of the ionic charge distribution, models more complicated than a parallel plate capacitor are needed to fully describe the observed behaviour.

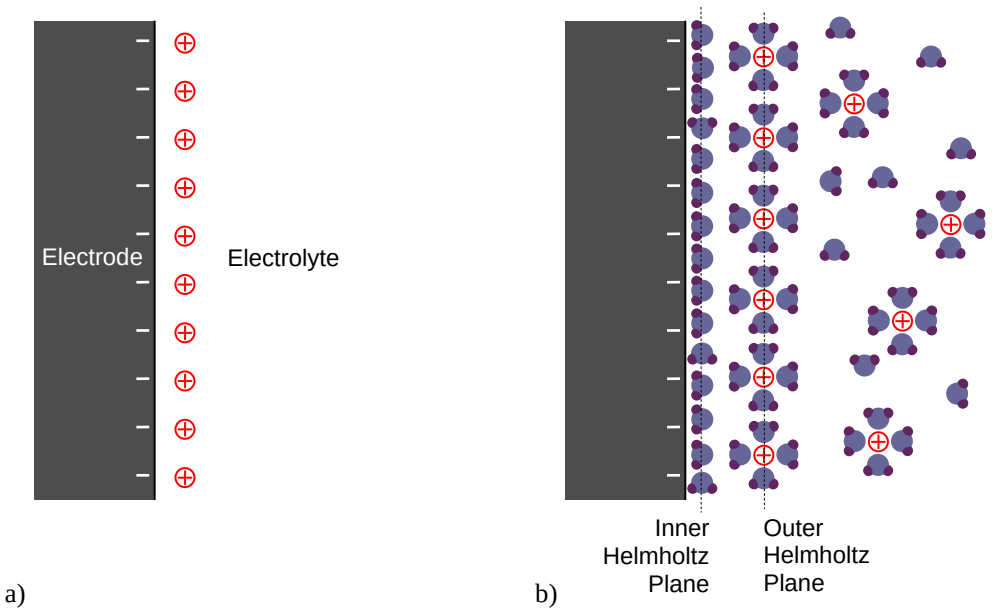

Figure 2.5 Common Representation (a) of the Double Layer, with a more accurate Representation shown in (b), adapted from Bockris and Reddy [12]

The membrane and electrode are commonly manufactured and sold as a single unit, a membrane electrode assembly (MEA). There are two main methods for MEA fabrication. The most common involves creating the electrodes directly on the membrane surface. For this method, an ink composed of activated carbon, platinum particles, solubilised ioniomer (Nafion in a liquid form) and solvent are sprayed or printed onto the membrane (in one or more steps) then dried. The alternative method for MEA fabrication is to apply the ink onto the gas diffusion layer, such as carbon fibre paper (a porous and conductive material described in the next section). The gas diffusion layer is then hot pressed onto a membrane, creating a MEA with gas diffusion layers attached. MEAs utilising Nafion membranes are wildly available, as are Gore MEAs as discussed previously.

Typical carbons used for electrode manufacture include XC72 (®Cabot) [3] as used by Saab *et al.* [13] or Vulcan XC-12 as used by Gode *et al.* [14]. The most common catalyst, used for the anode and cathode, is platinum. A number of platinum alloys have been investigated for the cathode and are shown to have better performance (reduced activation loss), however pure Pt is almost exclusively used commercially [15]. Fuel cells that operate on reformate gas (as opposed to pure hydrogen) will use an alloy such as Pt/Pd or Pt/Ru, as these catalysts are more tolerant to impurities such as CO. Typically, catalyst loadings are < 1 mg/cm^2, and usually range 0.1 – 0.4 mg/cm^2.

2.2.3 GAS DIFFUSION LAYER

The gas diffusion layer (GDL) is a porous, electrically conductive layer, which serves as a current collector and ensures that the reactant/product gases flow to and from the electrode surface uniformly. Gas diffusion layers are made from carbon, such as Toray™ Carbon Paper, (TGP-H-090) or carbon cloth. The gas diffusion layer will be wet proofed with PTFT, which prevents liquid water from forming and blocking gas flow to the electrode. In certain types of passive air breathing fuel cells the GDL may be quite thick and exposed to the air directly, thus, bipolar plates are not used. For example, Enabled produced a small, 12W stack consisting of 23 series connected cells. The stack is annular in design, with hydrogen introduced to the centre of the stack (from both ends). Each cell had a thick GDL on the cathode that allowed air to diffuse from the outer edges to the electrode surface. Most stacks will employ GDLs along with a bipolar plate as discussed below.

2.2.4 BIPOLAR PLATES AND STACK CONSTRUCTION

A single PEM cell produces a voltage of around 0.7V, so many cells (40 – 90) are connected in series, forming a stack, and achieving a useful voltage. The most common stack design is shown in Figure 2.2 where individual cells are connected using a bipolar plate. The bipolar plate is electrically conductive and gas impervious. Grooves, or flow channels on both sides of the bipolar plate, enable hydrogen and air to be delivered to the anode and cathode of adjacent cells, as shown in Figure 2.6a. Bipolar plates are generally made of carbon, either machined graphite plates or moulded plastics containing large amounts of carbon. In addition, metal bipolar plates have also been investigated [3].

Gasket seals are typically integrated into the bipolar plate as shown in Figure 2.6a, and the stack is clamped together under pressure to ensure the seals are gas tight, and to ensure good electrical contact between the electrodes, GDLs and bipolar plates. Due to the delicate nature of the MEAs, a stack cannot be taken apart for repair. Therefore, once a single cell fails, the stack fails. In addition, the weakest performing cell will dictate stack functionality, as will be described in following section.

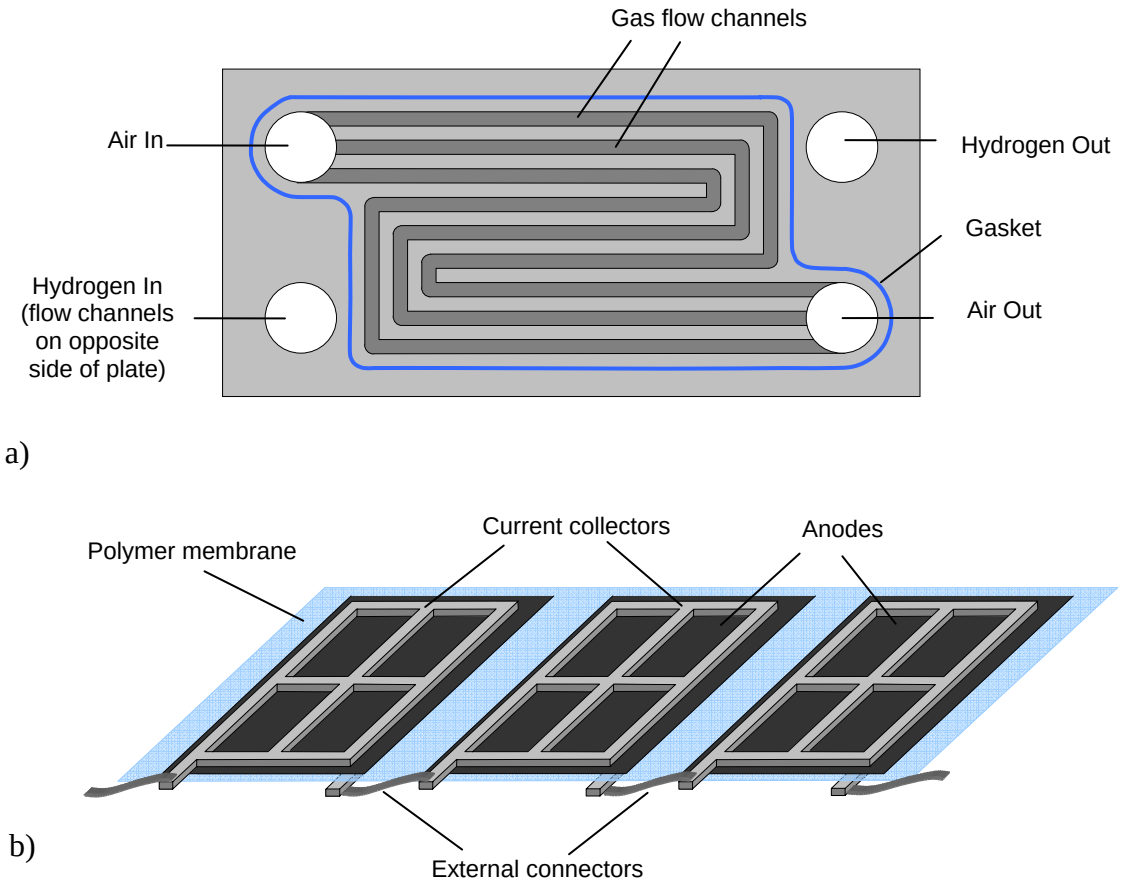

Figure 2.6 Typical Bipolar Plate (a) and Edge Current Collected Cells (b)

Utilizing bipolar plates is not the only way of constructing a stack. Instead, each cell can be edge current collected using a metal grid clamped on to the gas diffusion layer. Each edge current collected cell is then connected in series with external contacts as shown in Figure 2.6b.

2.2.5 FUEL CELL SYSTEM

A schematic fuel cell system is shown in Figure 2.7, and consists of a fuel cell stack, together with auxiliary components, commonly referred to as balance of plant, (BOP). The BOP enables the stack to operate and deliver power, and includes a range of equipment;

- solenoid valves for the hydrogen,
- air pump or fan for delivering reactant air (oxygen) to the stack
- a cooling system where air or a liquid is pumped through separate channels in the stack
- humidification system
- a monitoring and control system
- electronics for power conditioning

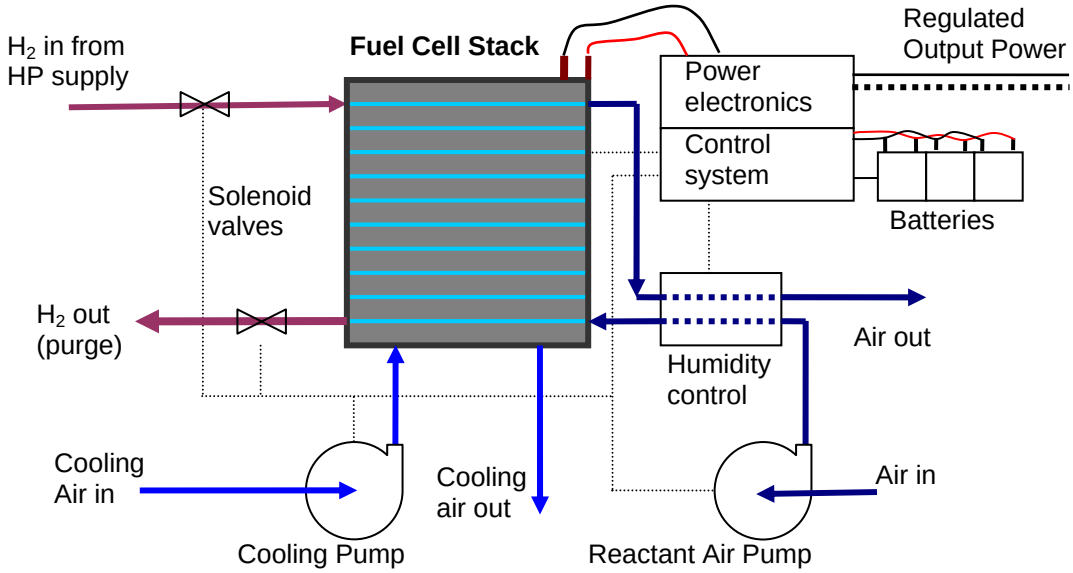

Figure 2.7 Schematic of a PEM Fuel Cell System Showing Balance of Plant (BOP) Components

A fuel processor that reforms a hydrocarbon fuel (i.e. natural gas or methanol) into a hydrogen rich fuel stream, can also be included as part of a fuel cell system. As this thesis focuses on back-up power systems that generally use pure hydrogen, fuel processors are not considered further.

The exact BOP in a PEM fuel cell system will vary depending on the system design. For example, a system manufactured by ReliOn, the Avista-SR12, is a relatively simple system consisting of a single convection fan for air supply, hydrogen solenoid valves, a simple monitoring & control system, and batteries for start-up. In contrast, a system manufactured by Plug Power, the GenCore, employs a humidification system, power-conditioning system, water cooling system, radiator, etc. The chosen system and stack design depends on the targeted application. For back-up power, where reliability is the most important factor, a relatively simple fuel cell system is desirable. Increased complexity, with a higher number of system components, introduces more points of failure. Fuel cell systems that do not have humidification control or specific cooling systems can not be operated at high-power densities. However, high power density is not a major consideration for backup applications as it is for mobile applications.

2.3 PERFORMANCE OF A PEM FUEL CELL

A detailed schematic of an operating fuel cell is shown in Figure 2.8. Each process shown in Figure 2.8 is described below, with subsequent subsections detailing the three main losses and common steady state equations.

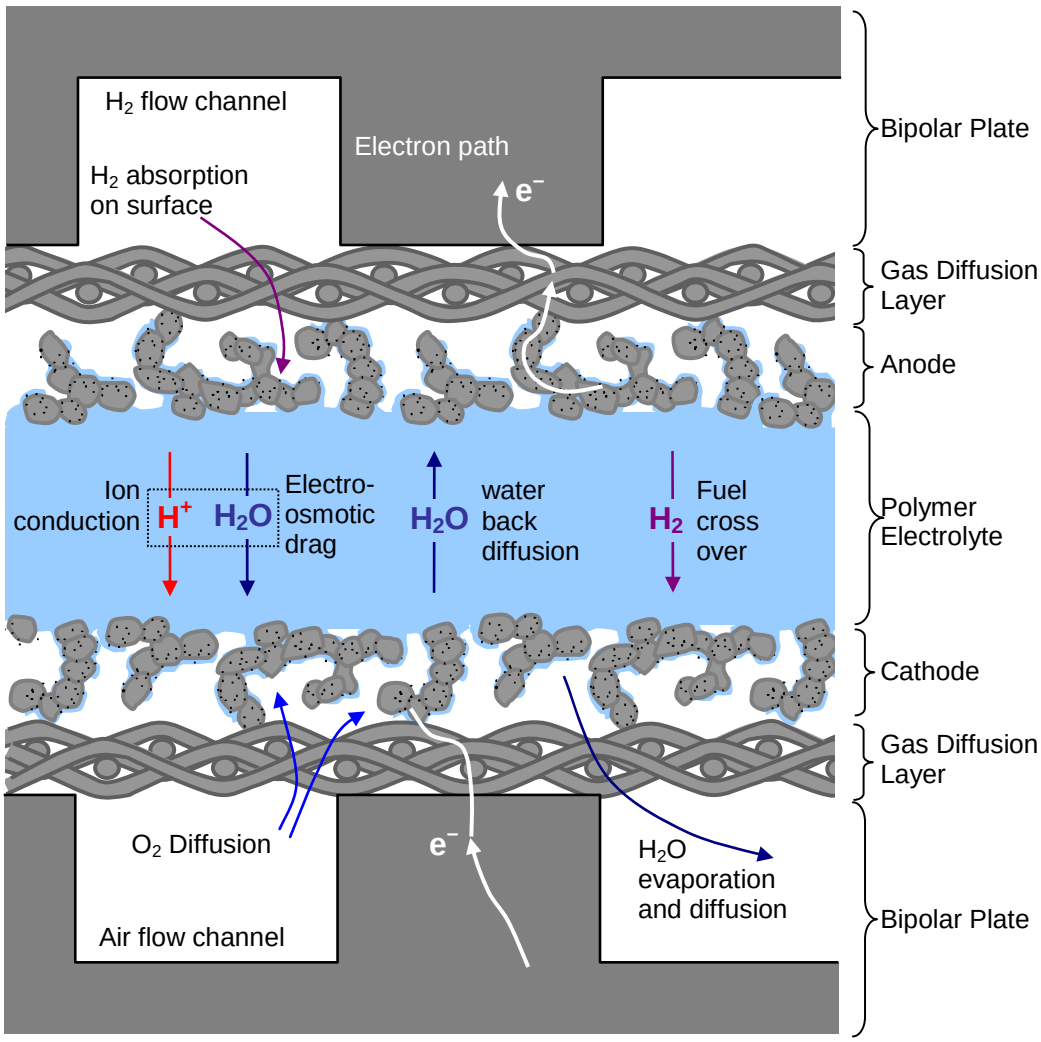

Figure 2.8 Processes Occurring in a Function PEM Fuel Cell

Air flows across the cell cathode, accomplishing both processes of O_2 supply and H_2O exhaust. As oxygen is consumed during operation, a concentration gradient is generated that drives oxygen diffusion to the electrode from the air flow stream. The electrodes, anode and cathode, have highly porous structures, consisting of very small flow channels, or micro channels. As oxygen moves into the electrode, it flows via capillary action, i.e. the affinity the flow channels have for the fluid flowing through them [16].

The half-cell reaction at the cathode occurs in multiple steps, including oxygen adsorption onto a catalyst site, the reaction with hydrogen ions, and finally the desorption of H_2O from the catalyst

site. In section 2.2.2, a three-phase boundary consisting of a catalyst, electrolyte, and gas phase was described as the only place where half-cell reactions could occur. In actuality, catalyst sites may be covered in a thin layer of electrolyte, with oxygen dissolving into the electrolyte liquid phase before migrating to the catalyst site. H_2O is generated at the cathode surface and will evaporate into the air stream depending on the relative humidity. By controlling the humidity, temperature and flow rate of the incoming air, H_2O evaporation can be controlled.

Excess air is always passed through the fuel cell, ensuring the partial pressure of the oxygen does not fall too low in any part of the cell, which would reduce performance. The airflow through the fuel cell is usually quantified by the stoichiometric value, which is the inverse of utilization, i.e. a stoichiometry of 4 corresponds to 25% of the oxygen in the air being consumed. The airflow stoichiometry, temperature and the operating pressure of the fuel cell will determine the H_2O evaporation rate. In most cases, ensuring the membrane retains an adequate hydration is the challenge. In many fuel cell systems, the air, hydrogen, or both, are externally humidified preventing the cell from drying out. Systems that do not use external humidification must operate at lower temperatures ($< 60^oC$), and lower current densities such that adequate voltages are maintained.

A similar sequence of gas adsorption and charge transfer occurs at the anode, with the resulting hydrogen ion entering the membrane electrolyte. As hydrogen ions are generated at the anode and consumed at the cathode, a hydrogen ion concentration gradient forms across the membrane driving hydrogen ion diffusion from the anode to the cathode. An additional mechanism for hydrogen ion transport is migration, where electrostatic repulsion of adjacent ions forces them toward the cathode. As stated in section 2.2.1, hydrogen ions move through the membrane as Hydronium ions, H_3O^+. Therefore, for each H^+ ion, at least one water molecule is "dragged" from the anode to the cathode. This phenomenon, known as electro-osmotic drag, is an important factor for membrane hydration management. Electro-osmotic drag is defined by the amount of water molecules per hydrogen ion, H_2O/H^+, and has been suggested to be as high as 3. However, detailed studies by Zawodzinski [17] found an electro-osmostic value of 1, which was independent of the water content in the membrane. Subsequent work, such as Buchi *et al.* [18], has appeared to back this finding.

H_2O formation at the cathode and electro-osmotic drag causes a water gradient to exist in the membrane. As a result, water will back diffuse from the cathode to the anode, thus re-hydrating

the anode. The rate of water back diffusion is dependent on the concentration gradient, and governed according to Fick's first law as shown in equation 2.14 [7], [18].

$$flux = D_{H_2O} \frac{dC_{H_2O}}{dx} \qquad 2.14$$

Water can be delivered to the anode by humidifying the hydrogen, thus, diffusion may not occur if the anode side of the membrane has the same water content as the cathode side.

The electrons generated at the anode flow through the electrode (catalyst layer), gas diffusion layer, the bipolar plate, and either to the cathode of the next cell, or through an external load. Electron flow is proportional to the active area of the fuel cell, so current density, [mA/cm^2] is used when analysing fuel cell performance. The typical current density of a PEM fuel cell lies in the range of 450 – 800 mA/cm^2.

2.3.1 THE ACTIVATION LOSS

The largest voltage loss in a PEM fuel cell is caused by the slow chemical kinetics of the electrode half-cell reactions. As with any chemical reaction a potential energy barrier, the activation energy, must be overcome for the reaction to proceed. Therefore, some of the electrochemical potential is used to drive the electrochemical half-cell reactions, resulting in a voltage loss. The activation energy of the cathode half-cell reaction is significantly larger than the anode. Hence, the observed activation voltage loss for a PEM fuel cell is due predominantly to the electrochemical kinetics occurring at the cathode.

The activation loss mechanism results in a voltage loss that is non-linear with current. Assuming no other loss mechanisms are present, Figure 2.9 shows an ideal VI curve of a fuel cell operating at low current densities.

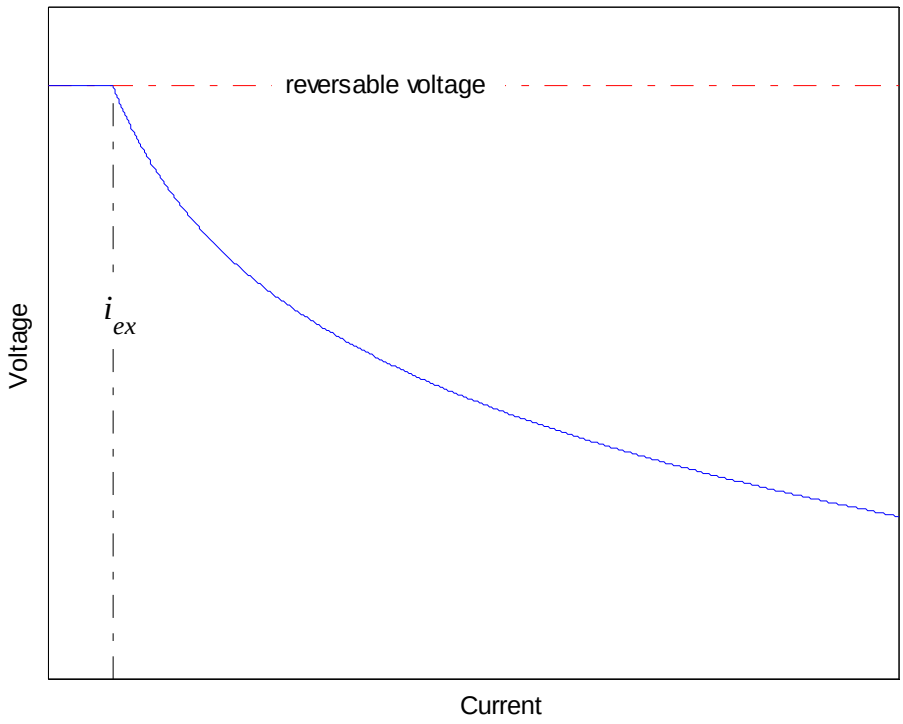

Figure 2.9 Ideal Voltage Behaviour of a Fuel Cell with Voltage Loss caused by the Activation Loss Mechanism Only

Figure 2.9 also shows there is no voltage loss up to a certain point, designated by the current density value i_{ex} [mA/cm^2]. Essentially, the exchange current density represents the rate of reactants interacting with the electrode that have enough energy to overcome the potential energy barrier. Thus, ideally, if the operating current were below this limit, the measured potential of the cell would equal the voltage as given by the Nernst equation. In practice, the crossover current exceeds the exchange current for all practical PEM fuel cells. This has the effect of shifting the whole VI curve to the left by the cross over current amount, resulting in the OCV being less than the reversible voltage.

Figure 2.9 shows a single exchange current density, i_{ex}. However, there are two distinct exchange current densities, one for each electrode. Each exchange current density defines the rate of the half-cell reactions while the fuel cell is in an open circuit state. This is shown in equations 2.15 and 2.16.

$$H_2 \xleftrightarrow{i_{ex,A}} 2e^- + 2H^+ \qquad 2.15$$

$$O_2 + 4e^- + 4H^+ \xleftrightarrow{i_{ex,C}} 2H_2O \qquad 2.16$$

Where $i_{ex,C}$ and $i_{ex,A}$ are the exchange current densities of the anode and cathode half-cell reactions. With the activation loss being dominated by the cathode electrochemical kinetics, the cathode exchange current density, $i_{ex,C}$ is much lower than that of the anode, $i_{ex,A}$ thus the current density reached before a loss is incurred is dictated by the exchange current density at the cathode, i.e. $i_{ex} = i_{ex,C}$ in Figure 2.9. In general, the higher the exchange current density, the more active the electrode is, resulting in a lower activation loss.

The voltage loss as a function of current can be derived from electrochemical theories developed by Butler-Volmer [21]. However, in practice a simplified semi-empirical equation is often used, the Tafel equation, which is given below [3].

$$\eta_{act} = \frac{RT}{2\alpha F}\ln\left(\frac{i}{i_{ex}}\right) \qquad 2.17$$

Where α is the charge transfer co-efficient, approximately 0.5 and η_{act} is the voltage drop due to the activation loss mechanism. It should be noted that the exchange current density, i_{ex} strongly dictates the shape (and hence voltage loss) for the entire VI range. It will be shown later that this equation is further simplified with the constants lumped together into a single parameter, the value of which is evaluated from experiment. Clearly, equation 2.17 only is true for $i > i_{ex}$.

Measures to reduce the activation loss are related to the manufacturing of the electrode, rather than the operating conditions of the fuel cell. The use of an electro catalyst, such as Pt is vital for PEM fuel cell operation for reducing the activation energy required for the half-cell reactions. Without a catalyst, the activation loss would be so high, no useful work could be extracted from the fuel cell. As the activation loss is far greater for the oxygen half-cell reaction, some fuel cell manufactures increase the catalyst loading on the cathode. The surface area is also vital, essentially increasing the exchange current density by providing more reaction sites per unit area.

The fuel cell operating conditions also affects the activation loss. As the fuel cell operating temperature increases, the activation loss decreases. Essentially, at higher temperatures a greater number of reactants have enough energy to overcome the activation energy barrier, thus increasing the exchange current density. Higher pressure also is known to decrease the activation loss through increased catalyst site occupancy [3]. Although the activation loss is

affected by the operating conditions, in practice, fuel cell operating conditions are dictated by membrane hydration rather than optimizing the operating conditions to minimise the activation loss.

2.3.2 THE RESISTANCE LOSS

The resistance loss, also referred to as the ohmic loss, arises from current flowing through the various conductors of the fuel cell stack. Ionic resistance of the membrane is the primary cause of resistance loss, although electronic resistance of the bipolar plates, gas diffusion layers, electrodes and contact resistances between these different materials also contributes. As the membrane resistance is most significant in a PEM fuel cell, this discussion will focus on the ionic resistance and how it is affected by the physical state of the membrane.

The water content of the membrane is the most important factor in determining the ionic resistance. The water content of a membrane is defined most commonly as the ratio of water molecules per sulfonic acid site, i.e. $\lambda = H_2O / SO_3^{-1}$. Zawodzinski *et al.* [20], measured the resistance of Nafion 117 at various states of hydration ($\lambda = 2 - 22$), and showed the resistance decreasing linearly with increasing water content. The relationship was quantified in a previous publication [21] and is shown in equation 2.18.

$$\sigma_{T=30^{\circ}\mathrm{C}} = 0.005139\lambda - 0.00326 \text{ for } \lambda > 1 \qquad 2.18$$

Where σ is the conductance, [S/cm] measured at 30°C. The ionic resistance as a function of temperature was also investigated and the following combined expression for Nafion 117 was derived [21].

$$\sigma(T_{cell}) = \sigma_{T=30^{\circ}\mathrm{C}} \exp\left[1268\left(\frac{1}{303} - \frac{1}{273 + T_{cell}}\right)\right] \qquad 2.19$$

Although the ionic conductance increases with increasing temperature, the variation over the operating temperature range is much smaller than the variation due to hydration.

Membrane hydration, hence the ionic resistance, is determined by the operating conditions of the fuel cell. For example, Cai *et al.* [22] measured the resistance of a PEM fuel cell operating with dry hydrogen to be 0.493 Ωcm^2 (Nafion 115, operating at 500 mA/cm^2), where as with saturated

hydrogen (at 333K), the ohmic resistance drops to 0.345 Ωcm^2. For both tests the cathode humidity was kept at 0.56 and the stoichiometry of the air and hydrogen was 1.1 and 2.5 respectively. The performance of the cell will clearly improve with lower resistance. For the two cases listed above the cell voltage while operating on dry hydrogen was 0.521 V compared with 0.618 V with saturated hydrogen.

The resistance as a function of current density has also been investigated. For example, Springer *et al.* [21] showed that the membrane (Nafion 117) resistance increased linearly with current destiny, from 0.24 Ωcm^2 at 0 mA/cm^2, to 0.40 Ωcm^2. However, Cai, *et al.*[22] found the resistance of Nafion 115 and 112 to decrease when measured at a current density of 500 mA/cm^2 compared with the resistance measured at 300 mA/cm^2. In both cases, the different current densities cause the water content in the membrane to change, leading to a change in resistance. Whether the water content increased or decreased depends on the operation conditions of the fuel cell, such as humidification of the reactant gases, stoichiometric flow, temperature and pressure.. Under certain operating conditions, a higher current will reduce the water content on the anode side of the membrane due to electro-osmotic drag, thus increasing the membrane resistance. Under a different set of operating conditions, the water content of the membrane will increase due to the increasing rate of water production at the cathode. The two experiments cited above were conducted under different operating conditions, leading to the different observed change in resistance with current density.

As with any ohmic resistance, the fuel cell resistance loss results in a voltage drop, η_{res} that is proportional to the operating current as shown in equation 2.20.

$$\eta_{res} = ri \qquad 2.20$$

If i, the current density is given as mA/cm^2, then r is given as the area specific resistance $k\Omega \cdot cm^2$ [3]. As will be shown in Section 2.3.4, the resistance loss is exclusively modelled as a constant, whose value is determined by fitting experimental data to a model that includes the other major loss mechanisms.

In summary, the resistance, and hence the fuel cell performance, is strongly dependent on the membrane water content. The amount of literature focusing on hydration and water management reflects the importance of this fuel cell aspect (for example [17], [18], [20], [22]-[27]).

2.3.3 THE MASS TRANSPORT LOSS

The mass transport loss occurs when the reaction rate approaches the maximum rate at which a reactant/product can be delivered/removed. Figure 2.6 shows numerous species are transported in a PEM fuel cell; reactant gas diffusion to the electrode surface, H^+ ionic conduction with associated electro-osmotic drag of H_2O, membrane back diffusion of H_2O, and H_2O evaporation and diffusion from the cathode. Any one of these species could have a low transport rate limit that when approached, would result in a voltage loss. The cause of voltage loss depends on the specific species involved, and is described below.

The limiting rate at which oxygen can diffuse to the surface of the cathode is often cited as the dominant mass transport loss mechanism [3]. As the maximum rate of O_2 diffusion is reached, the partial pressure of the O_2 at the cathode surface will decrease, resulting in a voltage loss as evident from the Nernst equation. Assuming the pressure of oxygen decreases in proportion to increasing current, and is zero at the limiting current, i_l, the voltage loss can be derived by a simple Nernst analysis [3]

$$\Delta V_{trans} = -B \ln\left(1 - \frac{i}{i_l}\right) \qquad 2.21$$

In theory, B equals RT/4F for oxygen, (and RT/2F if hydrogen is the limiting reactant). In practice, equation 2.16 or any other analytical model has not been used in the literature for modelling the mass transport loss. Instead, a purely empirical approach is employed, which is described in more detail in Section 2.3.4.

A mass transport mechanism related to oxygen access to the cathode, is the rate of H_2O evaporation and diffusion. If the rate of water removal from the cathode is less than the rate at which it is generated, liquid water can build up in the electrode or flow channels. This is commonly known as flooding. Clearly this will prevent oxygen from reacting at the cathode, resulting in voltage decline.

A likely cause of mass transport loss that has been cited more recently in the literature, originates from water transport within the membrane. At high current, the back diffusion of water may not be sufficient to compensate for electro-osmotic drag. Therefore, the anode side of the membrane becomes dehydrated leading to high ionic resistance and a high voltage loss. A number of authors have shown water back diffusion to be the limiting mass transport loss mechanisms. For example, Du *et al.* [8] investigated the performance of cells, each with a different membrane.

The mass transport loss was found to be higher for cells using a thicker membrane. Thus, it was concluded that the mass transport loss originates from changes in water distribution within the membrane (caused by H^+ transport) i.e. water cannot back diffuse as quickly in a thick membrane. However, in this experiment cells were operated with pure O_2, thus the mass transport loss from oxygen diffusion is not present. An air breathing planar fuel cell, where the cathode is exposed directly to the air, also showed a mass transport loss originating from water back diffusion in the work of Chu *et al.* [28]. With increased humidity operation at the anode, the mass transport loss was found to decrease (due to increased membrane hydration). In addition, the higher the operating temperature, the larger the mass transport loss, which was attributed to increased drying of the membrane.

The specific mass transport loss mechanism is dependent on the type of fuel cell and operating conditions. Most likely, water back diffusion in the membrane, or oxygen diffusion to the cathode will be the specific mass transport loss mechanism. Once again, the impact water has on the operation of the fuel cell is evident, not only effecting the resistance loss, but also dictating the mass transport loss and the limiting current of the fuel cell.

2.3.4 COMMON STEADY STATE EQUATIONS

The measured voltage from a practical fuel cell differs significantly from the reversible voltage of 1.23V. Figure 2.10 shows the characteristic voltage current curve.

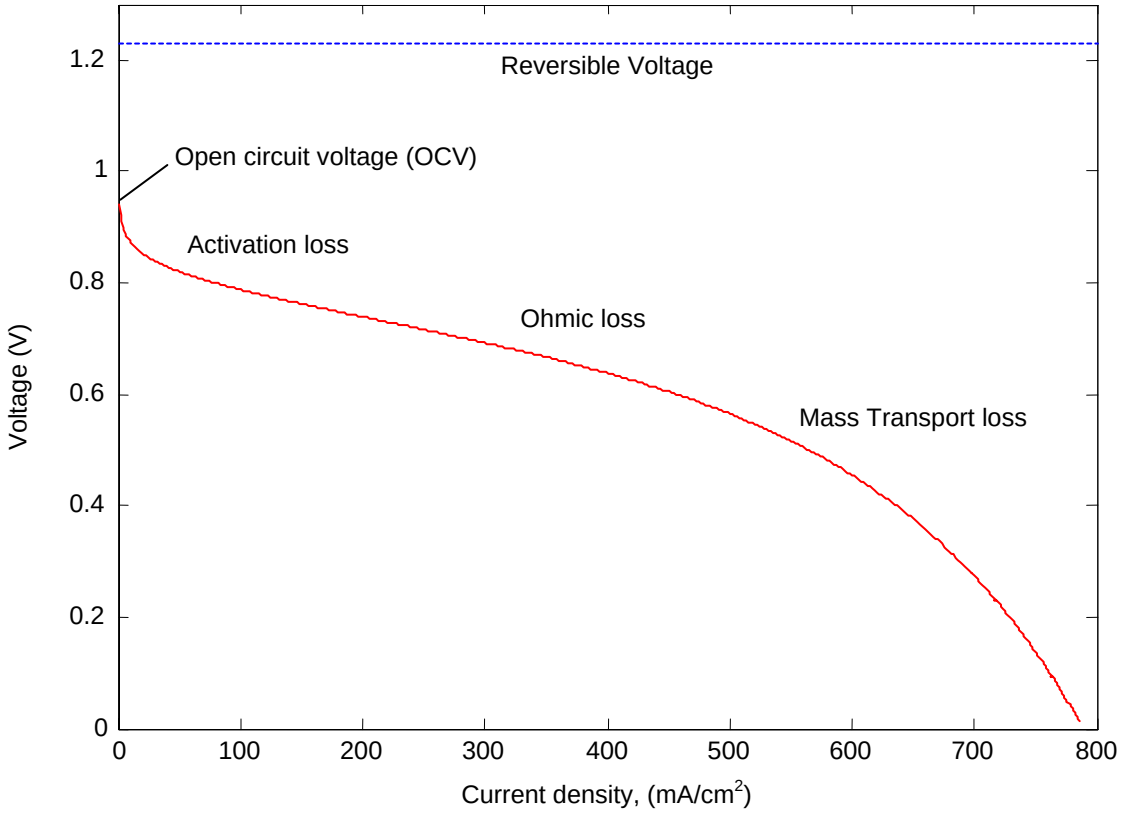

Figure 2.10 Typical PEM Fuel Cell VI Curve

In general, the three main loss mechanisms dominate the voltage behaviour at different current ranges. At low current values, the activation loss causes a steep decline in the voltage. Ionic resistance of the membrane together with electronic resistance of the electrodes and current-collectors, results in a linear decrease in the voltage at nominal operating currents. At high current, a rapid decay in voltage occurs due to the mass-transport loss mechanism.

Ideally, the open circuit voltage (OCV) would not be affected by the loss mechanisms, and should equal the reversible voltage 1.23V. Figure 2.10, is typical for all PEM fuel cells, and shows the OCV to be substantially less than 1.23V. This is due to internal currents flowing through the membrane effectively making the fuel cell current non-zero at OC, resulting in a voltage drop due to the activation loss. Fuel cross over, where molecular hydrogen travels through the membrane reacting with oxygen at the cathode is accepted to be the main cause of internal currents in a PEM fuel cell. Other mechanisms that cause internal currents to flow are conduction of the membrane (although very rarely documented) [3], and ion flow between adjacent cells(when a common membrane is used for multiple cells [29].

Mathematical definition of the VI curve in terms of fuel cell operating parameters has been the subject of much research. In general, the cell voltage, *E*, is described by a relation of the form

$$E = E_0 - \eta_{act} - \eta_{ohmic} - \eta_{mass} \qquad 2.22$$

Where η_{act}, η_{ohmic}, and η_{mass} are the losses associated with the activation, ohmic and mass transport mechanisms respectively. E_0 is the reversible voltage given by equation 2.13, (as derived in section 2.1). Each loss term in equation 2.22 is a function of the current and the operating conditions of the fuel cell such as temperature, humidity and pressure. For example, the activation loss reduces with increased temperature and pressure, thus increasing the cell voltage.

There are two main approaches for obtaining a mathematical expression of the loss terms in equation 2.22; mechanistic and empirical. A number of authors [30]-[34] have used a mechanistic approach. This involves deriving functions for each loss mechanism from electrochemistry first principles and the species transport fundamentals. The resulting loss terms are functions of many operating parameters, and depend on many electrochemical material properties. As many of these values are not easily found, mechanistic equations are not often used to represent real fuel cell behaviour. Instead, empirical models are used and are reviewed below.

Empirical models are formed by fitting an appropriate equation to experimental VI data. In most cases, the empirical equation will be a function of current only. A typical empirical model given by Larminie and Dicks [3] is shown in equation 2.23

$$E(i) = E_0 \quad - \eta_{act} \quad - \eta_{ohmic} - \eta_{mass}$$

$$E(i) = E_0 - b\log\left(\frac{i + i_n}{i_0}\right) - ri \quad - me^{ni} \qquad 2.23$$

E_0 = reversible voltage [V]

i = operating current density [mA/cm^2]

i_0 = exchange current density [mA/cm^2]

i_n = internal current (fuel cross over) [mA/cm^2]

b = empirical fitting value associated with activation loss [mV]

r = empirical fitting value associated with resistance loss [kΩ·cm^2]

m, n = empirical fitting value associated with the mass transport loss [V, cm^2/mA]

This type of equation is sometimes referred to as semi-empirical, as certain parts are derived from mechanistic considerations. For instance, the logarithmic drop in voltage due to the activation loss is derived from electrochemical fundamentals.

The mass transport loss term in equation 2.23 was first proposed by Charles E. Chamberlin, and described in the work of Kim *et al.* [9]. The empirical model used is shown in equation 2.24.

$$E(i) = E_{OCV} - b\log(i) - ri - me^{ni} \qquad 2.24$$

Again, *b*, *r*, *m* and *n* are fitted parameters, and E_{OCV} is the measured potential of the cell at open circuit, rather than the reversible voltage, E_0, as used in equation 2.23.
Equation 2.24 is most commonly used in the literature to model the VI performance of fuel cell. A number of slight variations are also used, for example, the model used by Chu *et al.* [28] is shown in equation 2.25

$$E(i) = E - B\log(1000i) - ri - i_m me^{(ni_m)} \qquad 2.25$$

$$i_m = i - i_d \quad \text{for } i > i_d$$

$$i_m = 0 \qquad \text{for } i \le i_d$$

In this model, the mass transport loss term only affects the voltage beyond a particular current, i_d, defined as the smallest current value where the voltage deviates from linearity in the ohmic loss dominated region of the VI curve.

Some empirical models are functions of physical parameters in addition to current. For example, equation 2.26 was used by Lee *et at.* [16] when modelling the current distribution, temperature, and humidity over an MEA surface,

$$E(i, P, P_{O_2}) = E_0 - b\log(i) - ri - me(ni) - b\log\left(\frac{P}{P_{O_2}}\right) \qquad 2.26$$

Where *P* is the total pressure and P_{O2} is the oxygen partial pressure.

Practical fuel cells are not operated near their limiting current values, due to the significant mass transport loss incurred. Therefore, the mass transport loss term is often not required for practical

modelling purposes. A simple empirical relation as given by equation 2.27 is often used [35], [8].

$$E(i) = E - b\log(i) - ri \qquad 2.27$$

All of the fuel cell models reviewed thus far only deal with the steady state performance of the fuel cell. The dynamics of the fuel cell, such as the voltage response to a change in current are also important aspects of fuel cell performance. These aspects will be addressed in Chapter 3, where methods of fuel cell testing, and equivalent circuit modelling of fuel cells is reviewed.

2.4 Degradation and Failure of PEM Fuel Cell Systems

An important consideration in a back-up power application is the degradation and potential failure of a fuel cell system. As PEM fuel cells are a relatively new and emerging technology, and one that is constantly evolving, degradation and lifetime issues are not well known. This lack of knowledge is further exacerbated by the proprietary nature of fuel cell research and development. The main degradation mechanisms and resulting effects are briefly discussed.

Catalyst poisoning occurs when contaminants in either the air or fuel supply, particularly CO and sulphur compounds, absorb onto the catalyst preventing electrochemical reactions from occurring. As a result, the activation loss increases, reducing performance. Catalyst poisoning is of particular concern when the fuel cell is operated on a reformate fuel stream, which can contain significant amounts of impurities. Contaminates are costly to remove and so poisoning is a real operational issue for UPS applications.

Catalyst agglomeration is a gradual process, where the fine catalyst particles combine. This process reduces the catalyst surface area, eliminating sites where electrochemical reactions can occur. Again, the effect is an increase of the activation loss, and a decrease in the performance.

The polymer membrane can degrade and lead to the failure of the fuel cell in a number of ways. The polymer is based on PTFE, which is chemically and physically stable and will not break down easily, or react chemically. However, the sulphonic acid groups, which enable the membrane to conduct, are susceptible to chemical attack. For example, contaminant ions can

take the place of the H^+ and cause cross linking of the polymer side chains [36]. This results not only in a reduction of charge carriers (H^+), but also in a reduction in the water carrying capacity of the membrane. Contaminant membrane degradation effectively increases the ionic resistance and reduces performance [37].

Membrane degradation can also be caused by operating the fuel cell at inadequate humidification levels, and in the extreme case, can lead to complete cell failure. At low membrane hydration, (hence high resistance), holes can form in the membrane [27]. As PEM fuel cells are operated with the anode at a higher pressure than the cathode, significant amount of H_2 gas to flow under pressure to the cathode. At high current, the electrode can delaminate from the membrane clearly leading to complete cell failure [36].

Degradation in a PEM fuel cell is exacerbated by start-up/shut-down cycling. The changes in hydration levels during cycling cause the membrane to swell and contract. Thermal cycling is known to increase the rate of degradation due to material stress [38].

Clearly, the cell is not the only point of failure in a fuel cell system. If any of the auxiliary systems fail, the stack will not be able to function. Fuel cell systems designed for backup power are most likely to have simple system designs, thus the source of failure is likely to be the stack or the cell itself. As stated previously, if a single cell performs poorly, this limits the operation and hence performance of the entire fuel cell stack. If a single cell fails, then the stack fails.

2.5 PHYSICAL SIMILARITY TO A DOUBLE LAYER CAPACITOR (DLC)

In the literature, fuel cells are generally analysed and compared with similar electrochemical devices such batteries or electrolysis cells. The comparative analysis taken in this research is to compare a fuel cell with a specific type of capacitor; the double layer capacitor (DLC). This approach is taken because a fuel cell in a passive state, is physically and electrically similar to a DLC

This section briefly describes the physical construction of a double layer capacitor, and the fundamental principles of operation. The similarity between a DLC and a passive PEM fuel cell is also discussed.

2.5.1 PHYSICAL DESCRIPTION OF A DLC

The basic construction of any DLC consists of two electrodes, separated by an electrolyte that contains free moving ions. Under an applied voltage, a double charge layer forms at the electrode–electrolyte boundary as the ions in the electrolyte are attracted to the charge on the electrode. As the charge separation between the electrolyte ions and electrode surface charge is very small, in the order of a number of molecules, the capacitance of a DLC is extremely large. Figure 2.11 shows a schematic of a charged DLC.

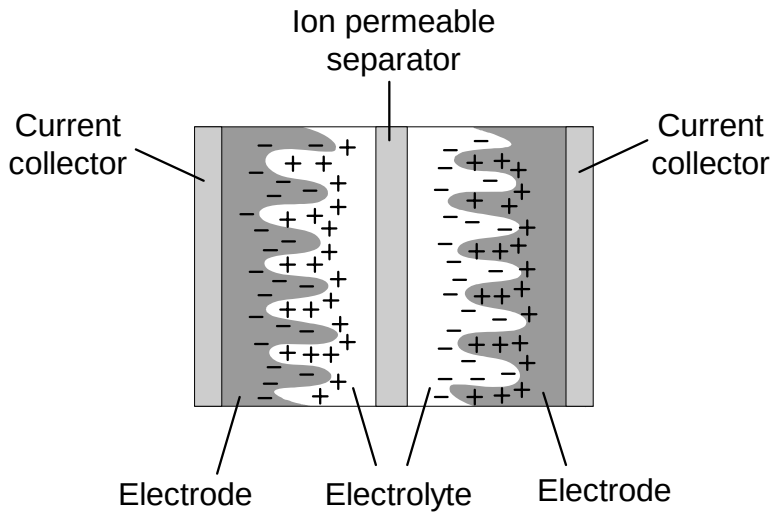

Figure 2.11 A Double Layer Capacitor (DLC) Under an Applied Potential

DLCs are sometimes referred to as super capacitors or ultra capacitors. However, these terms primarily refer to devices in which the primary charge storage mechanism is something other than the double charge layer, such as the absorption of electrolyte species into a solid crystalline electrode [39].

2.5.2 MATERIALS USED

The electrodes of a DLC consist of activated carbon, which possess a very high surface area. This is essentially the same electrode material in a PEM fuel cell, with the exception of the

platinum catalyst. The electrolyte in a DLC can be organic or aqueous. Usually organic electrolytes are used such as tetraethyl-ammonium tetrafluorborate and propylene carbonate [40], as higher voltages can be applied (up to 3V) before electrolyte breakdown occurs. Although a higher operating voltage means more energy can be stored, organic based electrolytes suffer from a high ionic resistance. Instead of an organic based electrolyte, an aqueous environment can be used such as H_2SO_4, similar to the acid in a PEM fuel cell. Aqueous electrolytes have a lower ionic resistance [41]; however, their potential is limited to 1.2 V, as water will decompose at higher voltages.

Recently, a number of DLCs have been constructed using Nafion®, the polymer membrane most commonly used for PEM fuel cells [42]-[44]. The construction method was essentially the same as for a PEM fuel cell and consisted of spraying an ink composed of Norit AS Super activated carbon ($1150 m^2/g$), Nafion solution and a solvent, on to two carbon cloths, forming the electrodes. The electrodes were then hot pressed together, separated by a sheet of Nafion® 115 [43].

Despite a DLC and a PEM fuel cell being physical similar, the processes occurring in each are distinctly different. In a DLC, only non-Faradaic processes can occur, such as the movement and accumulation of ions and electrons. However, in an operating fuel cell, Faradaic processes dominate, i.e., electrochemical reactions proceed due to a charge transfer between the electrolyte and the electrode.

Due to the similarity between a double charge layer capacitor and a PEM fuel cell, consideration is given to testing and modelling these devices throughout this thesis. The actual properties of the DLC will be examined when the testing procedures are discussed.

2.6 REFERENCES

[1] CRC handbook of chemistry and physics, 85th Edition Cleveland, Ohio, CRC Press 2004

[2] Sonntag R.E, Borgnakke C, Van Wylen G.J, "Fundamentals of Thermodynamics" 6th ed. New York, Wiley, c2003.

[3] Larminie J, Dicks A, "Fuel cell systems explained, 2nd Edition, West Sussex, J. Wiley, 2003

[4] Slade S, Campbell SA, Ralph TR, Walsh FC, "Ionic conductivity of an extruded Nafion 1100 EW series of membranes", Journal of the Electrochemical Society, Vol. 149, pp. A1556-A1564, Dec. 2002

[5] Paddison S.J. "First principles modeling of sulfonic acid based ionomer membranes", Handbook of Fuel Cells, Vol 3, Chap. 31, West Sussex, John Wiley & Sons Ltd, 2003

[6] Sumner JJ, Creager SE, Ma JJ, DesMarteau DD, "Proton conductivity in Nafion (R) 117 and in a novel bis[(perfluoroalkyl)sulfonyl]imide ionomer membrane"**,** Journal of the Electrochemical Society**,** Vol. 45, pp. 107-110, Jan. 1998

[7] Buchi FN, Srinivasan S, "Operating proton exchange membrane fuel cells without external humidification of the reactant gases - Fundamental aspects", Journal of the Electrochemical Society, Vol. 144, pp. 2767-2772, Aug.1997

[8] Du XZ, Yu JR, Yi BL, Han M, Bi KW, "Performances of proton exchange membrane fuel cells with alternate membranes" Physical Chemistry Chemical Physics Vol. 3, pp. 3175-3179, 2001

[9] Kim J, Lee S-M, Srinivasan S, "Modeling of Proton Exchange Exchange with an Empirical Equation", Journal of the Electrochemical Society, Vol. 142 pp. 2670-2674, Aug. 1995

[10] Sigma-Aldrich Co., Product information, Electrolyte Materials, http://www.sigmaaldrich.com/Area_of_Interest/Chemistry/Materials_Science/Energy_Source_Materials/Liquid_Electrolytes.html

[11] W. L. Gore & Associates, Inc., Product information, MEA http://www.gore.com/en_xx/products/electronic/fuelcells/index.html

[12] Bockris JO'M, Reddy AKN, "Modern Electrochemistry: An Introduction to an Interdisciplinary Area", Vol 2, Chapter 7, New York: Plenum Press, 1970

[13] Saab AP, Garzon FH, Zawodzinski TA, "Determination of ionic and electronic resistivities in carbon/polyelectrolyte fuel-cell composite electrodes", Journal of the Electrochemical Society, Vol. 149, pp. A1541-A1546, Dec 2002

[14] Gode P, Jaouen F, Lindbergh G, Lundblad A, Sundholm G, "Influence of the composition on the structure and electrochemical characteristics of the PEFC cathode", Electrochimica Acta, Vol. 48, pp. 4175-4187, Dec. 2003

[15] Thompsett D, "Pt alloys as oxygen reduction catalyst", Handbook of Fuel Cells, Chap. 37, West Sussex, John Wiley & Sons Ltd, 2003

[16] Lee JH, Lalk TR, Appleby AJ, "Modeling electrochemical performance in large scale proton exchange membrane fuel cell stacks", Journal of Power Sources, Vol. 70, pp. 258-268, Feb. 1998

[17] Zawodzinski T. A. Davey J, Valerio J, Gottesfeld S "The Water Content Dependence of Electro-Osmotic Drag in Proton-Conducting Polymer Electrolytes" Electrochimica Acta, Vol. 40, pp. 297-302, Feb. 1995

[18] Buchi FN, Scherer GG**,** "Investigation of the transversal water profile in nafion membranes in polymer electrolyte fuel cells", Journal of the Electrochemical Society, Vol. 148, pp. A183-A188, Mar. 2001

[19] Kordesch K, Simader G, “Fuel cells and their applications”, Weinheim, New York, 1996.

[20] Zawodzinski Ta, Derouin C, Radzinski S, Sherman Rj, Smith Vt, Springer Te, Gottesfeld S, “Water Uptake by and Transport Through Nafion(R) 117 Membranes”, Journal of the Electrochemical Society, Vol. 140, pp. 1041-1047 Apr 1993

[21] Springer TE, Zawodzinski TA, Gottesfeld S, “Polymer Electrolyte Fuel-Cell Model”, Journal of the Electrochemical Society, Vol. 138, pp. 2334-2342, Aug. 1991

[22] Cai YH, Hu J, Ma HP, Yi BL, Zhang HM, “Effect of water transport properties on a PEM fuel cell operating with dry hydrogen”, Electrochimica Acta, Vol. 51, pp. 6361-6366, Sep. 2006

[23] Nguyen TV, White RE, “Water and heat management model for proton-exchange-membrane fuel cells”, Journal of the Electrochemical Society, Vol. 140, pp. 2178-2186, Aug 1993

[24] Sena DR, Ticianelli EA, Paganin VA, Gonzalez ER, “Effect of water transport in a PEFC at low temperatures operating with dry hydrogen”, Journal of Electroanalytical Chemistry, Vol. 477, pp. 164-170, Nov. 1999

[25] Freire TJP, Gonzalez ER, “Effect of membrane characteristics and humidification conditions on the impedance response of polymer electrolyte fuel cells”, Journal of Electroanalytical Chemistry, Vol. 503, pp. 57-68, Apr. 2001

[26] van Bussel HPLH, Koene FGH, Mallant RKAM, Dynamic model of a solid polymer fuel cell water management, Journal of Power Sources, Vol. 71, pp. 218 – 222, Mar. 1998

[27] Yu JR, Matsuura T, Yoshikawa Y, Islam MN, Hori M, “Lifetime behavior of a PEM fuel cell with low humidification of feed stream”, Physical Chemistry Chemical Physics, Vol. 7, pp. 373-378, 2005

[28] Chu D, Jiang R, Walker C, “Analysis of PEM fuel cell stacks using an empirical current-voltage equation” Journal of Applied Electrochemistry, Vol. 30, pp. 365-370, Mar. 2000

[29] O'Hayre R, Fabian T, Lee SJ, Prinz FB, “Lateral ionic conduction in planar array fuel cells”, Journal of the Electrochemical Society, Vol. 150, pp. A430-A438, Apr. 2003

[30] Correa J.M, Farret, F.A, Canha L.N, “An analysis of the dynamic performance of proton exchange membrane fuel cells using an electrochemical model” IECON '01, The 27th Annual Conference of the IEEE Industrial Electronics Society, Vol. 1, pp. 141–146, Dec. 2001.

[31] van der Merwe JB, Turpin C, Meynard T, Lafage B, “The installation, modelling and utilisation of a 200 W PEM fuel cell source for converter based applications”, IEEE 33rd Annual Power Electronics Specialist Conference (PESC 02), Vol. 1, pp. 333-338, Jun. 2002

[32] Amphlett JC, Baumert RM, Mann RF, Peppley BA, Roberge PR, Harris TJ “Performance Modeling of the Ballard-Mark-IV Solid Polymer Electrolyte Fuel-Cell .1. Mechanistic Model Development”, Journal of the Electrochemical Society Vol. 142, pp. 1-8, Jan. 1995

[33] Amphlett JC, Baumert RM, Mann RF, Peppley BA, Roberge PR, Harris TJ “Performance Modeling of the Ballard-Mark-IV Solid Polymer Electrolyte Fuel-Cell .2. Empirical-Model Development”, Journal of the Electrochemical Society Vol. 142, pp. 9-15, Jan. 1995

[34] Mann RF, Amphlett JC, Hooper MAI, Jensen HM, Peppley BA, Roberge PR, “Development and application of a generalised steady-state electrochemical model for a PEM fuel cell”, Journal of Power Sources, Vol. 86, pp. 173-180, Mar. 2000

[35] Chu D, Jiang RZ, “Performance of polymer electrolyte membrane fuel cell (PEMFC) stacks Part I. Evaluation and simulation of an air-breathing PEMFC stack”, Journal of Power Sources, Vol. 83, pp. 128-133, Oct 1999

[36] Okada T, “Modeling Polymer Electrolyte Membrane Fuel Cell Performances”, Journal of New Materials for Electrochemical Systems, Vol. 4, pp. 209-220, Oct. 2001

[37] St-Pierr J, Wilkinson DP, Knights S, Bos ML, “Relationship between management, contamination and lifetime degradation in PEFC”, Journal of New Materials for Electrochemical Systems, Vol. 3, pp. 99-106, Apr. 2000

[38] Michael W. Fowler, Ronald F. Mann, John C. Amphlett, Brant A. Peppley, Pierre R. Roberge, “Incorporation of voltage degradation into a generalised steady state electrochemical model for a PEM fuel cell”, Journal of Power Sources, Vol. 106 pp. 274-283, Apr. 2002

[39] Huggins RA, “Supercapacitors and electrochemical pulse sources”, Solid State Ionics, Vol. 134, pp. 179-195, Oct. 2000

[40] Spyker RL, Nelms RM, “Classical equivalent circuit parameters for a double-layer capacitor” IEEE Transactions on Aerospace and Electronic Systems, Vol. 36, pp. 829 – 836, Jul. 2000

[41] Kotz R, Carlen M, “Principles and applications of electrochemical capacitors”, Electrochimica Acta, Vol. 45, pp. 2483 – 2498, May 2000

[42] Lufrano F, Staiti P, Minutoli M, “Evaluation of nafion based double layer capacitors by electrochemical impedance spectroscopy” Journal of Power Sources, Vol. 124 pp. 314-320, Oct. 2003

[43] Lufrano F, Staiti P, Minutoli M, “Influence of Nafion content in electrodes on performance of carbon supercapacitors”, Journal of the Electrochemical Society, Vol. 151, pp. A64-A68, Jan. 2004

[44] Staiti P, Minutoli M, Lufrano F, “All solid electric double layer capacitors based on Nafion ionomer”, Electrochimica Acta Vol. 47, pp. 2671-2870, Jul. 2002

3 TESTING AND EQUIVALENT CIRCUIT MODELLING OF PEM FUEL CELLS

This chapter reviews testing techniques and modelling commonly used to investigate a Proton Exchange Membrane (PEM) fuel cell. Double layer capacitor (DLC) testing and modelling is also reviewed given the similarity between a PEM fuel cell and a DLC as outlined in Section 2.4. As steady state modelling of a PEM fuel cell was reviewed in Section 2.3.4, this chapter focuses on dynamic modelling of a fuel cell and a DLC. Throughout this review, the practical aspects of fuel cell and DLC testing techniques are also considered. The primary focus of this thesis is the development of an application based testing method. Therefore, the practical requirements of the testing method are an important consideration for the deployment of the test as part of a UPS monitoring system, described in Chapter 1.

Section 3.1 describes specific techniques commonly used for testing PEM fuel cells. A review of equivalent circuit models used for modelling the dynamic behaviour of a PEM fuel cell is provided in Section 3.2, focussing on the representation of physical aspects such as the double layer capacitor and the resistance. An overview of DLC testing is provided in Section 3.4, with Section 3.5 reviewing DLC equivalent circuit models. A summary is provided in Section 3.5.

3.1 EXISTING FUEL CELL TESTING TECHNIQUES

The testing of Proton Exchange Membrane (PEM) Fuel Cells is wide ranging in terms of measured properties and testing techniques. Testing objectives may include identifying specific properties, evaluating overall performance, or determining the state of a functioning fuel cell for control purposes.

In general, fuel cell testing methods have been derived from, or are the same as those used in other areas of electrochemistry. For example, cyclic voltammetry has been used in a number of cases, usually with the PEM fuel cell in a half-cell configuration [1]. Material properties, particularly the membrane ionic resistance, have been measured ex situ using a variety of electrochemistry methods, such as 4 point Kelvin [2], and other techniques [3], [4].

This type of testing is predominately used when fundamental insights into fuel cell processes or properties are required. In addition, these testing techniques often require the fuel cell to be in physical configuration that is different from a commercially constructed stack. The testing methods focused on in this thesis are ones that could be used in an application setting. Therefore, the test techniques reviewed in this section have been implemented on a fully assembled, functional fuel cell, one that has been manufactured for an application rather than for fundamental study.

The next three subsections review testing techniques for commercial-ready fuel cell stacks while in operation;

- VI curve evaluation
- Electrochemical Impedance Spectroscopy
- Current interrupt/pulse techniques

In addition to these standard tests, a subsequent subsection reviews a number of tests conducted while the fuel cell is not operating, as this is the type of test developed in this thesis.

3.1.1 VI CURVE EVALUATION

The most common method of testing and characterising a PEM fuel cell or stack is to obtain a steady state voltage versus current (VI) curve. The VI curve is obtained by holding the fuel cell operating conditions, such as the temperature, gas stoichiometry, humidity etc. constant, and measuring the steady state voltage at set current values. For example, Figure 3.1 shows VI curves for cells using different membranes, as obtained by Du *et al.* [5].

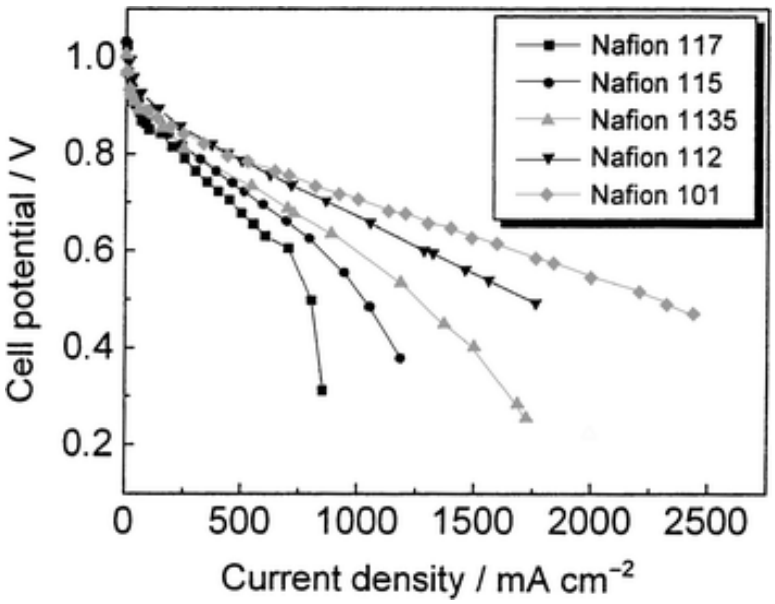

Figure 3.1 VI Curves of Cells Operating at 80^{o}C with Pure O_2 and H_2, Du *et al* [5]

As described in Section 2.3, the three main loss mechanisms dominate at different current ranges, thus the VI curve can be used to determine the magnitude of each loss mechanism. This can be done by either measuring specific aspects of the VI curve, or evaluating parameters of a model. For example, Forrai *et at.* [6] equated the slope of the linear region of the VI curve to the ohmic resistance, where as Kim *et al.* [7] found the ohmic resistance by fitting an empirical equation to the VI data. Using the VI curve to obtain loss values is not particularly accurate, as each loss mechanism affects the voltage at each current point. For example, the ohmic resistance value will depend on exactly which part of the VI curve was used, and Kim *et al.* found the ohmic resistance value to change substantially when a mass transport loss term is added into an empirical equation [7]. In general, the VI curve provides the net performance of an active stack under a certain set of operating conditions.

To assess the impact of operating conditions, or certain physical attributes of the fuel cell, a family of VI curves is often obtained. For example, the effect membrane thickness (see table 2.1) has on the voltage performance is clearly shown in Figure 3.1. With increasing membrane thickness, the ohmic resistance increases, as estimated by the slope in the linear region of the VI curve. The mass transport loss also increases with increasing membrane thickness, as the drop-off in potential is observed to occur at lower current densities with thicker membranes. This indicates that water back diffusion through the membrane is the specific mass transport loss mechanism in this case. The way operating conditions, such as humidity or pressure, effect the performance are also commonly examined using a set of VI curves. For example, Buchi and

Srinivasan [8] investigated the performance at different humidity levels, finding decreased ohmic and mass transport loss with increased humidity.

VI curve evaluation can be implemented on a single cell or a stack. If implemented on a stack, the VI curve of each cell is obtained by measuring the individual voltage of each cell. VI curves are obtained in a lab environment, where accurate control over testing conditions can be maintained.

3.1.2 ELECTROCHEMICAL IMPEDANCE SPECTROSCOPY (EIS)

Electrochemical Impedance Spectroscopy (EIS) or AC impedance testing is commonly cited in the scientific literature for determining fuel cell properties. The technique consists of applying a low amplitude sinusoidal voltage (or current) onto the fuel cell, and measuring the phase and amplitude of the current (or voltage), from which the impedance is calculated. A frequency sweep is used (typically 10mHz to 100kHz) in order to obtain a full AC impedance spectrum. Usually, a functioning fuel cell is tested, in which case the AC perturbation is superimposed onto a DC load. The DC load can be changed such that the AC response is obtained over the entire operating regime of the fuel cell.

The fuel cell impedance is displayed and analysed in one of two ways. A Bode plot is shown in Figure 3.2, where the absolute impedance and phase shift (not shown in this case) is plotted against the frequency. This bode plot by Andreas *et al.* [9] compares the impedance of three PEM cells, each having a membrane with a different EW. All cells were operated at 283 mA/cm^2, with the H_2 (humidified at 80^oC) and O_2 (dry) flowing at stoichiometric values of 2, and a cell temperature of 75^oC.

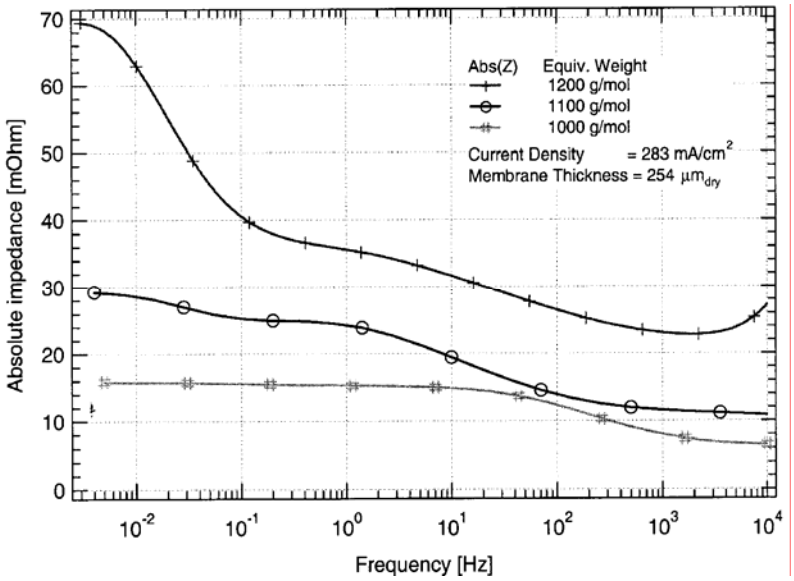

Figure 3.2 A Bode Plot of the AC Impedance Response of PEM cells Employing Membranes of Different Equivalent Weights, produced by Andreaus *et al.* [9]

The impedance spectrum can also be displayed as a Nyquist Plot, where the imaginary impedance is plotted against the real impedance. A typical Nyquist plot is shown in Figure 3.3, also obtained by Audreaus *et al.* [9], with the PEM fuel cell operated at 500 mA/cm^2, with the rest of the operating conditions the same as previously described.

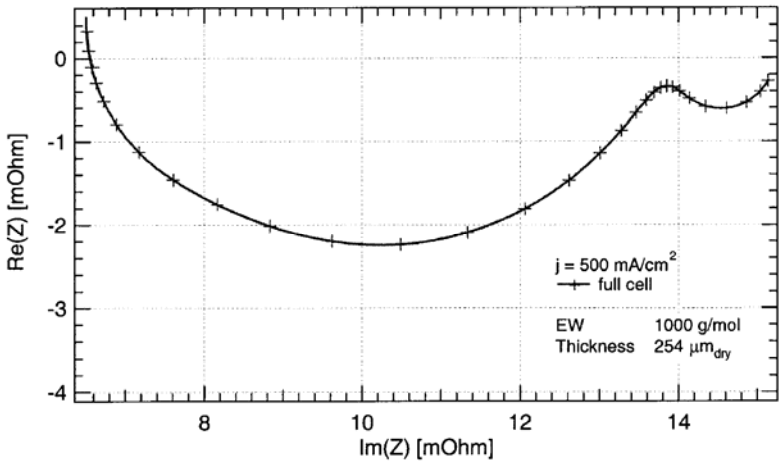

Figure 3.3 A Nyquist Plot of AC Impedance Response for a PEM Fuel Cell at 500mA/cm^2, produced by Andreaus *et al.* [9]

EIS is accepted to be superior over steady state VI curve evaluation for separating out and identifying the different loss mechanisms of a fuel cell, due to the association of certain loss mechanisms with particular frequency ranges [10]. For instance, at very high frequencies, the

impedance is only due to ohmic losses, predominantly the membrane ionic resistance. At intermediate frequencies, charge transfer resistance, coupled with the double layer capacitance, adds to impedance. Finally, at low frequencies, diffusion/mass-transport losses also contribute to the measured fuel cell impedance [9], [11].

Different loss mechanisms contribute to the impedance at different frequency limits. However, it is not always clear what specific features of the impedance spectrum relate to which processes and material properties of the fuel cell. In order to relate test results to cell conditions, multiple tests are conducted with the fuel cell held at different operating conditions for each test. For example, Andreaus *et al.* [12] obtained a number of impedance spectra, with the fuel cell operating at different hydrogen humidity levels for each spectra. With higher humidity, the impendence at low frequencies was found to decrease significantly. It was concluded that the low frequency impedance is attributed to low water content on the anode side on the membrane, thus the primary mass transport loss mechanism is water back diffusion through the membrane. This is further confirmed by the fact that cathode hydration has little effect on the impedance spectra.

EIS can only be implemented on a single cell, and requires substantial electronic equipment to generate the required signal and measure the corresponding response. The testing process itself can be difficult, particularly at the frequency extremes. At very low frequencies, the time for a single cycle will be long, in which time the physical state of the fuel cell may change. At high frequencies, stray inductance from the testing leads can be problematic. Thus, 50kHz is generally accepted as the upper limit with the impedance at higher frequencies having to be extrapolated [13]. With these practical considerations, most would agree that EIS is limited to laboratory testing only. However, some have considered how this technique could be used in an application as explained below.

A patent by Freeman *et al.* [14], describes a portable, self-contained testing system. The system consists of a CPU, AC signal generator and measurement/analysis components, which allows the fuel cell impedance to be measured at discrete frequencies. The ultimate intention of the test system is for active control of the fuel cell in automotive and stationery applications. The authors did not state how individual cells could be measured, therefore, it is assumed only bulk stack properties are obtained. The importance of individual cell measurements was treated in the patent of Kelly *et al.* [15]. To obtain individual cell properties, additional electrodes were integrated on to each cell and used for testing and monitoring. The electrodes are subject to

either AC or DC, enabling cell properties to be acquired. In general, the testing methods proposed in both patents are complex, requiring either a complex test signal and measurement, or individual test elements to be built onto each cell. Therefore, the test methods are not particularly suited for an application such as UPS, which requires the test method to be integrated into a fuel cell system.

3.1.3 CURRENT INTERRUPT/PULSE TESTING

Current interrupt methods have been proposed as a simpler technique than EIS for obtaining fuel cell properties, and are commonly used [6], [16]-[24]. The method involves subjecting a functioning fuel cell to a step change in current, with the voltage transient measured.

Forrai *et al.* [6] conducted a current interrupt on a small fuel cell, which has a nominal operating point of 0.2A and 0.7V. The imposed current interrupt was from approximately 0.4A to open circuit; the resulting voltage transient is shown in Figure 3.4.

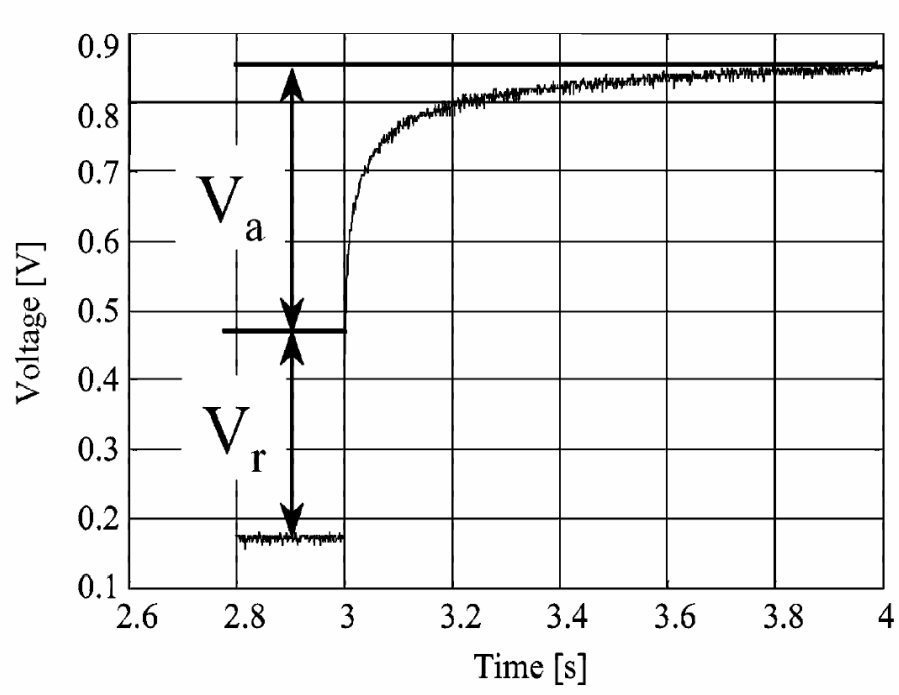

Figure 3.4 Voltage Transient Resulting in the Fuel Cell Current Being Instantly Reduced to Zero, reproduced from Forrai *et al.* [6]

The sudden change in voltage, V_r, is attributed to the ohmic loss in the fuel cell, with the exponential rise in voltage due to the capacitance and activation loss [16], [23]. These fuel cell properties are explicitly calculated in Section 3.2.2, with reference given to an equivalent circuit

model. Longer voltage transients have been attributed to diffusion losses when, for example, a molten carbonate fuel cell was subjected to a current interrupt test [18].

A variation of the current interrupt method involves subjecting a functioning fuel cell to a short duration current pulse. For, example Andreaus *et al.* [12] imposed a current pulse of 1A for 0.9ms on a cell with an active area of $28cm^2$ operating at $500mA/cm^2$. The ohmic loss, attributed primarily to the membrane ionic resistance, was calculated from the step change in voltage.

Current interrupt, as with EIS, is used for finding the properties of a single cell. An entire stack can be subject to a current interrupt test, but only net stack properties are obtained. For example, Kong *et al.* [17] showed through basic circuit analysis that multiple cells connected in series, act in the same manner as one cell. Thus, the ohmic resistance of the stack was measured from a stack current interrupt test, as was a combined activation and capacitance value.

Although the test process is simple, high quality data (high measurement rate) is required to clearly distinguish the different voltage quantities. In addition, subjecting a large (in terms of surface area) cell to a sudden change in current can be problematic, due to the large currents involved i.e. large switches would be required to obtain a clean current break, and arcing may be an issue.

The current interrupt method has been suggested for use in an application. For example, in the patent by Bai *et al.* [25], a functioning fuel cell had the ohmic resistance measured by current interruption. As with EIS, only net stack properties were obtained when current interrupt testing is implemented on a stack.

3.1.4 NON-ACTIVE FUEL CELL TESTING

Most reported fuel cell testing has been conducted while the fuel cell is in an active state, i.e. hydrogen and air are present at the anode and cathode respectively, with current flowing through an external circuit. Quantifying the individual loss mechanisms has been a primary objective. However, this can be challenging, particularly when separate activation losses at the anode and cathode are required. For other electrochemical devices, such as batteries, a reference electrode can be inserted in the electrolyte to isolate the losses occurring at each electrode. However, this is impractical for a PEM fuel cell. A few experiments reported in the literature, test the fuel cell

in a non-active state, the objective being the measurement of individual losses, particularly the anode and cathode activation.

A loss present at the cathode and not at the anode was demonstrated using a planar fuel cell, where the cells are formed on a common membrane [26]. When the cells are externally connected in series, internal currents flow due to lateral ionic conduction of hydrogen ions from the anode to the cathode of an adjacent cell. A voltage drop is observed on each cell at open circuit, except for the cell at the positive terminal of the stack, as no O_2 is being reduced. In this test, oxygen and hydrogen are present at the anode and cathode, thus the fuel is in an operating state. However, the fuel cell was not required to function for the test.

Wagner *et al.* [27] [28], conducted two AC impedance tests with the fuel cell at open circuit using a symmetrical gas arrangement. For one test, hydrogen was at the anode and cathode ($H_2|H_2$), for the other test, oxygen was at the anode and cathode ($O_2|O_2$). The objective of their testing was to measure the charge transfer resistance (or impedance) of the hydrogen half cell reaction (using the $H_2|H_2$ test) and the oxygen half cell reaction (using the $O_2|O_2$ test). In both tests, electrochemical reactions were occurring, due to the charge transfer between the electrode and electrolyte, (the objective of the test measurement). The impedance of the $O_2|O_2$ test was found to be much higher than the $H_2|H_2$ test, indicating a significant impedance at the cathode compared to the anode, as expected.

Andreas *at al*. [12] [9] also conducted AC impedance with a symmetrical gas arrangement; however, instead of imposing the AC signal with the fuel cell at open circuit, a DC current was forced through the cell at a current density of $500mA/cm^2$. Effectively, the cell was operated as a hydrogen pump, where the electrochemical reactions, $H_2 \rightarrow 2H^+$ and $2H^+ \rightarrow H_2$, occurred at the electrodes. Again, the objective was to isolate the activation loss associated with one electrode, (just the anode in this case).

Tsampas *et al.* [24] also conducted AC impedance using a symmetrical gas arrangement with the fuel cell at open circuit. These authors did not discuss or try to measure the charge transfer resistance, not because charge transfer was not occurring, but because a large amount of catalyst was used thus reducing the resistance of the change transfer process. Measuring the ionic resistance of the membrane was the objective of the test in this case.

All non-active operation test reported in the literature involve electrochemical reactions occurring, as determining the activation loss is the primary objective of the testing. H_2 is required to be in the cell for most of these tests. A compete summary of fuel cell testing is provided at the end of this chapter, together with conclusions drawn from the modelling and DLC testing reviewed below.

3.2 FUEL CELL EQUIVALENT CIRCUIT MODELLING

The steady state characteristics of a fuel cell are either modelled by mechanistic or empirical equations. As described in Section 2.3.4, the resulting models are very good at representing the steady state behaviour of the fuel cell, but do not include the dynamic behaviour. The most common method used for modelling the dynamic behaviour of the fuel cell, is to use an equivalent circuit model (ECM).

Many ECM's have been proposed, and they range widely in terms of complexity and form. The purpose of certain models has simply been to replicate a particular terminal behaviour of the fuel cell. For example, Figure 3.5a shows an ECM proposed by Yu and Yuvarajan [29], [30] that reproduces VI curve and voltage transient behaviour induced by load changes. A circuit that simulates the effects of inverter ripple current on a fuel cell was proposed by Choi *et al* [31], and is shown in Figure 3.5b.

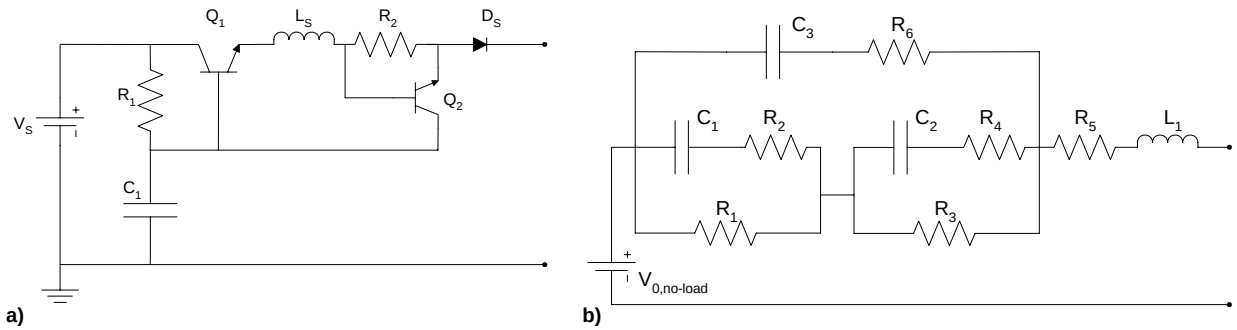

Figure 3.5 Behaviour Derived Equivalent Circuit Models Proposed by Yu and Yuvarajan (a) [29] and Choi *et al.* (b) [31]

Generally, these models are empirical or phenomenological in nature. Therefore, the structure and component values of the ECM do not relate directly to physical characteristics. Existing fuel cell (and related electrochemical) ECMs that have been derived by considering the physical

nature of the fuel cell are reviewed in Section 3.2.1. The techniques used for acquiring the circuit parameter values are reviewed in Section 3.2.2. During this research, a novel ECM was derived in which physical meaning was placed on the structure and components of the model. The novel structurally derived ECM is fully explained in Chapter 4.

3.2.1 PHYSICALLY BASED EQUIVALENT CIRCUIT MODELS

A number of physically based fuel cell ECMs have been put forward in the literature. Figure 3.6 shows how these models are related to one another, and how they are related to the physical structure of a PEM fuel cell.

A basic PEM fuel cell schematic is shown in Figure 3.6a, with the ECM most commonly used to model a fuel cell, (and other electrochemical cells) shown in Figure 3.6b [13]. R_{ionic}, represents the ionic resistance of the membrane, $R_{CT,A}$ and $R_{CT,C}$ represent the charge transfer loss/resistance across the electrolyte/electrode boundaries at the anode and cathode respectively. The capacitors $C_{DL,A}$ and $C_{DL,C}$ represent the double layer capacitance present at the anode and cathode electrolyte-electrode boundaries.

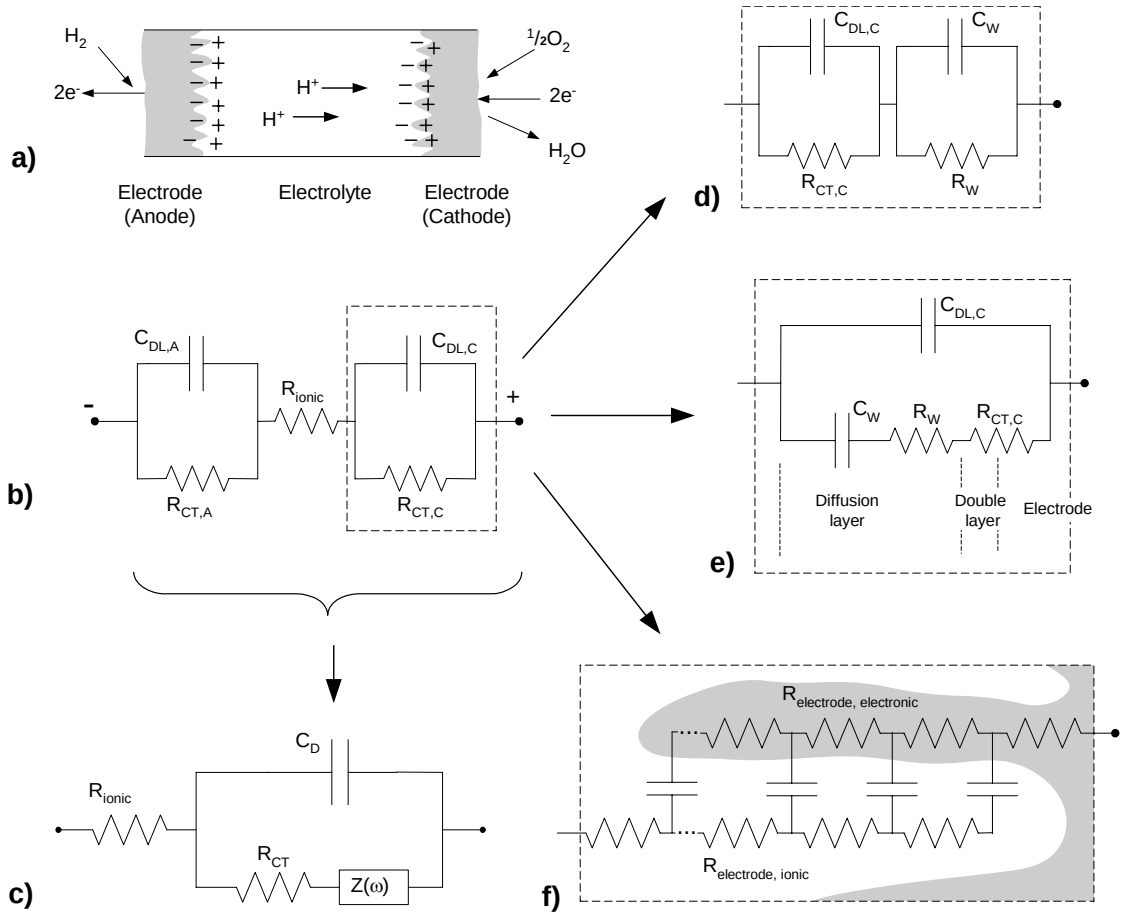

Figure 3.6 Operational Schematic of a PEM Fuel cell a), shown with a common ECM (b) [13]. Modifications on the Cathode side to take into account fuel cell diffusion (d) [27] and a general electrochemical cell (e) [13]. The classic transmission line model of porous electrode is shown in (f) [11]. A simplified fuel cell ECM often used (c) [32]

Identification of individual electrode activation and capacitance properties is not often carried out as it requires non-standard testing techniques as described in Section 3.1.4. Therefore, a simplified model shown in Figure 3.6c is often used (as in [32] [33]), and is commonly referred to as the Randle's equivalent circuit. In this circuit, the double charge layers and the activation resistances have been combined into a single resistor and capacitor respectively. Occasionally, a complex, frequency dependent component is added to account for diffusion losses (as explained below). This circuit has been used for interpreting the results of current interrupt and EIS test methods, as in [12]. Section 3.2.2 describes how the circuit model, basic circuit theory and test results are used for acquiring specific loss terms.

The mass transport or diffusion loss, commonly referred to as the Warburg impedance, has been modelled using an additional resistor R_W and capacitor C_W, and have been incorporated into a fuel cell ECM in a number of ways. For example, Wagner *et al.* [27] models the Warburg impedance as an additional parallel branch as shown in Figure 3.6d. An equivalent circuit model of a general electrochemical cell is shown in Figure 3.6d [13], where R_W and C_W have been added in series with the activation loss at the cathode. The mass transport loss, or diffusion impedance, is commonly attributed to oxygen diffusion [27]. Therefore, the Warburg impedance is incorporated on the oxygen side (cathode) of the ECM. It is commonly accepted that the diffusion impedance possesses a long time constant, with slow voltage transients induced by load changes are attributed primarily to diffusion effects [18].

The classic transmission line model of a porous electrode, shown in Figure 3.7 has been used when specific properties of the catalytic layer were investigated [11], [34]. The model consists of an electronic resistor rail connected to an ionic resistor rail through capacitors, such that ionic and electronic charges must move through a range of resistance paths to charge the double layer completely. Clearly, the model does not take into account charge transfer losses or any other active processes. Instead, the model represents the physical nature of the electrolyte/electrode interface, or catalytic layer.

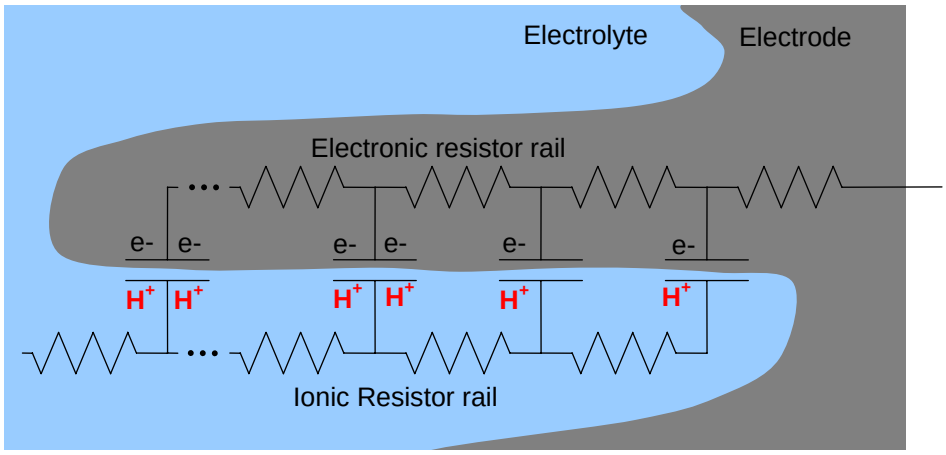

Figure 3.7 Transmission Line Model of a Porous Electrode-Electrolyte Interface

The proposed models shown in Figure 3.6 are simple representations of a fuel cell, thus they are somewhat limited in their behaviour prediction. For example, the activation loss magnitude is logarithmically dependent on fuel cell operating current. However, as a simple resistor is used to model the activation loss, the voltage drop increases linearly with current. In order to capture fuel cell characteristics more accurately, the functional nature of certain circuit components has

been modified. For example, as the Warburg impedance is theoretically phase independent at high frequencies, Boillot *et al.* [23] used a constant phase element in place of a capacitor. O'Hayre *et al.* [26] used a voltage dependant current term instead of a resistor for modelling the activation loss, thus encompassing the logarithmic nature of this mechanism.

None of the equivalent circuit models shown in Figure 3.6 show a source term, which represents the potential generated by the cell. In many cases, a model representing an active fuel cell may not require a source term, as the ECM aims to model the loss and dynamic characteristics related to testing procedures, particularly in the case of EIS and current interrupt/pulse testing. When the full performance of the cell is required, a source term can be added in a number of ways, as shown in Figure 3.8.

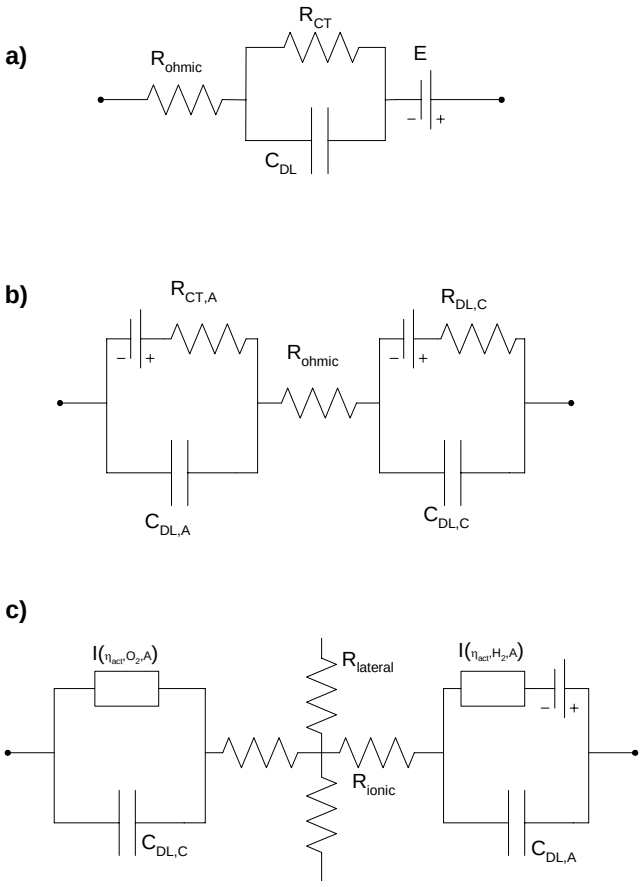

Figure 3.8 Fuel Cell ECMs Including Potential Terms with Randle's Circuit Model (a), Source Term in Attributed to Each Half Cell Reaction (b) [26] and a Source Term in the Anode Only [16] (c)

A simple Randle circuit has the potential term placed in series as shown in Figure 3.8a, and is the most commonly used circuit. Alternatively, a source term has been placed in series with one or both of the activation loss terms as shown in Figure 3.8b [26] and 3.8c [16].

3.2.2 CIRCUIT PARAMETER IDENTIFICATION

The circuit models reviewed thus far are physically based. Therefore, identifying the values of the circuit components provides information on the physical state of the fuel cell such as the magnitude of different loss mechanisms or the capacitance of the fuel cell.

The circuit parameter values of an ECM are determined in a number ways, depending on how the fuel cell is tested. Using a VI curve, the values of R_{ionic} and R_{CT} can be found, as discussed in Section 3.1.1. However, as a VI curve only reveals the steady state performance of the cell, the capacitance values must be found by alternative transient testing techniques.

An EIS impedance spectrum is used to find the circuit parameters of an ECM in one of two ways. In both cases, the impedance as a function of frequency, $Z(\omega)$, is determined for the circuit model in terms of the circuit parameters. In the first method, the circuit parameters are found by fitting $Z(\omega)$ to the experimental impedance spectrum. This method can be used for finding the circuit parameters of a single cell, irrespective of circuit model complexity. However, a good fit to a complex model, does not necessarily mean a unique or physically meaningful circuit model and parameter values. Instead of fitting to the impedance spectrum, the circuit parameter values can be estimated from particular regions of the spectrum. For instance, at very high frequencies, the circuit model impedance tends to R_{ohmic} as the capacitors act as short circuits.

Voltage transients produced by current pulse/interrupt testing, together with simple circuit theory can also be used to calculate circuit parameters. For example, Figure 3.9 shows the voltage response of a fuel cell, when current is instantaneously reduced to zero. A fuel cell equivalent circuit model is also shown in Figure 3.9. The parameter values of the circuit models are obtained as follows.

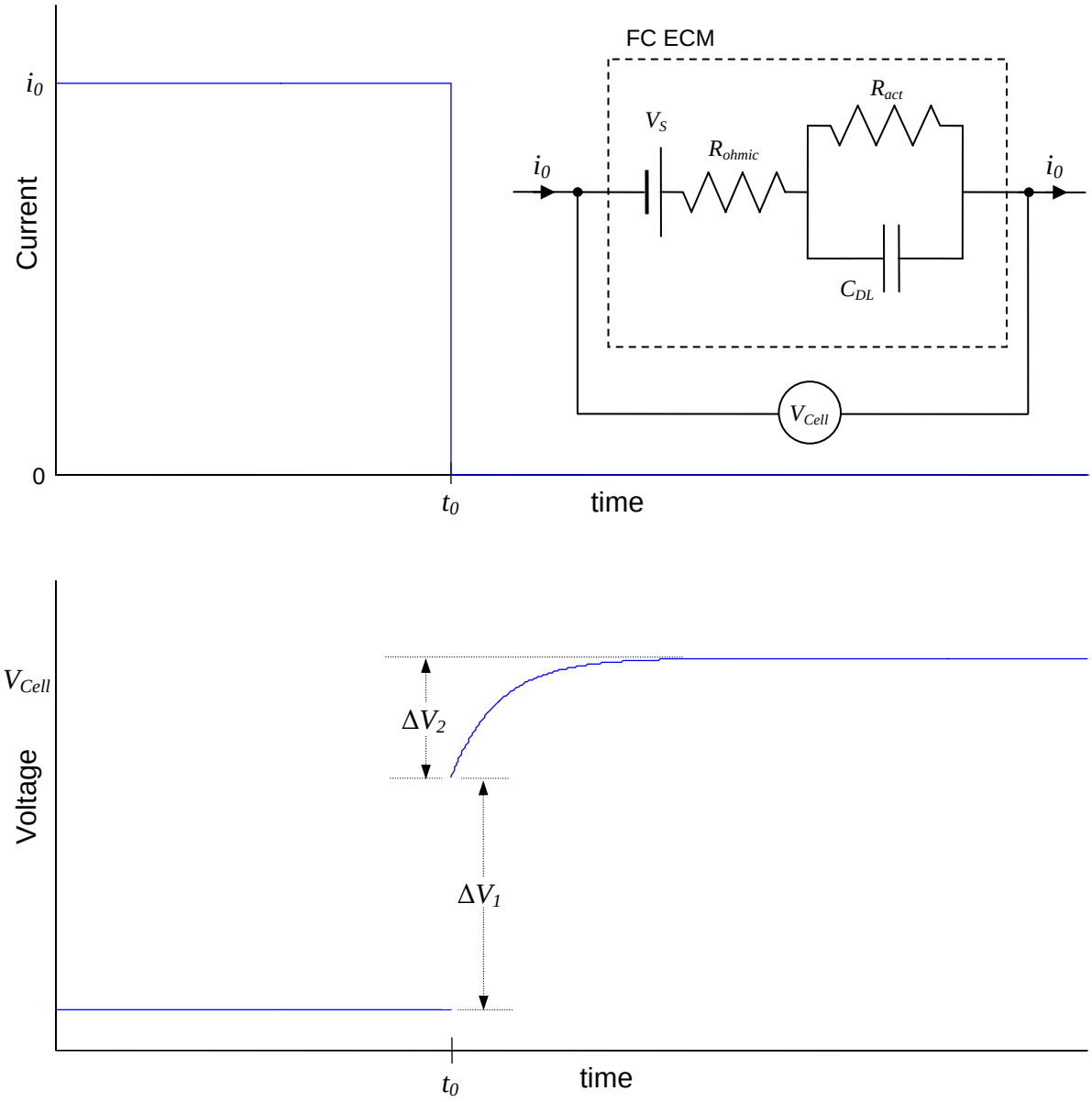

Figure 3.9 A Current Interrupt Test, Shown with the Common Fuel Cell ECM

Initially, at constant current i_0, the measured voltage across the cell, V_{Cell}, is the sum of the voltage source, V_S and the voltage drop across the model resistors i.e.

$$V_{Cell}\big|_{t<t_0} = V_S - i_0 R_{ohmic} - i_0 R_{act} \qquad 3.1$$

Given Kirchoff's law, the voltage across C_{DL} will be $-i_0 R_{act}$, with respect to V_S. Immediately after the current is reduced to 0, $t = t_0$, the potential drop across R_{ohmic} also reduces to 0. However, the potential drop across R_{act} remains $i_0 R_{act}$ due to the voltage across C_{DL}. Therefore, the measured voltage across the cell at t_0 is thus

$$V_{Cell}\big|_{t=t_0} = V_S - i_0 R_{act} \qquad 3.2$$

The instantaneous change in voltage at t_0 is

$$\begin{aligned}\Delta V_1 &= V_{Cell}\big|_{t=t_0} - V_{Cell}\big|_{t<t_0} \\ &= \left(V_S - i_0 R_{act}\right) - \left(V_S - i_0 R_{act} - i_0 R_{ohmic}\right) \\ &= i_0 R_{ohmic}\end{aligned} \qquad 3.3$$

Thus, the ohmic resistance is calculated using

$$R_{ohmic} = \frac{\Delta V_1}{i_0} \qquad 3.4$$

The cell voltage will eventually reach V_S, as the capacitor will discharge through R_{CT}. Therefore the change in voltage of the cell from just after t_0 is given by

$$\begin{aligned}\Delta V_2 &= V_{Cell}\big|_{t\to\infty} - V_{Cell}\big|_{t=t_0} = V_S - \left[V_S - i_0 R_{act}\right] = i_0 R_{act} \\ &= V_S - \left(V_S - i_0 R_{act}\right) \\ &= i_0 R_{act}\end{aligned} \qquad 3.5$$

Therefore, the activation resistance is calculated using

$$R_{act} = \frac{\Delta V_2}{i_0} \qquad 3.6$$

As the charge on C_{DL} is dissipated through R_{CT}, the voltage across C_{DL} reduces according to

$$V_{C_{DL}}(t) = -i_0 R_{act} \exp\left(\frac{-t}{R_{act} C_{DL}}\right) \qquad 3.7$$

Thus, the transient voltage across the cell after t_0 is given by

$$V_{Cell}(t) = V_S - i_0 R_{act} \exp\left(\frac{-t}{R_{act} C_{DL}}\right) \qquad 3.8$$

As R_{act} is calculated, C_{DL} can be found by evaluating the voltage at a certain time, or fitting equation 3.8 to experimental data. Although this method appears straight forward, measuring ΔV_1 and ΔV_2 is difficult, as high quality data (high scan rate), is required for an accurate evaluation.

Current interrupt testing can be implemented on a stack to evaluate net stack properties. Kong *et al.* [17] showed how the circuit model of a stack is the same as a single cell, and calculated the circuit values by subjecting the stack to a current interrupt test.

Current interrupt has been used to find the parameters of circuit models with greater complexity than that shown in Figure 3.6. Larmine [15] evaluated the circuit parameters of a model consisting of an R_{act} and C_{DL} for each electrode (shown in Figure 3.8b). However, as alluded to earlier, additional half cell experiments are required to distinguish specific anode and cathode properties. Therefore, only the circuit parameters of a simple ECM shown in Figure 3.9 are found with current interruption.

3.3 DOUBLE LAYER CAPACITOR (DLC) CHARACTERISTICS AND TESTING TECHNIQUES

The behaviour of a DLC differs significantly from an ideal capacitor because of the charge storage mechanism. Charge is stored by the formation of the double charge layer at the electrode-electrolyte interfaces. The following subsections describe the two main test techniques used for characterising a DLC; charge/discharge methods, and electrochemical Impedance spectroscopy. The behaviour and properties of a DLC is described, and compared to ideal capacitor.

3.3.1 CHARGE/DISCHARGE TESTING

Tests involving a simple DC charge and/or discharge are frequently used to characterise a DLC [35]-[41]. This method involves subjecting a single DLC to a controlled, constant-current charge and/or discharge, with the voltage response measured. A typical voltage transient produced by Zubieta and Bonert [37] is shown in Figure 3.10, and is the result of a 470F DLC being subjected to a 30A charge, followed by an open circuit period and then being discharge at 30A.

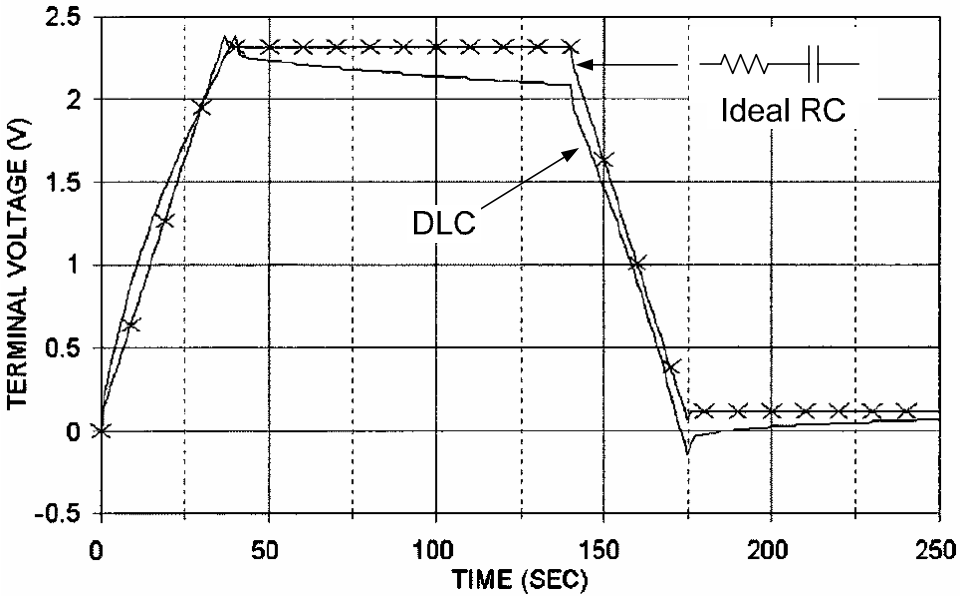

Figure 3.10 Constant Charge, Open Circuit, then Discharge of a DLC (——) and a ideal capacitor (–|(–), Zubieta and Bonert [37]

Figure 3.10 also plots an ideal capacitor of the same value, modelled with a series resistance. Clearly, there is a significant difference between an ideal capacitor and a DLC. The remainder of this section details specific DLC properties that cause it to deviate from ideal behaviour.

Unlike an ideal capacitor, the capacitance of a DLC is linearly dependent on the terminal voltage [37], [39], [42]. For example, a DLC rated at 470F had a measured capacitance of 375F at 0.5V, and 750F at 2.5 V [39]. Therefore, during a constant current charge, the voltage rate of change is observed to decrease as the voltage across the DLC increases. For an ideal capacitor charged at a constant current, a constant increase in the voltage would be expected as shown in Figure 3.10.

After the charge process ends and the DLC is held at open circuit, Figure 3.10 shows the voltage decaying. Part of this voltage decay is due to leakage current. For example, a DLC sold commercially by Maxwell™ Technologies, loses up to 1.5% of the stored energy per day through leakage current. In addition, the variation in leakage current between many series connected cells requires voltage balancing to be employed [43], [44]. Although leakage current has been documented numerous times, the exact mechanism has not been explicitly described in the literature. Electron flow directly across the DLC is assumed here.

Leakage current is not the only phenomena responsible for the observed voltage decay. After charging, the potential decays rapidly to a new open circuit voltage value, then continues to decay at a slow rate. Clearly, the initial fast decay in voltage is not due to leakage current, if this

were the case, the voltage would continue to decrease rapidly at a rate proportional to the cell voltage. Instead, the continuing ion movement, primarily at the porous electrode-electrolyte interface is responsible for the initial decay. This is most often referred to as charge redistribution, and can be understood by considering the transmission line model of the porous electrode-electrolyte interface as shown in Figure 3.7. Assuming the electronic resistance rail has negligible resistance compared to the electrolyte, the model capacitor nearest the electrolyte will contain more charge during the charging process. After the charge step has ceased, ions will continue to penetrate further into the porous electrode, thus distributing the charge across all of the capacitors in the model and reducing the potential across the cell.

The distributed capacitance is also believed to be responsible for a non-zero OCV, or rest potential. Effectively, a DLC will retain a small OCV after being short-circuited, as some of the R C values (considering the transmission line model, Figure 3.7) will possess very long time constants. For example, Zubieta and Bonert [36] found that a 450F with an initial voltage of 1.82V, recovered to a voltage of 0.39V after being short-circuited for 48 hours.

In summary, DC charge/discharge testing is relatively straight forward, requiring a constant current source and measurement of the transient voltage response. Only single cells are tested and analysed using this method. How a voltage transient of a DC test can be used for acquiring the values of an ECM will be shown in Section 3.4.

3.3.2 DLC ELECTROCHEMICAL IMPEDANCE SPECTROSCOPY

Electrochemical Impedance Spectroscopy (EIS) has been widely used to test DLCs [45]-[48]. The testing process is similar to that described for a fuel cell. However, the AC signal is imposed around a constant voltage, thus a set state of charge, as opposed to a constant operating current in the case of a fuel cell. As with fuel cell EIS, the results are displayed and analysed using either a Bode plot or a Nyquist Plot. For example, Figure 3.11 shows a Bode plot obtained by Lufrano *et al.* [49] where the EIS of DLCs employing different electrolytes were examined. The N115 data refers to Nafion 115, a membrane commonly used in a PEM fuel cell. The other two electrolytes used, FVH_2SO_4 and NRG50, are a porous glass fibre matrix impregnated with 1 M H_2SO_4, and a recast Nafion prepared with 5% Nafion 1100 solution.

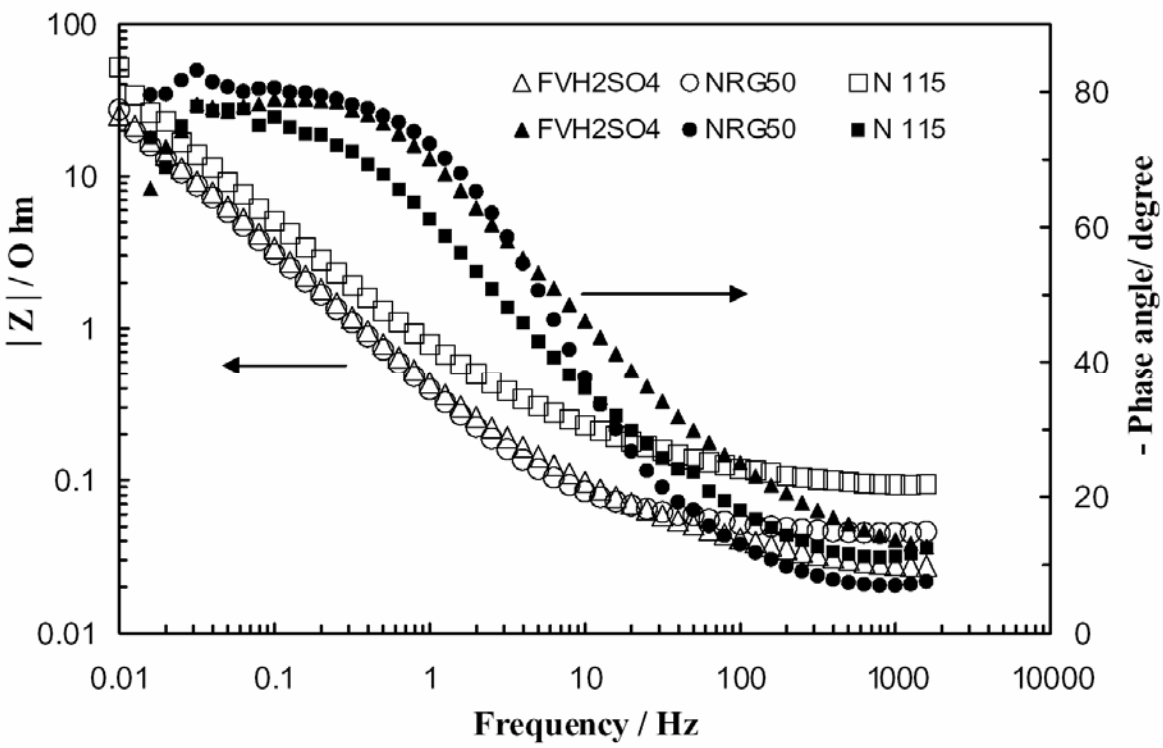

Figure 3.11 Bode Plot of Three DLCs Employing Different Electrolytes, Lufrano *et al* [49]

A schematic Nyquist plot drawn by Kötz and Carlen [50] is shown in Figure 3.12, and again shows the difference between an ideal capacitor and a DLC.

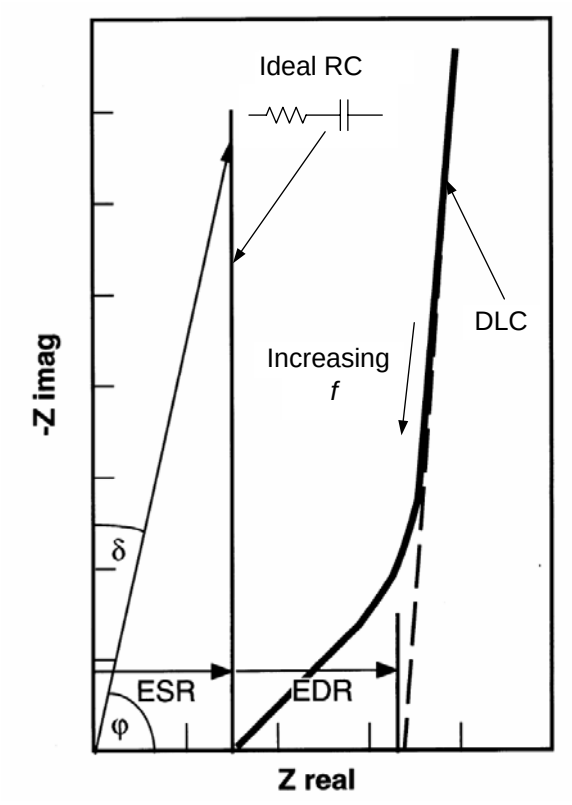

Figure 3.12 Schematic Nyquist Plot of an Ideal Capacitor and a DLC, Kötz and Carlen [50]

The impedance of a capacitor is defined by equation 3.9

$$Z(\omega) = \frac{1}{j\omega C} \qquad 3.9$$

where ω is the angular frequency.

The capacitance of any device can be calculated given the absolute impedance, $|Z(f)|$, at a particular frequency, f , and the phase angle ϕ,

$$C_{cell} = \frac{1}{2\pi f\left(-|Z(f)|\sin(\phi)\right)} \qquad 3.10$$

The capacitance and equivalent series resistance (ESR) value of an ideal capacitor, as measured by EIS, are independent of frequency. Thus, a straight line is obtained on the Nyquist plot, as shown in Figure 3.12.

The capacitance and resistance of a DLC to decrease with increasing frequency. Thus, a distorted (from vertical) line results in a Nyquist Plot, as shown in Figure 3.12. The frequency dependent capacitance of a DLC is attributed to the to the porous electrode-electrolyte interface. At high frequencies, the ions to not have time to fully penetrate deep into the porous structure of the electrode, thus the capacitance value of the device is reduced. A number of authors have investigated capacitance as a function of frequency, each finding frequency dependent capacitance characteristic [46], [49]-[51].

3.4 Equivalent Circuit Modelling (ECM) of Double Layer Capacitors (DLC)

A standard electrostatic capacitor is simply modelled as an ideal capacitor with an equivalent series resistance. As shown by Sections 3.3.1 and 3.3.2, a simple R-C model is inadequate to fully for represent the behaviour of a DLC due to properties such as leakage current, distributed capacitance, and voltage dependent capacitance. Figure 3.13a shows a DLC schematic, together with an ECM occasionally used, as by Belhachemi *et al.* [41] and Spyker and Nelms [42], to discuss the properties exhibited by a DLC.

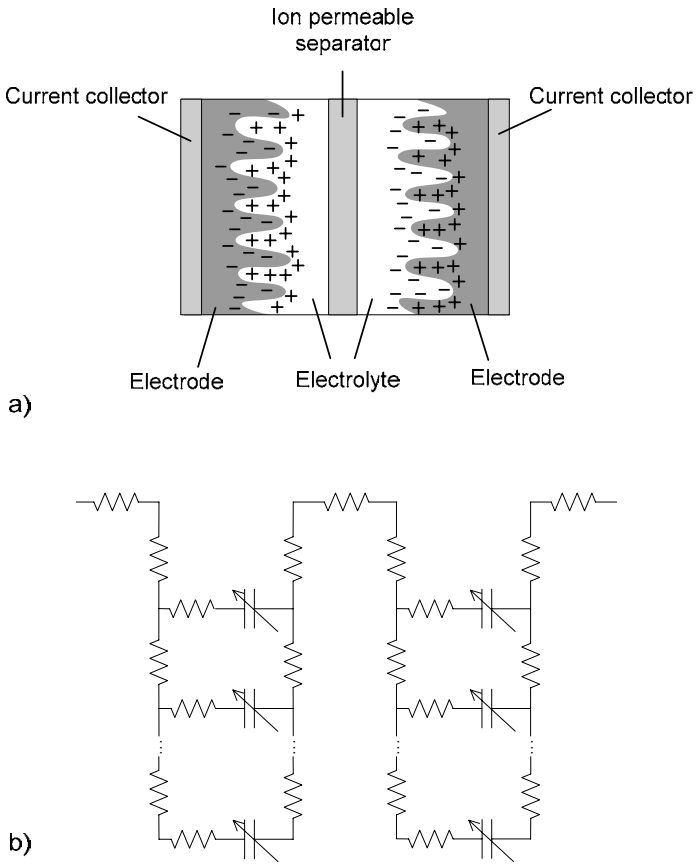

Figure 3.13 A DLC Shown in a) with a ECM based the Electrode-Electrolyte Transmission Line Model, Belhachem *et al* [41]

The ECM is based on the transmission line model of a porous electrode-electrolyte interface, two of which are connected in series representing the cell. The model is complex, consisting of many elements, and has little practical use, i.e. it is not used to simulate or predict the terminal behaviour of a DLC. Instead, numerous, simpler ECMs have been proposed and are reviewed in the following section.

3.4.1 COMMON ECM OF DLC

The most common ECMs used to simulate the terminal behaviour of a DLC are shown in Figure 3.14.

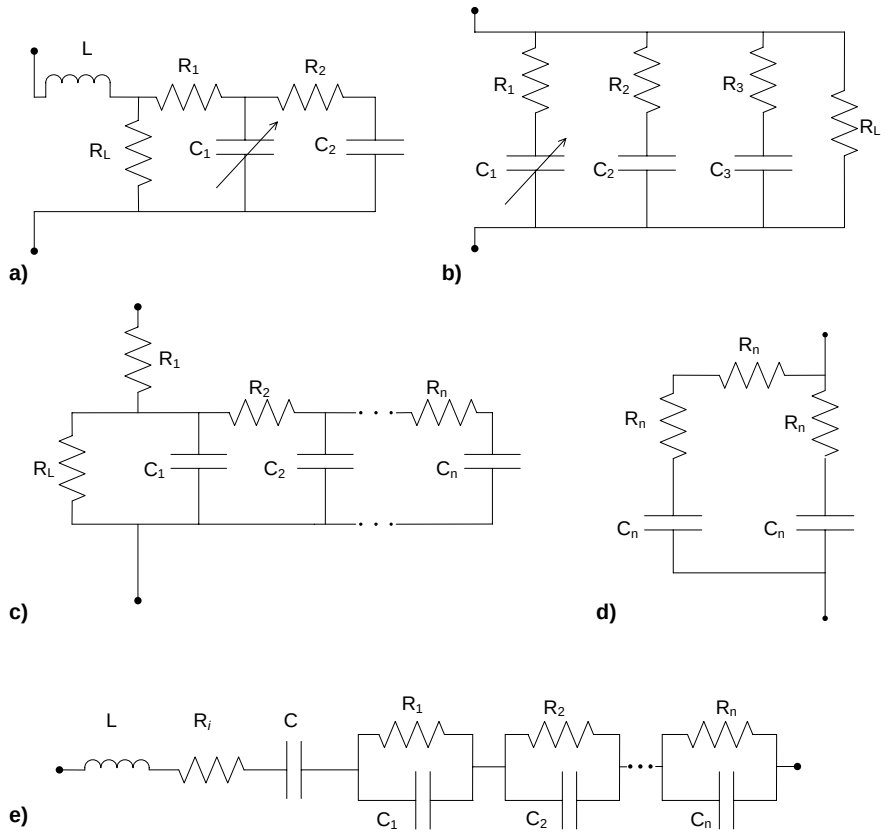

Figure 3.14 ECM of DLC as used by Gualous *et al.* (a) [40], Bonert & Zubieta (b) [36], Dougal *et al.* (c) [47], Larmaine (d) [16] and Buller *et al.* (e) [45].

The most dominant feature of the ECM presented in Figure 3.14, is the use of multiple R–C branches. A model using two R–C branches, Figure 3.14d, is used by Larmaine [16]. Figure 3.14a shows a slightly different two branch model as used by Gualous et al [40]. Bonert and Zubieta [36]-[39] used a three branch R–C as shown in Figure 3.14b. The model parameters of a 5 branch ECM were obtained by Dougal *et al.* [47] and Nelms *et al*. [48]. Figure 3.14e shows a circuit used by Buller *et al.* [45] where 10 R–C circuits were used. However, each R_i and C_i (i = 1–10) were derived from only 2 independent parameters. In general, increasing the number of R–C branches increases the accuracy of the model, which is particularly important when long time scales are being simulated.

The capacitance of a DLC is dependent on the terminal voltage. Thus, a voltage dependent capacitor is used in some models, as shown in Figure 3.14a and b. A linear function is used, as shown by equation 3.11 where a and b are empirical constants, determined by charging a DLC to various voltage levels.

$$C(V) = a + bV \qquad 3.11$$

An inductor element is sometimes included, as show in Figure 3.14a and 3.14e when high frequencies are being modelled. However, the inductance value is often ignored as it tends to be very small, in the order of nH.

Most proposed ECMs of DLCs include a resistance that models leakage current, R_L. If highly dynamic regimes are being modelled, the leakage current would not have a significant effect and can be ignored as in the case of Buller *et al.* [45]. With the exception of $R_{L,}$ which corresponds directly to the leakage current, the other components of the model have no direct physical interpretation. All models reviewed are empirical, and aim to reproduce the terminal behaviour of the DLC.

3.4.2 DETERMINING ECM PARAMETERS OF A DLC

The technique used to determine circuit parameter values clearly depends on the test method used, i.e EIS, or DC charge/discharge techniques. For EIS, the ECM parameters are obtained by fitting the impedance expression (as a function of frequency) to the experimental data using a least squares fitting routine. This method can be applied irrespective of circuit model complexity. Fuel cell ECM values are also obtained in this way as discussed in Section 3.2.2.

Using charge/discharge voltage transients for calculating the circuit parameters requires a number of assumptions. The R–C branches are assumed to have distinctly different time constants. Therefore, the voltage transient at a particular time is primarily due to a single R–C branch. For example, the voltage transient immediately after a charge period, which is a rapid decline in voltage, is attributed just to the R–C branch with the smallest time constant. In addition, capacitors in the ECM are assumed to have an initial voltage of zero, thus, the DLC itself must have a near zero initial voltage. For this condition to be satisfied, Zebieta and Bonert [36] showed that a DLC must be short-circuited for a significant time. For example, a 470F capacitor regained 26.5% of its voltage after being shorted for 12hrs, and regained 17% after being shorted for 48hrs.

Whether EIS or DC charge/discharge testing is employed, the technique and corresponding analysis has only been reported in the literature for a single cell. As with fuel cell testing discussed in Section 3.1 and 3.2, the techniques and analysis methods used to test a DLC are implemented on a single cell only. The methods used for acquiring circuit parameters of a DLC are also only applicable for a single cell analysis.

3.5 SUMMARY OF TESTING TECHNIQUES AND MODELS FOR FUEL CELLS AND DLCS

The vast majority of fuel cell testing has been conducted while the fuel cell is in an active state, i.e. producing power by electrochemically reacting hydrogen and oxygen at the anode and cathode. A common testing objective is the identification of individual loss mechanisms, how these change with fuel cell operating conditions, and the impact different fuel cell materials have. Even tests where the fuel cell was not in an operational state, such as AC impedance with a symmetrical gas flow arrangement, the objective of the testing procedure was to measure electrochemical processes, such as anode and cathode charge transfer losses.

DLC testing was reviewed as the construction and materials of a DLC are similar to a PEM fuel cell. DLC's have been constructed using almost identical materials i.e. utilising Nafion as the electrolyte. Testing methods used to characterise a DLC included EIS and DC charge/discharge methods. A DLC was shown to behave differently than an ideal capacitor, specific properties including: voltage dependent capacitance, leakage current, and internal charge redistribution. Clearly, the properties associated with the ionic membrane and electrodes are exposed during this testing method even though no electrochemical reactions are occurring.

A common method of modelling the dynamic behaviour of a fuel cell and a DLC is to use and equivalent circuit model (ECM). Fuel cell and a DLC ECMs were reviewed. Although many such models can be connected in series, thus representing a fuel cell stack, techniques for acquiring ECM parameter values are only applicable for a single cell.

Throughout the testing review, the practical aspects of the fuel cell test methods were also considered, as the objective of this thesis is the development of a testing methodology that can be implemented into an application. Of the three test methods reviewed in Section 3.1, only a VI curve test can be used to evaluate each cell within a stack, provided the voltage of each cell is monitored. EIS and current interrupt/pulse can only be implemented on a single cell, and are rarely used for testing cells within a stack. As described in Section 2.2.4, one bad cell can dictate stack performance and can mean the end of a stack's useful life. Therefore, a commercial

testing methodology, one that is integrated into the system must be able to measure properties of each cell in a stack. In summary, existing fuel cell testing and analysis methods are not well suited for implementation into a backup power application.

3.6 REFERENCES

[1] Papageorgopoulos DC, Keijzer M, de Bruijn FA, "The inclusion of Mo, Nb and Ta in Pt and PtRu carbon supported 3electrocatalysts in the quest for improved CO tolerant PEMFC anodes"**,** Electrochimica Acta, Vol. 48, pp. 197-204, Nov. 2002

[2] Slade S, Campbell SA, Ralph TR, Walsh FC, "Ionic conductivity of an extruded Nafion 1100 EW series of membranes", Journal of the Electrochemical Society, Vol. 149, pp. A1556-A1564, Dec. 2002

[3] Verbrugge MW, Schneider EW, Conell RS, Hill RF**, "**The Effect of Temperature on the Equilibrium and Transport Properties of Saturated Poly(Perfluorosulfonic Acid) Membranes", Journal of the Electrochemical Society, Vol. 139, pp. 3421-3428, Dec. 1992

[4] Sumner JJ, Creager SE, Ma JJ, DesMarteau DD, "Proton conductivity in Nafion (R) 117 and in a novel bis[(perfluoroalkyl)sulfonyl]imide ionomer membrane"**,** Journal of the Electrochemical Society, Vol. 45, pp. 107-110, Jan. 1998

[5] Du XZ, Yu JR, Yi BL, Han M, Bi KW, "Performances of proton exchange membrane fuel cells with alternate membranes" Physical Chemistry Chemical Physics Vol. 3, pp. 3175-3179, 2001

[6] Forrai A, Funato H, Yanagita Y, Kato Y, "Fuel-Cell Parameter Estimation and Diagnostics", IEEE Transactions on Energy Conversion, Vol. 20, pp. 668-675, Sep. 2005

[7] Kim J, Lee S-M, Srinivasan S, "Modeling of Proton Exchange Exchange with an Empirical Equation", Journal of the Electrochemical Society, Vol. 142 pp. 2670-2674, Aug. 1995

[8] Buchi FN, Srinivasan S, "Operating proton exchange membrane fuel cells without external humidification of the reactant gases - Fundamental aspects", Journal of the Electrochemical Society, Vol. 144, pp. 2767-2772, Aug.1997

[9] Andreaus B, McEvoy AJ, Scherer GG, “Analysis of performance losses in polymer electrolyte fuel cells at high current densities by impedance spectroscopy”, Electrochimica Acta, Vol. 47, pp.2223-2229, May 2002

[10] Springer TE, Zawodzinski TA, Wilson MS, Gottesfeld S, “Characterization of polymer electrolyte fuel cells using AC impedance spectroscopy”, Journal of the Electrochemical Society, Vol. 143, pp. 587-599, Feb. 1996

[11] Li GC, Pickup PG, **“**Ionic conductivity of PEMFC electrodes - Effect of Nafion loading”, Journal of the Electrochemical Society, Vol. 150, pp. C745-C752, Nov. 2003

[12] Andreaus B, Scherer GG, “Proton-conducting polymer membranes in fuel cells - humidification aspects”, Solid State Ionics, Vol. 168, pp. 311-320, Mar. 2004

[13] Hamann CH, Hemnett A, Vielstich W, “Electrochemistry”, Wiley-VCH 1998 Verlag GmbH, Weinheim, Germany

[14] Yoon CO, Barsukov Y, Kim JH, “Method and apparatus for determining Characteristic parameters of a charge storage device”, United States Patent 6,160,382, Dec. 2000

[15] Kelley RJ, Mulligan RJ, Pratt, SD, Muthuswamy S, Landreth BD, Pennisi, RW, “Integral sensors for monitoring a fuel cell membrane and methods of monitoring” United States Patent, 6,214,487 B1, Apr. 2001

[16] Larminie JRJ, “Current interrupt techniques for circuit modelling” Electrochemical Measurement, IEE Colloquium on, pp. 12/1-12/6, 1994

[17] Kong X, Khambadkone AM, Soy Kee Thum, “A hybrid model with combined steady-state and dynamic characteristics of PEMFC fuel cell stack”, Industry Applications Conference, Fourtieth IAS Annual Meeting, Conference Record of the 2005, Vol. 3, pp. 1618-1625, Oct. 2005

[18] Lee CG, Nakano H, Nishina T, Uchida I, Kuroe S, “Characterization of a 100 cm(2) class molten carbonate fuel cell with current interruption” Journal of the Electrochemical Society, Vol. 145, pp. 2747-2751, Aug. 1998

[19] Correa J.M, Farret, F.A, Canha L.N, “An analysis of the dynamic performance of proton exchange membrane fuel cells using an electrochemical model” IECON '01, The 27th Annual Conference of the IEEE Industrial Electronics Society, Vol. 1, pp. 141–146, Dec. 2001.

[20] Buchi FN, Marek A, Scherer GG, “In-Situ Membrane Resistance Measurements in Polymer Electrolyte Fuel-Cells by Fast Auxiliary Current Pulses”, Journal of the Electrochemical Society, Vol. 142, pp. 1895-1901, Jun. 1995

[21] Maruyama J, Abe I, “Cathodic oxygen reduction at the catalyst layer formed from Pt/carbon with adsorbed water” Journal of Electroanalytical Chemistry, Vol. 545 pp. 109-115, Mar. 2003

[22] Ceraolo M, Miulli C, Pozio A “Modelling static and dynamic behaviour of proton exchange membrane fuel cells on the basis of electro-chemical description” Journal of Power Sources, Vol. 113, pp. 131-144, Jan. 2003

[23] Boillot M, Bonnet C, Jatroudakis N, Carre P, Didierjean S, Lapicque F, “Effect of gas dilution on PEM fuel cell performance and impedance response”, Fuel Cells, Vol. 6, pp. 31-37, Feb. 2006

[24] Tsampas M N, Pikos A, Brosda S, Katsaounis A, Vayenas C G, “The effect of membrane thickness on the conductivity of Nafion”, Electrochemica Acta, Vol. 51, pp. 2743-2755, Mar. 2006

[25] Bai L, Lott DR, Martin VL, “Method and apparatus for monitoring equivalent series resistance and for shunting a fuel cell” United States Patent 6,620,538, Sep. 2003

[26] O'Hayre R, Fabian T, Lee SJ, Prinz FB, “Lateral ionic conduction in planar array fuel cells”, Journal of the Electrochemical Society, Vol. 150, pp. A430-A438, Apr. 2003

[27] Wagner N, “Characterization of membrane electrode assemblies in polymer electrolyte fuel cells using a.c. impedance spectroscopy”, Journal of Applied Electrochemistry, Vol. 32, pp. 859-863, Aug. 2002

[28] Wagner N, Schnurnberger W, Muller B, Lang M, “Electrochemical impedance spectra of solid-oxide fuel cells and polymer membrane fuel cells” Electrochimica Acta, Vol. 43, pp. 3785-3793, Aug. 1998

[29] Yuvarajan S, Dachuan Yu, “Characteristics and modeling of PEM fuel cells” ISCAS '04, Proceedings of the 2004 International Symposium on Circuits and Systems, Vol. 5, pp. V880-V883, May 2004

[30] Yu D, Yuvarajan S, “A novel circuit model for PEM fuel cells” APEC '04, Nineteenth Annual IEEE Applied Power Electronics Conference and Exposition, Vol. 1, pp. 362–366, 2004

[31] Choi W, Enjeti PN, Howze JW, “Development of an equivalent circuit model of a fuel cell to evaluate the effects of inverter ripple current” APEC '04. Nineteenth Annual IEEE Applied Power Electronics Conference and Exposition, Vol. 1, pp. 355-361, 2004

[32] Bard AJ, Faulkner LR, “Electrochemical Methods: Fundamentals and Applications” second edition, New York: John Wiley, c2001

[33] Larminie J, Dicks A, “Fuel cell systems explained, 2nd Edition, West Sussex, J. Wiley, 2003

[34] Jia NY, Martin RB, Oi ZG, Lefebyre MC, Pickup PG, “Modification of carbon supported catalysts to improve performance in gas diffusion electrodes”, Electrochimica Acta, Vol. 46, pp. 2863–2869, May 2001

[35] Staiti P, Minutoli M, Lufrano F, “All solid electric double layer capacitors based on Nafion ionomer”, Electrochimica Acta Vol. 47, pp. 2671-2870, Jul. 2002

[36] Bonert R, Zubieta L, “Measurement techniques for the evaluation of double-layer power capacitors” IAS '97, IEEE Industry Applications Conference, Thirty-Second IAS Annual Meeting, Vol. 2, pp. 1097-1100, Oct. 1997

[37] Zubieta L, Bonert R, “Characterization of double-layer capacitors for power electronics applications”, IEEE Transactions on Industry Applications, Vol. 36, pp. 199-205, Jan. 2000

[38] Zubieta L, Bonert R, “Experimental 400 kW sec double-layer capacitor energy storage system”, IEEE Industry Applications Conference, Thirty-Fourth IAS Annual Meeting, Vol. 4, pp. 2448-2453, Oct. 1999

[39] Zubieta L, Bonert R, “Characterization of double-layer capacitors (DLCs) for power electronics applications”, IEEE Industry Applications Conference, Thirty-Third IAS Annual Meeting, Vol. 2, pp. 1149-1154, Oct. 1998

[40] Gualous H, Bouquain D, Berthon A, Kauffmann JM, “Experimental study of supercapacitor serial resistance and capacitance variations with temperature” Journal of Power Sources, Vol. 123, pp. 86-93, Sep. 2003

[41] Belhachemi F, Rael S, Davat B, “A physical based model of power electric double-layer supercapacitors”, IEEE Industry Applications Conference, Thirty-Fifth IAS Annual Meeting, Vol. 5, pp. 3069-3076, Oct. 2000

[42] Spyker RL, Nelms RM, “Classical equivalent circuit parameters for a double-layer capacitor” IEEE Transactions on Aerospace and Electronic Systems, Vol. 36, pp. 829 – 836, Jul. 2000

[43] Maxwell Technologies “Cell Balancing in Low Duty Cycle Applications” Application Note, Available at: http://www.maxwell.com/pdf/uc/app_notes/AN-002_Cell_Balancing.pdf

[44] Linzen D, Buller S, Karden E, De Doncker RW, “Analysis and evaluation of charge-balancing circuits on performance, reliability, and lifetime of supercapacitor systems”, IEEE Transactions on Industry Applications, Vol. 41, pp. 1135-1141, Sep. 2005

[45] Buller S, Karden E, Kok D, De Doncker RW, “Modeling the dynamic behavior of supercapacitors using impedance spectroscopy”, IEEE Transactions on Industry Applications, Vol.38, pp. 1622–1626, Nov. 2002

[46] Emmenegger C, Mauron P, Sudan P, Wenger P, Hermann V, Gallay R, Zuttel A, “Investigation of electrochemical double-layer (ECDL) capacitors electrodes based on carbon nanotubes and activated carbon materials”, Journal of Power Sources, Vol. 124, pp. 321-329, Oct. 2003

[47] Dougal RA, Gao L, Liu S, “Ultracapacitor model with automatic order selection and capacity scaling for dynamic system simulation” Journal of Power Sources, Vol. 126, pp. 250-257, Feb. 2004

[48] Nelms RM, Cahela DR, Tatarchuk BJ, “Modeling double-layer capacitor behavior using ladder circuits”, IEEE Transactions on Aerospace and Electronic Systems, Vol. 39, pp. 430 – 438, Apr. 2003

[49] Lufrano F, Staiti P, Minutoli M, “Evaluation of nafion based double layer capacitors by electrochemical impedance spectroscopy” Journal of Power Sources, Vol. 124 pp. 314-320, Oct. 2003

[50] Kotz R, Carlen M, “Principles and applications of electrochemical capacitors”, Electrochimica Acta, Vol. 45, pp. 2483 – 2498, May 2000

[51] Lufrano F, Staiti P, Minutoli M, “Influence of Nafion content in electrodes on performance of carbon supercapacitors”, Journal of the Electrochemical Society, Vol. 151, pp. A64-A68, Jan. 2004

4 PASSIVE STATE DYNAMIC BEHAVIOUR (PSDB) TEST METHOD: PROTOCOL DESCRIPTION AND MODELLING

Existing fuel cell testing and analyses methods are not designed for testing in an application setting such as telecommunications back-up power. The requirements for such a test method include simplicity, and the ability for each cell to be analysed without compromising run time or inducing stress in the fuel cell. Of the testing methods reviewed in Section 3.1, the only possibility to test a stack in an application setting is to start the fuel cell system, and examine the voltage performance of each cell. However, for back-up power applications there are some drawbacks to this approach. Hydrogen fuel is consumed, thus, the run time of the system would be decreased after each test. Eventually, the system would require servicing for the hydrogen to be replenished. In Section 2.4, degradation of the fuel cell was exacerbated by thermal and hydration cycling caused by start-up and shut-down sequences. In summary, as existing test methods are not suited for telecommunications back-up power, a novel test procedure is developed, named the passive state dynamic behaviour (PSDB) test.

The PSDB is based on electronically probing the fuel cell while in a passive, non-functioning state. While in a passive state, the fuel cell is claimed to act as an RC circuit, and by obtaining the parameter values of an equivalent circuit model, information about the active performance of the cells can be determined.

The PSDB test is introduced in Section 4.1, with an in-depth description provided in Section 4.2. A new equivalent circuit model is derived in Section 4.3, with subsections discussing model uniqueness, and the voltage response of a fuel cell as determined from the model. Section 4.4 briefly discusses the limitations of the new test, with concluding remarks given in Section 4.5.

4.1 TEST METHOD INTRODUCTION

The PSDB test is implemented while the fuel cell is in a passive, non-functioning state. No hydrogen is present in the stack, with air at both the anode and cathode. Therefore, no electrochemical potential can form across any of the cells during the test. The fuel cell is tested electronically by imposing a sequence of DC electrical conditions, thereby charging and discharging the fuel cell in a capacitive sense. As no electrochemical reactions will occur during the test process, the fuel cell response is attributed to electrical properties, such as the double layer capacitance, and resistance of the fuel cell. It is hypothesized that the electrical characteristics of the cell, while in a passive state, will provide information on the physical properties and potential functionality of the fuel cell. For example, if the electrodes of a cell have a high surface area, indicating good functionality, a high capacitance value would be measured when tested in a passive state.

The results from the passive fuel cell test will be analysed primarily using an equivalent circuit model. As all existing ECMs represent an active fuel cell, a novel, passive fuel cell ECM is developed. A novel method for acquiring the circuit model parameters is described in Chapter 7. As each cell in the stack must be tested, the passive test method and equivalent circuit modelling must be applicable for multiple cell testing and analysis.

4.2 DESCRIPTION OF THE PSDB TEST

The fuel cell is electrically perturbed using a simple test circuit shown in Figure 4.1. The test circuit consists of a DC voltage source, V_{Charge}, two resistors, R_{Charge} and $R_{Discharge}$, and two switches, S_1 and S_2. The same test circuit is used for testing a single cell or a stack of cells. If a fuel cell stack is being tested, the test circuit is attached across the stack terminals and the voltage of each cell in the stack is monitored.

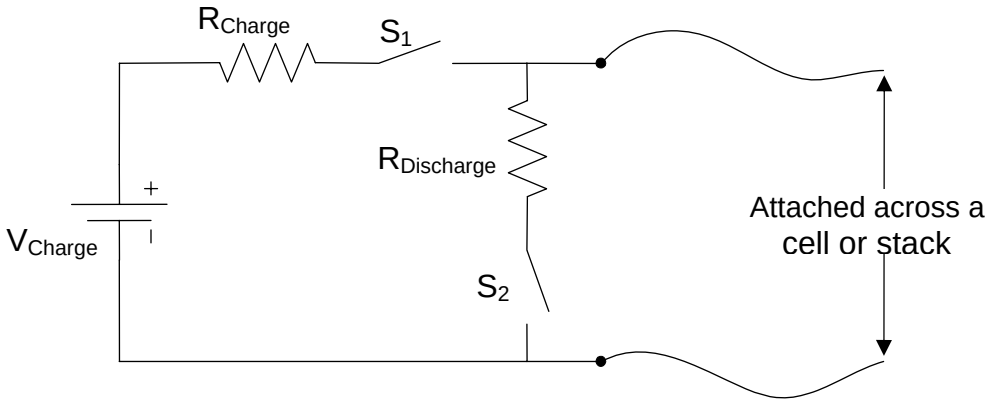

Figure 4.1 Test Circuit used for Implementing the Test Protocol

The test circuit imposes a series of DC electrical conditions onto a cell or stack by closing and opening switches S_1 and S_2. The following sequence is used;

1. **S_1, S_2 open:** The initial voltages of the cells and stack terminals are measured
2. **S_1 closed:** The fuel cell is charged using a constant voltage source, V_{Charge}, in series with the resistor R_{Charge}
3. **S_1 opened:** The voltage source is disconnected, thus placing the fuel cell in an open circuit condition
4. **S_2 closed:** Charge held by the fuel cell is dissipated through the resistor $R_{Dischage}$
5. **S_2 opened:** The stack remains at open circuit for the remainder of the test

An import aspect of the test is the value of the voltage applied across the stack. Only small voltages are used ensuring no electrochemical reactions can occur, i.e. significantly less than 1.2 V is across each cell at any point in the test. Thus, there is no charge transfer across the electrode-electrolyte boundary, with only non-Faradic reactions occurring. The test produces little stress on the PEM materials due to the low voltage used.

Clearly, the five-step protocol could be modified. For example, an additional charge or discharge sequence could be added to the test protocol. However, the test protocol as described is used throughout this thesis, as it adequately demonstrates the behaviour of a passive fuel cell.

The PSDB test process is simple, making it appropriate for an application setting. The test circuit itself is very basic, and could easily be incorporated into a system. The PSDB test requires the voltage on each cell to be monitored, which is a feature already built into most fuel cell the systems. For example, the Avista SR-12, Plug Power Gen–Sys, and Plug Power Gen-Core, constantly measure the voltage on each cell during operation for monitoring and control

purposes. However, the voltage measurement accuracy would need to be improved, as at present, the Plug Power provides a 2 decimal place value, with a measurement rate of 1s, and the Avista SR-12 provides a 3 decimal place voltage value, but only updates cell voltages every 40 seconds. In general, the passive test method could be integrated into an application with minimal cost and design modification.

4.3 Novel ECM for a Fuel Cell in a Passive State

This section details the novel passive fuel cell ECM developed in this research. A physically based ECM is desired, such that the circuit parameter values when found from a PSDB test can be related to the physical aspects of the fuel cell, and in turn the functionality of the active fuel cell. The ECM is derived by considering the basic physical structure of a fuel cell. Figure 4.2 shows a PEM fuel cell in two states, without, and with an applied potential.

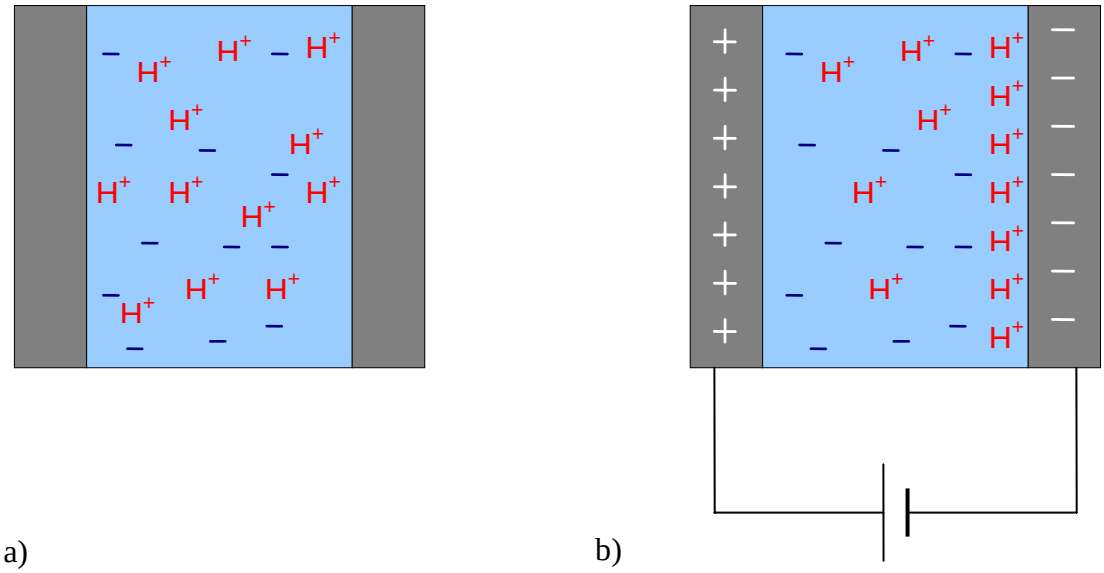

Figure 4.2 Fuel Cell in a Passive state shown without (a) and with (b) an Applied Potential

The electrodes are essentially two high surface-area conductors parallel to one another, thus a capacitor, C_a, is placed across the terminals of the circuit model as shown in Figure 4.3. For charge to be stored on the electrodes (on C_a), current must be able to pass through each electrode with a related contact resistance. Therefore resistor R_c is placed before capacitor C_a. The presence of the membrane has a number of effects, one of which is the presence of leakage

current. Hence, resistor R_a is placed across capacitor C_a. The main effect that the membrane has on the cell is to increase the capacitance value. Therefore, capacitor C_b is placed in parallel with C_a, with the addition of resistor R_b, which models the ionic resistance.

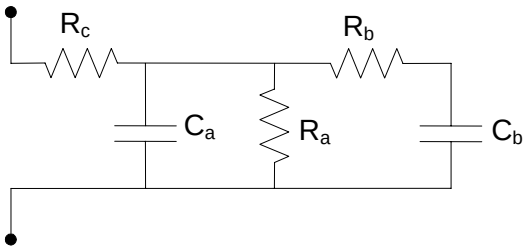

Figure 4.3 Equivalent Circuit Model (ECM) of a Passive Fuel Cell

The passive ECM model is significantly different from existing fuel cell ECMs, as a passive rather than active fuel cell is being modelled. The following four subsections discusses these differences in detail. Model uniqueness is discussed, and the behaviour of a cell and stack subjected to a passive fuel cell test is described.

4.3.1 COMPARISON TO EXISTING ECMS

A significant difference between the passive ECM and existing fuel cell ECMs, is the placement and physical interpretation of the two capacitors. In existing models, the capacitors represent the electronic-ionic charge accumulation of each electrode and are connected in series. In the passive ECM, one of the capacitors is due to the electronic charge on the electrodes, the other due to the charge distribution of the ions in the electrolyte.

The passive ECM was derived by considering the fuel cell in a passive state, with the resulting model being different to existing models, thus the resulting model is expected to be different. However, taking a standard ECM of a fuel cell and reducing to a passive state, still results in a different model as is shown in Figure 4.4.

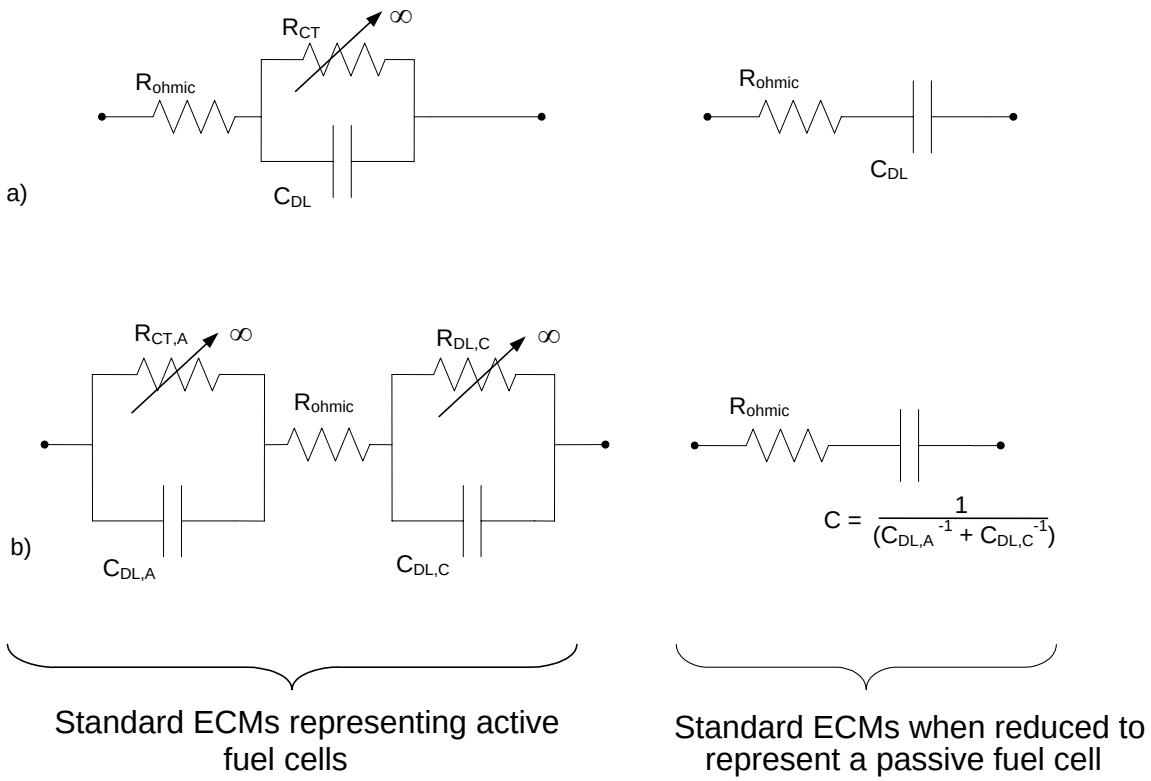

Figure 4.4 Reduction of Standard ECMs to Model a Passive Fuel Cell

No electrochemical reactions occur in a passive fuel cell. Therefore, no charge crosses the electrolyte-electrode boundary. As a result, the activation resistance, or charge transfer impedance, R_{CT}, will have an infinite resistance value (open circuit). When the charge transfer resistances are replaced with an open circuit (infinite resistance), the active fuel cell models reduce to simple R-C circuits. The same circuit derivation was achieved when considering a cell composed of an ideal reversible electrode and an ideal polarisable electrode, which by definition, means no charge can be transferred across the electrode electrolyte boundary [1].

Based on the similarity between a passive fuel cell and a DLC, a simple R-C model is predicted not to model the passive fuel cell adequately. As will be shown when the results are examined, a simple RC circuit cannot represent the electrical response of a passive fuel cell to the testing protocol.

The proposed model is very similar to DLC ECMs, and is the same as the 2-branch DLC model proposed by Nelms *et al.* [2]. However, physical meaning has been attributed to each component of the passive ECM.

4.3.2 MODEL UNIQUENESS

As a two terminal device, the fuel cell, is being modelled by a circuit containing 5 elements, the circuit form and thus circuit component values are not unique. Figure 4.5a shows the original passive ECM proposed (excluding the R_c value), together with 3 other circuits that are electrically identical at the circuit terminals.

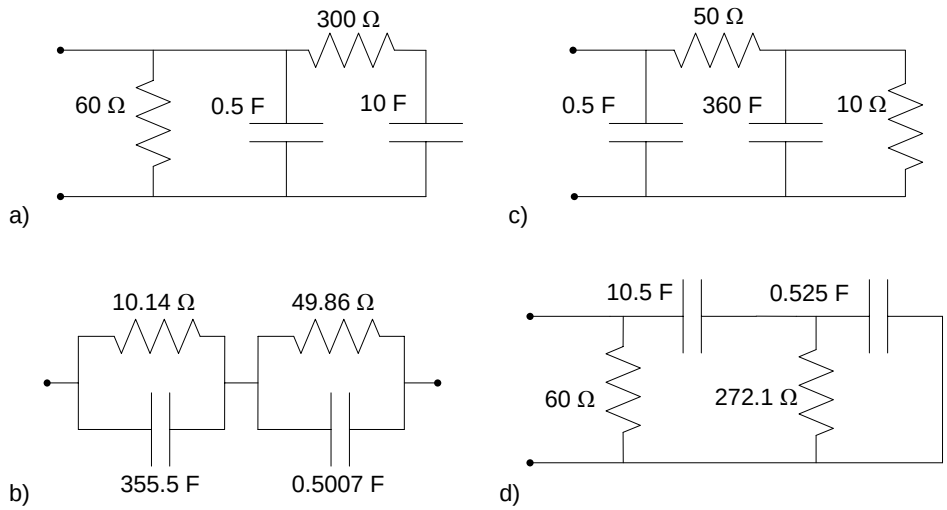

Figure 4.5 ECMs that are Electrcally Identical from the Circuit Termainls

The circuit values of the 3 alternative models, Figure 4.5b, c, and d, were obtained by observing that the series resistance must be the same for each circuit, and equating the impedance spectrum to that of the proposed circuit, Figure 4.5a. As more than one model could replicate the electrical properties of the fuel cell, using a different model would change the physical interpretation of the results. For example, Figure 4.6 shows two models of a fuel cell, the proposed passive model and the standard model of an active fuel cell. Circuit values for both models can be chosen, such that they are electrically identical from the circuit terminals.

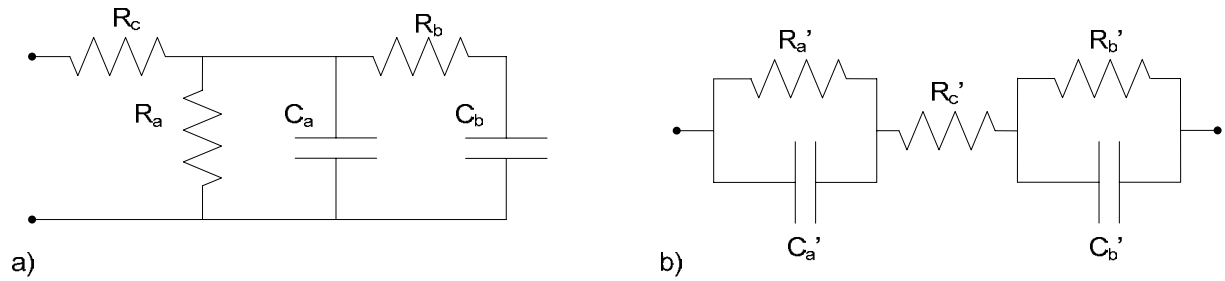

Figure 4.6 The Passive ECM a) and a Standard ECM of an Active Fuel Cell b)

In this case the value of R_c is the same as R_c'. However, the physical interpretation of these two values is different. The resistor R_c in Figure 4.6a represents the electrical resistance of the electrodes and contacts, whereas R_c' in Figure 4.6b represent the ionic resistance of the membrane.

A method to verify the circuit model, and physical attributes of the circuit components, is to change the physical state of the fuel cell, and measure the corresponding change the circuit parameter values. For example, if the hydration level of the fuel cell were to increase, an increase in the capacitance of the fuel cell would be expected, as well as a decrease in the resistance associated with the ionic resistance. This test, together with circuit model analysis is presented in Chapter 8.

4.3.3 Predicted Behaviour of a Passive Cell using the Novel ECM

The passive equivalent circuit model can be used for predicting the electrical response of a cell when subject to the testing technique. Figure 4.7 shows the test circuit applied to a fuel cell represented by the passive ECM.

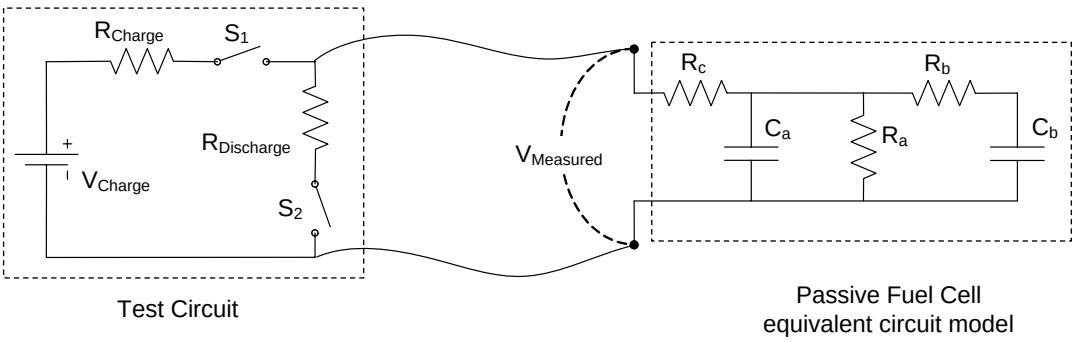

Figure 4.7 Test circuit and ECM of a Passive Fuel Cell

The test protocol consists of 5 steps as described in Section 4.2. At each step, the voltage behaviour across the circuit model, $V_{measured}$ is described. It should be noted that R_c, which represents series electrical resistance, is assumed to be small and is thus neglected in this discussion.

1. **S_1, S_2 open**; The initial charge on the capacitors is measured (if any).

2. **S_1 closed**; capacitor C_a is charged by V_{Charge} through resistor R_{Charge}. The voltage across C_a will therefore rise exponentially. The rise in voltage will not be a simple exponential, as some charge will flow through R_a, and C_b will also be charged through $R_{Charge} + R_b$.

3. **S_1 open**; The charge across C_a will dissipate through R_a, thus the voltage will decline exponentially. The decay will not follow a simple exponential decline, as charge on C_b will also decline though $R_b + R_a$ during this period.

4. **S_2 closed**; As $R_{Discharge}$ has a small resistive value, the charge held by C_a is rapidly dissipated. The charge on C_b will also decline but at a slower rate due to R_b. Thus, the fuel cell voltage declines rapidly when S_2 is closed.

5. **S_2 open**; At this point, the charge on C_a has all but gone, but C_b will have retained some charge due to the increased resistance of R_b. Therefore, charge will flow from C_b to C_a, thus increasing the voltage across the circuit terminals. As R_a continues to dissipate charge, the voltage across the fuel cell will eventually fall back down in this last period.

4.3.4 STACK BEHAVIOUR TO THE PSDB TEST

Given the voltage behaviour of the cell during a passive test as described above, the behaviour of the fuel cell stack terminals can also be described. Following the methodology by Kong *et al* [3], the behaviour of the stack can be predicted by examining the combined impedance of many cells. Based on the passive ECM shown Figure 4.3, the impedance of a single passive fuel cell is given by equation 4.1. Again, R_c has not been included.

$$Z(\omega) = \left[\frac{1}{R_a} + i\omega C_a + \left(R_b + \frac{1}{i\omega C_b} \right)^{-1} \right]^{-1} \qquad 4.1$$

Therefore, a stack of N identical cells, connected in series, has an impedance given by equation 4.2

$$N \cdot Z(\omega) = N \cdot \left[\frac{1}{R_a} + i\omega C_a + \left(R_b + \frac{1}{i\omega C_b} \right)^{-1} \right]^{-1}$$

$$= \left[\frac{1}{N \cdot R_a} + \frac{i\omega C_a}{N} + \frac{1}{N} \left(R_b + \frac{1}{i\omega C_b} \right)^{-1} \right]^{-1}$$

$$= \left[\frac{1}{N \cdot R_a} + \frac{i\omega C_a}{N} + \left(N \cdot R_b + \frac{N}{i\omega C_b} \right)^{-1} \right]^{-1}$$

$$= \left[\frac{1}{R_a'} + i\omega C_a' + \left(R_b' + \frac{1}{i\omega C_b'} \right)^{-1} \right]^{-1} \qquad 4.2$$

where $R_a' = NR_a$, $R_b' = NR_b$, $C_a' = \frac{1}{N} C_a$, $C_b' = \frac{1}{N} C_b$

As the impedance of the stack has the same form as the impedance of a single cell, the stack voltage behaviour will have the same form as a single cell.

4.4 Limits of the Passive Fuel Cell Test Method

The passive test method cannot measure all factors influencing fuel cell performance. For example, gas delivery to the anode and cathode as determined by the flow field plate and adjacent manifold, clearly influence performance when active. A good cell, in terms of the physical structure, may still perform poorly due to a defect in the bipolar plate. The operating conditions as determined by the balance of plant will also affect the performance. A malfunction (such as an air pump not working) will clearly cause cells to perform poorly. In essence, the PSDB test only assesses the cell, more specifically the MEA and inter-cell resistances. This is a very important part of a complete fuel cell system, as it is the cell, or MEA itself that is most likely to degrade over time and ultimately determine stack life. This is particularly true for a system designed for back-up power, where due to system simplicity, many other BOP components will not be present. Finally, the PSDB test is intended to add to existing management strategies (such as periodic start-up testing), rather than acting as a substitute.

4.5 SUMMARY

In this chapter, the passive state dynamic behaviour (PSDB) testing methodology has been presented. The method is simple, allowing all cells in a fuel cell stack to be tested, thus making it appropriate for back-up power applications testing. A novel equivalent circuit model of a passive fuel cell has also been proposed. The passive ECM is based on the physical structure of a passive fuel cell, thus, determination of the ECM parameter values can be related to the physical state of the fuel cell, thus indicating functionality.

4.6 REFERENCES

[1] Bard AJ, Faulkner LR, “Electrochemical Methods: Fundamentals and Applications” second edition, New York: John Wiley, c2001

[2] Nelms RM, Cahela DR, Tatarchuk BJ, “Modeling double-layer capacitor behavior using ladder circuits”, IEEE Transactions on Aerospace and Electronic Systems, Vol. 39, pp. 430 – 438, Apr. 2003

[3] Kong X, Khambadkone AM, Soy Kee Thum, “A hybrid model with combined steady-state and dynamic characteristics of PEMFC fuel cell stack”, Industry Applications Conference, Fourtieth IAS Annual Meeting, Conference Record of the 2005, Vol. 3, pp. 1618-1625, Oct. 2005

5 TEST EQUIPMENT AND ANALYSIS METHODS

This chapter describes the automated test system developed for implementing and analyzing the results of the passive state dynamic behaviour (PSDB) test. As the active performance of the PEM fuel cell stacks is also evaluated, this chapter details the active test systems and lists the specifications of each stack tested.

Section 5.1 details the passive test system, with subsections describing the data acquisition equipment, test circuit and software. Section 5.2 describes the three fuel cell stacks tested, along with the test systems used for evaluating their active performance. Section 5.3 provides an example data set, and verifies the measured voltage response is purely due to the electrically properties of the fuel cell under test.

5.1 PASSIVE TEST SYSTEM

Figure 5.1 shows a schematic diagram of the experimental setup used for conducting the PSDB test.

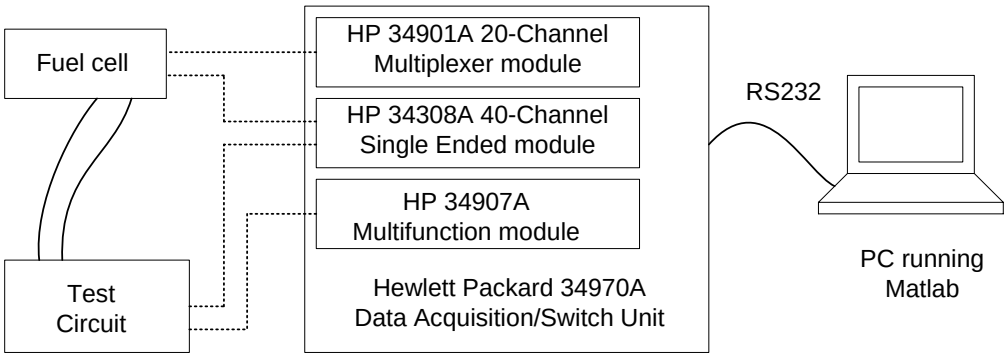

Figure 5.1 Test System Overview

A Hewlett & Packard 34970A data acquisition/switch unit is the primary component for test implementation. It controls the test circuit, hence the test process, and measures the fuel cell

response. The HP meter is programmed through a PC, which also reads and stores the data from the meter. The subsequent subsections describe HP unit, test circuit and PC software.

5.1.1 DATA ACQUISITION EQUIPMENT

The Hewlett Packard HP34970A data acquisition/switch unit is shown in Figure 5.2.

Figure 5.2 The HP 34970A Data Acquistion/Switch Unit

This multipurpose meter is used for measuring multiple voltages, with digital and analogue output used to control the test circuit. The unit possesses an internal digital multimeter, (DMM), real time clock, data interfaces, and a front panel user interface and display. The HP unit can accommodate up to three removable modules that slot into the back of the HP unit. Figure 5.3 shows one of the modules, the HP34901A 20-Channel Multiplexer.

Figure 5.3 Removable Module – the HP 34901A 20-Channel Multiplexer

This module contains multiple relays, each of which connects to the internal DMM allowing isolated measurements to be made. Each channel can be configured to measure DC/AC voltage, frequency, temperature or resistance. Table 5.1 lists all of the removable modules used for this research, together with an overview of their capabilities and uses.

Table 5.1 HP Modules Used for Testing

Module type	Description	Use
HP34901A 20-Channel Multiplexer	Contains 20 isolated channels that connect to the DMM. Also, 2 channels for direct current measurement up to 1A	Voltage sensing of the cells, stack, applied test circuit voltage, current shunt, and resistance measurements
HP 39407A 40-Channel Multiplexer	Contains 40 single ended channels (common ground) that connect to the DMM	Used when more than 20 voltage measurements were required
HP 34907A Multifunction module	Contains two analogue voltage outputs (+12 to –12, 8-bit resolution) and two 8-bit digital IO.	Used for test circuit control; digital output used for switch control, and voltage output used as test circuit source

Voltage readings were set at 5 ½ digits, i.e. if the voltage range is set to 100mV, the first digit is either 1 or 0 (the ½ digit) with five digits following, for example, 126.274mV or 053.674mV. The integration time for each measurement is 1PLC (power line cycle). The impedance of the meter is 10MΩ, with some experiments repeated with the impedance set to >10GΩ, verifying the meter did not affect test results in any way. The maximum scan rate of the meter is 19 channels a second. Although the meter can be programmed using the front panel, it was controlled using a PC communicating via an RS232, which is further described in Section 5.1.3.

5.1.2 TEST CIRCUIT

Figure 5.4 shows a schematic of the test circuit used for implementing the passive test protocol.

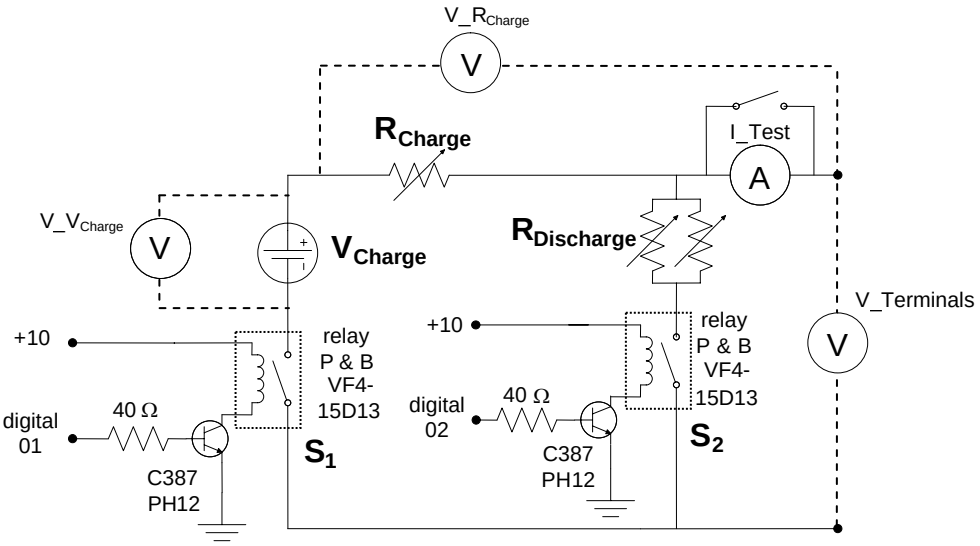

Figure 5.4 Test Circuit Detail

The relays, controlled with the HP 34907A multifunction module (digital 01, digital 02), allowed the testing process to be automated. A Reid Controls Power Supply, (0-15V and 1.5A) provided a 8V source for energizing the relays. The HP34907A multifunction module also supplied the voltage source (V_{Charge}) for some passive testing, otherwise, a Solstat Regulated DC Supply Model 3S2PB was used.

Variable resistors were used for R_{Charge} and $R_{Discharge}$, allowing the desired resistance values to be set for a particular passive test. Once set, the resistance values were measured at the test circuit terminals using the 4-wire method (separate source and sense). By closing just S_2, $R_{Discharge}$ was measured, and by closing S_1 with V_{Charge} shorted, R_{Charge} was measured. This ensured any resistance from the relays, wires and connections was included in the $R_{Discharge}$ and R_{Charge} values.

A number of voltage measurements, along with a current measurement is also shown in Figure 5.4. During a passive test, only V_V_{Charge} and V_Terminals are recorded, which measure the test circuit voltage source (V_{Charge}) and the voltage across the cell/stack. V_R_{Charge} and I_Test are redundant measurements, in that their values can be derived from the other values measured. However, V_R_{Charge} and I_Test provided a useful check in the construction of the test circuit and preliminary passive testing conducted. The two voltages, V_V_{Charge} and V_Terminals are

measured directly using the HP34901A 20-Channel Multiplexer module. If only one cell is tested, the scan list will only consist of these two voltage measurements. For stack testing, each cell, as well as the stack terminals (V_Terminals) and the voltage source (V_V_{Charge}) are measured.

For each test, the HP meter must be programmed. This includes the configuration of each channel i.e. for voltage, temperature etc. The number of measurements (scans) and the time between each scan must also be defined. Although this can be achieved using the front interface panel of the meter, a PC was used, and is described in detail below.

5.1.3 SOFTWARE USED

MATLAB version 6.5 (and above) has the ability to directly communicate with external devices using the Standard Commands for Programmable Instruments (SCPI) language. Commands are sent to the HP meter as text strings, and data is read from the meter as text strings. An overview of the program is shown in Figure 5.5. A complete listing of the code is given in Appendix II. Two smaller programs are also listed in Appendix II; one is used for creating the HP meter as a Matlab object and for setting the communication parameters (such as baud rate, and COMM port). The other small program is used for closing and clearing the device from the Matlab workspace.

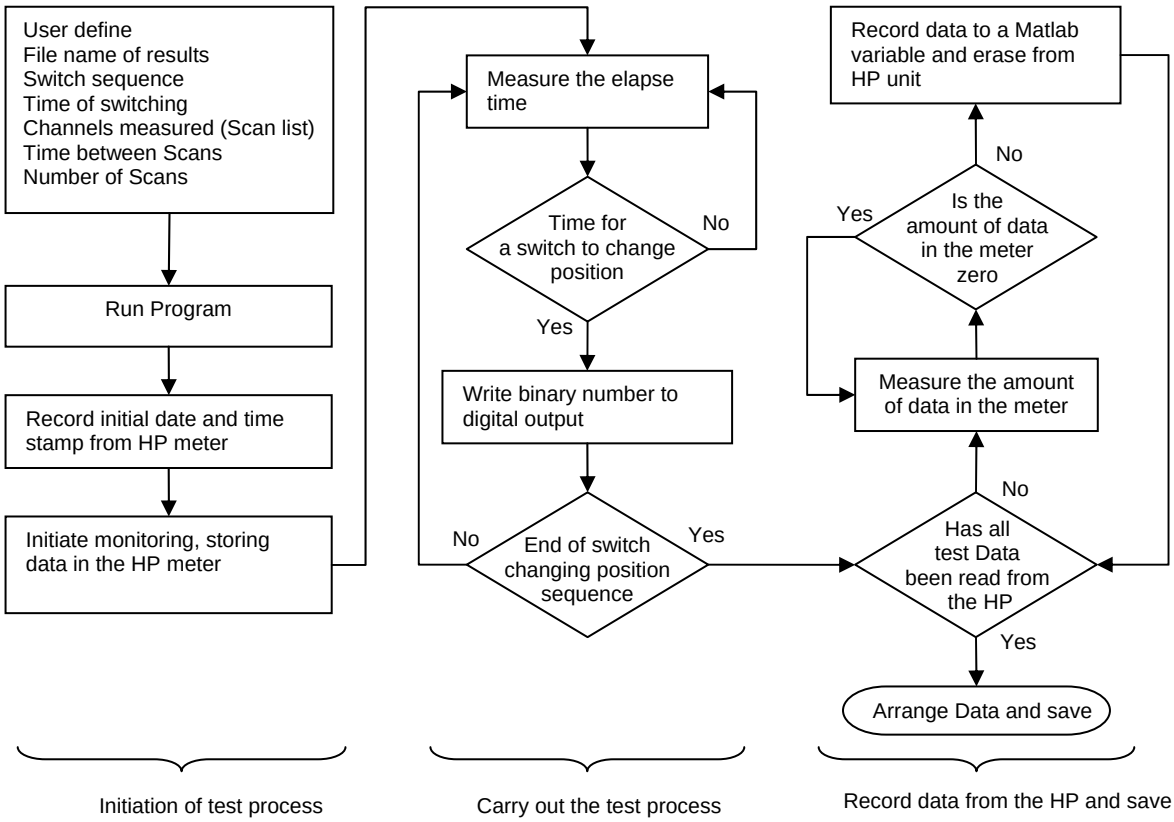

Figure 5.5 Matlab Program for Test Implementation and Data Acquisition

Once the programme is started, the meter is configured and scanning begins. The scanning continues irrespective of additional commands sent to the HP meter, such as switch commands or data being read and erased from the meter. Once all measurements have been taken, and all data has been recorded from the meter, the test data is arranged in a readable format and saved as a Matlab variable, (`.mat`). Figure 5.6 shows the format of a data file with the initial time stamp, the channel number and elapse time recorded with each measurement. Matlab is also used for analysing and graphing the results of all tests. It should be noted that the initial time stamp was not always accurate (due to HP internal clock resetting on occasion), thus the time and date of testing can be taken from the file modification date.

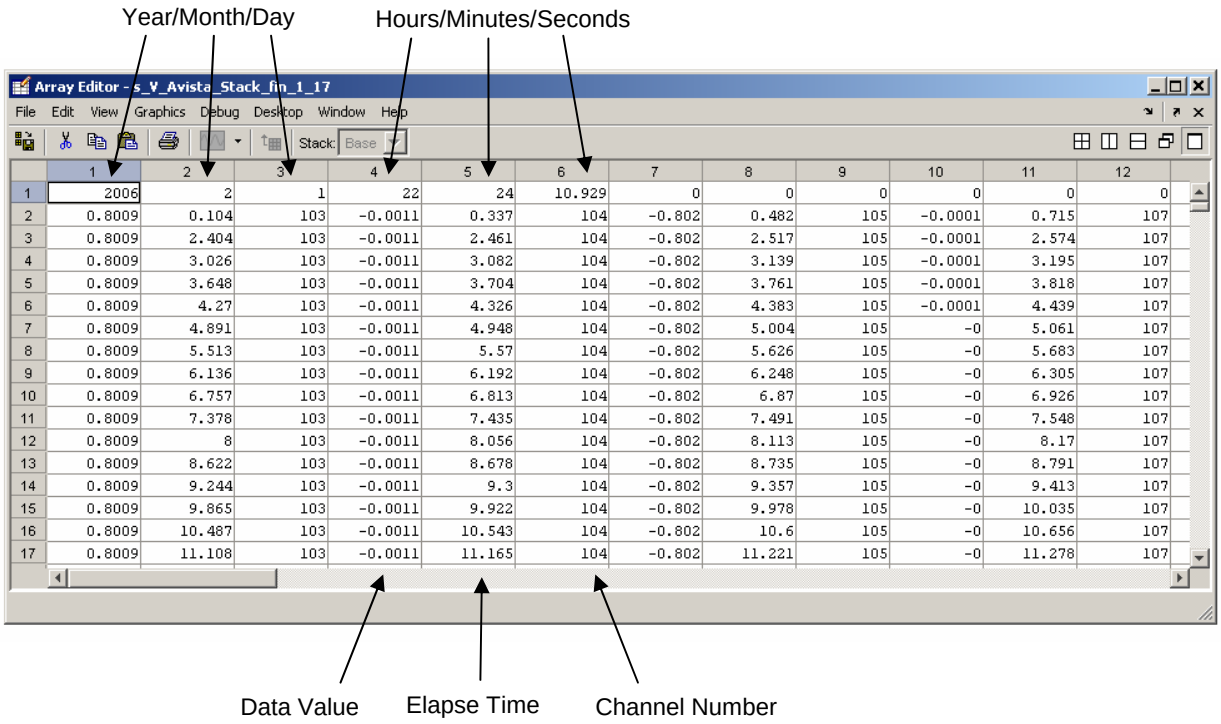

	1	2	3	4	5	6	7	8	9	10	11	12
1	2006	2	1	22	24	10.929	0	0	0	0	0	0
2	0.8009	0.104	103	-0.0011	0.337	104	-0.802	0.482	105	-0.0001	0.715	107
3	0.8009	2.404	103	-0.0011	2.461	104	-0.802	2.517	105	-0.0001	2.574	107
4	0.8009	3.026	103	-0.0011	3.082	104	-0.802	3.139	105	-0.0001	3.195	107
5	0.8009	3.648	103	-0.0011	3.704	104	-0.802	3.761	105	-0.0001	3.818	107
6	0.8009	4.27	103	-0.0011	4.326	104	-0.802	4.383	105	-0.0001	4.439	107
7	0.8009	4.891	103	-0.0011	4.948	104	-0.802	5.004	105	-0	5.061	107
8	0.8009	5.513	103	-0.0011	5.57	104	-0.802	5.626	105	-0	5.683	107
9	0.8009	6.136	103	-0.0011	6.192	104	-0.802	6.248	105	-0	6.305	107
10	0.8009	6.757	103	-0.0011	6.813	104	-0.802	6.87	105	-0	6.926	107
11	0.8009	7.378	103	-0.0011	7.435	104	-0.802	7.491	105	-0	7.548	107
12	0.8009	8	103	-0.0011	8.056	104	-0.802	8.113	105	-0	8.17	107
13	0.8009	8.622	103	-0.0011	8.678	104	-0.802	8.735	105	-0	8.791	107
14	0.8009	9.244	103	-0.0011	9.3	104	-0.802	9.357	105	-0	9.413	107
15	0.8009	9.865	103	-0.0011	9.922	104	-0.802	9.978	105	-0	10.035	107
16	0.8009	10.487	103	-0.0011	10.543	104	-0.802	10.6	105	-0	10.656	107
17	0.8009	11.108	103	-0.0011	11.165	104	-0.802	11.221	105	-0	11.278	107

Figure 5.6 Example of Test Data File

All data from a single day of testing (or group of sequential days) is stored in a separate directory, together with an analysis file describing each results file, and the conditions of the test.

5.2 Fuel Cell Descriptions with Passive and Active Test Methods

Three PEM fuel cell stacks were used in this research, and are described in the next 3 subsections. All of the fuel cells are prototypes and none are being manufactured today. Only one manufacturer, ReliOn Inc. (previously Avista Laboratories, Inc) is continuing with fuel cell development. Due to the proprietary nature of fuel cell development and manufacture, explicit fuel cell specifications were not available. Along with a description of the fuel cell, the passive and active operation of each is described in the following three subsections.

5.2.1 MerCorp Stack

Figure 5.7 shows the PEM stack manufactured by Materials and Electrochemical Research (MER) Corporation, or MerCorp.

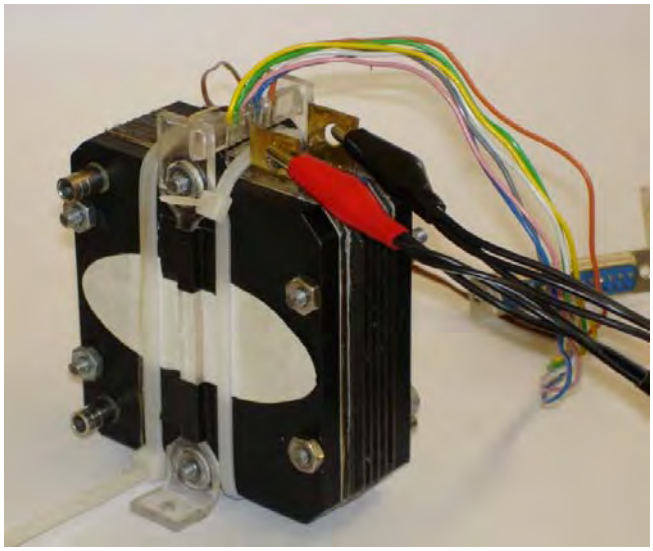

Figure 5.7 MerCorp Stack

The stack consists of six cells in a typical bipolar arrangement. The cells have an active area of 31cm^2, employ a Nafion based membrane, and the bipolar plates are made from machined graphite. Two identical MerCorp Stacks were purchased at a cost of US$ 1500 each. As one of the stacks did not function, it was disassembled and is shown in Figure 5.8.

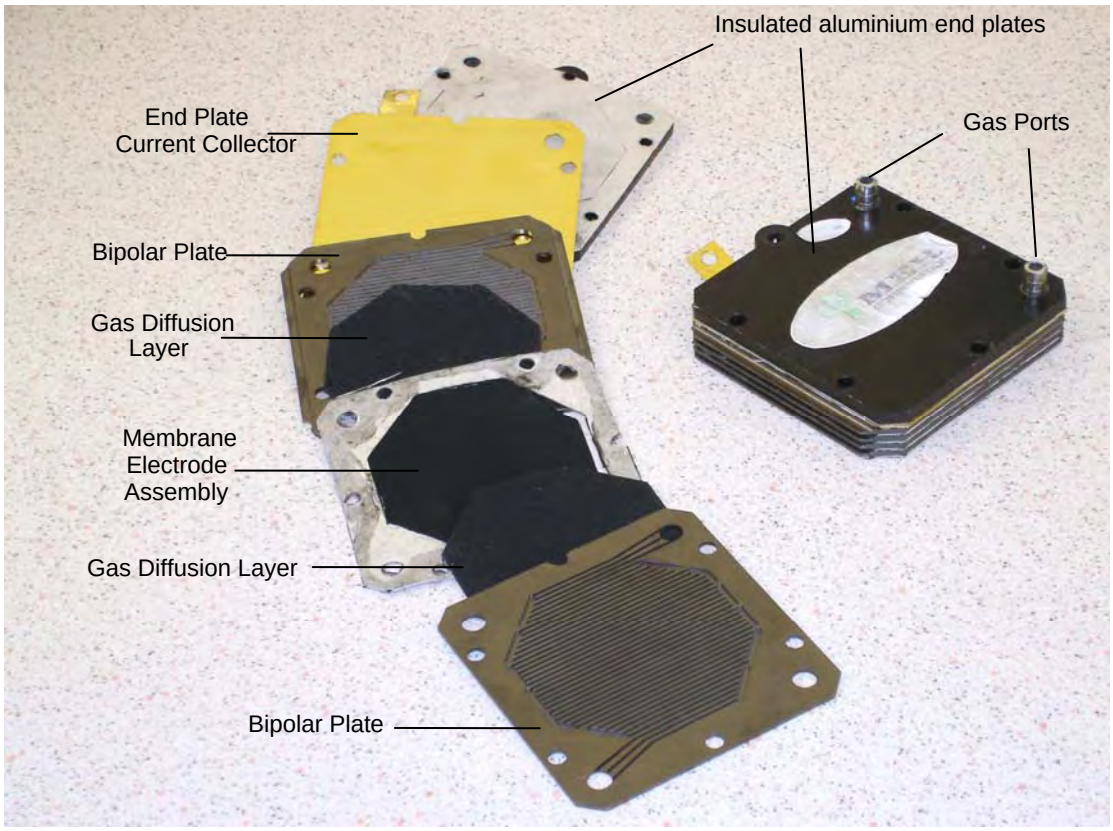

Figure 5.8 Disassembled MerCorp Stack showing Cell Components

The bipolar plates have a serpentine flow field pattern for gas distribution. The air and hydrogen are in a counter flow arrangement, i.e. the hydrogen enters the cell near the point where the air exits, and the gases flow across the MEA in opposite directions. The stack is completely symmetrical in design, in that the electrode composition and flow field pattern are identical for the anode and cathode [1]. Therefore, even though the stack has gas inlets specifically labelled "H_2 In" and "Air In", the hydrogen can enter the "Air In" port and visa versa, resulting in a reversal of stack polarity.

The MerCorp stacks were in the developmental stage, and their performance was very limited. The stack shown in Figure 5.8 was taken apart because it never produced power. When hydrogen was passed through this stack, one of the cells did not produce any voltage at all. The cause of this may be due to the seal around the edge of the stack, which was found to protrude into the gas flow channels.

For active and PSDB testing, each cell voltage was measured using metal pins clamped onto the side of each bipolar plate, which were wired to the HP meter. This is shown schematically in Figure 5.9

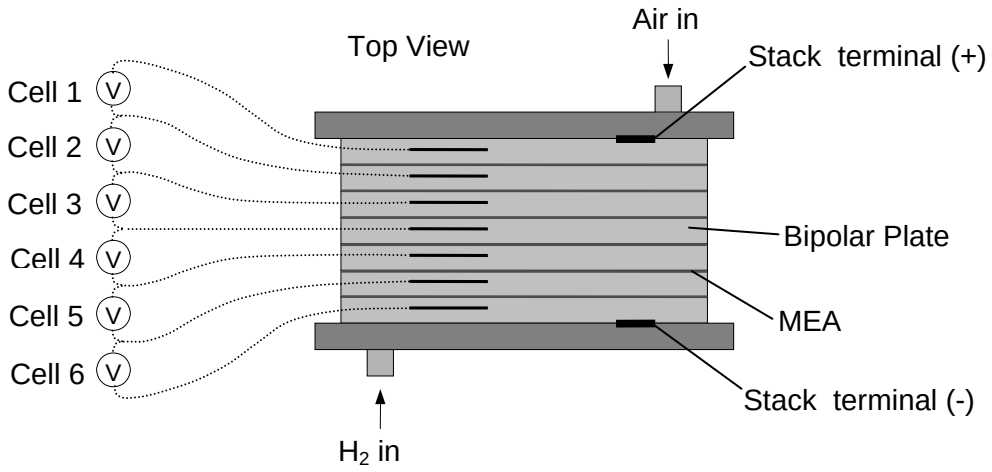

Figure 5.9 MerCorp Stack showing Cell Voltage Labels

Fuel cell active testing required a number of other components, effectively the balance of plant, a schematic of which is shown in Figure 5.10.

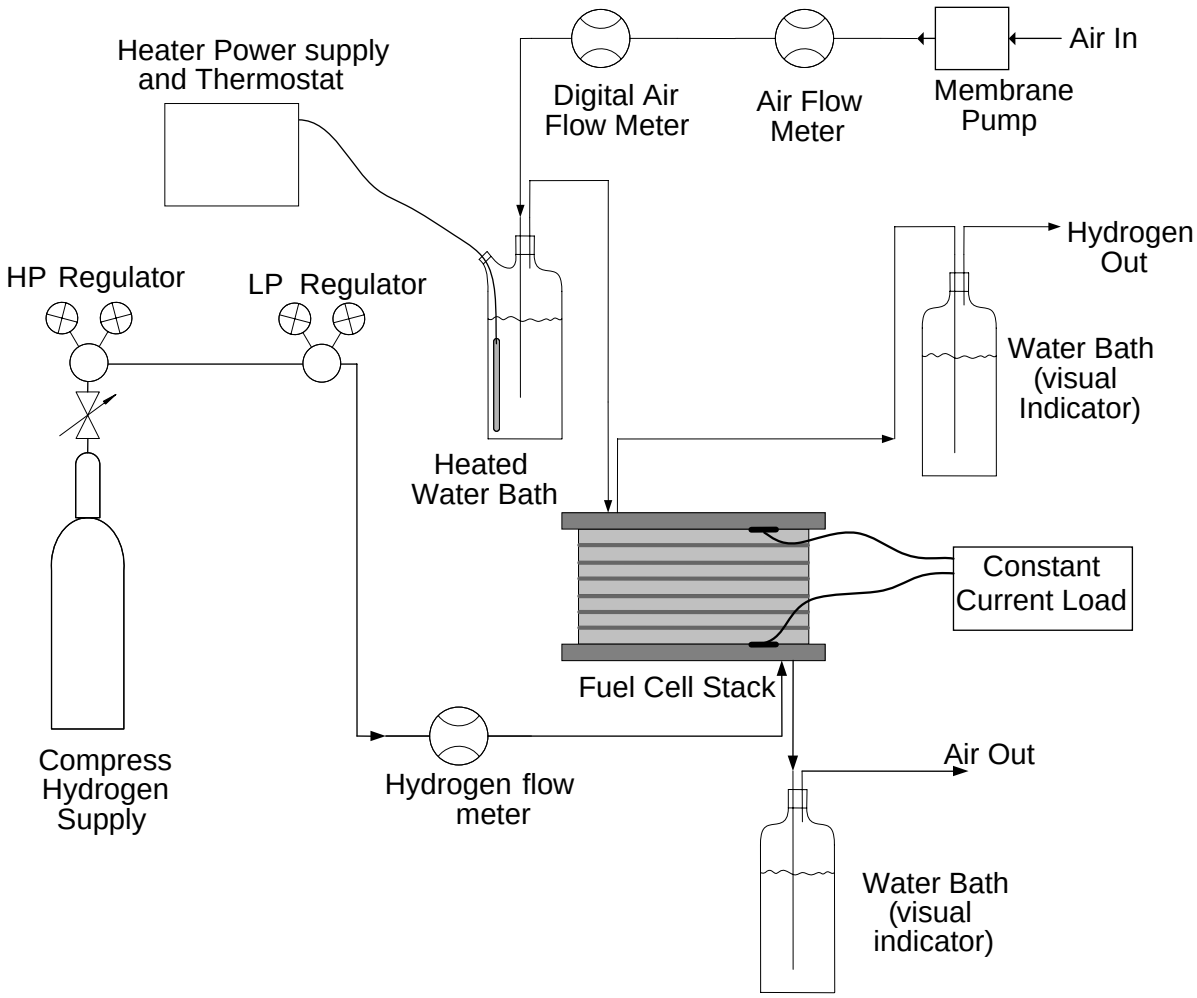

Figure 5.10 Active Testing Setup for the MerCorp Stack

Both the air and hydrogen exited via a water column of equal height, limiting any pressure drop across the membrane, thus reducing possible stress on the fuel cell. All of the equipment shown in Figure 5.10 is detailed in Table 5.2.

Table 5.2 MerCorp Active Testing Eqipment List

Component	Details
Compressed Hydrogen Supply	Zero Grade, 99.995%,
Hydrogen Flow Meter	GAP meter 0 – 2 l/min Hydrogen
Air Flow meter	GAP meter 0 – 5 l/min Air
Digital Flow Meter	Hastings mass flowmeter. Model HFM-200, Serial 1259, Hastings Instruments, Power Supply Model 200
Membrane Pump	Silent Flow 9000
Constant current load	*Described below*

The electronic flow meter outputs a voltage directly proportional to flow, and was calibrated using the GAP airflow meter. A constant current load [2] shown in Figure 5.12, was used for all

active testing of the MerCorp fuel cell. The current value was set by an input potential, achieved with a constant voltage source and a variable resistor.

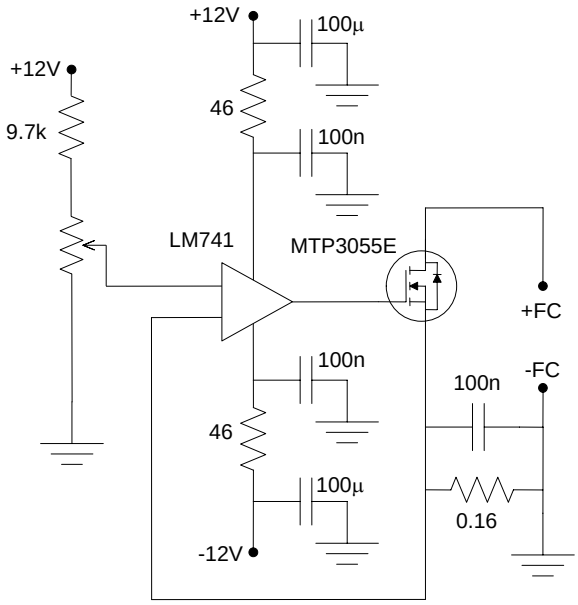

Figure 5.11 Constant Current Load Circuit for Active Testing of the MerCorp Stack

Additional voltage channels were used for monitoring the digital flow meter output, with the current measured using a shunt resistor. Figure 5.12 shows the complete equipment layout for the active operation of the MerCorp Fuel cell.

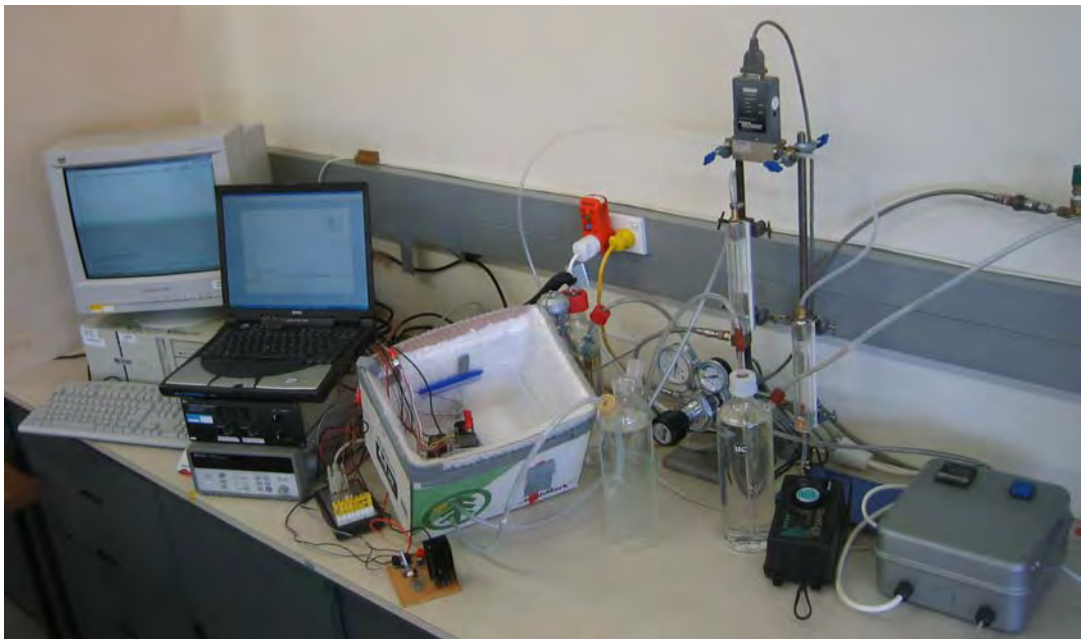

Figure 5.12 Photo of the MerCorp Test Layout

As stated previously, neither fuel cell performed as designed, with one of the stacks not functional. Through trial and error operation of the other fuel cell, maximum performance was found to occur using a large air flow rate. The specific airflow rates are provided with the active tests results in Chapter 8.

5.2.2 ENABLE FUEL CELL

A 12W (1A and 12V) Enable fuel cell stack is shown in Figure 5.13. The stack consisted of 23 series connected cells, each with an active area of 12cm^2. The stack is annular in design. Hydrogen enters the centre of the stack at each end, and diffuses across a gas diffusion layer (GDL) to the anode surface. A thick GDL on the cathode allows oxygen from the surrounding air to naturally diffuse to the electrode surface. Therefore, although the stack is configured in a typical series arrangement, bipolar plates are not required.

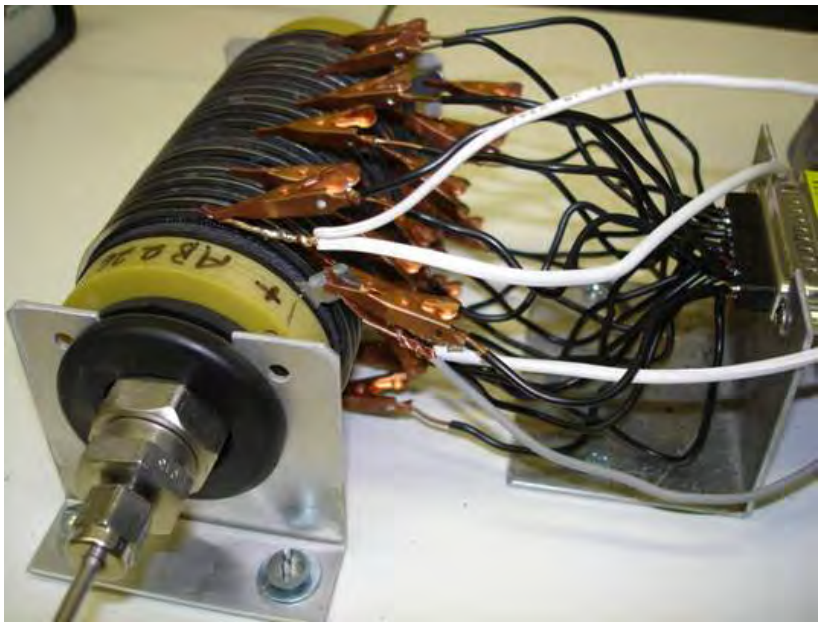

Figure 5.13 Enable Fuel cell

Adjacent cells are separated by a round metal plate, which is in electrical contact with the anode of one cell, and the GDL of the adjacent cell [3]. Small clips were attached to the metal separator plates, allowing individual cells to be tested and monitored.

As the number of cells exceeded the number of inputs to the 20 channel card, the 40 channel card was used, with each cell measured to a common ground as shown in Figure 5.14. In order to obtain the voltage of a single cell, the voltage reading of the previous cell (as measured to the common ground) was subtracted. This introduced a slight measurement error, as all voltages are measured at slightly different times. This error was usually insignificant, as the voltage across a single cell changes very little in the time between adjacent voltage measurements. However, if

periods of rapid voltage change were being analyzed, the raw data was first interpolated using a 2nd order polynomial, such that each voltage measurement in a single scan was defined at the same time.

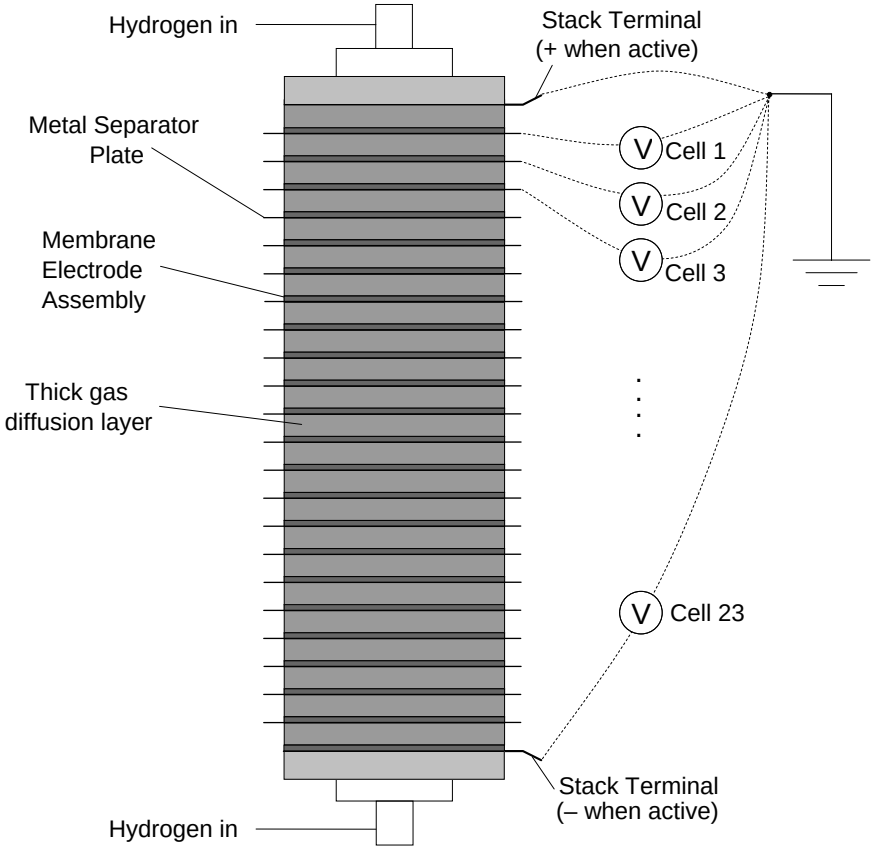

Figure 5.14 Enable HP Channel Connections for Conducting the Passive Test

Figure 5.15 shows a schematic of the active test set up. The balance of plant (BOP), designed and produced by Enable, is very simple. It consists of a pressure regulator, flow divider, purge valve and solenoid valves, which alternate which end of the stack the hydrogen enters. The alternating flow of hydrogen is designed to prevent inert gas areas building up within the stack. The cycle time was measured to be 120 seconds. Thus, every 60 seconds, the hydrogen switches, and enters the stack from the other end. The stack terminals are connected to the BOP through a control, which takes a small amount of stack power for solenoid valve operation. As active stack performance was required without any interference, the Enable BOP is connected to an external power supply that acts as a "dummy stack", providing power for solenoid valve operation. A series of variable resistors is used as the load, allowing a VI curve to be obtained. As the current produced by the stack has a 1A max value, the current was measured directly with the HP unit.

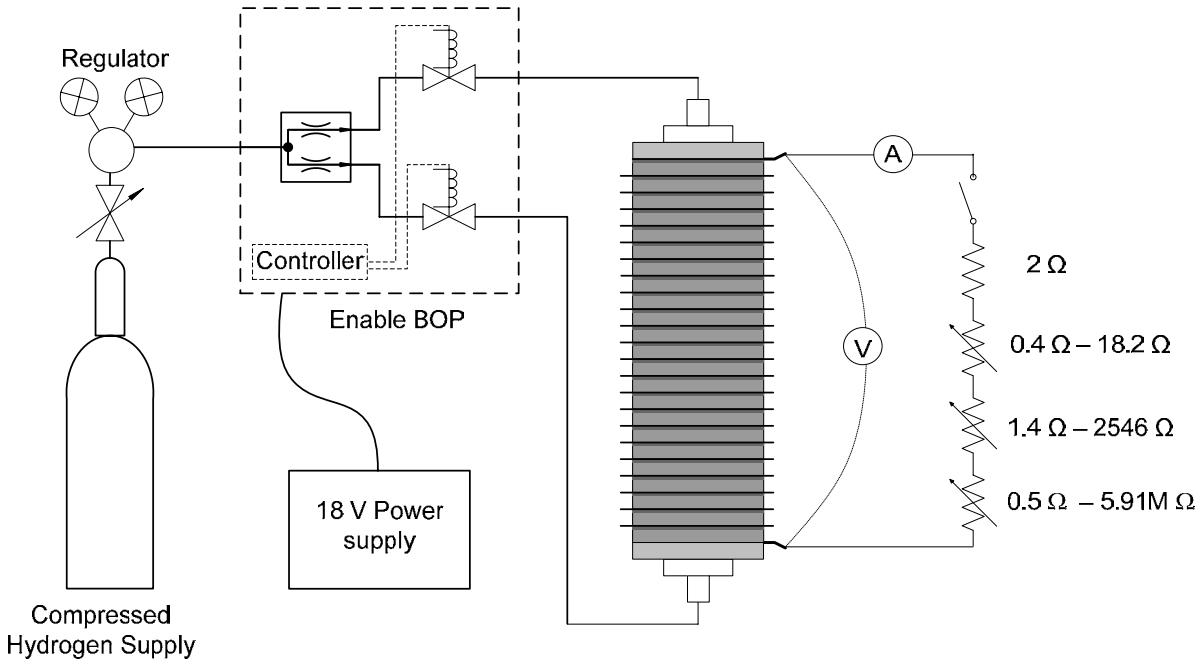

Figure 5.15 Active Setup of the Enable Fuel Cell

5.2.3 AVISTA SR-12 FUEL CELL

An Avista SR-12 PEM fuel cell system is shown in Figure 5.16. A description of the system is provided, followed by a description of the passive and active testing setup.

Figure 5.16 Avista SR 12 System showing 6 (of 12) catridges installed

The Avista SR-12 system is designed to produce up to 500W (25V at 20A). The specifications of the SR-12 system, as provided by Avista, are detailed in Table 5.3.

Table 5.3 Avista SR-12 System Performance [4]

System Parameter	Value
Power Output – Continuous	500W
Output Voltage	25 – 39 dynamic (120 VAC Single Phase available with optional inverter)
Fuel Source	Hydrogen
Fuel Consumption	7.0L/min @ 500W (<1.0L/min @ no load)
System Start Time	7 minutes @ room temperature
Turndown Ratio	500W to no load, infinite
Operating Temperature Range	5ºC to 35ºC
Dimensions (W x D x H)	0.56m x 0.615m x 0.345m
Weight	44kg w/cartridges

The stack is composed of 48 series connected cells, which are grouped into 12 removable cartridges. Figure 5.17 shows a picture of a cartridge, together with a schematic detailing the electrical configuration of the 4 cells contained.

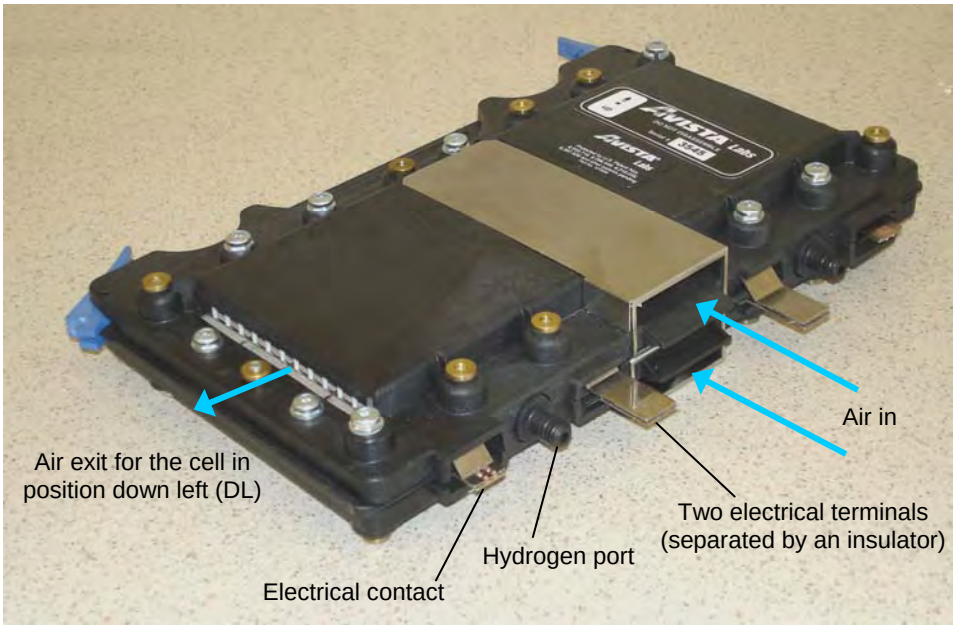

a)

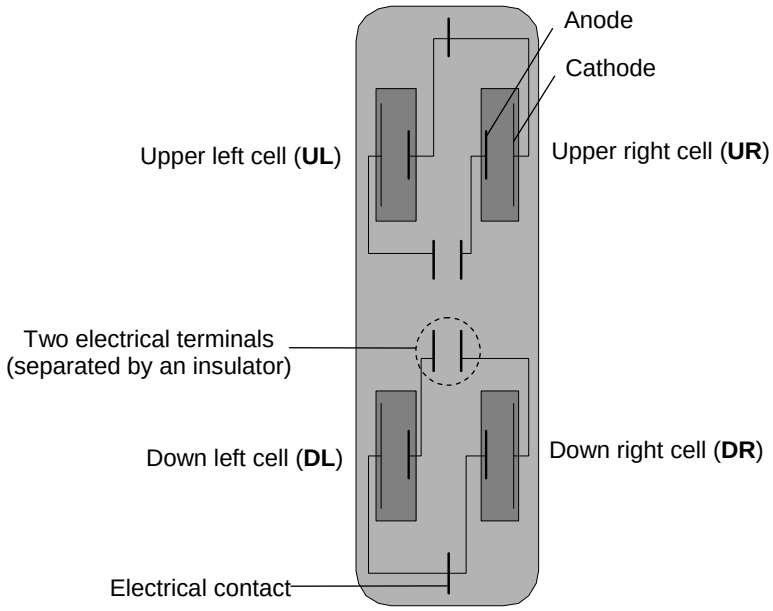

b)

Figure 5.17 An Avista Cartridge (a) with an Electrical Schematic (b)

Each cell has an active area of 50cm^2, and uses a Nafion based membrane electrolyte [5]. A thick gas diffusion layer (GDL), made of a porous graphite plate, covers each electrode. A metal grid is clamped onto the GDL, which serves as the current collector and cell electrical contacts. When the cartridge is fitted into the SR-12 system, hydrogen enters the cartridge at the bottom hydrogen port. The hydrogen is effectively dead ended, with the top hydrogen port used for

periodic purging, preventing the build-up of any gases such as nitrogen. Air is blown into the middle of the cartridge, and flows across the cathode of each cell, before exiting at the top and bottom of the cartridge.

The 12 cartridges form a stack of 48 series connected cells when inserted into the system. Figure 5.18 shows the details of the electrical connections.

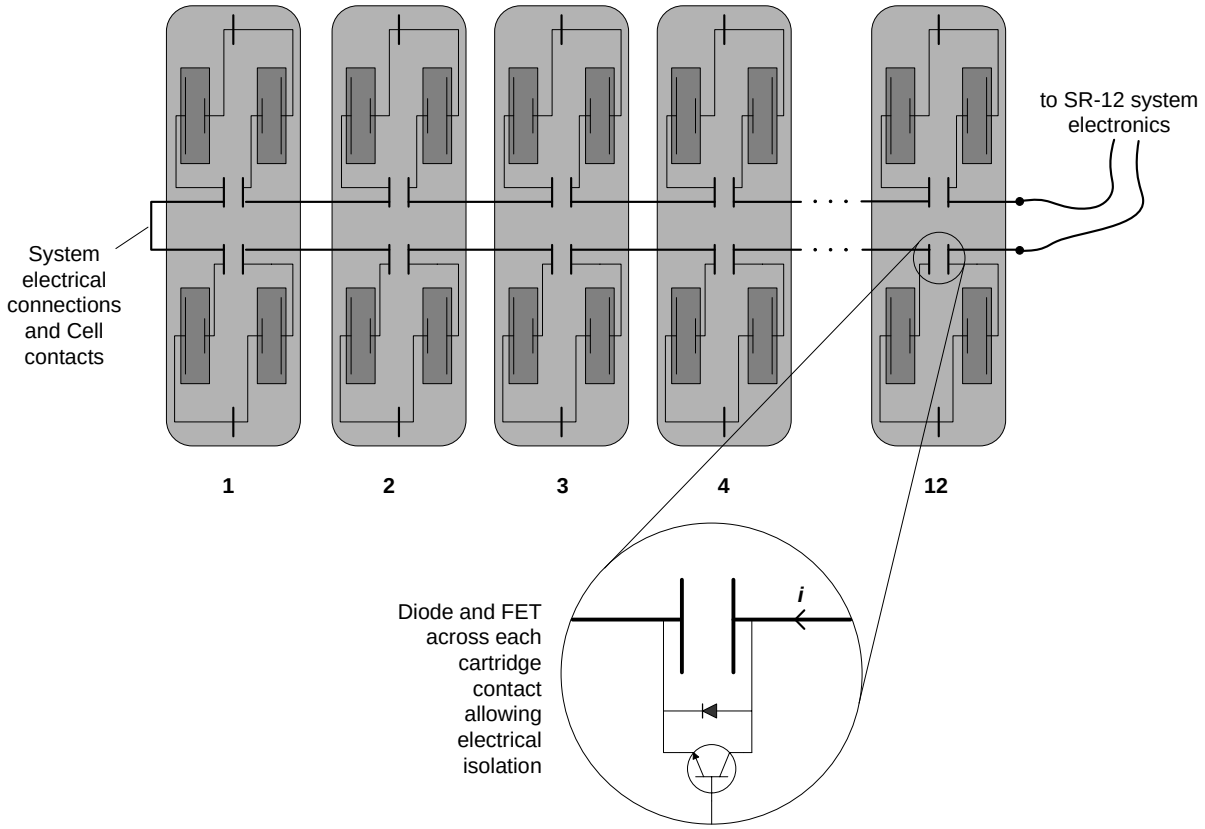

Figure 5.18 Avista SR-12 System Configuration

The Avista-SR12 has a number of unique design features, specifically designed for a back-up power application. Compared to other PEM systems, the balance of plant is relatively simple and consists of:

- a single convection fan for reactant air flow, which also provides cooling
- hydrogen solenoid valves for each cartridge, and common plenum purge
- lead acid batteries for system start-up
- power electronics for battery charging from the fuel cell stack
- controller, including hydrogen and temperature sensors, voltage monitoring on each cell and the stack, and stack current monitoring

As the fuel cell stack is subdivided into 12 cartridges, only a single cartridge needs to be replaced if a cell fails. In addition, the system electrical contacts shown in Figure 5.18, together

with hydrogen solenoid valves, allows a cartridge to be disconnected from the system in the event of poor performance, (i.e. if the voltage of any cell in a cartridge falls below 0.1V the system automatically shuts off the hydrogen and shunts current around the affected cartridge). The cartridges are also hot swappable, i.e. they can be replaced while the system continues to produce power.

A communication port on the back of the Avista SR-12 system, allowed the internal monitoring system to be accessed and recorded during the active operation of the system. An Avista Labs communication board links the fuel cell system to a PC. A software program, DAQ – SR12 Fuel Cell Monitor, running on the PC, records the operating variables to a txt file. Figure 5.19 shows the typical test setup, with Table 5.4 listing all variables recorded.

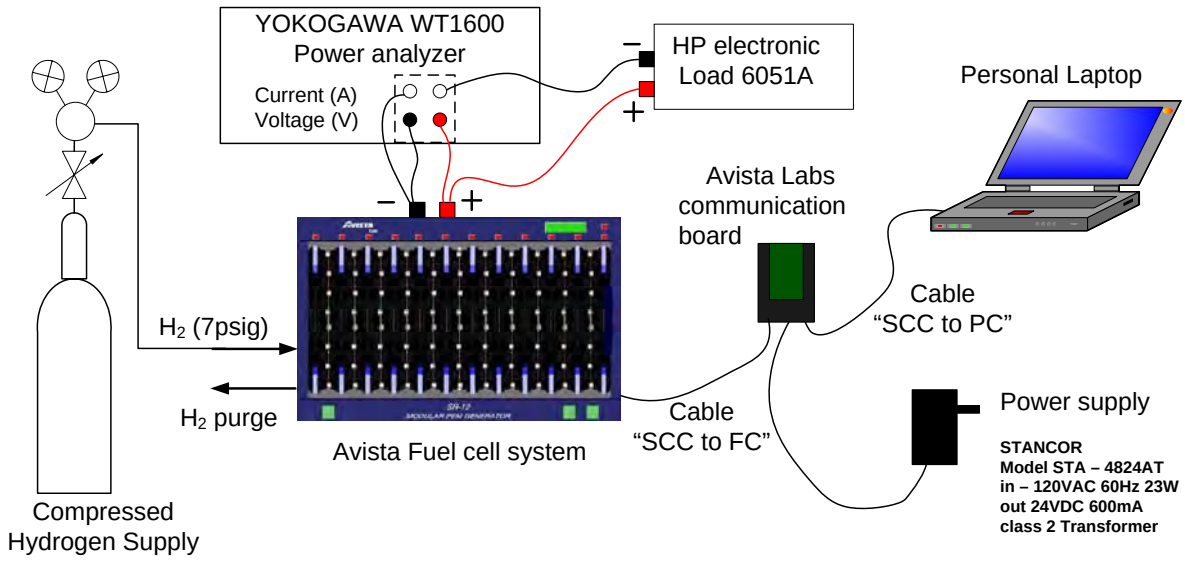

Figure 5.19 Operational Setup of the Avista SR-12 system

Table 5.4 Variables Recorded by the DAQ – SR12 Fuel Cell Monitor

Parameter	Description
Date Time	Timestamp of the data
MEA-1UL	MEA (Membrane Electrode Assembly) Voltage, UL = Upper Left, LR lower right etc
AMP Proc State	The AMP Processor State. On-line, Off-line, etc
Lower Plenum H2	The lower plenum H2 sensor voltage. This value correlates to the amount of Hydrogen concentration in PPM detected by the safety systems.
Lower Plenum Temp	The lower plenum temperature reading in degrees Celsius.
CFRAME Proc State	The CFRAME Processor State. On-line, Off-line, etc
Upper Plenum H2	The upper plenum H2 sensor voltage. This value correlates to the amount of Hydrogen concentration in PPM detected by the safety systems.
E-Bay H2	The electronics bay H2 sensor voltage. This value correlates to the amount of Hydrogen concentration in PPM detected by the safety systems.
Fan Speed	The system fan speed in RPM's.
Current Load	Amperage draw on the system. This is inclusive of parasitic loads.
Upper Plenum Temp	The upper plenum temperature reading in degrees Celsius.
E-Bay Temp	The electronics bay temperature reading in degrees Celsius.
ENV Proc State	The Environmental Processor State. On-line, Off-line, etc
System Voltage	The combined voltage of all MEA's in all Cartridges
60V Supply	The voltage on the 60v power supply
12V Supply	The status of the 12 volt power supply
External Voltage	The voltage on the external terminals
Power Proc State	The Power Processor State. On-line, Off-line, etc
Display Proc State	The Display Processor State. On-line, Off-line, etc
Power Output	Calculated Power Output in Watts

Although many parameters are recorded, including the individual cell voltages, data quality was relatively poor. The voltage on each cell was only recorded every 40s, and was measured with an 8-bit resolution over the range 0.000 – 0.999V. Measurement of the open circuit potential and low current performance of the stack was not possible due to the power requirements of the auxiliary systems, i.e. the convection fan, and battery charging etc. The power electronics in the SR-12 system, used for producing the correct voltage/current for the auxiliary systems, also interfered with the system/stack voltage, causing it to fluctuate (±1 – 2V). Therefore, the SR-12 system did not provide an adequate environment for assessing the active performance of the fuel cell.

The PSDB testing of the Avista stack could not be conducted when the cartridges are installed in the SR-12 system. As shown in Figure 5.18, a diode and FET are connected across each cartridge. Clearly, these will interfere with the test protocol. Therefore, all active and PSDB testing of the Avista fuel cell was conducted on cartridges that were removed from SR-12

system. Figure 5.20 shows the experimental set up for testing the Avista cartridges without using the SR-12 system.

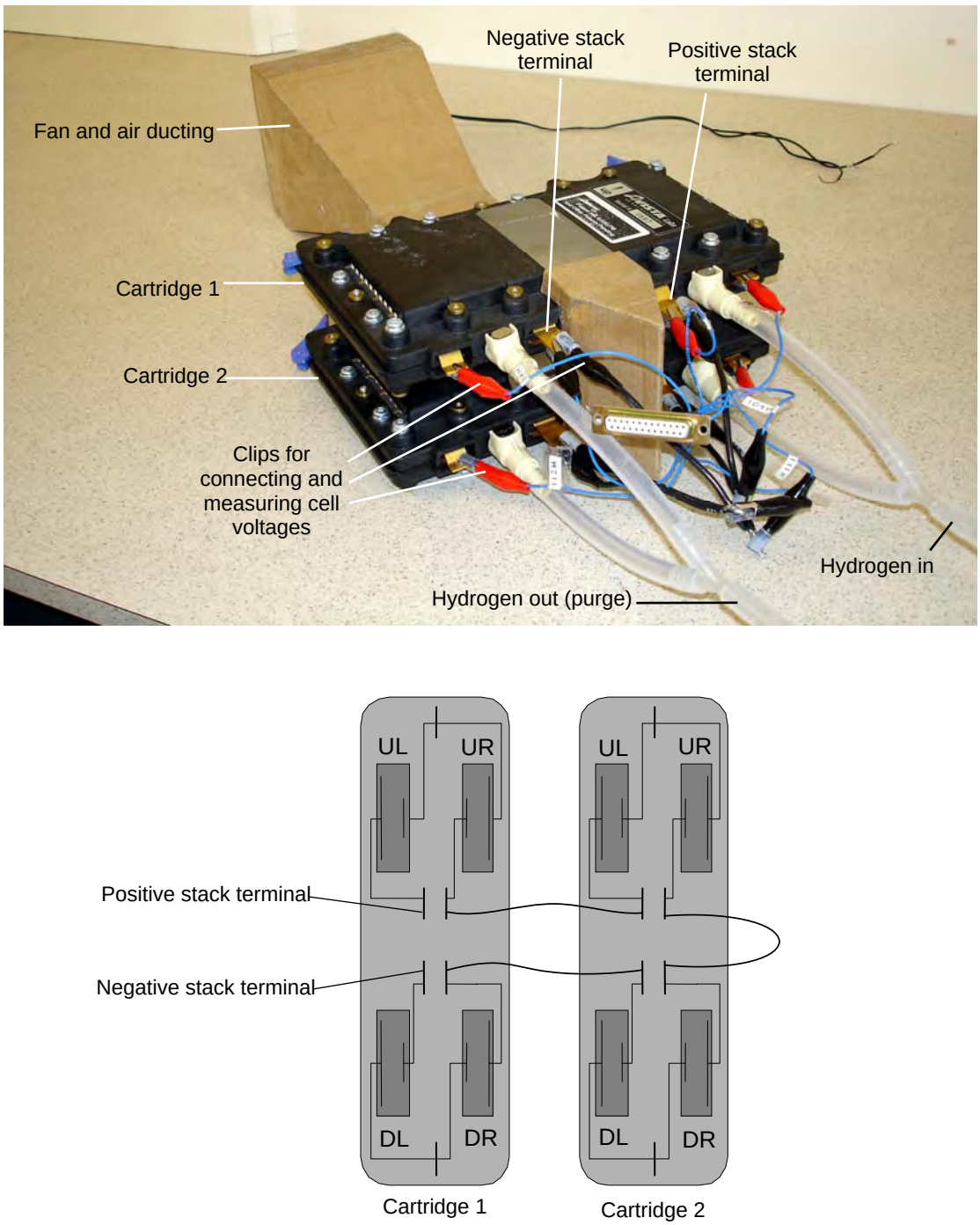

Figure 5.20 Avista Cartridge Testing without the SR-12 System

A stack of eight series connected cells is formed by electrically connecting two Avista cartridges. Designating a particular cell by its cartridge number, 1 or 2, and the cell position, upper left (UL), down right (DR) etc, the order in which the cells are connected is

Positive terminal – 1UL – 1UR – 2UL – 2UR – 2DR – 2DL – 1DR – 1DL – Negative terminal

Stack active and PSDB testing results presented in this thesis are also in this order. Alligator clip were attached to each electrical terminal, allowing the voltage of each cell to be monitored.

For active testing, Hydrogen is introduced to the top port of both cartridges, with the bottom hydrogen ports connected to a purge valve, thus dead-ending the hydrogen. The Hydrogen is held at 5psig for all active testing. A brushless DC San Ace fan, model 109R1224H102 operated at 25V, served as the air blower. Air is ducted between the cartridges, and flows through each cartridge in the normal fashion (see Figure 5.17a). A series of variable resistors is used as a load, allowing the VI performance of the fuel cell to be obtained.

For PSDB testing, the hydrogen lines are disconnected, and the fan remains inactive. The test circuit is attached to the stack terminals, which are located on cartridge 1 as shown in Figure 5.20. Figure 5.21 shows a compete schematic of the active and PSDB testing systems with a photo of the test setup shown in Figure 5.22

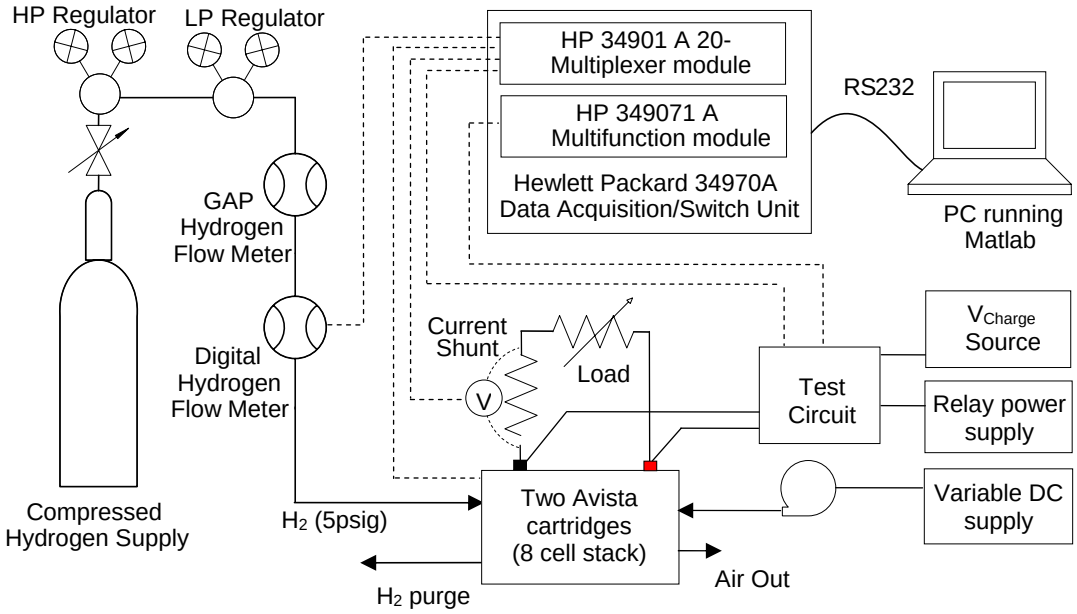

Figure 5.21 Active and Passive testing setup of two Avista Cartridges

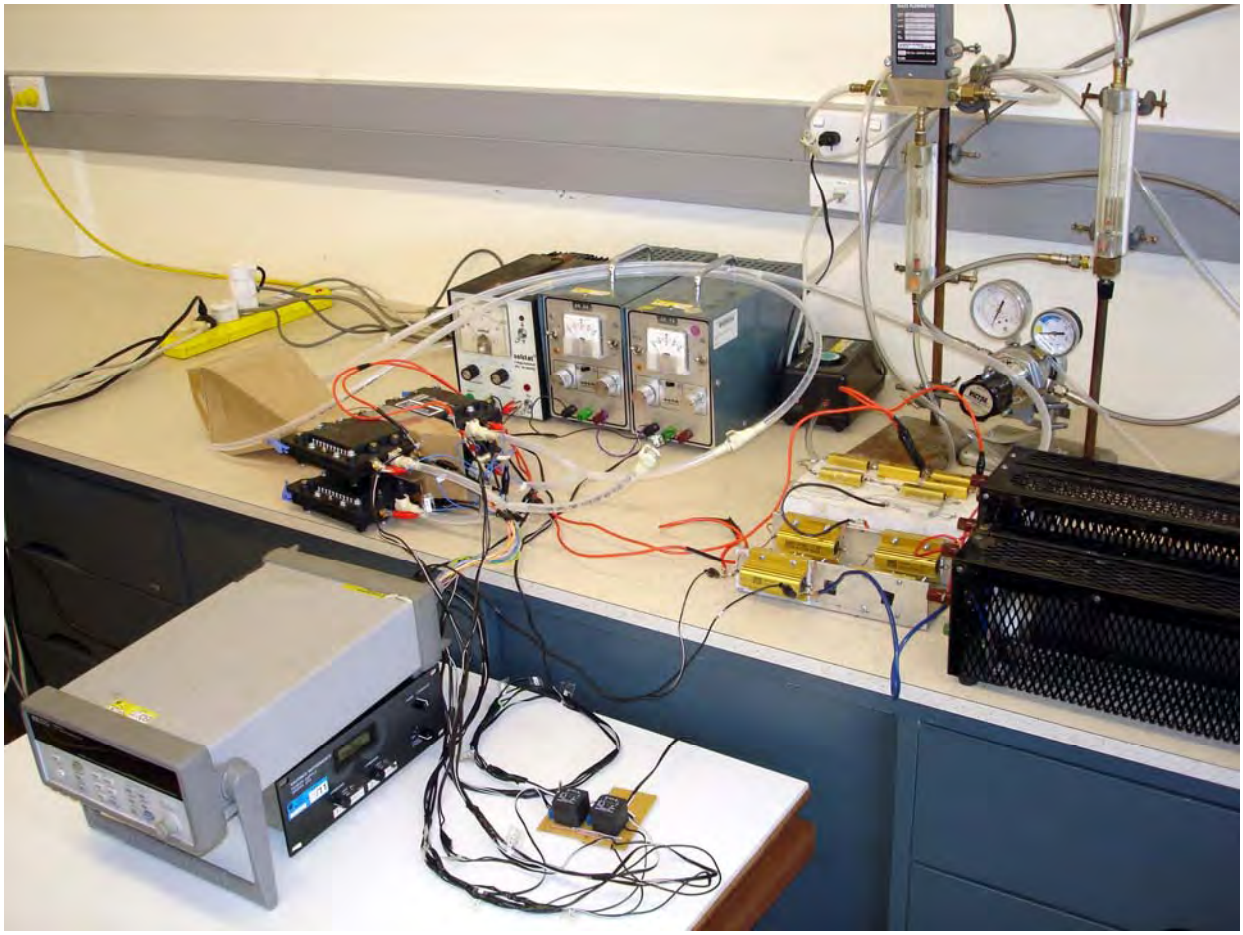

Figure 5.22 Equipment Layout of Avista Cartridge Testing, Active and Passive (the high-pressure regulator, hydrogen supply and PC not shown)

5.3 INTERFERENCE CHECKING

As the HP meter is used to control the test circuit and record the voltage response of the cell, possible interference was checked by conducting a number of passive experiments. A single cell of the MerCorp stack was subjected to three identical passive tests, i.e. switch times and test circuit values remained the same. However, in each test the voltage monitoring, method of switching, and voltage source was altered, in order examine if these experimental changes caused a change in the fuel cell voltage response.

The first test was conducted using the test system as described, i.e. the multifunctional module was used for relay switching and supplied the voltage output for the test circuit. All three voltages were recorded (see Section 5.1.2) together with the test current using the HP internal current measurement. The measurements were taken every 0.5 seconds.

In the second test, the multifunction module was removed from the HP unit. An independent power supply (Solstat Regulated DC Supply, Model 3S2PB) was used for the test circuit voltage, with the test circuit relays being manually shorted at the appropriate times. The cell voltage was recorded together with a disconnected channel. Therefore, the cell was only connected to the DMM briefly to obtain a measurement. Measurements were taken every 0.1 seconds.

The last test was very similar the second. However, just the cell was monitored, thus the DMM was permanently connected to the cell for the duration of the test, with measurements taken every 0.1 seconds. The results of all three tests are shown in Figure 5.24.

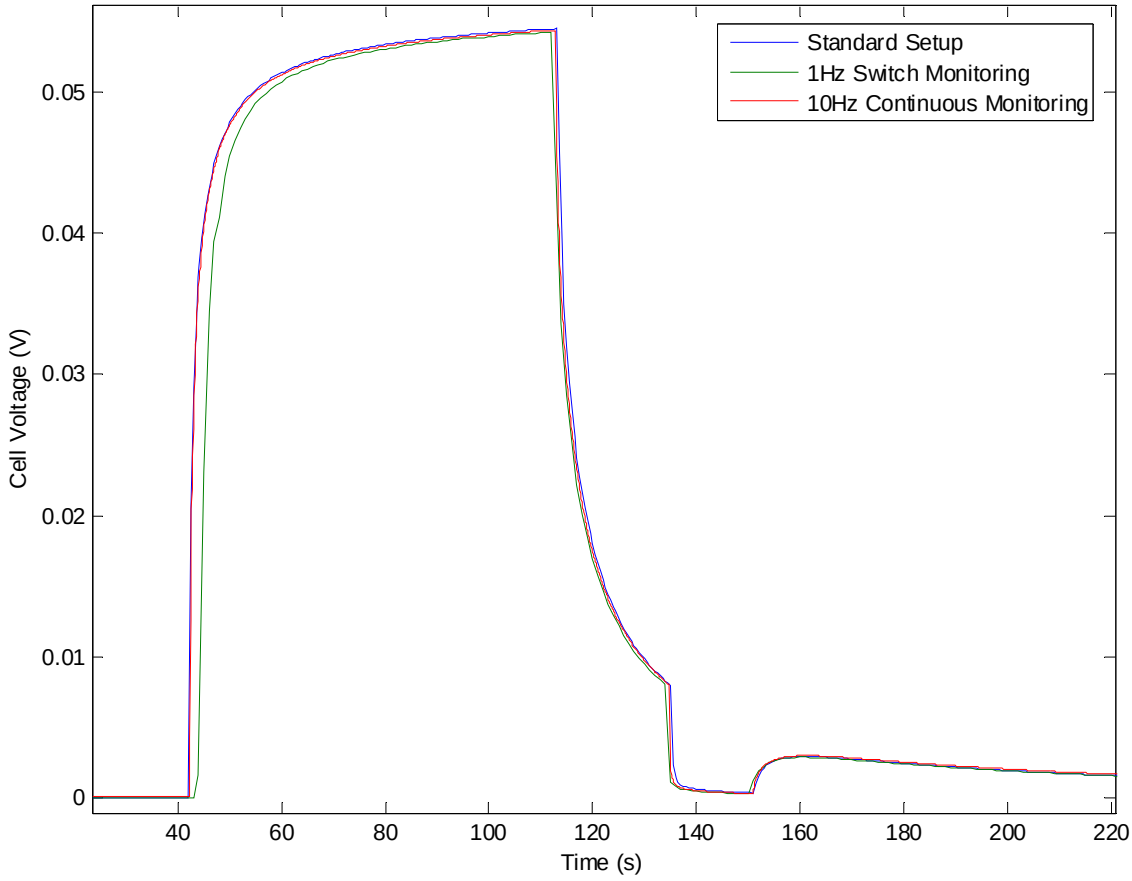

Figure 5.23 Verification of the Test System, using cell #3 of the MerCorp Stack; Test Circuit Parameters V_{Charge} = 95.0mV, R_{Charge} = 106.5Ω, and $R_{Discharge}$ = 15.0Ω

As can be seen from the results, there is very little difference between each test. The slight discrepancies are attributed to slight differences in the switch timings. In fact, the passive fuel cell response is robust to slight differences in the switch timing. For instance, in the experiment conducted with 1Hz timing, the charge time was approximately 2 seconds off, but did not affect the resulting voltage transient in a noticeable fashion. In summary, the results presented here can be confidently attributed the characteristics of the fuel cell only.

5.4 REFERENCES

[1] Hecht H, previously of MER Corporation, Tucson, AZ, Personal Communications, Sep. 2003

[2] Lyster M, Constant Current Load Development, Personal Communications, University of Canterbury, Oct 2003

[3] Kenyon KH, Doeppers MM, Ibrahim SE, “Passive air breathing fuel cells” United States Patent 6,423,437, Jul. 2002

[4] Avista Laboratories, Inc. SR-12 Modular PEM Generator, Operator’s Manual, Spokane, WA, Jul. 2000

[5] Gerry Snow, ReliOn Product Manager, Personal Communications, Spokane, WA. Aug. 2004

6 QUALITATIVE RESULTS AND ANALYSIS

This chapter describes the transient voltage behaviour of a fuel cell when subjected to the passive test protocol. Numerous passive tests were conducted on each fuel cell, and an example of the cell and stack response of each is provided. This chapter focuses on the results of the passive test only, and does not discuss the circuit model or active performance of the fuel cells.

Section 6.1 provides a detailed, qualitative description of the transient voltage response produced by a single cell. Each distinct region of the voltage response is described in a physical sense. Typical single cell testing results from the MerCorp, Enable and Avista fuel cells are presented in Section 6.2. Multiple cell (stack) testing is discussed in Section 6.3, with typical results from the three fuel cell stacks presented. A conclusion is provided in Section 6.4.

6.1 SINGLE CELL VOLTAGE RESPONSE

Figure 6.1 shows a typical voltage response of a single cell when subjected to the passive test protocol. The test was conducted on Avista cartridge #0588, cell DR (down right).

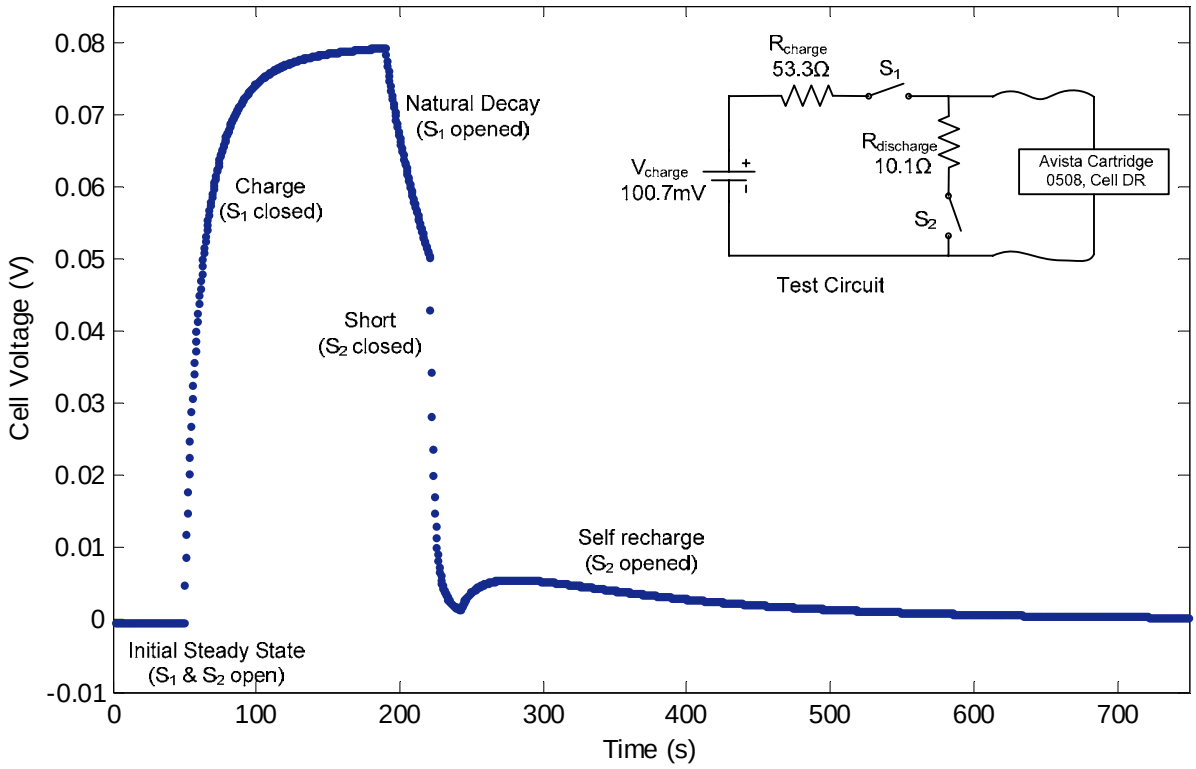

Figure 6.1 Single Cell Response to the Passive Test Protocol

The test protocol creates five distinct regions, which have been labelled;

1. Initial steady state: the cell is at open circuit (S_1 & S_2 open)
2. Charge: the cell is connected to a supply (S_1 closed)
3. Natural Decay: the cell is at open circuit (S_1 open)
4. Discharge: the cell is connected to a resistor (S_2 closed)
5. Self-recharge: the cell is at open circuit (S_2 open)

Primarily, the fuel cell in a passive state acts as a capacitor. The presence of electronic conduction is evident from the natural decay region, with additional non-ideal behaviour exhibited in the self-recharge region. The cell voltage response was predicted in Section 4.4.2, using the equivalent circuit model. The experimental voltage response shown in Figure 6.1 corresponds well to the predicted behaviour. A detailed description of the physical phenomena occurring in the cell during each region is now discussed in the following 5 subsections.

6.1.1 INITIAL STEADY STATE:

At the beginning of a test, each cell to possessed a small “resting” potential. Due to the voltage scale of Figure 6.1, the resting potential cannot be seen in the results presented. Initially, it was thought the resting potential was caused by fuel cell operation days prior to the passive test However, the majority of cells tested possessed a negative resting potential with respect to their polarity when functioning. Figure 6.2 shows the resting potential of 48 Avista Cells, 34 of which have a negative resting potential.

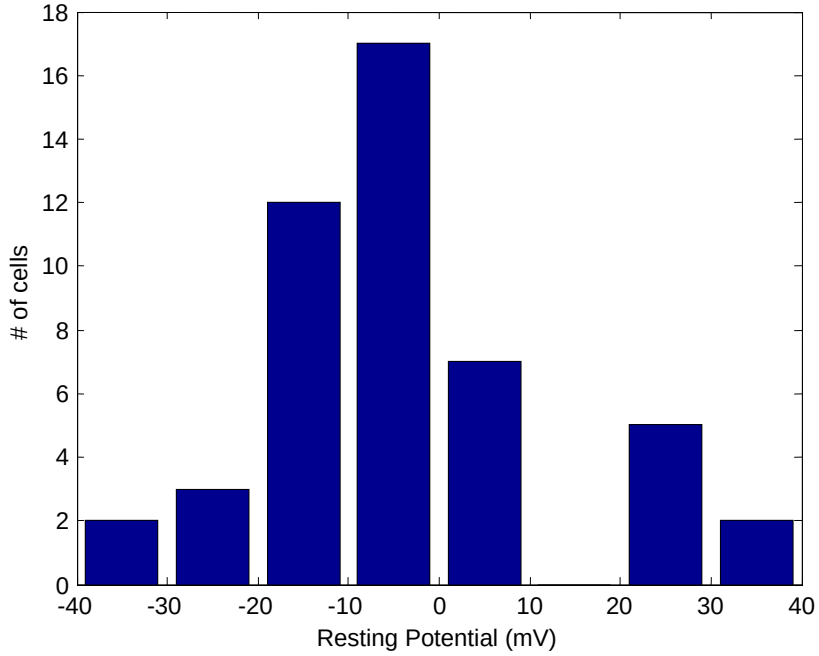

Figure 6.2 Resting Potential of 12 Avista Cartridges (48 Cells)

Figure 6.3 shows the resting potential of each cell in the Enable stack, measured 7 days after an active test. In this case, every cell possessed a negative resting potential.

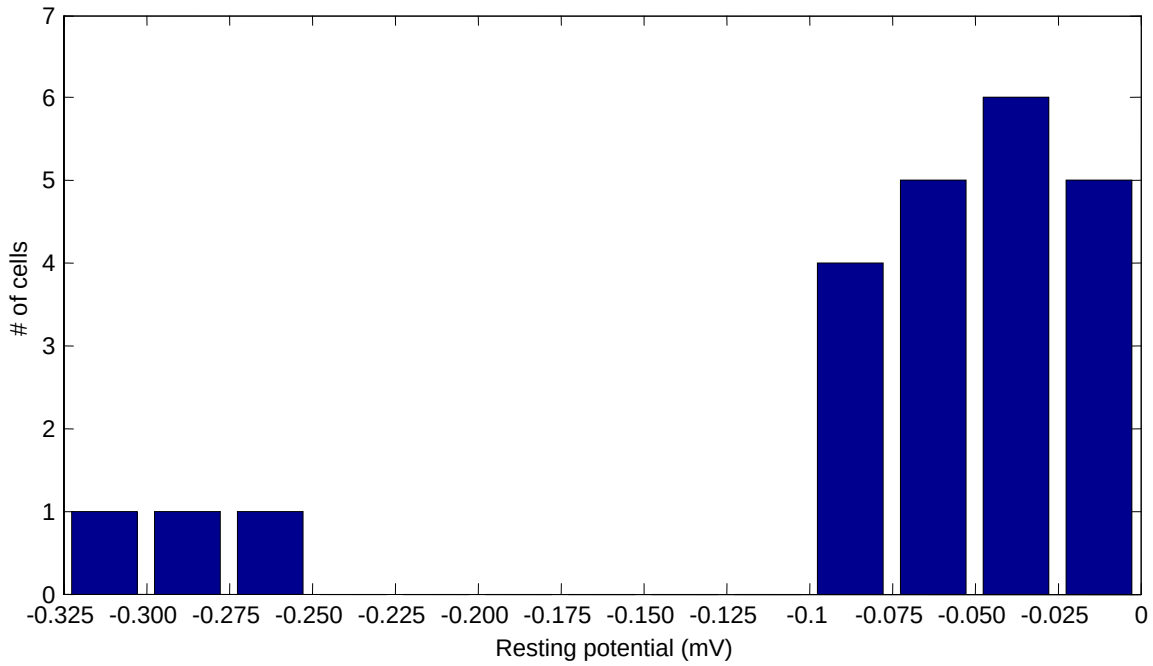

Figure 6.3 Resting Potential of the Enable Fuel Cell

The resting potential was found to persist particularly for the Avista cells. For example, when the polarity of a cell is forced to be positive, due to the PSDB test, the cell potential eventually returns to a negative value, and approaches the original potential.

Slight differences in the surface chemistry of the electrodes, particularly surface functional groups, is a possible cause of the resting potential. For example, Nakamura *et al*. [1], showed the resting potential of activated carbon increases with higher oxygen content, and acid functional groups. The resting potential, although persistent, is small (< 1%) compared to the voltage involved in the test process. As will be described in the following chapter, the resting potential is modelled by setting the initial voltage of the ECM capacitors to the measured resting potential.

6.1.2 CHARGE

In the charge phase, a voltage is applied across the cell in series with resistor R_{Charge} as illustrated in Figure 6.4. As the cell acts primarily as a capacitor, the cell potential rises in an exponential manner. As with any capacitor, electronic charge will accumulate on the electrodes during this period. In addition, charges will move inside the membrane, as the hydrogen ions will move

toward the negatively charged electrode. The rise in the stack voltage is not a pure exponential function, as the fuel cell, (like a DLC) does not behave as an ideal capacitor.

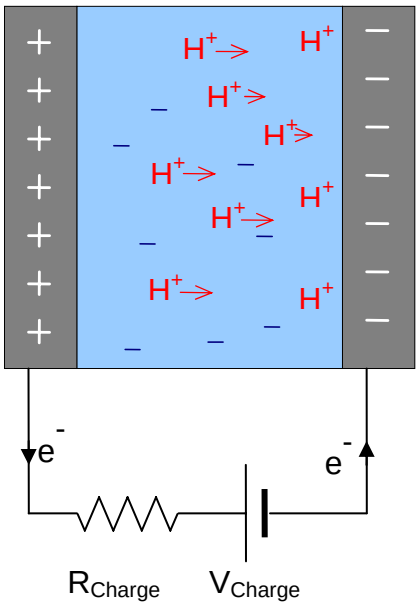

Figure 6.4 Charge Phase of the Test Protocol

6.1.3 NATURAL DECAY

During the decay phase, the voltage source is disconnected (S_1 opened) and the cell remains at open circuit. The potential of the cell clearly decays during this time. There are two processes thought to be responsible for the observed decay; leakage current, and ion movement in the membrane.

The leakage current of a DLC is well documented. Due to the physical similarity between a fuel cell and a DLC, it is postulated that leakage current also occurs in the fuel cell. As described in Section 3.3.1, the mechanism by which current leaks through a DLC has not been stated in the literature, thus a number of mechanisms are considered for the fuel cell. Direct electronic conduction across the cell is most likely, occurring through a defect in the membrane electrode assembly (MEA) or through the surrounding cell assembly. This is shown in Figure 6.5a. Alternatively, as oxygen is present at both electrodes, and dissolved in the water present in the membrane, electrochemical reactions could occur at the positive and negatively charged electrode, shown in equation 6.1, resulting in a net current flow across the cell.

$$H_2O \rightarrow \tfrac{1}{2}O_2 + 2e^- + 2H^+ \text{ and } \tfrac{1}{2}O_2 + 2e^- + 2H^+ \rightarrow H_2O \qquad 6.1$$

This reaction is shown schematically in Figure 6.5b, where the electrons are supplied/consumed by the negatively/positively charged electrode, rather than from an external circuit.

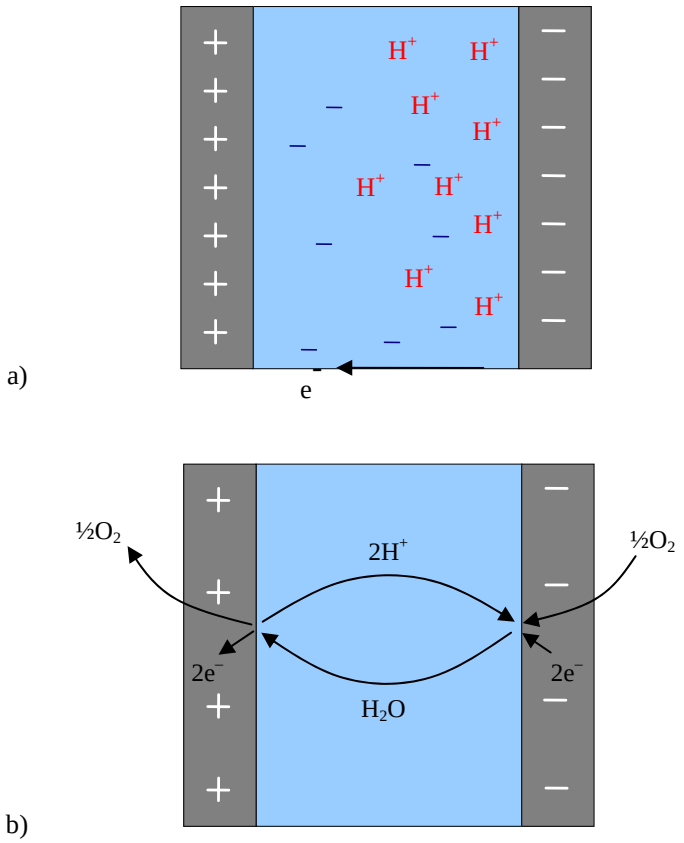

Figure 6.5 Leakage Current Caused by Electronic Conduction (a) and Electrochemical Reactions (b)

Andreaus et al. [2], [3], have documented a similar reaction to that shown in Figure 6.5b. However, instead of oxygen being present at the electrodes, Hydrogen was present, and the cell was operated as a hydrogen pump using an applied potential. If hydrogen was present at the electrodes of a cell undergoing a passive test, then it may provide another mechanism for the discharge of the cell during an open circuit phase.

Although the reaction shown in equation 6.1 is theoretically possible, it is not thought to occur to a significant degree. As described in Section 2.3.1 the oxygen reaction involves a large activation loss. Considering the low potential across the cell, the activation loss would be a significant barrier to the reaction.

Movement of hydrogen ions (H^+) towards the negatively charged electrode would also result in a potential decay. This process can be compared with phenomena known to occur in a DLC. As described in Section 3.3.1, after a DLC is charged, the initial decrease in potential is attributed to continued ion movement, primarily at the electrode-electrolyte interface. The transmission line

model of an electrode-electrolyte interface was considered in explaining the phenomenon, and the resulting decline in the potential. A more detailed explanation of how ion movement affects the potential of the cell is provided in Section 6.1.5, where the Self Recharge region of the results is discussed.

In summarising the decay region, two possible phenomena are considered; leakage current, and hydrogen ion movement in the membrane. If not for the other testing regions, the voltage in Figure 6.1 appears to approach zero, therefore, the decay is primarily attributed to leakage current.

6.1.4 DISCHARGE

During the discharge period, S_2 is closed, and the cell dissipates the accumulated charge through a resistor, $R_{Discharge}$. The resistance of $R_{Discharge}$ is small (~10Ω), thus, nearly all of the charge is removed from the electrodes during the discharge period of the test protocol. The potential decays rapidly in an exponential manner during discharge, as expected with any capacitor. Together with electronic charge being removed from the electrodes, the hydrogen ions will move from the negatively charged electrode and take up a more homogenous position in the membrane, as shown in Figure 6.6.

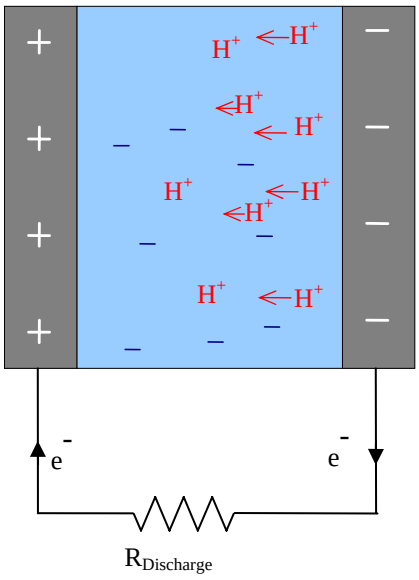

Figure 6.6 A Single Cell Undergoing the Discharge Phase of the PSDB Test Protocol

6.1.5 SELF RECHARGE

After the $R_{Discharge}$ is disconnected from the cell, Figure 6.1 shows the potential rising then declining as in the natural decay region. Clearly, charges are still moving during this period, giving rise to the self-recharge behaviour. Continued movement of the hydrogen ions is thought to be the primary cause of the self-recharge behaviour. At the end of the discharge region, most of the charge on the electrodes has been dissipated with the potential approaching zero. However, due to the relatively high ionic resistance of the membrane, the hydrogen ions will still be non-uniformly distributed within the membrane. Therefore, at the end of the discharge step, the ions will continue to move away from the electrode that held a negative charge, as is shown in Figure 6.7.

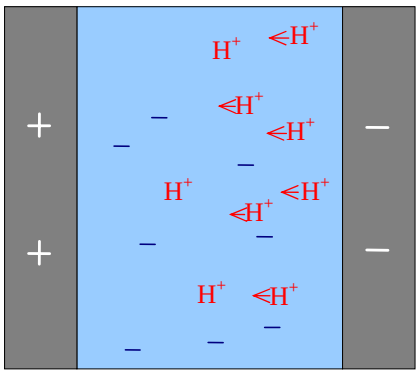

Figure 6.7 Ion Movement During the Self-Recharge Step

Exactly how the movement of ions results in a measured potential decrease is explained based on the equivalent circuit model (ECM) for a passive fuel cell proposed in Section 4.3. The model was constructed using one capacitor representing the charge held by the electrodes, and one capacitor representing the increased capacitance due to the dielectric property of the membrane. The membrane is considered to possess a variable dielectric value depending on the position of the hydrogen ions within it. For instance, the closer the ions are to the negative electrode, assuming a fixed charged on the electrode, the higher the dielectric value. Therefore, if a fixed charge remains on the electrodes, and the dielectric value of the membrane decreases due to hydrogen ion movement, the voltage across the cell will increase.

Using a simple mathematical consideration of the fuel cell and its capacitive properties, the predicted voltage rise can be shown. Equations 6.3 and 6.4 show the governing equations for an ideal parallel plate capacitor [4].

$$Q = CV \tag{6.3}$$

$$C = \frac{\varepsilon_0 \varepsilon_r A}{d} \tag{6.4}$$

C = capacitance [F]

V = voltage [V]

Q = charge [C]

A = surface area [m^2]

d = distance between the two plates/electrodes [m]

ε_0 = permittivity of the vacuum [$C^2/N \cdot m^2$]

ε_r = relative permittivity of the dielectric material

Consider the cell at time t and $t + \Delta t$, both of which are during the self-recharge phase. During the time interval, Δt, the ions continue to move away from the negatively charged electrode. Thus, in the time Δt, the relative permittivity of the membrane, ε_r, will decrease by a finite amount, say $\Delta\varepsilon_r$. Therefore, assuming the same amount of electronic charge, Q, remains on the electrodes, the voltage across the cell at time t and time $t + \Delta t$ is given by equations 6.5 and 6.6.

$$V(t) = \frac{Qd}{A\varepsilon_0 \varepsilon_r} \tag{6.5}$$

$$V(t + \Delta t) = \frac{Qd}{A\varepsilon_0 (\varepsilon_r - \Delta\varepsilon_r)} \tag{6.6}$$

Therefore, the change in voltage, in the time Δt is given by equation 6.7

$$\Delta V = V(t + \Delta t) - V(t)$$

$$= \frac{Qd}{A\varepsilon_0 (\varepsilon_r - \Delta\varepsilon_r)} - \frac{Qd}{A\varepsilon_0 \varepsilon_r}$$

$$\Delta V = \frac{Qd\Delta\varepsilon_r}{A\varepsilon_0 \varepsilon_r (\varepsilon_r - \Delta\varepsilon_r)} \tag{6.7}$$

Which is a voltage increase as expected. After a maximum is reached, the voltage begins to decline, caused by leakage current through the cell as detailed in Section 6.1.3.

6.1.6 SUMMARY OF SINGLE CELL BEHAVIOUR

By measuring the transient voltage response of the cell, features related to the cell physical structure are revealed such as the movement of ions and the capacitance of the cell. In order to analyze the behaviour quantitatively, an analysis using the equivalent circuit model is provided in Chapter 8, with the method used to identify the circuit parameters described in Chapter 7. Although the discussion in the above Section is based on the results of one cell only, the same behaviour is exhibited by other cells tested, and shown in the following Section.

6.2 SINGLE CELL TESTING OF MERCORP, ENABLE AND AVISTA CELLS

The PSDB test was conducted on many individual cells from each fuel cell stack. Figures 6.8, 6.9 and 6.10, show typical results obtained from the Enable, MerCorp and Avista cells.

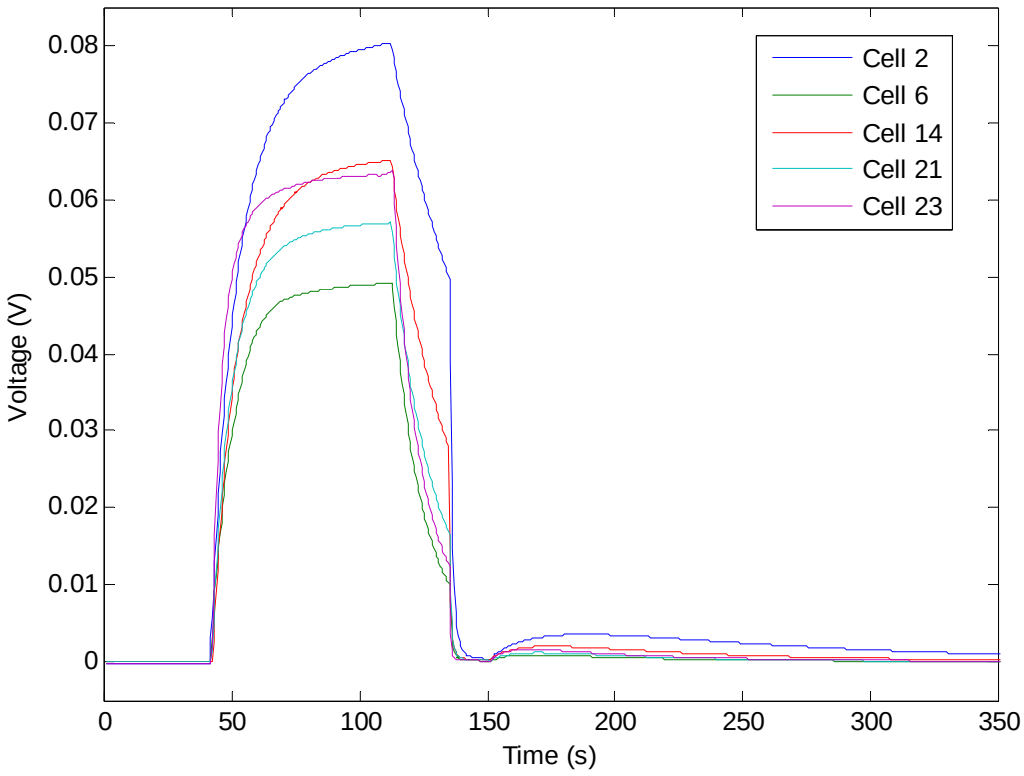

Figure 6.8 PSDB Test Results when Implemented on Single Cells in the Enable Stack; Test Circuit Values: V_{Charge} = 108mV, R_{Charge} = 98.4Ω and $R_{Discharge}$ = 5.6Ω

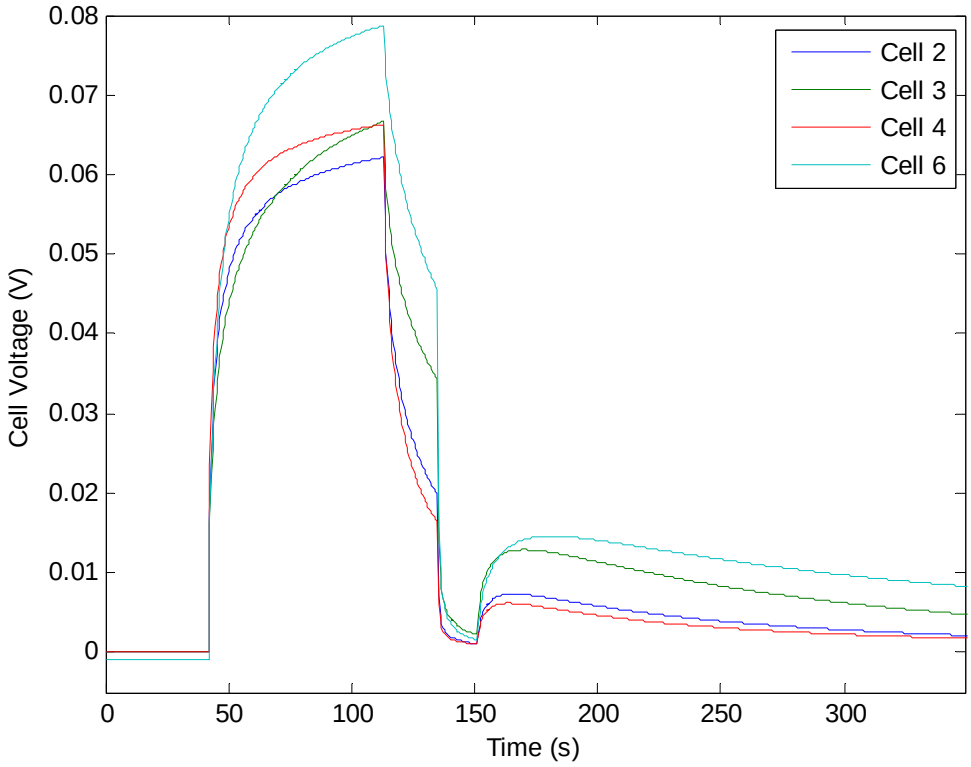

Figure 6.9 PSDB Test Results when Implemented on Single Cells in the MerCorp Stack; Test Circuit Values: V_{Charge} = 101mV, R_{Charge} = 100Ω and $R_{Discharge}$ = 6.1Ω

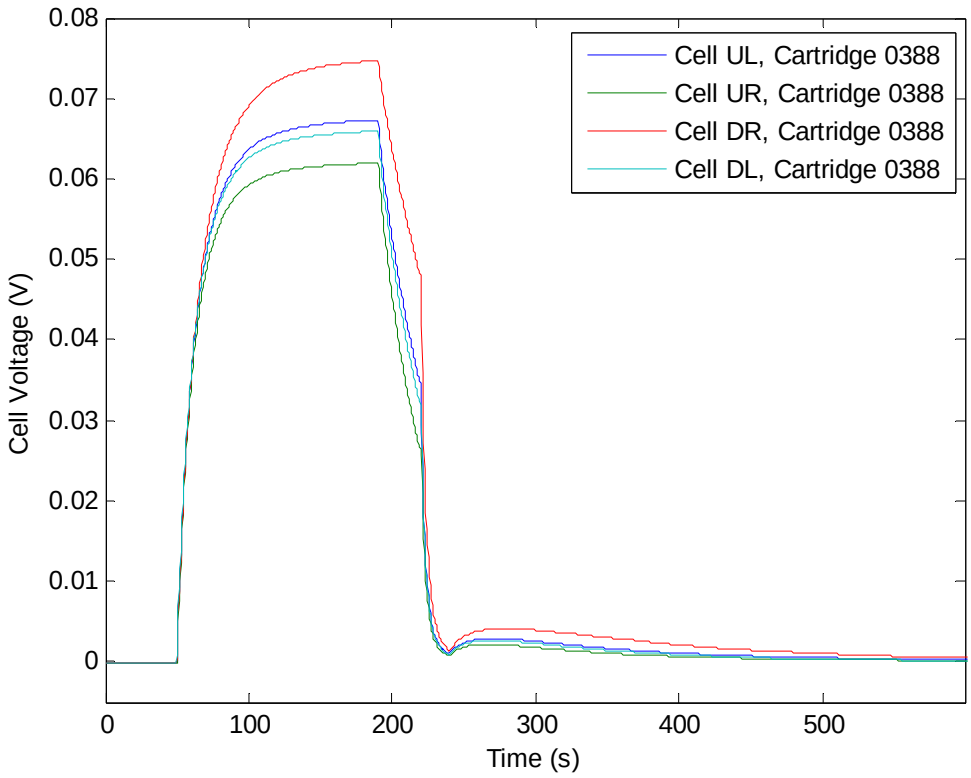

Figure 6.10 PSDB Test Results when Implented on Single Avista Cells; Test Circuit Values: V_{Charge} = 101mV, R_{Charge} = 53.3Ω and $R_{Discharge}$ = 10.1Ω

Each voltage transient in Figures 6.8 – 6.10, exhibits the same basic behaviour, with the distinct charge, decay, and recharge behaviour being present. For a given fuel cell stack, the voltage response of each cell is slightly different, despite being subjected to exactly the same test process because each cell possesses slightly different electrical properties.

In order to test an entire stack, individual tests could be carried out on each cell. However, this may be impractical in an application setting. The time to test an entire stack may become significant, considering a single test takes around 300s, and a stack may contain 80 cells. In addition, an isolated test signal is required for each cell, i.e. a set of test circuit terminals must be attached to each cell. An ideal testing procedure for an application setting is one where all cells can be tested simultaneously. The following section discusses how the PSDB test protocol is implemented on a stack, and the resulting voltage behaviour of the cells.

6.3 STACK RESULTS TO THE PSDB TEST

The PSDB test method can be used to test an entire stack, simply by attaching the test circuit across the stack terminals. By monitoring the individual cell voltages, every cell in the stack is tested simultaneously. Figure 6.11 shows the results of a typical stack test.

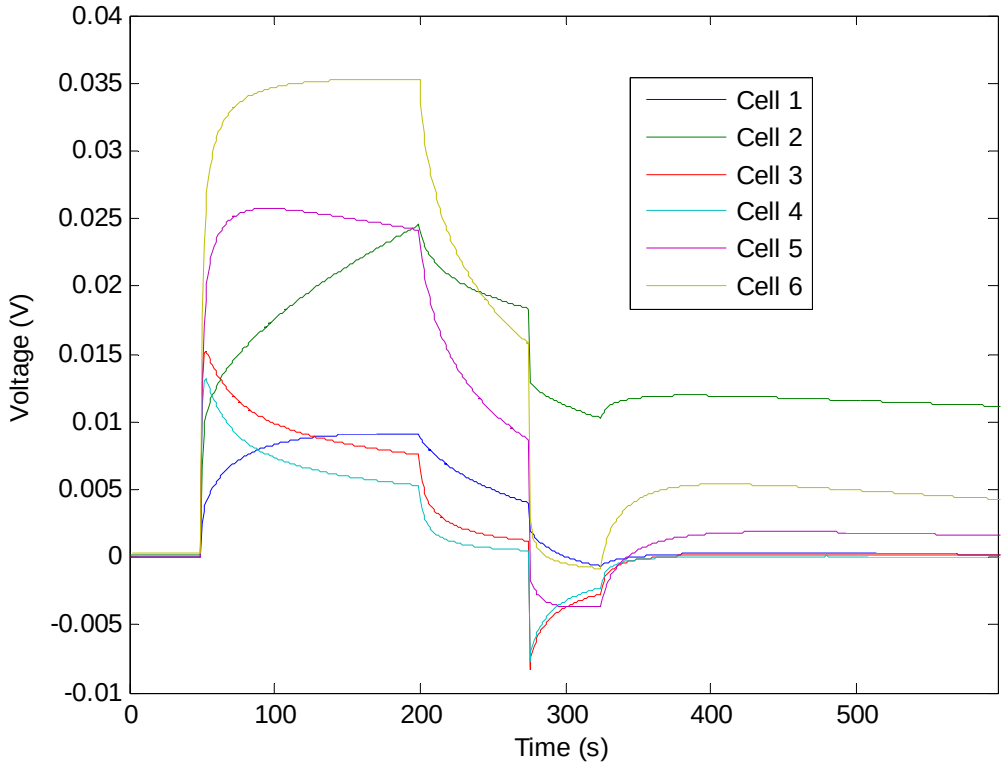

Figure 6.11 MerCorp PSDB Test Results Showing Individual Cell Behaviour; Test Circuit Values: V_{Charge} = 116mV, R_{Charge} = 99.8Ω and $R_{Discharge}$ = 4.7Ω

The variations in electrical properties of each cell, together with the electrical interaction of the cells during the test, results in each cell producing a significantly different voltage transient. The interconnected cells have a dynamic inter-relationship, which effectively results in each cell being subjected to a different charge/discharge pattern as reflected in the voltage responses. The undershoot and overshot transients exhibited by some cells is a stack phenomena, rather than properties of individual cells. Significant overshoot and undershoot as shown in figure 6.11 is a result of stack imbalance i.e. electrical properties of each cell are significantly different. The stack voltage (the sum of all cells) is shown in Figure 6.12 for the same test.

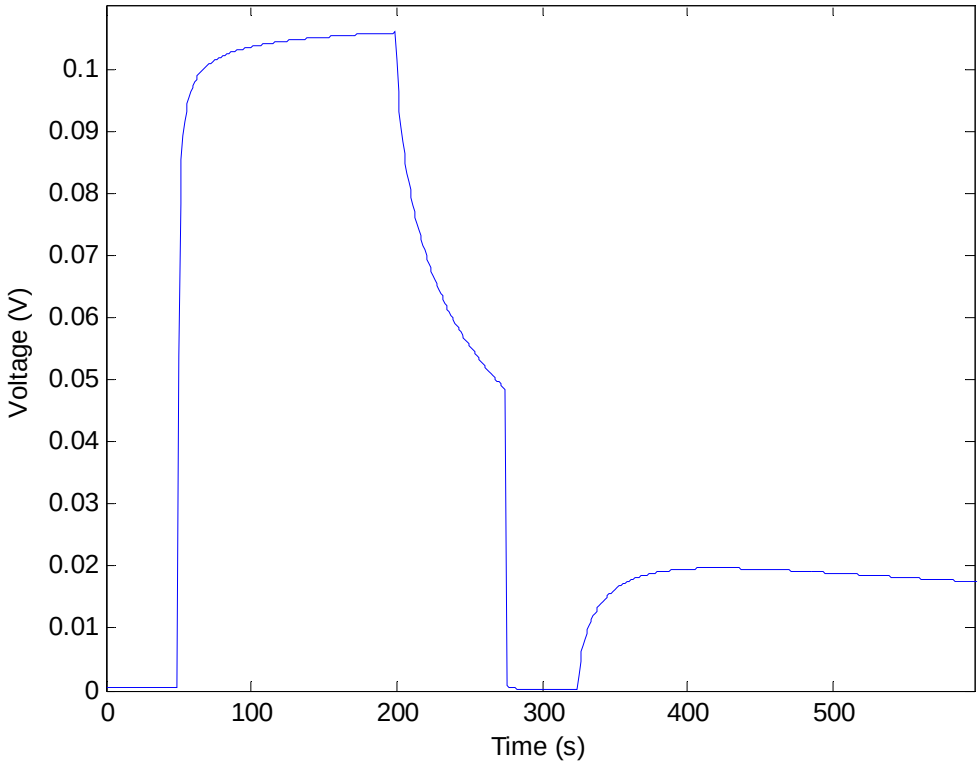

Figure 6.12 MerCorp Stack PSDB Test Showing Stack Terminal Behaviour

As predicted in Section 4.3.3, the stack voltage response has a similar pattern to a single cell, exhibiting the same charge, decay, discharge and self-recharge behaviour. Figure 6.14 and Figure 6.15 show the cell and stack voltage behaviour of the Enable and Avista stacks. For clarity, only 5 (of 23) cells are shown for the Enable results in Figure 6.13a.

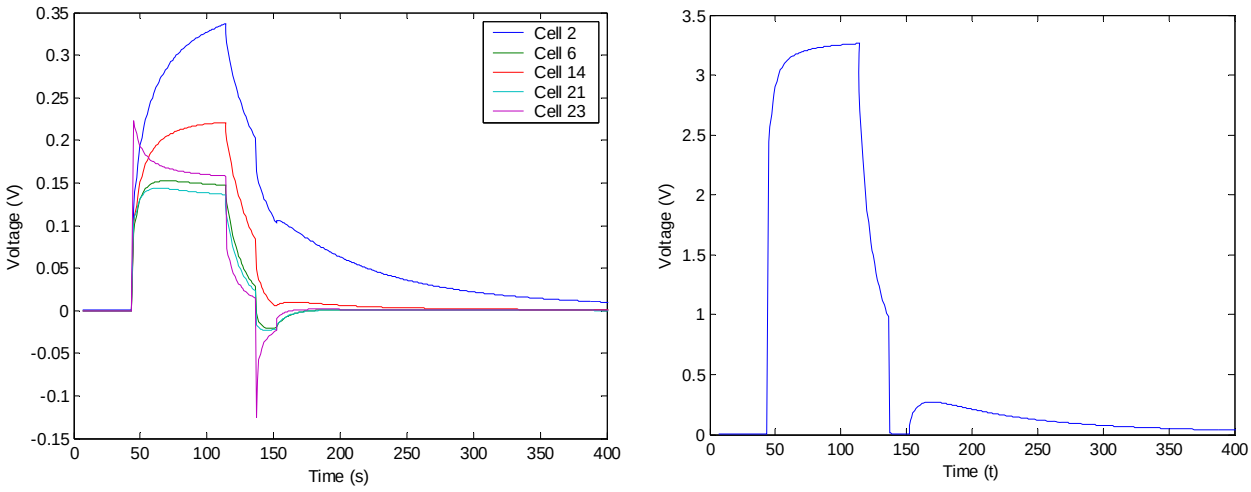

a) **b)**

Figure 6.13 Enable Stack PSDB Test Showing the Behaviour of Indiviudal Cells (a) and the Stack Terminal (b); Test Circuit Values: V_{Charge} = 4.001V, R_{Charge} = 98.4Ω and $R_{Discharge}$ = 5.5Ω

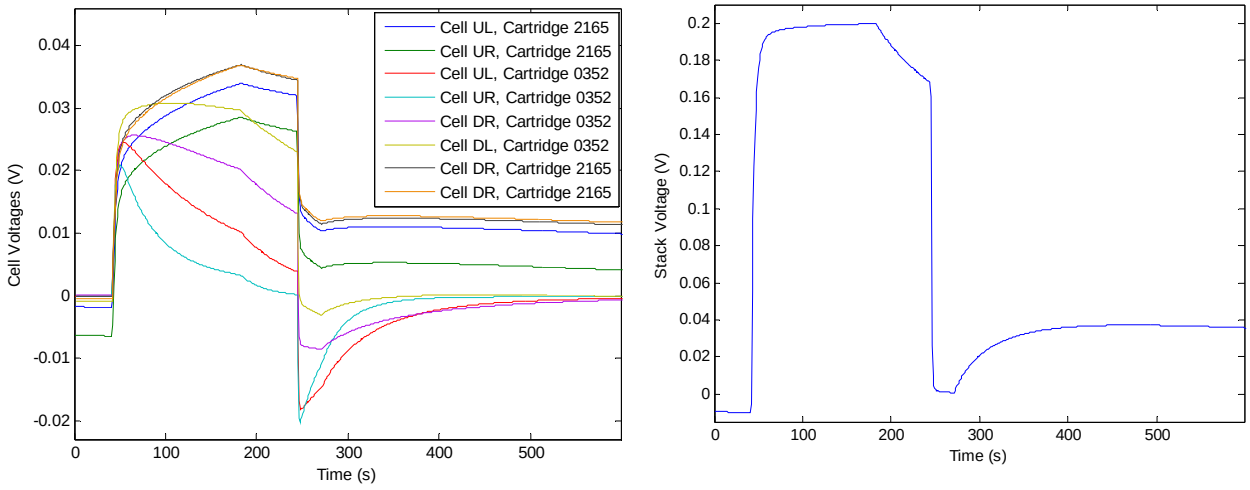

a) **b)**

Figure 6.14 Avista Stack PSDB Test (2-cartridges) Showing Individual Cell Behaviour (a) and Stack Terminal Behaviour (b); Test Circuit Values: V_{Charge} = 200.2mV, R_{Charge} = 53.1Ω and $R_{Discharge}$ = 9.9Ω

The Avista stack results shown in Figure 6.14b are particularly interesting, as a clear difference between cartridge 2165, and cartridge 0352 is observed. One of the main differences is the rate of voltage decay immediately after the charge step. For cells in cartridge 0352, the rate of voltage decay is much higher, indicating a higher leakage current than the cells in cartridge 2165. Many pairs of Avista cartridges were tested in this manner, with a clear difference between the cells in each cartridge. A simple way of quantifying the different voltage responses is to measure the voltage decay rate at beginning of the decay region. Figure 6.15 shows the decay rate for each cell in the 14 cartridges tested.

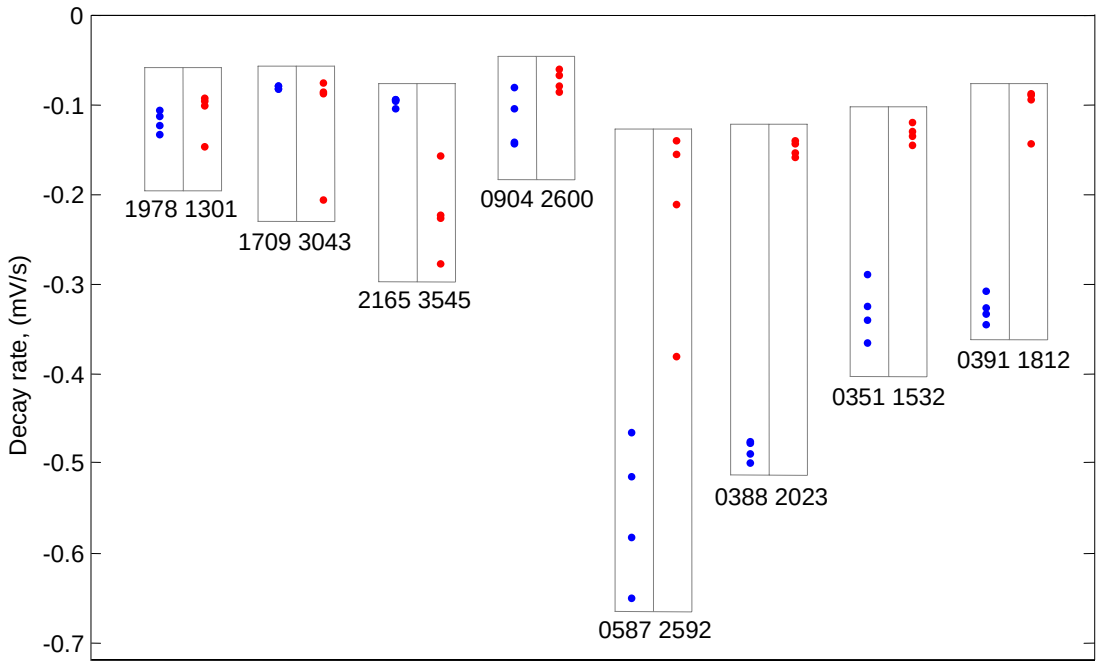

Figure 6.15 Voltage Decay Rate Measured at the Beginning of the Decay Region of the PSDB Test, Catridges Tested in Pairs; Test Cicuit Paramters: V_{Charge} = 304mV, R_{Charge} = 52.6 Ω, and $R_{Discharge}$ = 10.1Ω

The difference in voltage responses between the cells, as measured by the decay rate is most noticeable when the cells are from a cartridge having a serial number beginning with a zero, i.e. cartridges 0587, 0388, 0351 and 0391. The cells of these cartridges most often possessed a steeper decay rate than the cells in other cartridges. The cause of this difference is believed to originate from the age and physical composition differences in the cartridges. The Avista cartridges constantly went through improvements as more were produced, thus cartridges having a high serial number, are newer, and more advanced than those with a low serial number [5].

As stated, the voltage transient of cell is governed not only by the electrical properties of the cell, but that of the fuel cell stack. It is conceivable that the position of a cell within the stack may influence the voltage transients. If this were the case, the comparative analysis conducted above would not be valid. The following section experimental investigates the impact of cell order on the measured voltage response of a stack subjected to the PSDB test.

6.3.1 Influence of Cell Configuration

The cells within an Avista cartridge are edge current collected, and are connected externally in order to form a stack. This allows a stack to be formed with the cells in a number of different

configurations. Figure 6.15 shows a schematic of two Avista cartridges, connected in two different configurations, a and b. Configuration b is achieved by interchanging the positions of the cartridges, and rotating cartage 0578 by 180^{o} compared with configuration a.

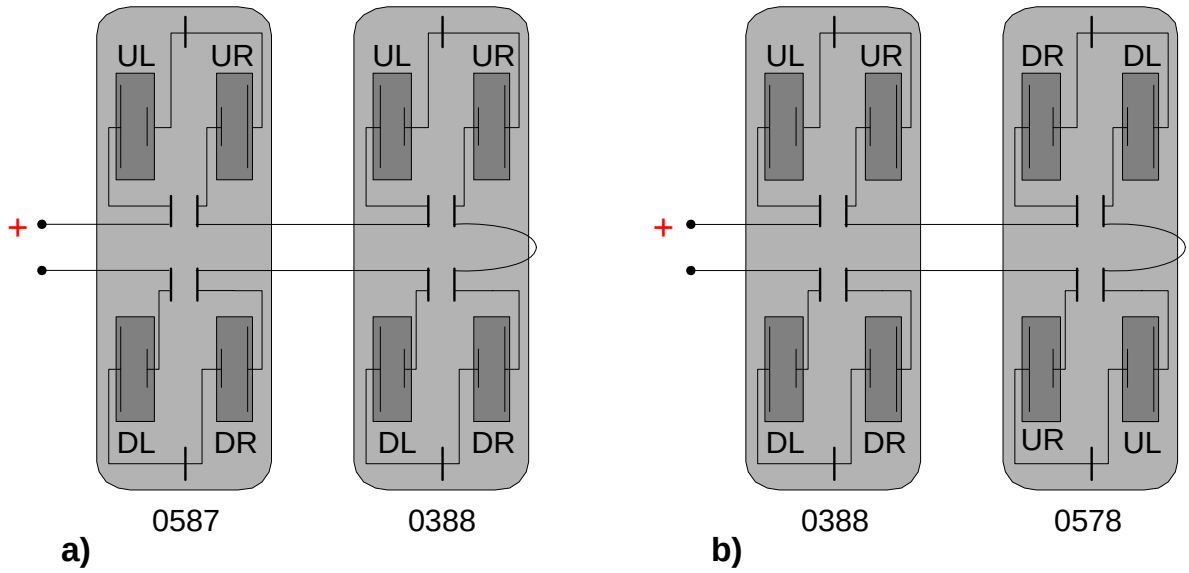

Figure 6.16 Two Avista configurations used

The two configurations show in Figure 6.16 result in the cells having the following series connection order.

a) + **0587** UL – **0587** UR – **0388** UL – **0388** UR – **0388** DR – **0388** DL – **0587** DR – **0587** DL –

Alternatively labelled + 1 – 2 – 3 – 4 – 5 – 6 – 7 – 8 –

b) + **0388** UL – **0388** UR – **0587** DR – **0587** DL – **0587** UL – **0587** UR – **0388** DR – **0388** DL –

Alternatively labelled + 3 – 4 – 7 – 8 – 1 – 2 – 5 – 6 –

Figure 6.17 shows the results of a PSDB test conducted on the stack in both configurations.

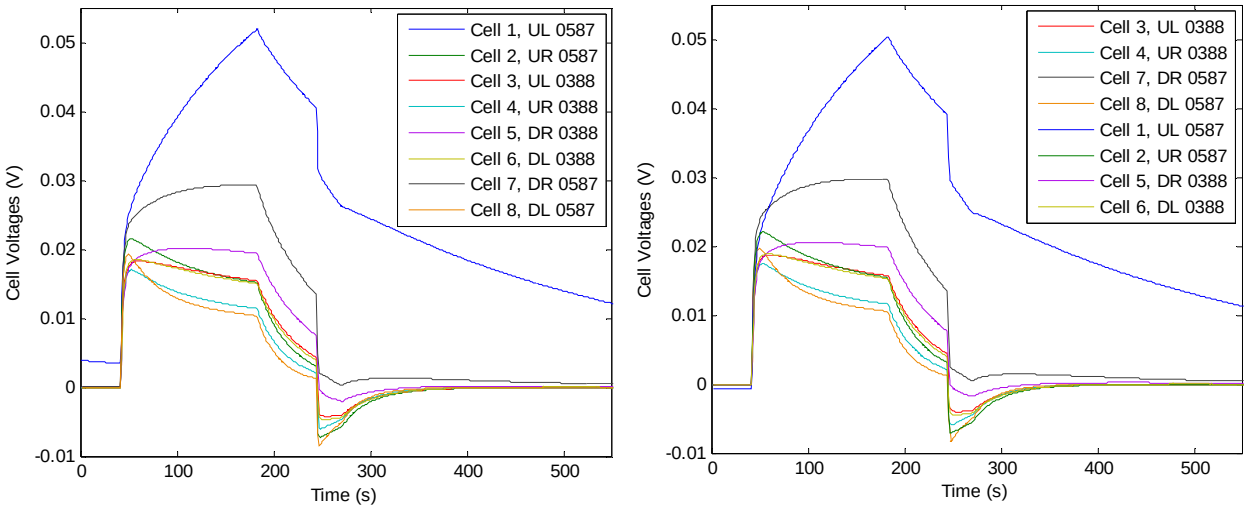

a) b)

Figure 6.17 Avista Stack Test Results Using Different Series Connection Arrangements; Test Circuit Values; V_{Charge} = 175mV, R_{Charge} = 101Ω and $R_{Discharge}$ = 9.9Ω

Clearly, from Figure 6.17, the cell order plays no part in the voltage response of each cell. Therefore, using features of individual cell results, such as the voltage gradient in the previous section, is a valid method for comparing cells, and potentially forming conclusions about their relative functionality. In addition, the measured voltage transients are almost identical for each test, evidence of the repeatability of the PSDB test.

6.4 CONCLUSION

The fuel cell response to the PSDB test protocol has been qualitatively described in this chapter. The results of a single cell test have been described in detail, with reference given to the physical processes occurring in the cell. The characteristic response was found to be the same for different cells within a stack, and for cells from different stacks. When individual tests were conducted on many cells from the same stack, slight variations between the results were evident. These variations, together with cells interacting with one another, caused large variations in the cell voltage response when a stack is subjected to the passive test protocol. The order in which the cells are connected to form a stack was shown to have no effect on the results of a stack test. In order to analyse the results quantitatively, the ECM proposed in Chapter 4 will be used. However, a method to determine the circuit parameter values is first required, and is the topic of the following chapter.

6.5 REFERENCES

[1] Nakamura M, Nakanishi M, Yamamoto K, “Influence of physical properties of activated carbons on characteristics of electric double-layer capacitors”, Journal of Power Sources, Vol. 60, pp. 225-231, Jun. 1996

[2] Andreaus B, McEvoy AJ, Scherer GG, “Analysis of performance losses in polymer electrolyte fuel cells at high current densities by impedance spectroscopy”, Electrochimica Acta, Vol. 47, pp.2223-2229, May 2002

[3] Andreaus B, Scherer GG, “Proton-conducting polymer membranes in fuel cells - humidification aspects”, Solid State Ionics, Vol. 168, pp. 311-320, Mar. 2004

[4] Halliday D, Resnick R, Walker J, “Fundamentals of physics” 5th ed. New York, Wiley 1997

[5] Gerry Snow, ReliOn Product Manager, Personal Communications, Spokane, WA. Aug. 2004

7 DETERMINATION OF CIRCUIT PARAMETER VALUES

This chapter describes the technique developed for determining the circuit parameter values of the passive equivalent circuit model (ECM). As described in Chapter 3, existing techniques can only be applied in the case of individual cell testing and analysis. The technique described allows the circuit parameter values of many cells to be obtained from a single stack test.

The method is described in Section 7.1, with Sections 7.2 and 7.3 detailing the software and programming. Section 7.4 provides a verification of the results obtained, and includes a sensitivity analysis. Section 7.5 discusses further aspects of the fitting technique, with Section 7.6 examining optimization possibilities. A summary is provided in Section 7.7.

7.1 METHOD

The method is described for the single cell case. Determining ECM parameters of multiple cells is discussed in Section 7.2 and 7.3, where the details of the software and programming are provided. Therefore, for a single cell, the ECM parameter values, P_i that need to be determined are shown below.

$$P_i = \begin{bmatrix} R_a & R_b & C_a & C_b \end{bmatrix} \tag{7.1}$$

In addition, the voltage across both ECM capacitors, C_a and C_b, at the beginning of the test, t = t_0 is required.

$$V_{Cj} = \begin{bmatrix} V_{C_a} & V_{C_b} \end{bmatrix} \tag{7.2}$$

The strategy used for determining the values is outlined in Figure 7.1.

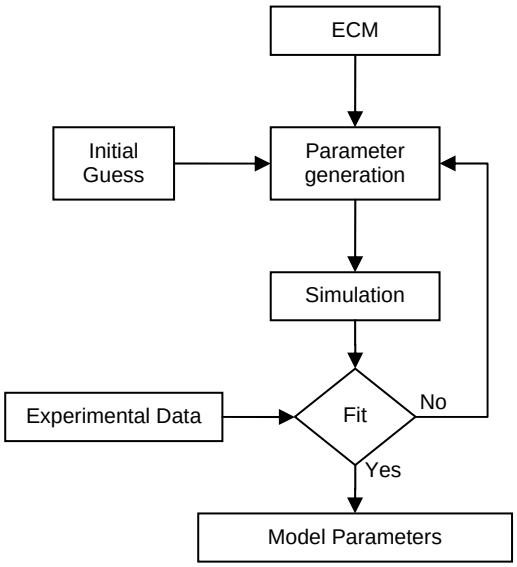

Figure 7.1 Overview of the Fitting Method Used for Determining the Circuit Paramter Values of the ECM

The circuit parameter values are determined by fitting the voltage response of the ECM, $V_S(t_n)$, to the measured cell response, $V_E(t_n)$, when subject to the passive state dynamic behaviour (PSDB) test. Starting with an initial guess for P_i and V_{Cj}, an iterative fitting routine is employed where each circuit parameter is modified in sequence to improve the fit. The fit is evaluated as the least squares difference between the voltage response of the ECM, $V_S(t_n)$ and the experimental fuel cell response, $V_E(t_n)$ as shown in equation 7.3.

$$\sigma = \left\{ \sum_n \left(V_E(t_n) - V_S(t_n) \right)^2 \right\}^{1/2} \qquad \text{where time index } t_n = 0 \quad 1 \quad 2 \quad .... \quad 500 \qquad 7.3$$

A solution for P_i and V_{Cj} is found when the error, σ is minimised subject to a tolerance on the circuit model parameters. This tolerance is defined in equation 7.4

$$\sigma\big|_{P_i} < \sigma\big|_{P_i \pm tol} \forall i \quad \text{and} \quad \sigma\big|_{V_{Cj}} < \sigma\big|_{V_{Cj} \pm tol} \forall j \qquad 7.4$$

Essentially, the error is minimised, hence a solution has been found, when a further change in any P_i or V_{Cj} by the tolerance value results in an increased error. The tolerance value was typically set at 0.1%, thus a solution is found when a change in any of the circuit parameters of

±0.1% resulted in a larger error. The iterative process used for finding the values such that equation 7.4 is satisfied, is explicitly described below.

An initial guess for P_i and V_{Cj} is defined, with each individual value being modified in sequence. For instance, take P_1. A number of other values for P_1 in the neighbourhood of the original value are generated by multiplying the original value by a neighbourhood vector, N_k as shown below.

$$P_{1,k} = P_1 N_k \tag{7.5}$$

$$N_k = \left[1-10^2 tol \quad 1-10tol \quad 1-tol \quad 1 \quad 1+tol \quad 1+10tol \quad 1+10^2 tol\right] \tag{7.6}$$

The $P_{1,k}$ values generated included the original value (k = 4), the original value ± the tolerance (k= 3, 5) and 4 additional values, which differ from the original P_1 by 10 and 100 times the tolerance value.

For each $P_{1,k}$, the error, σ_k between the voltage response of the ECM, $V_S(t_n)_k$ and experimental data $V_E(t_n)$ is evaluated as shown in equation 7.7. In practice, a slightly modified error value is calculated (described in Section 2.3.1.2), in order to reduce the propagation of errors present in experimental data.

$$\sigma_k = \left[\sum_n \left(V_E(t_n) - V_S(t_n)_k\right)^2\right]^{1/2} \tag{7.7}$$

The values of V_{Cj} and the other values of P_i are held constant for each $V_S(t_n)_k$. A new value of P_1 is assigned, using the $P_{1,k}$ value that resulted in the smallest error, σ_k. The next P_i value is selected, P_2, and the process is repeated. A full iteration is completed when each P_i and V_{Cj} value has been reassigned. This process is repeated until σ_k is the smallest when k = 4 for every P_i and V_{Cj}. Thus equation 7.4 is satisfied.

The software program used for generating the voltage response of the ECM is described in Section 7.3, with Section 7.4 describing details of the iterative fitting technique.

7.2 SIMULATION MODEL

The voltage response of the ECM to the applied test protocol, $V_S(t_n)$ is generated using PLECS V1.0.9, (Plexim™ GmbH). PLECS is a linear piece wise circuit simulation program that operates in the MATLAB Simulink environment. PLECS contains a multitude of circuit elements, allowing the test circuit and the ECM of a fuel cell stack to be modelled as shown in Figure 7.2.

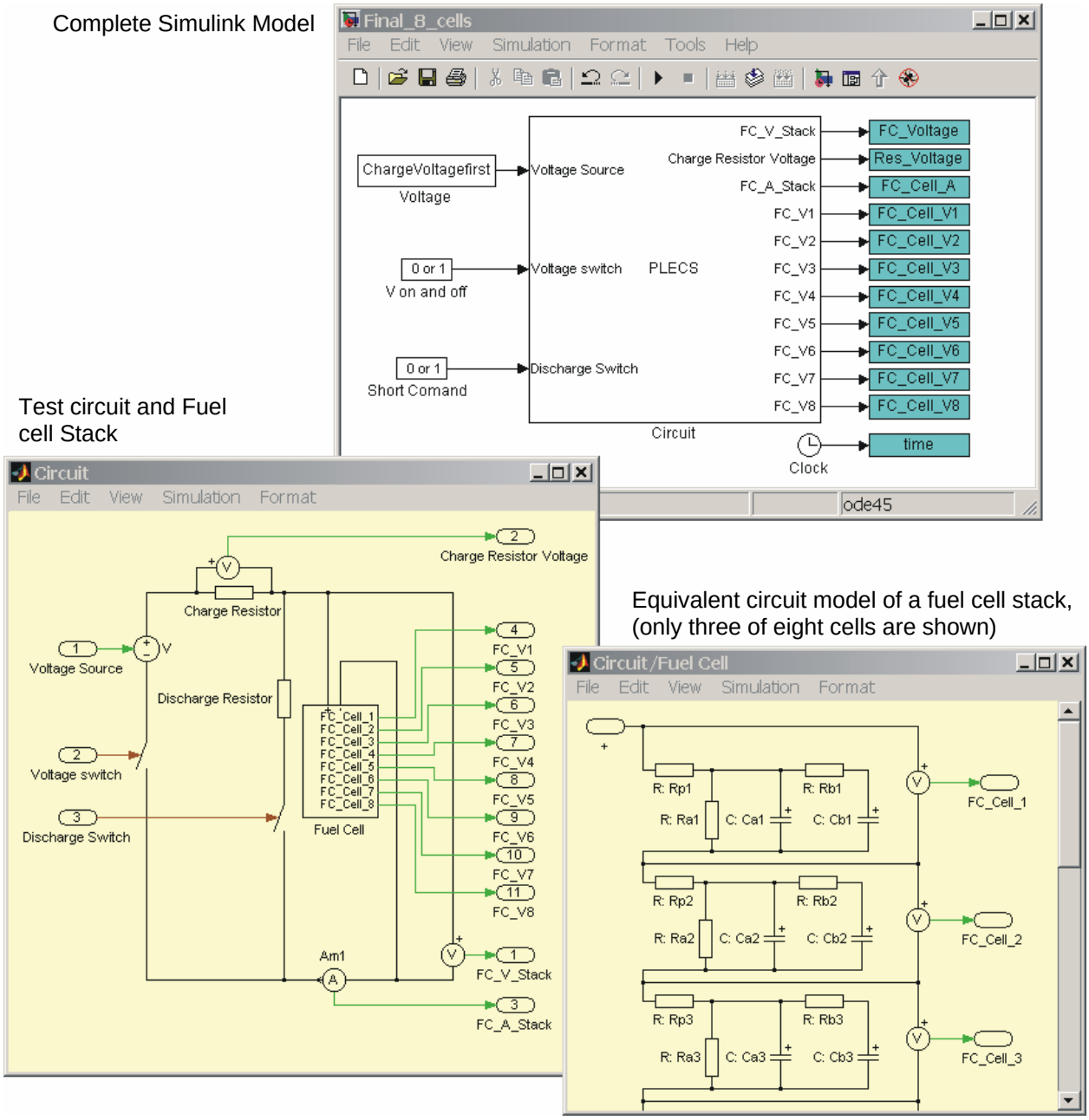

Figure 7.2 Fuel Cell Stack ECM and Passive Test Circuit Simulated using MATLAB Simulink and PLECS

All model parameter values and the test protocol conditions are defined in a separate script file (**`fitting_algorithm.m`**). The simulation results are obtained by calling the model file (**`Fuel_Cell_ECM.mdl`**) from the script. Effectively, the Simulink/PLECS model acts as a function; the inputs are the ECM parameter values, and the outputs are cell voltage transients.

7.3 ALGORITHM

The iterative routine, as described in Section 7.1, is programmed in MATLAB using a single script file (**`fitting_algorithm.m`**). The circuit parameter values, P_i and the capacitor voltage values, V_{Cj} are treated separately, due to the particular values of $V_S(t_n)$ and $V_E(t_n)$ used to evaluate the error, σ. Therefore, the algorithm script file is composed of three main elements; initialization, circuit component loop and initial capacitor voltage loop. An overview of the algorithm is shown in Figure 7.3a. The following subsections detail the three main parts of the algorithm; Initialization, Circuit component loop and Initial capacitor voltage loop.

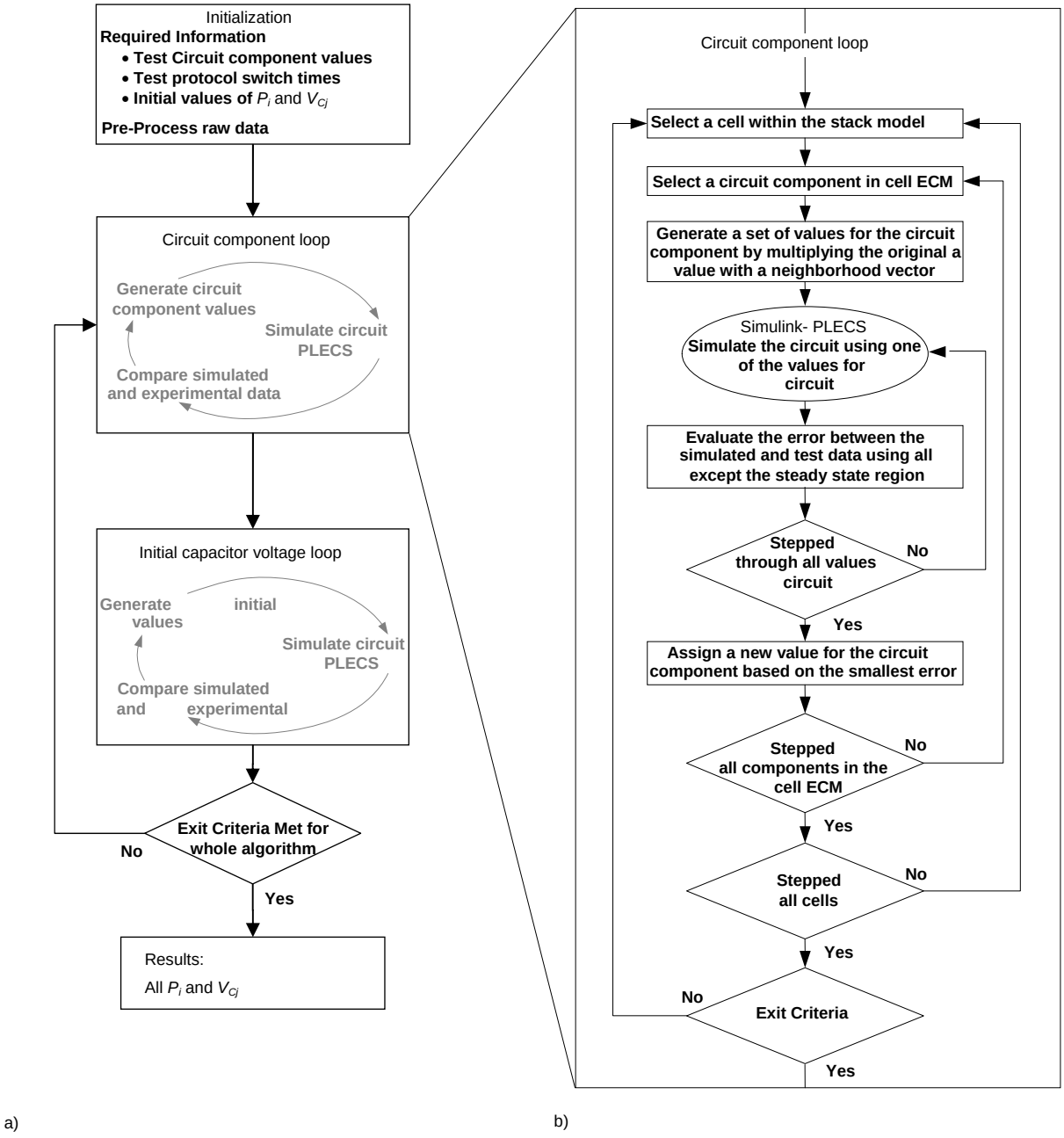

Figure 7.3 Overview of the Algorithm Used for Finding Circuit Parameter Values (a), and Details for Finding the Circuit Parameter Values (b)

7.3.1 INITIALISATION

During the initialisation step, data is loaded into the Matlab workspace, raw data is pre-processed and a number of fitting details, such as the tolerance values and neighbourhood vectors are defined. All conditions of the PSDB test protocol must be known and defined, i.e. the switch times ($T_1 – T_4$), and the test circuit values (V_{Charge}, R_{Charge} and $R_{Discharge}$). If the ECM parameter values for many cells are to be determined from a stack test, the voltage transient produced from

each cell is required. Starting values (the first guess) of each circuit parameter must be defined including the initial voltage on each capacitor in the ECM. Before the iteration routine begins, the raw data is pre-processed, and the least squares error evaluation is precisely defined. The following two subsections described these two aspects detail.

7.3.1.1 RAW DATA PRE-PROCESSING

The least squares error between the simulated data, $V_S(t_n)$, and experimental data, $V_E(t_m)$, cannot be computed directly, as the voltage values for each data set are recoded at different times, i.e. time index $t_n \neq t_m$. All outputs from the Simulink model have a sampling rate fixed at 1 sample/s. Therefore, all voltage values from each cell are specified on the second, i.e. time index, $t_n = 1, 2, 3\ldots$. On the other hand, each experimental voltage measurement is recorded at a different time, as the digital multi meter contained in the data acquisitions switch unit can only measure the voltage on one channel (which is connected to one cell) at a time (see Figure 5.6). In order to compared the experimental and simulated data, and evaluate the least squares error, the experimental data set is modified such that all voltage values are defined on the second.

Figure 7.4 shows the raw experimental data of two cells, shown as ×. Clearly, each experimental data point occurs at a different time, as opposed to the simulated data (shown as •) which occur on the second. To obtain an experimental data set such that each voltage value is defined on the second, a 2^{nd} order polynomial was used to interpolate the raw data voltage values. The interpolated voltage values are also shown in Figure 7.4 as ○. The least squares difference is then evaluated between the interpolated and the simulated data values.

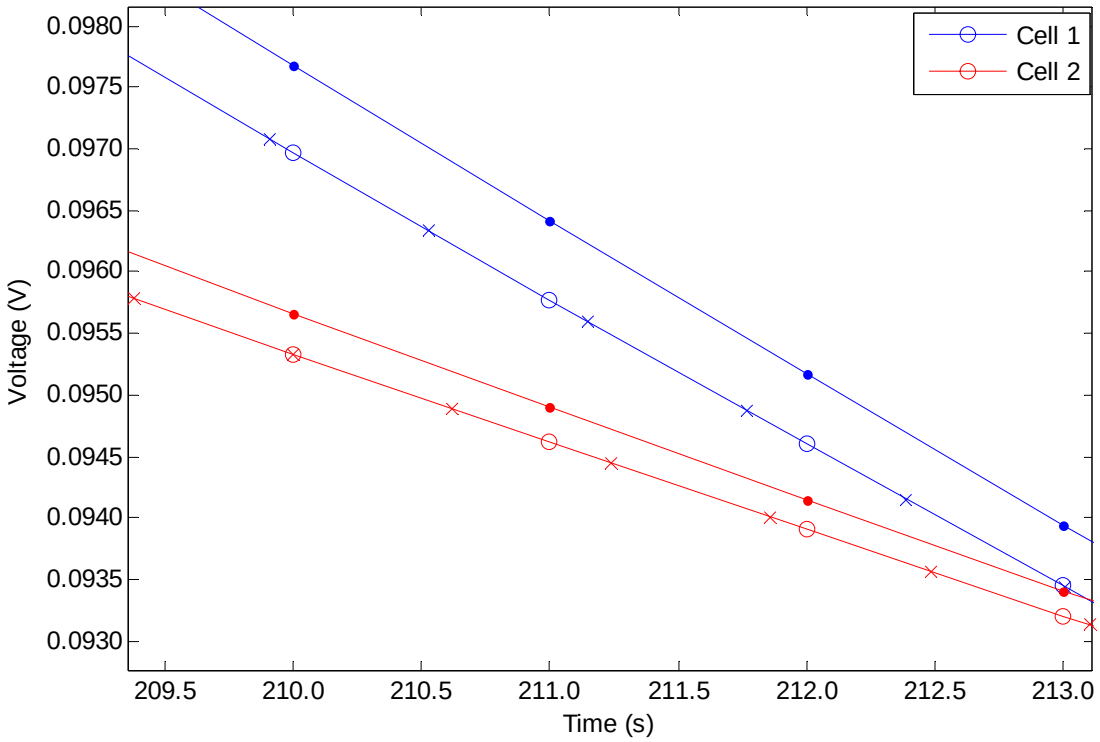

Figure 7.4 Experimental Data of Two Cells (×) with PLECS Model Simulation (•) and Interpolated Data (○)

The interpolation program is integrated into the fitting algorithm code, and is shown in Appendix II. As shown in Figure 7.4, the interpolated data values fall between the experiment data values as expected. However, this did not occur for each interpolated data value. At points of discontinuity, i.e. at the switching times, interpolated values in one region may have been calculated using experimental values in another region. Thus, when comparing simulated and interpolated data, only certain data values are used. The following section describes which sections (data values) are used for comparing the simulated and interpolated data sets, and calculating the error value, σ.

7.3.1.2 Least Squares Error Calculation Details

An even spread (in time) of data points cannot be used in calculating the error between the simulated and experimental (interpolated) data values. As the voltage response of a PSDB test contains regions of rapid voltage change, these regions will be preferentially fitted as the large errors present will dominate the sum of squares. Although the algorithm will converge, the solution may not adequately capture the cell response to the PSDB test. Therefore, the data

points used for comparing the experimental and modelled data (comparison points) do not include areas of rapid voltage change.

A simple vector, $CP(t_n)$ containing either ones or zeros, is used for including/excluding data points in the error calculation. Equation 7.8 defines $CP(t_n)$ such that data values close to the switch times are excluded, (due to interpolation errors), and areas of rapid voltage change are also excluded.

$$CP(t_n) = \begin{cases} 0 & \text{if} \quad T_p - 2 < t_n < T_p + 2 \\ 0 & \text{if} \quad T_1 < t_n < T_1 + 35 \\ 0 & \text{if} \quad T_3 < t_n < T_3 + 8 \\ 1 & \text{if} \quad \text{otherwise} \end{cases} \qquad \text{where the switch times } T_P = \begin{bmatrix} T_1 & T_2 & T_3 & T_4 \end{bmatrix} \qquad 7.8$$

Figure 7.5 shows the data values (comparison points) used for evaluating the error. In the algorithm script file, the comparison points are defined as a series of time intervals, along with the number of points contained in each interval. In the example shown in Figure 7.5, seven time intervals were defined, each containing 10 – 13 comparison points.

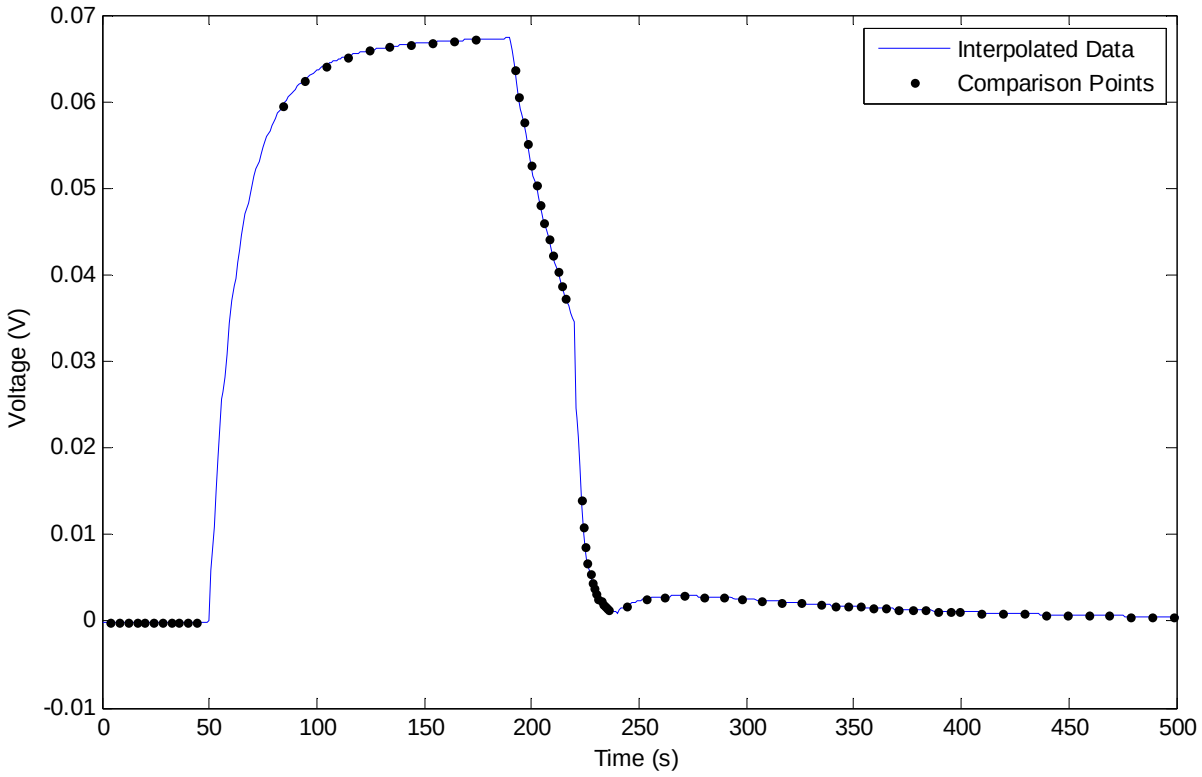

Figure 7.5 Data Values (Comparison Points) used for Computing the Error

The solution for P_i may result in the ECM response not capturing all of the measured fuel cell behaviour, due to large relative differences in the voltage transient behaviour at different times. For example, if the self-recharge region is very small in comparison to other regions, the essential form of the voltage transient may not be captured. To rectify this, a weighting factor can be applied such that comparison points with lower absolute voltage values have a higher weighting factor attached. The weighting factor is defined as a simple vector, and is shown below.

$$CW(t_n) = \begin{cases} 1 & \text{if} \quad t_n < T_1 \\ 3 & \text{if} \quad T_1 < t_n < T_2 \\ 1 & \text{if} \quad T_2 < t_n < T_3 \\ 2 & \text{if} \quad T_3 < t_n < T_4 \\ 10 & \text{if} \quad T_4 < t_n \end{cases} \tag{7.9}$$

The combination of the weights and fitting areas results in a modified error equation shown below

$$\sigma = \left[\sum_n CP(t_n) CW(t_n) \left(V_E(t_n) - V_S(t_n) \right)^2 \right]^{1/2} \tag{7.10}$$

Finally, when the circuit model parameters of a cell are being determined from the results of a stack test, the error is calculated using the simulated and experimental values of the cell in which the model parameter is being modified. For example, if a component in cell #3 was being modified, the error used is given by equation 7.11.

$$\sigma_{3,k} = \left[\sum_n CP(t_n) CW(t_n) \left(V_E(t_n)_3 - V_S(t_n)_{3,k} \right)^2 \right]^{1/2} \tag{7.11}$$

Clearly, the values of P_i and V_{Cj} determined will be effected by the $CP(t_n)$ and $CW(t_n)$ used. However, as $CP(t_n)$ and $CW(t_n)$ are the same for each cell, and the same for subsequent passive tests, the values of P_i and V_{Cj}, can still be used for comparing the properties of cells within a stack, and comparing the properties of cells at different times to detect changes in the state of the fuel cell.

7.3.2 Determination of Circuit Component Values

Once the initialisation process has been completed, the circuit component values, P_i are iterated through as described in the Section 7.2. Figure 7.3b shows how the method is coded into the

algorithm, taking into account multiple cells from a stack test. The process continues until the circuit parameter values found satisfy equation 7.4, thus a solution with minimum error has been achieved. As the circuit component values and capacitor voltage values are determined separately, this part of the algorithm will exit if a predetermined number of iterations have been completed. This ensures that a significant amount of time is not spent converging to a solution when the initial voltage values of the ECM model capacitors are significantly different to the initial voltage state of the fuel cell. In calculating the error between the simulated and experimental voltage data, all regions of the voltage response are used, except the initial steady state region, i.e $t_n < T_1$. This region is only used for calculating the initial voltage values of the capacitors, which is described in detail in the following sub-section.

7.3.3 Determination of the Initial Capacitor Voltage Values

The initial voltage values of the ECM capacitors are determined in the same way as the circuit parameter values as described above. However, the error between the experimental data and model simulation is evaluated using the steady state region only. Again, the iterative loop will exit if a predetermined number of iterations is completed, or the minimum error condition has been satisfied. Once the circuit parameter values, P_i, and the initial voltage values V_{Cj}, have been found subject to the error condition, the solution is saved and the program stops. Otherwise, the circuit component parameters will be iterated through again.

7.3.4 Features of the Method and Implementation

The fitting method has all of the features for determining the circuit parameter values of an ECM. The technique is not limited to the analysis of a single cell. Instead, parameter values of many ECM's (one for each cell) can be determined from the results of a single stack test. The fitting technique can also be used irrespective of the exact test protocol implemented. For example, if an additional charge/discharge sequence were included in the test process, this added sequence is simply added to the simulation. In general, the fitting technique is designed for flexibility and robustness rather than speed, enabling the parameters of a stack containing any number of cells to be obtained irrespective of the exact testing process or ECM.

7.4 VERIFICATION AND SENSITIVITY ANALYSIS

7.4.1 SENSITIVITY TO INITIAL GUESS

Determination of circuit parameter values using the fitting technique is explicitly shown by examining the iteration process as applied to the analysis of a single cell. Figure 7.6 shows the voltage response of a single cell (Avista cartridge 0508, cell DR) when subjected to the PSDB test. This data set, together with the testing conditions, is loaded into the Matlab workspace during the initialisation step. As described in Section 7.3.1, initial values (the first guess) of all circuit parameter values are required. The algorithm generates new values in an iterative fashion, by minimising the error between the experimental and simulated voltage response. The specific initial guess values chosen should not influence the final solution. To verify this, the fitting technique was applied twice, designated "Run 1" and "Run 2", each run using a different set of initial guess values. Table 7.1 shows the initial guess values used for Run 1 and Run 2.

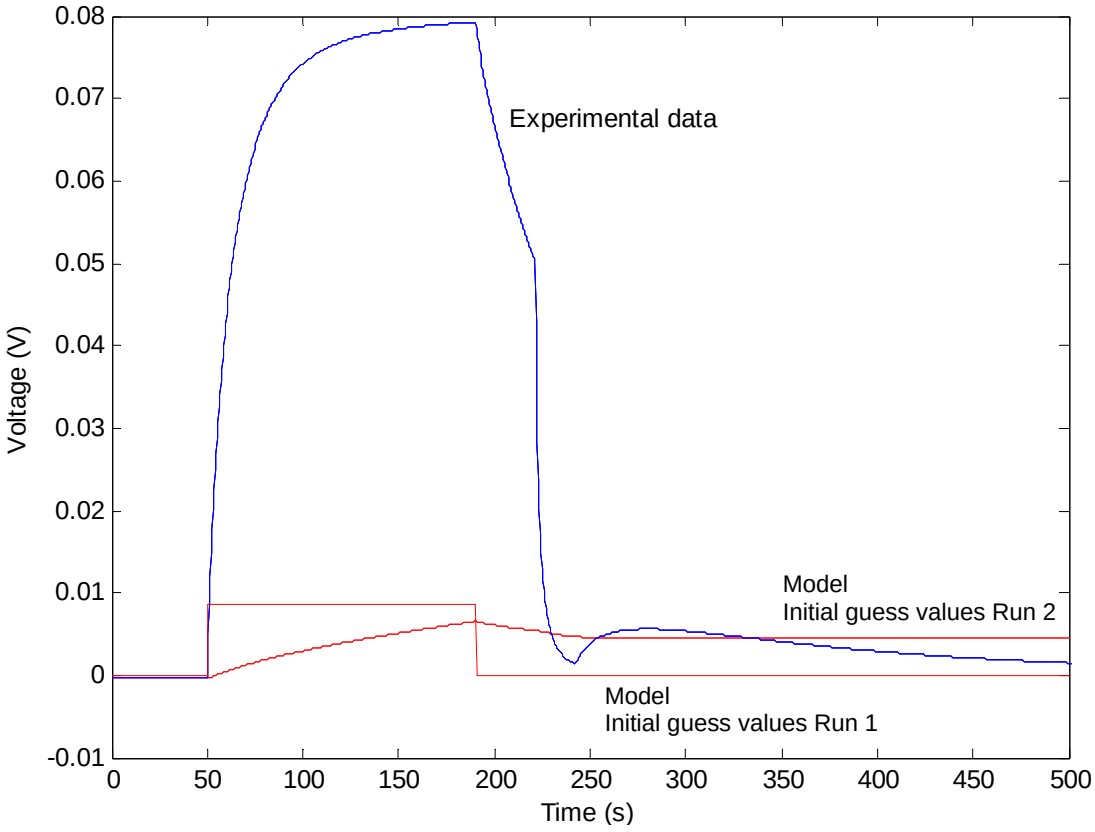

Figure 7.6 Single Cell Response to the Passive Test Method, with ECM Results Using Two Different Sets of Initial Guess Values; Test Circuit Values: V_{Charge} = 100.6mV, R_{Charge} = 53.3Ω, and $R_{Discharge}$ = 10.1Ω

Table 7.1 Initial Guess Values for the Fitting Method

Cell	Circuit Parameter Values			
	R_a (Ω)	R_b (Ω)	C_a (F)	C_b (F)
Run 1	5	600	0.01	0.01
Run 2	800	3	20	30

Also shown in Figure 7.6, are the simulated results of the ECM, having circuit values shown in Table 7.1. Clearly, the initial set of circuit values chosen for either Run 1 or Run 2, do not represent the cell behaviour. Figure 7.7 shows how the circuit values change as the fitting technique proceeds. The corresponding error is shown in Figure 7.8.

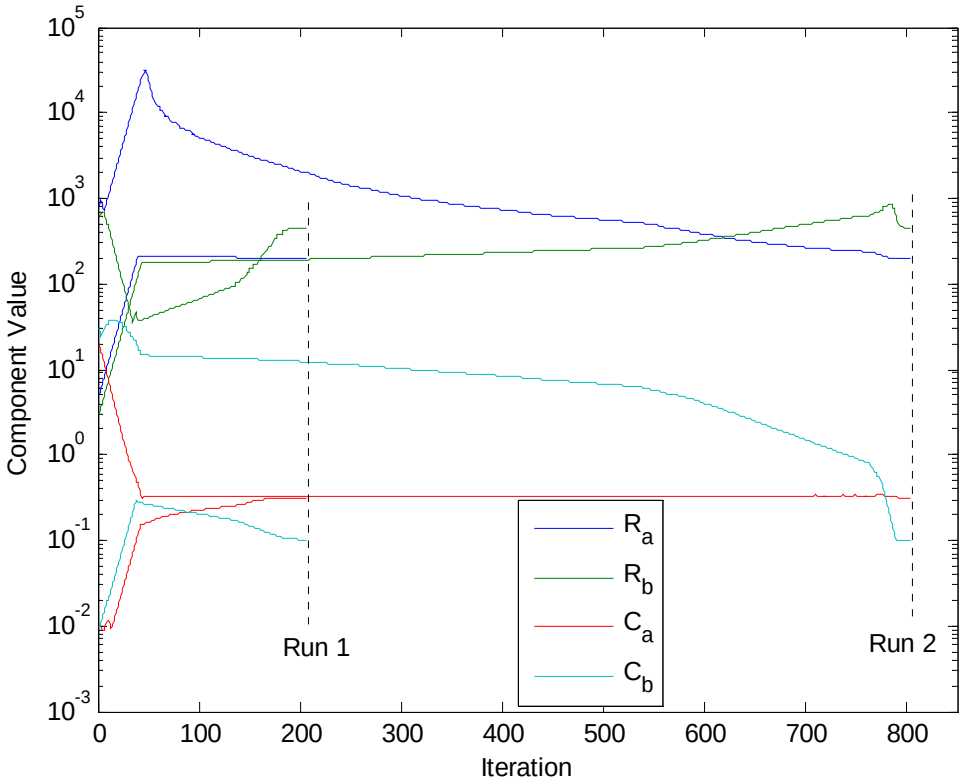

Figure 7.7 Circuit Values vs Iteration for Run 1 and Run 2

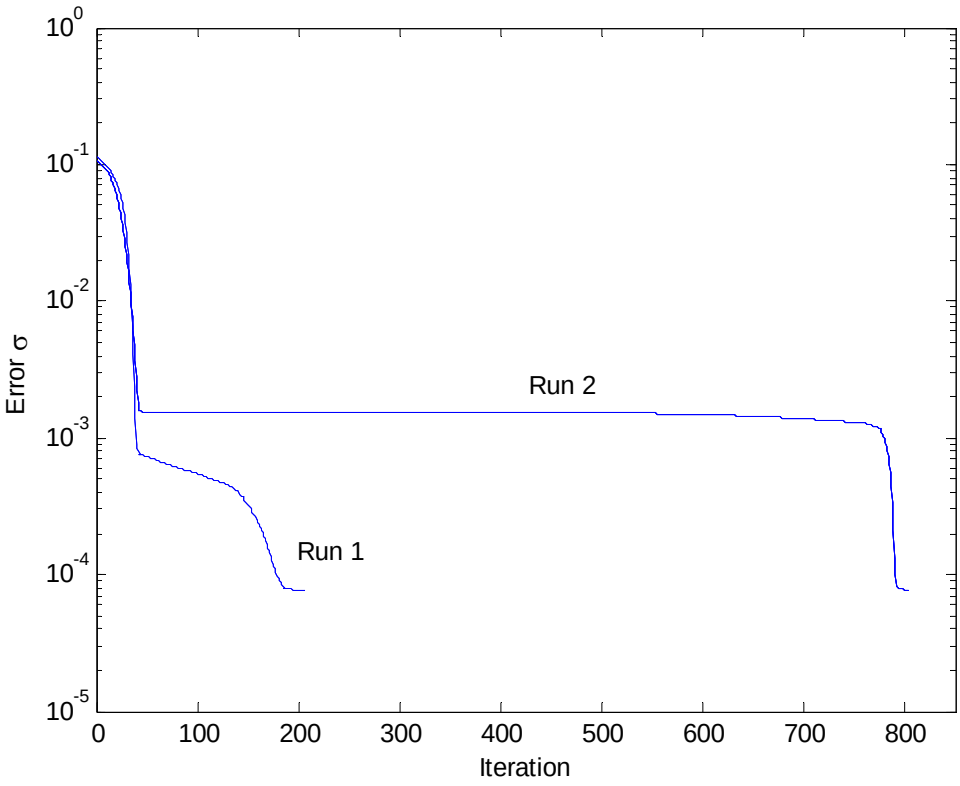

Figure 7.8 Error vs Iteration for Run 1 and Run 2

The initial circuit values chosen clearly affect the number of iterations required before a solution is found. In this case, Run 2 required 4 times as many iterations before converging on a solution. However, the final solution was the same in both cases and is shown in Table 7.2. The resulting modelled response shown in Figure 7.9.

Table 7.2 Final Values Obtained with the Fitting Method

	Circuit Parameter Values			
	R_a (Ω)	**R_b (Ω)**	**C_a (F)**	**C_b (F)**
Run 1 (206 iterations required)	201.69	448.86	0.30907	0.10246
Run 2 (804 iterations required)	201.87	450.32	0.30881	0.10228
% difference	0.089	0.330	0.085	0.180

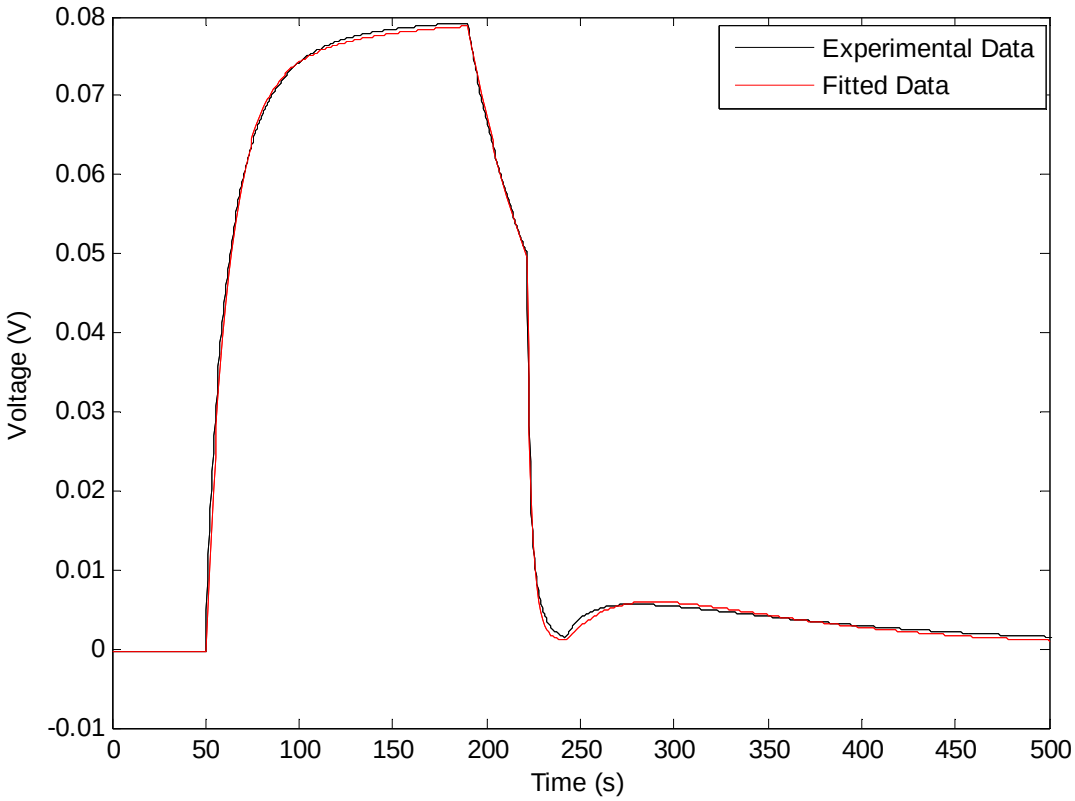

Figure 7.9 Experimental Data Shown with Fitted Results

In conclusion, the ECM values found using the fitting technique are independent of the initial guess values chosen. However, the number of iterations required before the solution converges is dependent on the initial guess values.

In the example shown above, the solution obtained is assumed to be "correct", in that the values obtained result in the best fit. However, it is possible that the fitting technique converged to a local minimum. The next section aims to verify the circuit parameters found using the fitting technique, are in fact the correct values, representing a global optimum.

7.4.2 Verification of Global Optima: Single Cell Results

To verify the circuit parameter values found are the global optima, the fitting technique was applied voltage transients generated by the PLECS model simulation, as opposed to real, experimental test data. This allows the circuit parameter values determined with the fitting technique, to be verified against the circuit values used in the PLECS simulation. Table 7.3 shows the test protocol values, and model values used to create the data set. The ECM voltage

response from the simulation is treated as the experimental data set, to which the fitting technique is applied. Table 7.3 also shows the results of the fitting technique.

Table 7.3 Simulated Data Set Values and Fitting Results

Simulated Data	**Test Circuit Values**	R_{Charge} = 53Ω	$R_{Discharge}$ = 10Ω	V_{Charge} = 0.1V	
	Switch times	T_1 = 50s	T_2 = 190s	T_3 = 220s	T_4 = 240s
	ECM values	R_a = 150 (Ω)	R_b = 200Ω	C_a = 0.6F	C_b = 0.15F

Fitting method results		**R_a (Ω)**	**R_b (Ω)**	**C_a (F)**	**C_b (F)**
	Starting Values	1	900	2	5
	Results	149.97	200.38	0.6005	0.14985
	% difference	-0.0200	0.1900	0.0833	-0.1000

Clearly, the fitting technique converged to a set of circuit parameter values that are the same as those used to create the simulated data set. The small % difference is attributed to the minimum change made to the circuit values, i.e. either a reduction or increase of 0.1% (0.999 or 1.001 in the neighbourhood vector, N_k, used for generating alternative values).

7.4.3 VERIFICATION OF GLOBAL OPTIMA: STACK RESULTS

A very similar test can be applied to a set of stack data. Table 7.4 shows the circuit values used to create a simulated set of data for a stack consisting of 8 series connected cells. The starting values for the algorithm are also shown, together with the circuit parameter values determined. Again, the circuit parameter values determined with the fitting technique are very close to those used for creating the data set. The % difference is slightly higher with stack testing, with a maximum difference of 1.3% found for competent R_b in cell number 8.

Table 7.4 Verification of Stack Test Data

	Cell	Circuit Parameter Values			
		R_a (Ω)	R_b (Ω)	C_a (F)	C_b (F)
Equivalent Circuit Model Values Used for Producing Simulated Stack Data (Treated as an Experimental Data Set)	**1**	240	400	0.42	0.23
	2	70	570	0.58	0.21
	3	300	180	0.42	0.19
	4	95	600	0.51	0.17
	5	160	500	0.59	0.28
	6	150	200	0.60	0.15
	7	210	190	0.32	0.22
	8	30	520	0.38	0.18
Fitting Method Starting Values	**1–8**	200	600	1	1
ECM Results	**1**	239.22	398.39	0.42178	0.23061
	2	69.774	565.57	0.58246	0.21112
	3	299.07	179.1	0.42174	0.19055
	4	94.693	596.06	0.51214	0.17083
	5	159.47	498.22	0.59253	0.28052
	6	149.51	201.89	0.60409	0.14922
	7	209.34	188.96	0.32118	0.22093
	8	29.899	513.25	0.3813	0.18185
% difference	**1**	-0.326	-0.405	0.421	0.264
	2	-0.324	-0.783	0.422	0.530
	3	-0.312	-0.503	0.414	0.291
	4	-0.324	-0.660	0.417	0.487
	5	-0.335	-0.357	0.427	0.187
	6	-0.326	0.937	0.677	-0.521
	7	-0.314	-0.553	0.367	0.419
	8	-0.337	-1.315	0.342	1.016

7.4.4 SENSITIVITY TO MEASUREMENT ERROR

In a real experimental test, there will be some measurement error in the test circuit values (R_{Charge}, $R_{Discharge}$, and V_{Charge}), and timing of the test protocol (T_1 – T_4). Therefore, the simulation of the testing protocol may not match exactly the testing conditions experienced by the passive fuel cell. To examine the propagation of measurement error onto the circuit parameter values obtained, the fitting technique was applied to a simulated data set, but with errors introduced. Table 7.5 shows the values used to create the simulated data, together with the

algorithm values and the results of the fitting process. The difference between the simulated and algorithm values represents an overestimation in measurement error for a real experiment.

Table 7.5 Algorithm Defined Values and Iteration Results

Simulated data values	**Test Circuit Parameters**	R_{Charge} = 53Ω	$R_{Discharge}$ = 10Ω	V_{Charge} = 0.1 V	
	Switch times	T_1 = 50s	T_2 = 190s	T_3 = 220s,	T_4 = 240s
	ECM values	R_a = 150 Ω	R_b = 200 Ω	C_a = 0.6 F,	C_b = 0.15 F
Algorithm Values	**Test Circuit Parameters**	R_{Charge} = 53.2Ω	$R_{Discharge}$ = 10.2Ω	V_{Charge} = 0.0998V	
	Switch time	T_1 = 50.2s	T_2 = 189.8s	T_3 = 220.2s,	T_4 = 239.8s
	Starting Values	R_a = 1Ω	R_b = 900Ω	C_a = 2F,	C_b = 5F
Results	**ECM values**	R_a = 150.78Ω	R_b = 207.08Ω	C_a = 0.59151F	C_b = 0.1469F
	% difference	0.5200	3.540	-1.4150	-2.0667

Table 7.5 also shows that the resulting circuit parameter values differ to a larger degree when compared to the circuit values used to generate the data set. This is particularly true for circuit component R_b, which is 3.5% larger. This type of test, where the fitting algorithm was applied to a data set with error, was repeated a number of times. In many cases, the values determined for R_a and C_a were very similar as those used to for the simulation data, with the largest difference in circuit component R_b. Based on the 3.5% error, and considering a larger error is found when the fitting method is applied to a stack of cells (Section 7.4.3), a statistical uncertainty of ±5% is attributed to the circuit parameters determined using the fitting method. This uncertainty could be reduced through further refinement/optimization of the fitting method, as discussed the following section.

7.5 POTENTIAL AREAS FOR OPTIMIZATION

The convergence time, and the exact solution found, depends on a number of algorithm parameters. For example, the size of the neighbourhood vector, N_k will change how fast the algorithm converges, as will the number of voltage points used to compare the simulated and experimental results. In addition, not all circuit parameters need to be found using the algorithm, as they can be found directly (or with minimal computation) from the passive fuel cell test results. These aspects are discussed below.

A number of the circuit parameters may be calculated by direct inspection of the results. The initial voltage across C_a equals the voltage measured at the start of the testing protocol, thus, this voltage value is not found with the fitting technique. In theory, the value of C_a can be calculated using the voltage gradient at the beginning of the charge step. Provided no significant charge is present on C_a at $t = T_1$, current is assumed to flow through R_a into C_a only. Using the measured value of dV/dt at the start of the charge step, and assuming that $R_c << R_{Charge}$, C_a can be calculated using equation 7.12.

$$C_a = \frac{V_{Charge}}{R_{Charge} \left. \frac{dV}{dt} \right|_{t=T_1}} \qquad 7.12$$

Although this equation has been derived by considering a single cell, it can be applied to each individual cell in a series connected stack, provided dV/dt is obtained with negligible voltage across any cell, (i.e. every other C_a in the stack model acts as a short circuit in the initial charge period). Finally, the value of R_c could, in theory, be calculated by measuring a sudden change in voltage at the beginning of the charge step. The calculation is very similar to that described in Section 3.2.2, where the series resistance of a cell is calculated from a current interrupt test. The problem with calculating C_a and R_c in this fashion is the high quality data required, specifically, a high sampling rate for each cell. As the test method is designed for an application setting, such as back-up power, the testing and measurement equipment would be as simple as possible, thus high-resolution data would not be available. As a result, the fitting technique would be used for determining the circuit parameters.

The fitting technique determines the circuit parameter values of every cell from a single stack test. However, the values of a single cell can be determined without having to acquire the circuit values of every other cell in the stack. This may be useful if the stack contains many cells, in which case the fitting technique may take considerable time, but only one, or a few cells are of interest. To find the circuit parameters of just one cell, a stack ECM composed of only two cells is used. One cell in the ECM models the cell of interest, where as the other cell in the ECM model represents the net electrical properties of the other cells in the stack. As shown in Section 6.3, many cells added together behave as a single cell. Therefore, the voltages of every other cell in the stack are added together, and can be treated as a single cell. The fitting technique is applied, thus acquiring the circuit parameters of a single cell, and one other cell only, which represents the rest of the cells in the stack.

7.6 CONCLUSION

This chapter has described a technique to determine the circuit model parameter values of every individual cell using the results of a stack test. The results obtained were shown to be independent of the initial guess values. The fitting technique was also applied to a set of simulated cell and stack data. The circuit parameter values determined in both cases were in agreement with the values used to create the simulated data. The fitting technique is flexible; it can be used irrespective of the exact testing protocol or ECM.

8 PEM FUEL CELL ANALYSIS USING THE PASSIVE STATE DYNAMIC BEHAVIOUR (PSDB) TEST PROTOCOL

The objectives set out at the beginning of this thesis were to develop a testing procedure for a fuel cell in an application setting, back-up power for telecommunications. Although the theory and practical aspects of the passive state dynamic behaviour (PSDB) test have been developed, the usefulness of the test method has not yet been demonstrated. This chapter demonstrates how the PSDB test provides information on the active functionality of the fuel cell.

Section 8.1 details a direct correlation between the voltage decay rate in the PSDB test results, and the active operation of a fuel cell. Section 8.2 demonstrates how the circuit parameter values, obtained from a stack PSDB test, are used to predict a change in the functionality of certain cells within the stack. A summary is provided in Section 8.3.

8.1 PSDB TEST RESULTS AND ACTIVE FUNCTIONALITY CORRELATION

The thesis of the PSDB test is that electrical properties measured while the fuel cell is in a passive state, provide information on the active functionality of the fuel cell. This section directly compares stack behaviour in both passive and active mode. Specifically, the voltage transients of the PSDB test results are compared with the active functionality of the fuel cell. This type of analysis is conducted on the MerCorp and the Avista stacks, and is detailed in the following two subsections.

8.1.1 MERCORP CORRELATION RESULTS

Figure 8.1a shows the response of the MerCorp stack when subjected to the PSDB test. Immediately after the PSDB test, an active test was conducted in which the VI performance of the fuel cell stack was obtained. This is shown in Figure 8.1b.

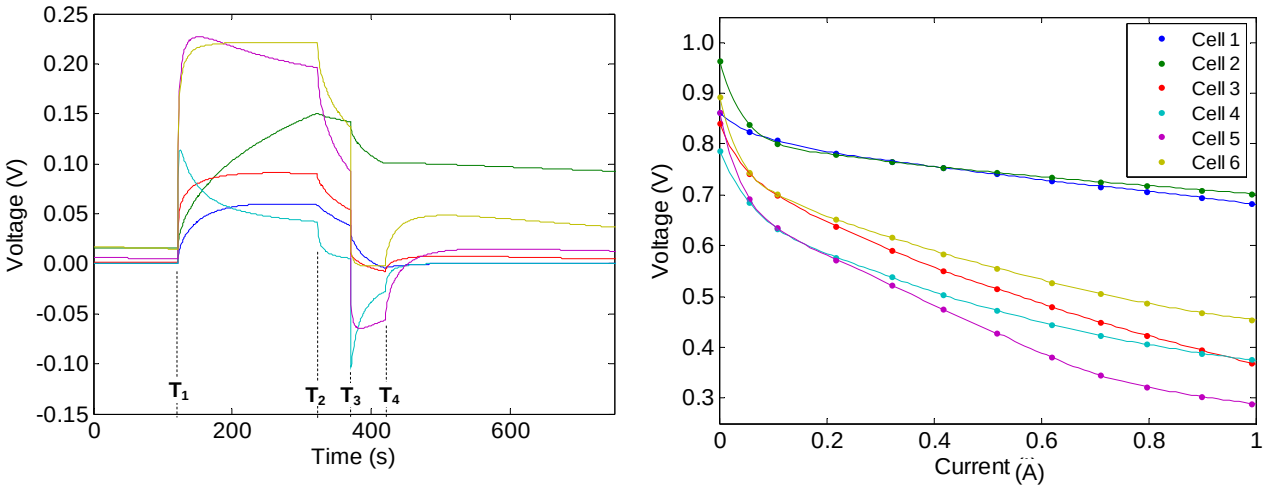

a) **b)**

Figure 8.1 MerCorp Stack PSDB Test Result (a); Test Circuit Values V_{Charge} = 806mV, R_{Charge}= 99.8Ω, $R_{Discharge}$ = 4.8Ω, (b) the Active VI Performance of the Stack

The VI curve was obtained 100s after hydrogen was introduced into the cell. This allowed the anode compartment to be purged of air, ensuring only hydrogen remained. The stack remained in an open circuit state for this time. The VI curve was obtained over a period of 190s, from 0-0.993A, with each current value shown in Figure 8.1b held for approximately 15s. The airflow varied between 2.06 and 2.08 l/min during the VI evaluation.

To determine if there is a relationship between the PSDB test results and the active functionality of the cells, the PSDB test results were characterised by measuring certain aspects of the cell voltage transients. These included;

- The rate of voltage increase at the beginning of the charge region, t = T_1
- The maximum voltage reached by each cell during the charge region
- The voltage decay rate at the beginning of the natural discharge region, t = T_2
- The step change in voltage when the stack was discharged, t = T_3
- The maximum voltage reached in the natural decay region

Two of the properties, the voltage decay rate after T_2 and the voltage step size at T_3, were found to correlate with the active functionality of the fuel cell. Table 8.1 lists these passive fuel cell

properties, along with the voltage performance of the cells when operating at a current of 0.556A. The active voltage is measured at this current value to maintain consistency with additional results presented in this section.

Table 8.1 PSDB Test Properties Compared to the Active Functionality: Experiment One

Cell (in order of voltage performance)	Cell voltage@ 0.556A (V)	Gradient at T_2 (mV/s)	Size of the voltage step at T_3 (mV)
2	0.744	-0.340	0.00716
1	0.741	-0.717	0.00942
6	0.556	-6.50	0.124
3	0.516	-2.45	0.0445
4	0.473	-5.62	0.109
5	0.429	-7.80	0.133

By inspection of the results in Table 8.1, a smaller decay rate is associated with a cell that functions with a higher voltage. Also, a smaller voltage step in the passive test results, is associated with a cell having a higher voltage when active. This is particularly true of cells #1 and #2. The voltage of these cells was significantly higher than the other four cells, and the corresponding voltage decay and voltage step were significantly smaller than the rest of the cells in the stack.

A stack PSDB test, followed by an active VI evaluation of the stack, was conducted a number of times to confirm repeatability of the correlation. Two additional experiments, consisting of the a PSDB test and an active test are discussed below, the first of which is shown in Figure 8.2.

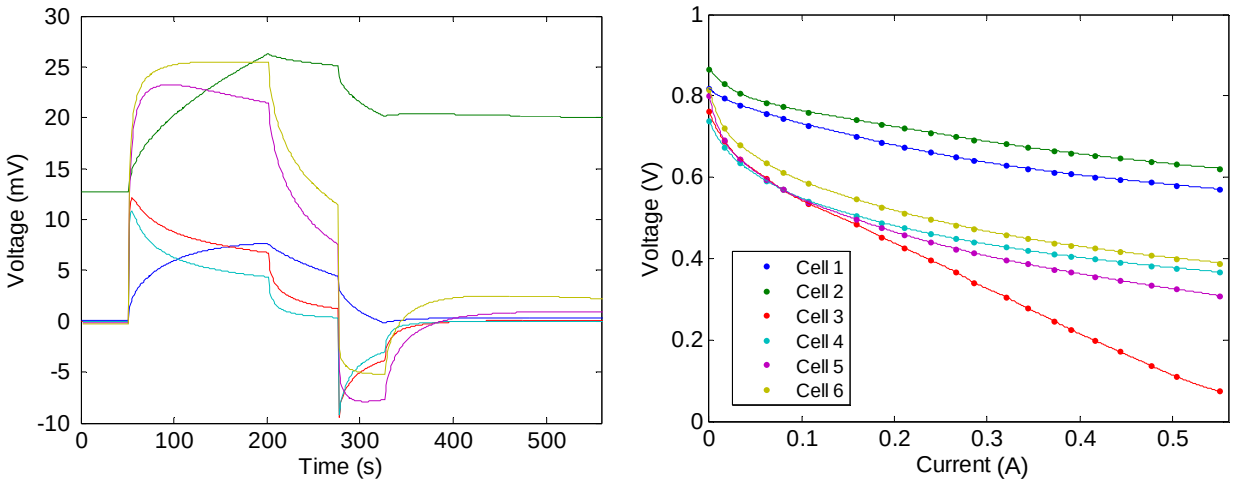

a) **b)**

Figure 8.2 MerCorp Stack PSDB Test Result (a), Test Circuit Values: V_{Charge} = 97.0mV, R_{Charge}= 99.8Ω, $R_{Discharge}$ = 4.8Ω, (b) the Active VI Performance of the Stack.

In this particular active test of the stack, the current was limited to 0.55A, due to the poor performance of cell #3. The VI curve was obtained after the stack had been functioning for some time. Initially, the stack was kept in an open circuit condition for 126s from when hydrogen first entered the stack, ensuring only hydrogen is present in the anode compartment. The stack was then operated at a variety of currents for 36.9 minutes, before the VI curve was obtained. During this time, the airflow was varied in order to obtain maximum performance. An airflow of 0.57-0.59 l/min was used for the VI curve, which was measured over a period of 161s, from open circuit to a maximum current of 0.55A. Table 8.2 lists the voltage performance and the passive test characteristics.

Table 8.2 PSDB Test Properties Compared to the Active Functionality: Experiment Two

Cell (in order of voltage performance)	Voltage @ 0.550 A (V)	Decay rate at T_2 (mV/s)	Size of the voltage step at T_3 (mV)
2	0.624	-0.0508	1.11
1	0.572	-0.0914	1.27
6	0.386	-0.911	14.0
4	0.364	-0.560	9.57
5	0.307	-0.869	12.3
3	0.0605	-0.623	10.7

A similar correlation between the passive and active tests is observed from Table 8.2, with cells performing well actively, possessing a small gradient and voltage step in the PSDB test.

The correlation was found to persist even after the performance of certain cells was altered, due to a change in the active operating conditions of the stack. As the flow field pattern on the bipolar plates and electrodes was identical, the stack could be operated with the hydrogen and air flows switched, resulting in a reversal of polarity. Under this operational arrangement, the performance of cell number 2 was significantly reduced and the performance of cell number 3 improved. After a number of active tests in this arrangement, a PSDB test was conducted followed by an active test. These results are shown in Figure 8.3.

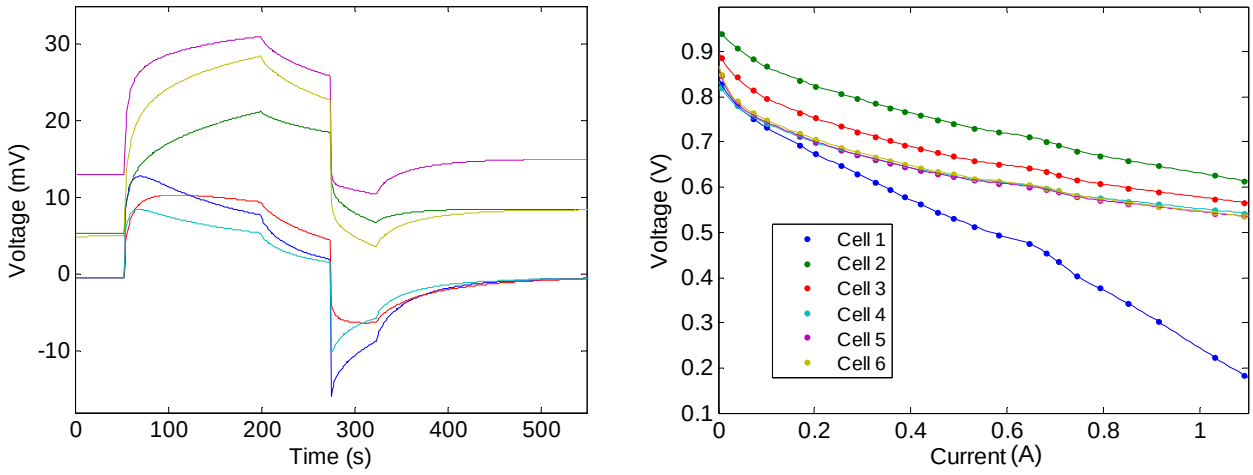

a) **b)**

Figure 8.3 MerCorp Stack PSDB Test Result (a); Test Circuit Values: V_{Charge} = 109mV, R_{Charge}= 99.8Ω, $R_{Discharge}$ = 4.8Ω, (b) the VI Performance of the Stack Obtained with the Air/Hydrogen Flows Switched

For this active test, the stack was kept in an open circuit condition for 81 seconds from when hydrogen first entered the stack, ensuring only hydrogen is present in the anode compartment. The fuel cell was then operated at variety of currents for 389s, with the VI curve taken over a time of 157s, from open circuit to a current of 1.1A. A constant airflow of 1.25l/min was used. A major difference in the performance of the stack is in the behaviour of cell #1. In the previous active tests presented, cell #1 functioned with a relatively high voltage over the entire current range. However, with the air and hydrogen flowing on opposite sides of the fuel cell, the performance of cell #1 is now the lowest, as evident from Figure 8.3. Along with the decline in the cells performance, the voltage transient of cell #1 in the passive test also changes. Table 8.3 lists the voltage performance and the passive test properties measured.

Table 8.3 PSDB Test Properties Compared to the Active Functionality: Experiment Three

Cell (in order of voltage performance)	Voltage at 0.560 A (V)	Voltage decay at T_2 (mV/s)	Size of the voltage step at T_3 (mV)
2	0.725	-0.105	6.28
3	0.652	-0.174	8.58
6	0.614	-0.223	13.3
4	0.612	-0.217	11.7
5	0.610	-0.225	12.5
1	0.501	-0.336	17.8

Cell #1, which now possesses the lowest voltage performance when active, has now the steepest gradient, and the largest voltage step when tested passively. The correlation in this case, is clearly linear, as shown by Figure 8.4.

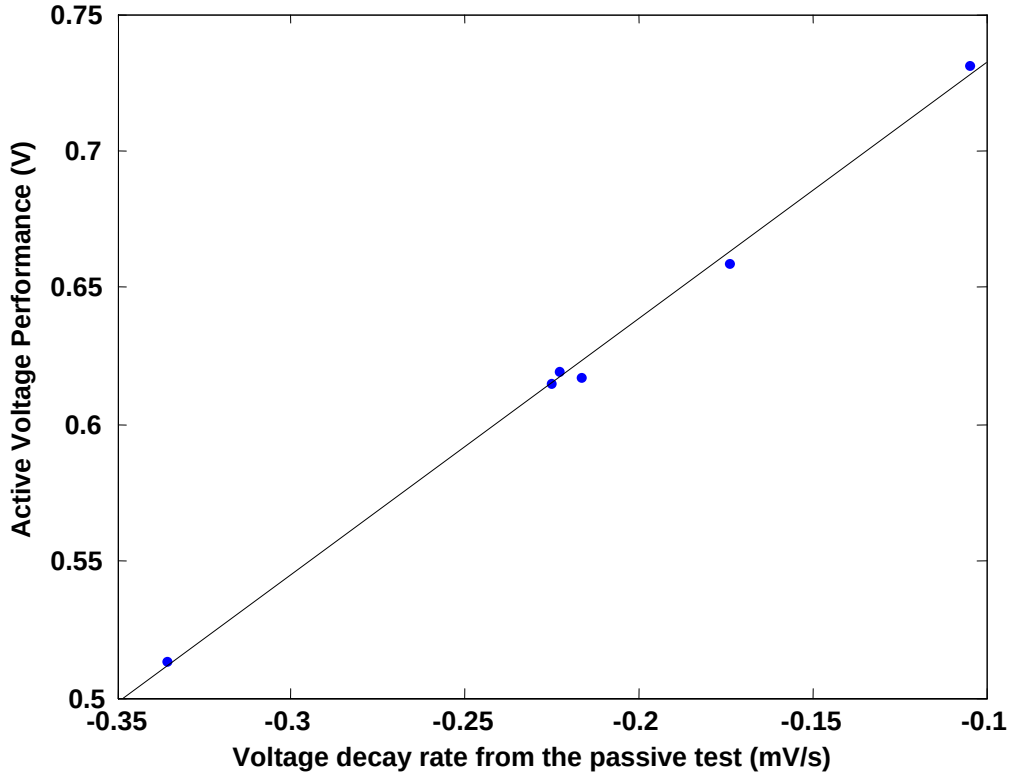

Figure 8.4 Correlation between the Active and Passive Tests for the MerCorp Stack

By scaling the results of the three Experiments such that all values lie in the range 1-0, the correlation results can be presented on the same graph as shown in Figure 8.5.

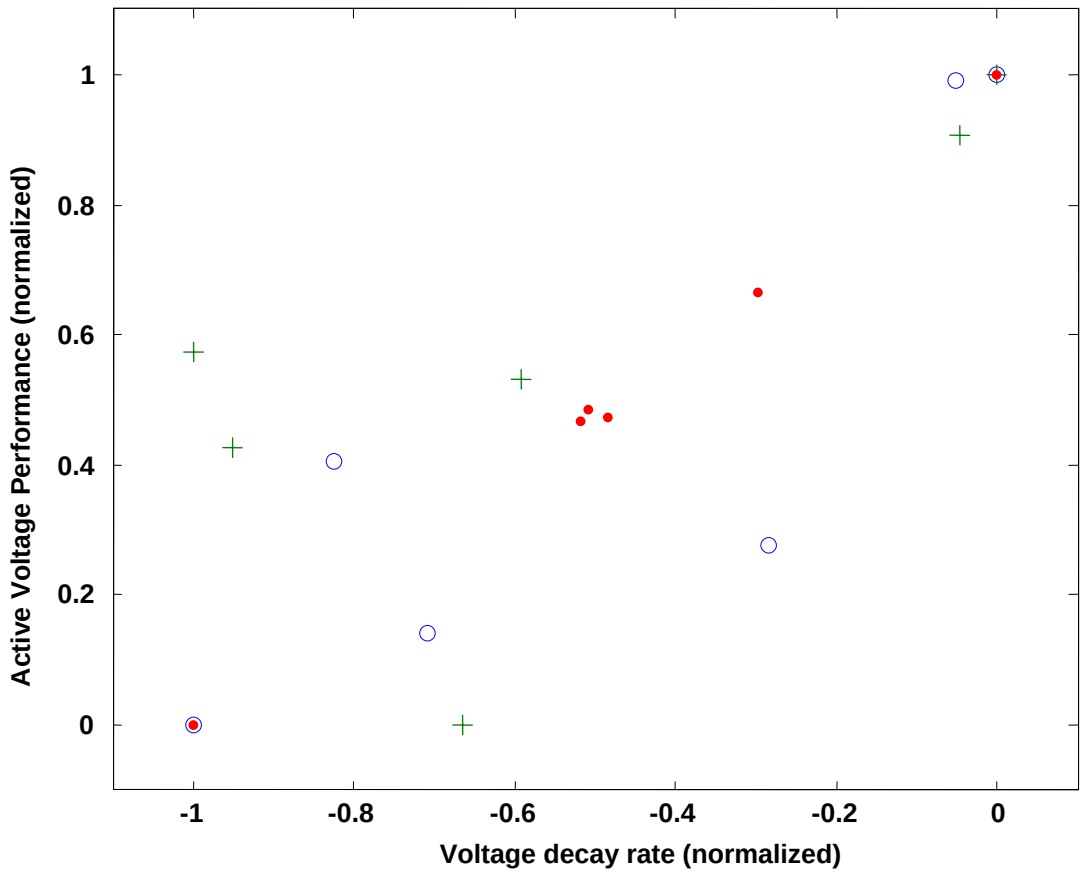

Figure 8.5 Correlation between Passive and Active testing for Experiment One (○), Experiment Two (+) and Experiment Three (•)

In summary, a direct correlation between PSDB testing and active functionality of the MerCorp stack is observed. The correlation is repeatable, despite differences in the active testing conditions resulting in changes in performance of the cells. For instance, in the three experiments presented, the stack was actively operated for various lengths of time before the VI curve was obtained. It should be noted that the active functionality of the stack was far below the excepted performance of a PEM stack. The maximum current was around 1A, and with an active area of 36cm^2, the current density of 27mA/cm^2 is significantly below the 400-700mA/cm^2 typical of PEM fuel cell. In general, the PSDB test predicts the relative performance of the cells.

8.1.2 AVISTA CORRELATION RESULTS

PSDB testing, followed by active testing was implemented on each Avista cartridge, tested in pairs as described in Section 5.2.3. The voltage decay rate was measured at the start of the decay region and compared with the active performance of the fuel cell. A similar correlation between the passive and active tests was also observed, but only under particular conditions. If there was a clear distinction between the voltage decay rates of the two cartridges, then a performance difference could also be observed in the active functioning of the cell at low current densities. Figure 8.6 shows the PSDB test results, followed by the VI assessment for two Avista stacks, each composed of eight cells (two cartridges).

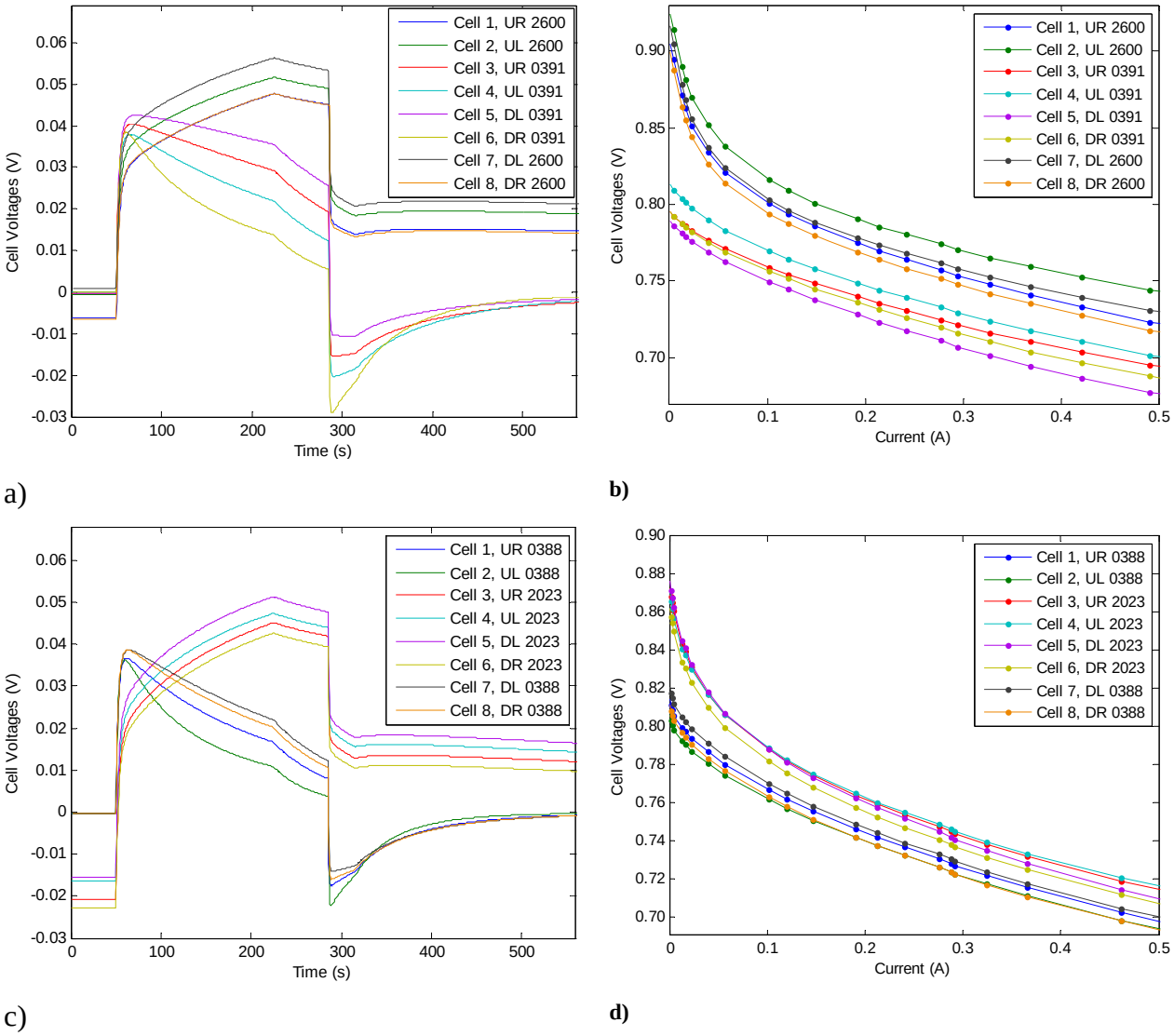

Figure 8.6 PSDB tests (a) and (c) Conducted on Pairs of Cartridges, Followed by Active Testing (b) and (d); Test Circuit Resistor Values are the same for both Passive Tests, R_{Charge} = 52.7 and $R_{Discharge}$ = 10.2Ω, with V_{Charge} = 308mV for (a) and V_{Charge} = 260mV for (c)

For the active tests shown in Figure 8.6b and 8.6d, the stacks underwent a simple warm up procedure before obtaining the VI curves. The warm up procedure consisted of first purging the anode compartment of air by flowing hydrogen through the stack for approximately 10s. The stack was then operated at a current of 7-8A for 100s. After being disconnected from the load, the stack remained at in an open circuit state for 100s. The VI curve was recorded over a time period of 520s, the load being increased every 10s. The resulting VI curve shown in Figure 8.6b and 8.6d is obtained by taking the V and I of each cell at the end of each 10s time period. The voltage performance of each cell when operating at a low current is listed in Table 8.4 together with the measured voltage decay rate at the beginning of the natural decay region.

Table 8.4 Correlation of Avista Cells

Test 1				Test 2			
Cartridge	**Cell**	**Voltage decay rate (mV/s)**	**Voltage @ 0.0569A (V)**	**Cartridge**	**Cell**	**Voltage decay rate (mV/s)**	**Voltage @ 0.0563A (V)**
2600	UR	-0.0732	0.821	**2023**	UR	-0.0867	0.806
	UL	-0.0670	0.838		UL	-0.0877	0.807
	DR	-0.0752	0.814		DR	-0.0868	0.800
	DL	-0.0744	0.824		DL	-0.0946	0.807
0391	UR	-0.243	0.771	**0388**	UR	-0.256	0.780
	UL	-0.237	0.783		UL	-0.243	0.774
	DR	-0.244	0.769		DR	-0.256	0.777
	DL	-0.233	0.763		DL	-0.253	0.784

Again, a cell exhibiting a low voltage decay rate will possess a higher voltage when active. However, this is only true at low current densities. Figure 8.6 shows a clear difference in the active performance at low currents, but this difference becomes less clear at higher load current of the fuel cell. The current density of the cell at 0.5A is 10mA/cm^2.

8.1.3 CORRELATION DISCUSSION

A direct correlation between the results of the PSDB test and the active operation of the stack has been demonstrated. Both the MerCorp stack and certain Avista Stacks exhibit a correlation between the rate of voltage decay during the PSDB test, and the operating voltage of the cells.

Direct conduction across the cell is a possible cause of the observed correlation. A cell that possesses a larger conduction value would self-discharge more rapidly after a charge period. Thus, the decay rate would be higher as measured from a PSDB test. When the same cell is tested actively, the current leaking through the cell coupled with the activation loss, leads to a lower voltage measurement at a particular current value. Attributing the observed correlation to direct conduction across the cell, also explains why the correlation has only been observed at low current densities. As the fuel cell current is increased, the leakage current becomes insignificant when compared to the ionic current flowing through the cell. Thus, the voltage will be dictated by the other loss mechanisms present, instead of being dominated by the leakage current and activation loss.

The correlation was not present on all the active and PSDB testing conducted. As stated previously, a correlation could not be established on all Avista cartridges tested. In addition, despite numerous testing on the Enable stack, a passive-active correlation could not be established. Therefore, using the rate of voltage decay from a PSDB test result, cannot be used for indicating the relative performance of cells for every PEM fuel cell stack. A direct inspection of the PSDB test results may still be useful in some cases. For instance, a shorted cell would easily be detected by examining the result of a stack PSDB test. The intended method of determining active fuel cell information from the results of a PSDB test is to use the passive ECM, which is described in detail in the following section.

8.2 Relating ECM Parameters to the Operation of the Stack

This section demonstrates how the PSDB test, including circuit model analysis, is used to predict the active performance of individual cells within the fuel cell stack. In addition, this section verifies the physical aspects of a fuel cell attributed to the circuit parameters of the passive ECM. These two objectives are realised by altering the physical state of the fuel cell, and exploring the impact this has on the PSDB test results and the active performance.

Membrane hydration is the specific physical property of the fuel cell that is altered. As discussed previously, the hydration of the fuel cell is an important aspect in determining the active performance of the cells. The remainder of this section explicitly details the experimental

method, results and analysis. All experiments were conducted on an Avista fuel cell stack composed of cartridges 0587 and 0388.

Initially, a PSDB test followed by an active test was conducted on the fuel cell stack. The results of these tests will provide base line performance data, which will be compared with subsequent testing results. Figure 8.7 shows the stack PSDB test results, with the circuit parameter values given the Table 8.5.

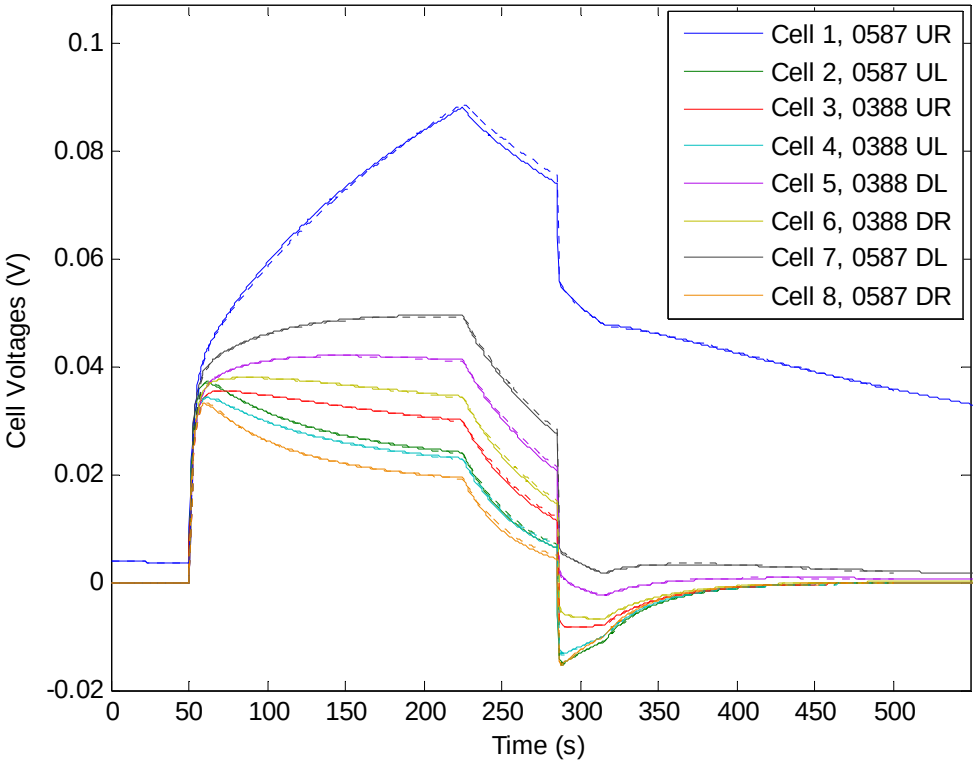

Figure 8.7 PSDB Test Response of Avista Cartridges 0587 0388, Solid Line Experimental, Dashed Line ECM; Test Circuit Values: V_{Charge} = 322mV, R_{Charge} = 52.6Ω and $R_{Discharge}$ = 10.1Ω

Table 8.5 Initial Circuit model Parameters

Cell	Circuit Parameter Values			
	R_a (Ω)	R_b (Ω)	C_a (F)	C_b (F)
Cell 1, 0587 UR	781	411	0.512	0.141
Cell 2, 0587 UL	92.4	445	0.452	0.128
Cell 3, 0388 UR	115	433	0.510	0.127
Cell 4, 0388 UL	87.7	417	0.492	0.133
Cell 5, 0388 DL	164	513	0.513	0.113
Cell 6, 0388 DR	133	468	0.496	0.119
Cell 7, 0587 DL	206	427	0.471	0.126
Cell 8, 0587 DR	74.1	370	0.490	0.143

The circuit model parameter values are approximately the same for all cells. Thus, the voltage performance of each cell is expected to be similar. Figure 8.8 shows the VI performance of each cell in the Avista stack.

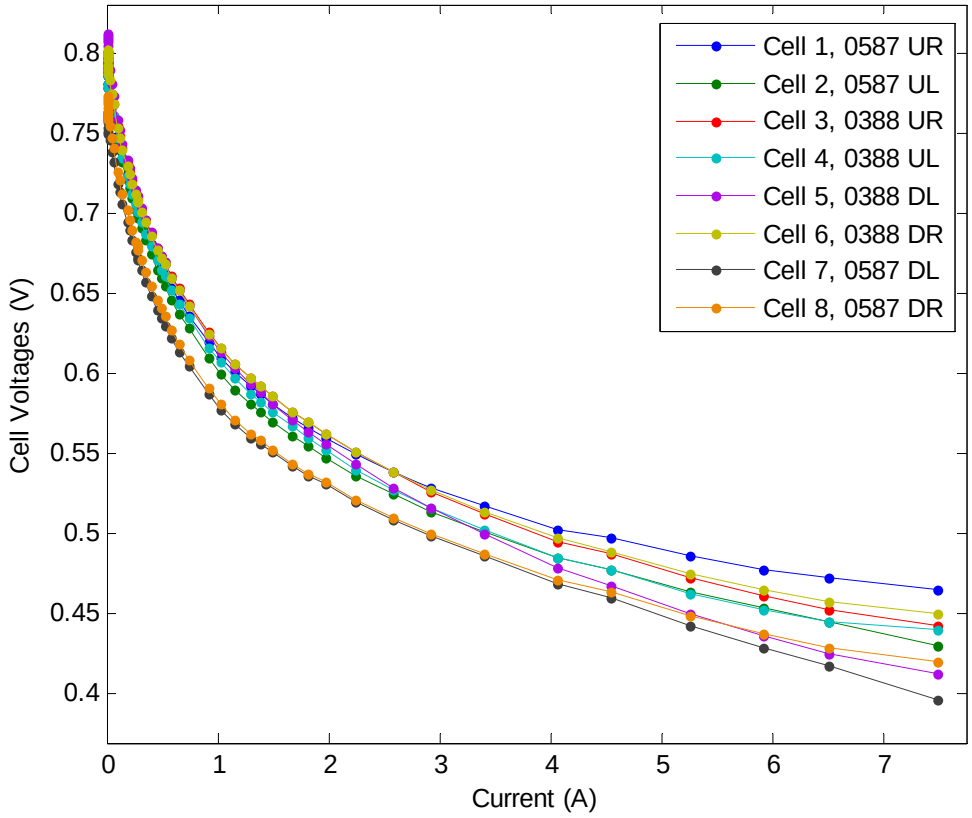

Figure 8.8 Initial Active Performance of an Avista Fuel Cell Stack

Before the VI curve was obtained, the stack underwent a quick warm-up procedure. This consisted of purging the hydrogen compartment of air for 10s, operating the stack at a current of

7A for approximately 70s, followed by an open circuit period of 90s. The VI curve was obtained over period of 510s, with each VI point measured after the load was held constant for 10s. The VI performance of the stack and the PSDB test results establishes baseline performance for comparison to subsequent testing.

After the PSDB test and active testing, the hydrogen lines and load were disconnected. The stack remained in this condition for two days, with no further testing over this period. After two days, the passive stack test was repeated. The results of are shown in Figure 8.9, with the circuit model parameter values given in Table 8.6

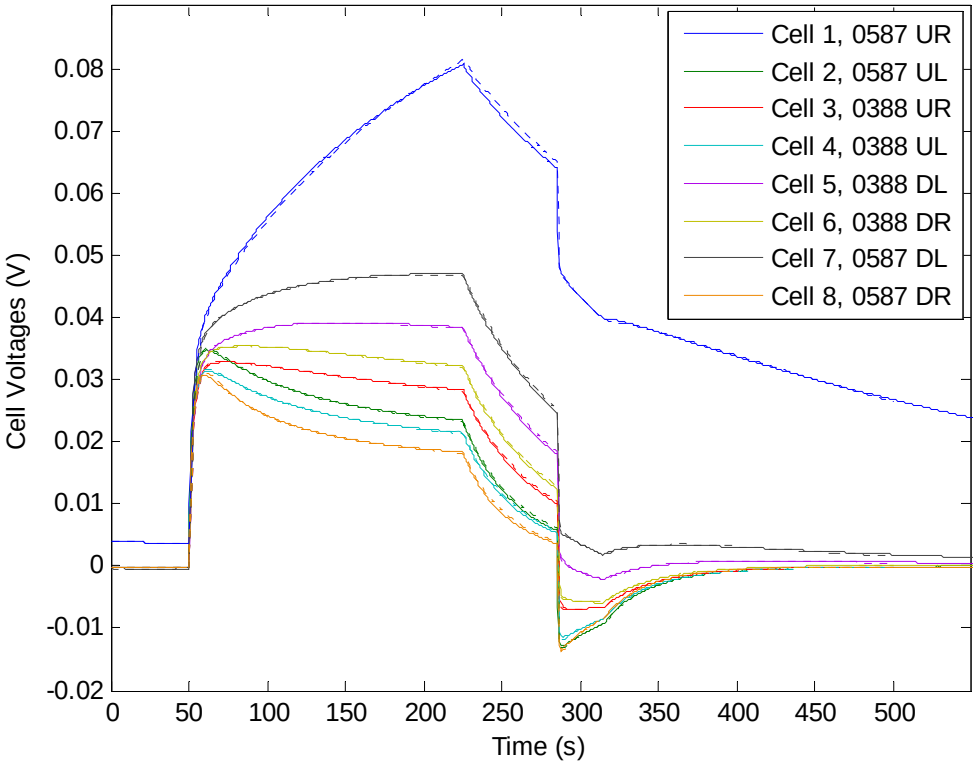

Figure 8.9 Results of the Stack PSDB Test Prior to the Humidification of Cartridge 0587, Solid Line Experimental, Dashed Line ECM; Test Circuit Values: V_{Charge} = 303mV, R_{Charge} = 52.6 Ω and $R_{Discharge}$ = 10.1 Ω

Table 8.6 Circuit Parameter Values Determined from Stack Passive Test Results

Cell	Circuit Parameter Values			
	R_a (Ω)	R_b (Ω)	C_a (F)	C_b (F)
Cell 1, 0587 UR	548	387	0.507	0.162
Cell 2, 0587 UL	85.0	397	0.444	0.123
Cell 3, 0388 UR	103	368	0.510	0.127
Cell 4, 0388 UL	77.5	357	0.491	0.126
Cell 5, 0388 DL	144	445	0.511	0.122
Cell 6, 0388 DR	118	406	0.492	0.123
Cell 7, 0587 DL	184	374	0.463	0.138
Cell 8, 0587 DR	66.5	326	0.481	0.136

The results from the PSDB test shown in Figure 8.9 and Table 8.6 are similar to the PSDB test results shown previously. Thus, if the fuel cell stack were actively tested, a similar VI performance of the cells would be expected.

Before additional testing, active or passive, the membrane hydration of the cells in cartridge 0587 was altered. This was achieved by passing humidified air through the stack (2.4 l/m), entering at the hydrogen port by the upper cells. This process was continued for approximately 700s, with the temperature of the humidified air entering the cell at approximately 70^{o}C. Immediately after this humidification procedure, the PSDB test was repeated using exactly the same test circuit values and switch times. The results are presented in Figure 8.10.

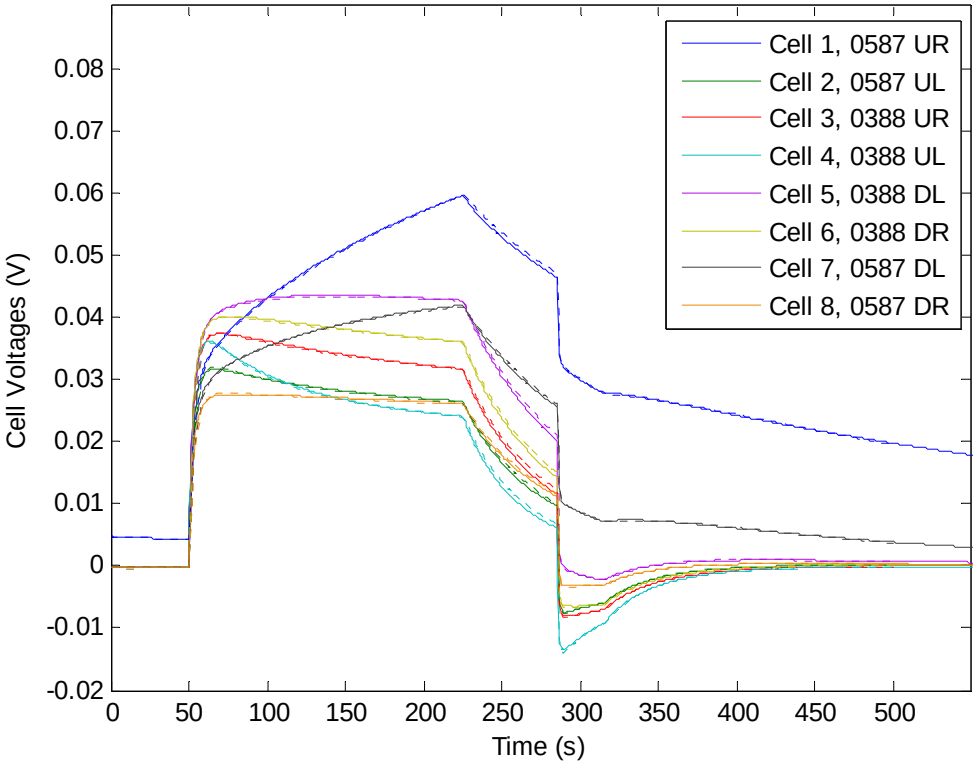

Figure 8.10 Results of the Stack PSDB Test after the Humidification of Cartridge 0587, Solid Line Experimental, Dashed Line ECM; Test Circuit Values: V_{Charge} = 303mV, R_{Charge} = 52.6Ω and $R_{Discharge}$ = 10.1Ω

Figure 8.10 shows each cell in the stack possesses a different voltage transient when compared to the passive test results obtained prior to the humidification of cartridge 0587, (shown in Figure 8.9). The increased hydration of the cells in cartridge 0587 has predictably altered the electrical properties of the cells. Specifically, a membrane possessing a higher water content will have a lower ionic resistance. In addition, the capacitance of the cell would also increase due to the increased mobility of the hydrogen ions. The PSDB test method results clearly reveal the change of electrical properties of cartridge 0587.

Upon close inspection of Figure 8.10, the voltage transients of the cells in cartridge 0388 have also changed, despite the cells not undergoing the humidification procedure. The change in results is to be expected as the voltage transient of a particular cell is partially dictated by the electrical properties of the other cells in the stack. Therefore, as the electrical properties of the cells in cartridge 0587 have been altered due to the humidification procedure, the voltage transients of all the cells in the stack will have changed.

From inspection of the test results alone, it is not be possible to identify which cells have undergone a change in their physical state, and which cells have remained the same. However,

by acquiring the circuit model parameters of each cell, the humidified cells should be easily identifiable. The circuit parameter values obtained after the humidification of cartridge 0587 are shown in Table 8.7. For comparison purposes, the circuit parameter values of the stack prior to the humidification procedure are reproduced in Table 8.7.

Table 8.7 Circuit Parameter Values Before and After the Humidification of Cartridge 0587, Humidified Cells Shaded

Cell	Before Humidification of cartridge 0587				After Humidification of cartridge 0587			
	R_a (Ω)	R_b (Ω)	C_a (F)	C_b (F)	R_a (Ω)	R_b (Ω)	C_a (F)	C_b (F)
Cell 1, 0587 UR	548	387	0.507	0.162	357	253	0.770	0.315
Cell 2, 0587 UL	85.0	397	0.444	0.123	86.1	281	0.619	0.202
Cell 3, 0388 UR	103	368	0.510	0.127	103	364	0.534	0.138
Cell 4, 0388 UL	77.5	357	0.491	0.126	77.7	351	0.513	0.141
Cell 5, 0388 DL	144	445	0.511	0.122	143	437	0.529	0.127
Cell 6, 0388 DR	118	406	0.492	0.123	118	398	0.512	0.132
Cell 7, 0587 DL	184	374	0.463	0.138	161	261	0.725	0.232
Cell 8, 0587 DR	66.5	326	0.481	0.136	86.5	225	0.744	0.238

In general, the circuit parameter values of the cells in cartridge 0388 remained the same, while the values of the cells in cartridge 0587 changed. In addition, the circuit model values have changed according to the physical properties attributed to them. For instance, the ionic resistance of the membrane decreases with increasing humidity. Table 8.7 shows the circuit parameter R_b for each cell in cartridge 0587 has decreased. As the ions in a hydrated membrane have a higher mobility, the capacitance effect of the membrane also increases. Table 8.7 shows that all values of C_b, attributed to capacitance effect of the membrane, have increased for the humidified cells.

In the derivation of the passive equivalent circuit model, Section 4.3, the capacitor C_a was attributed to the capacitance effect of just the electrodes, i.e. the value is related to the real surface area and separation of the anode and cathode. Therefore, the value of capacitor C_a is not expected to change significantly with an increase in membrane hydration. Table 8.7 shows that the value of C_a did in fact increase significantly for the hydrated cells. Clearly, the value of capacitor C_a is partially dictated by the ions present in the membrane. As discussed in Section 2.2.2, the ionic charge distribution near the surface of a charged electrode is somewhat complicated. A plane of solvated ions exists near the surface of the electrode, defined as the outer Helmholtz layer, with a more random distribution of ions extending into the bulk electrolyte. It is likely that the value of C_a includes the effects of the ions in the immediate

vicinity of the electrode, whereas C_b accounts for the ions more in the bulk of the electrolyte, which are subject to ionic resistance.

The value of R_a, representing direct conduction across a cell, changed irregularly for the cells that were humidified. Cells UR and DL decreased, while cells UL and DR increased in value. The change in R_a cannot be attributed to any error in the testing process, or subsequent determination of the circuit parameter values, as the values of R_a for cartridge 0388 are very similar for both tests, shown in Table 8.7. Even though the cause of R_a changing is unknown, its value does not strongly indicate active fuel cell performance. For example, taking the two extreme values of R_a 66.5Ω and 548Ω, at a voltage of 0.6V this accounts for a leakage current of 9.0mA and 1.1mA respectively. Both of these values are insignificant compared with the ionic current of up to 7A. Only when the fuel cell is operating at a low current, would leakage current influence the operating voltage, as discussed in the previous section.

The circuit model parameters most important in predicting a change in active performance of the stack are R_a, C_a and C_b. Figure 8.11 shows the percentage change in these circuit model parameters.

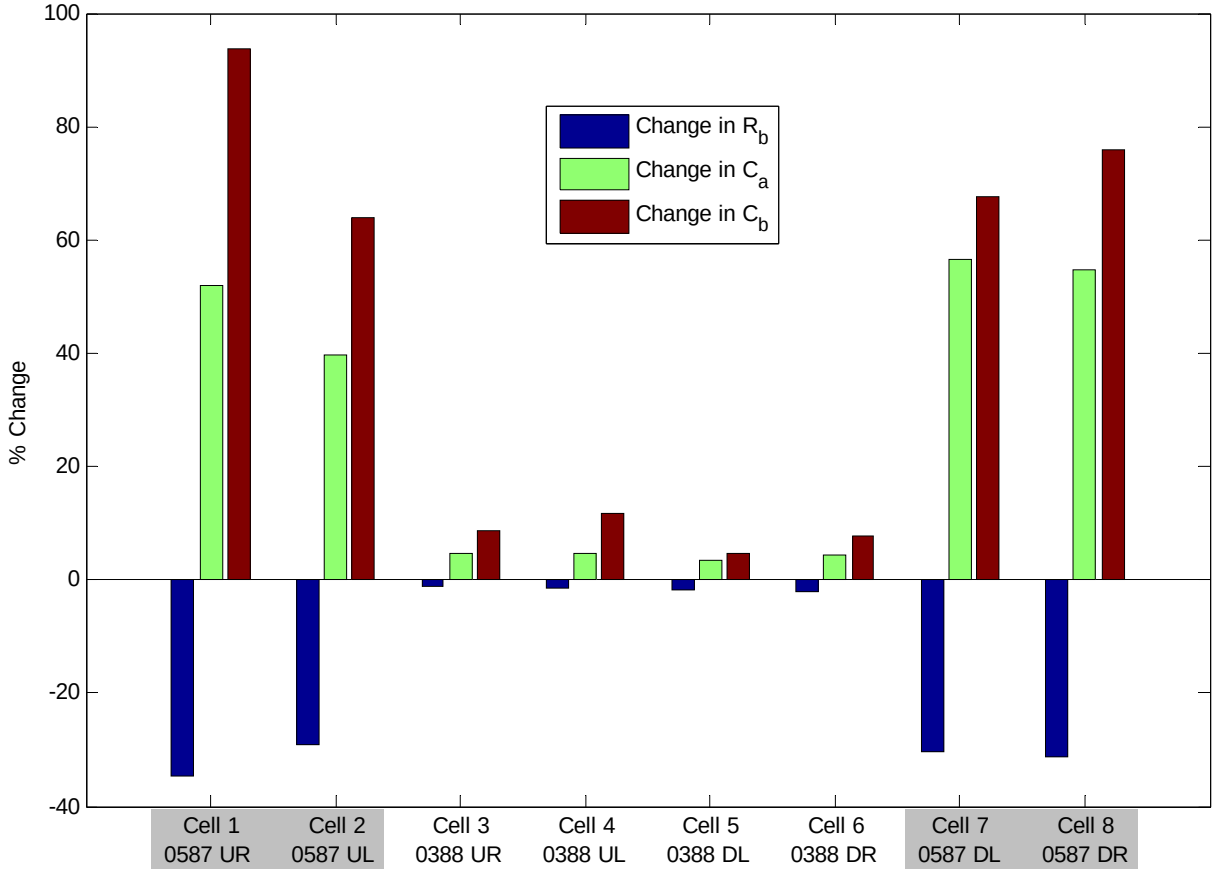

Figure 8.11 The Change in Circuit Model Parameters Due to Humidification of Cartridge 0587

By examining the change in circuit model parameters, shown in Figure 8.11, the cells that underwent the humidification procedure are clearly identifiable. Ideally, the circuit model values for the cells in cartridge 0388 should be the same for both tests, thus the percentage difference between the two tests should be zero. Considering the ±5% uncertainty on each parameter value, as determined in Section 7.4.4, all of the circuit values for the cells in cartridge 0388 do in fact agree within uncertainties, except one. Parameter C_b in cell 0388 UL is found to be significantly higher in the second test. As the cell did not undergo any physical change in the time between the two passive tests, the different values obtained are attributed to errors in fitting method.

The primary goal of the PSDB test method is to predict the active performance, or a change in active performance of each cell within a fuel cell stack. Therefore, without being aware of the humidification procedure, the results of the passive test alone should provide information on the active functionality of the cells in comparison to the prior established baseline performance. For the cells in cartridge 0587, the value of R_a has decreased, indicating a decrease in the ionic resistance. Hence, the expected voltage performance of the cells in cartridge 0587 would be higher than the baseline performance. A performance increase is also predicted by observing that the capacitance values for the cells in cartridge 0587 have also increased. As all of the circuit parameter values for cartridge 0388 have not changed significantly, the performance of these cells is expected to be the same as the base line performance. In summary, the performance of the cells in cartridge 0587 should improve, while the cells in cartridge 0388 remain the same as determined from the PSDB test.

In order to confirm the predictions made above, the active performance of the fuel cell stack was determined by obtaining the VI curve. The warm-up procedure and method for obtaining the VI curve is the same as the previous active test conducted. Figure 8.12 shows the resulting VI curves for each cell. For comparison purposes, Figure 8.12 also shows the original, baseline performance. For clarity the results have been separated, with the cells in cartridge 0388 shown in 8.12a, and those of cartridge 0587 shown in 8.12b.

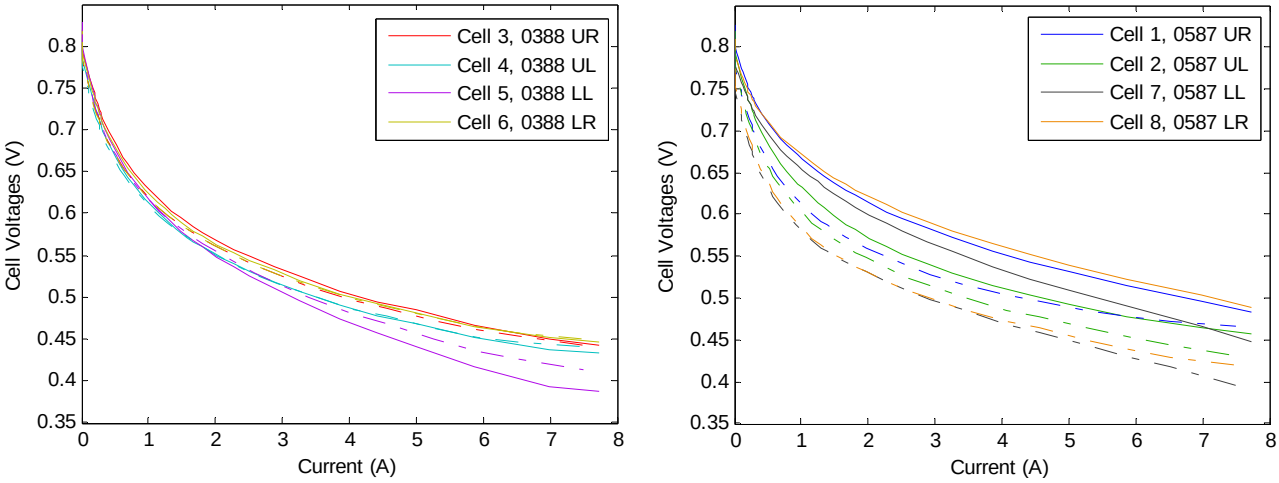

a) **b)**

Figure 8.12 The Active Performance of the Stack After the Humidification of Cartridge 0587 (solid line) Shown in Comparison to the Base Line Performance (dashed line)

As predicted, the performance of the humidified cartridge 0587 has clearly improved whilst the performance of cells in the cartridge 0388 remained the same. In Figure 8.12b, the voltage performance of each humidified cell is higher at each current value tested, compared to the original baseline performance. The cell in cartridge 0587 that underwent the smallest improvement in performance, although still significant, is Cell 2, 0587 UL. By close inspection of Figure 8.11, the percentage change in each circuit parameter of cell 2 is actually the smallest when compared to the rest of the cells in cartridge 0587. Figure 8.12 shows that Cell 8, 0587 LR under went the largest change in active performance. Hence, the passive test results should show that this cell underwent the largest change in the values of the circuit parameters. Figure 8.11 shows that this is only the case for circuit parameter C_a, with circuit parameters R_a and C_b exhibiting a larger change for Cell 1, 0587 UR. Considering the uncertainty in the circuit parameter values, ±5%, the specific change in a circuit model parameter, is not expected to predict the level of improvement observed in the active test. In summary, the active functionality of each cell in cartridge 0578 has improved, as predicted using the PSDB test.

The performance of each cell in cartridge 0388 has remained very similar for both active tests, with the exception of Cell 5, 0388 LL. The voltage performance during the second test is clearly lower than the original, baseline performance. A likely cause for the poorer than expected performance was airflow interference. As the position of cell 5 lies directly on the bench top, obstructions, such as wires lying on the bench, occasionally drifted across the outlet of the cathode. This would have obstructed the airflow, thus reducing the performance of the cell. As discussed in Section 4.4, the passive test only indicates the performance of the cell, based on the

physical state of the electrode membrane assembly. Cleary, other factors such as an airflow obstruction, can affect cell performance.

8.2.1 EXPERIMENTAL SUMMARY

The PSDB test, including circuit model analysis, has been used to successfully identify which cells in a stack have undergone a change in their physical state, specifically, hydration. The circuit model values changed in a way that agreed with the physical properties attributed to them. For instance, R_b, which is associated with the ionic resistance decreased, while the capacitance values increased with an increase in the cells hydration. This verifies the physical properties attributed to the cells, described when the passive circuit model was derived in Section 4.3. The corresponding change in the active performance of the cells was predicted from the circuit model analysis, and confirmed by obtaining the VI curve of the fuel cell stack.

8.3 CONCLUSIONS

This chapter has demonstrated the effectiveness of the PSDB test method for indicating the active functionality of the fuel cell. The results of the PSDB test method were related to the active functionality of the fuel cell in two ways. A direct correlation was observed between the PSDB test results and the relative functionality of the active cells. However, the correlation was only present if the active voltage of the fuel cell is measured at a low current value. In addition, the correlation was not observed in all fuel cells tested. Analysing the PSDB test results using the circuit model parameters provided much more insight into the fuel cell active operation.

An important aspect of the circuit model analysis and subsequent performance prediction was the establishment of base line performance data. A PSDB test, followed by an active test, enabled a set of circuit model parameters to be associated with a particular level of fuel cell functionality. Subsequent PSDB testing and ECM parameter evaluation is used for predicting performance changes of cells within the stack, in comparison to the base line performance data.

With the establishment of base line performance data, the PSDB test method could add value to the monitoring and management strategy of a telecommunication based fuel cell system. For example, environmental conditions may excessively dehydrate the cells over time. This change in state of the fuel cell would be detected by the PSDB fuel cell test, as a change in the circuit

model parameters. With this knowledge, corrective action could be taken. This may include a slower warm-up procedure, providing the required battery capacity is present. A process to humidify the stack could be undertaken, such as introducing a small amount of hydrogen into the cell, which would react on the electrode surface and produce water. It is interesting to note that if the stack was simply started, as part of a periodic testing program, the cause of reduced performance would not be known. Conducting a PSDB stack test provides further information for diagnosing the cause of a performance reduction. Clearly, further development of the PSDB test could be conducted, such as examining whether particular contaminants can be detected. This is future work which is outlined in the final chapter.

9 CONCLUSIONS AND FUTURE WORK

This chapter summarises the research presented in this thesis, and suggests further avenues of research. Section 9.1 outlines the research motivation and hypothesis. Section 9.2 states the findings of the literature and technology review. The experimental method, modelling and analysis used in this thesis is explained in Section 9.3. The achievements and novel aspects of this work are highlighted in Section 9.4, with a discussion on future work being presented in Section 9.5.

9.1 RESEARCH MOTIVATION AND HYPOTHESIS

The primary objective of this thesis was to develop a testing method for a Proton Exchange Membrane Fuel Cell in an application setting, specifically telecommunications backup power. As reliability is the most important feature for this application, the goal was to develop a testing method and subsequent analysis procedure that could provide information on the operational status of the fuel cell. This capability would represent important progress in the commercialization of PEM fuel cells.

This thesis proposes that a fuel cell can be tested, and can provide valuable information on the operational status while in a in a passive, non-functioning state. The novel test method developed in this thesis has been named the passive state dynamic behaviour (PSDB) test. The PSDB is based on electronically perturbing the fuel cell while in a passive state, and measuring the voltage response. The fuel cell is claimed to act as an RC circuit, and by obtaining the parameter values of an equivalent circuit model, information about the active performance of the cells can be determined.

9.2 LITERATURE AND STATE OF THE ART REVIEW

Testing method requirements were defined by reviewing PEM fuel cell technology, and considering the constraints of backup power systems. A testing method that assesses the condition of individual cells was found to be a primary requirement, as the failure of a single cell will cause the entire fuel cell stack to fail. Degradation and subsequent failure is most likely to occur in the membrane electrode assembly (MEA), so the MEA was the focus of a testing method. Further requirements included test simplicity and system integration. In addition, as hydrogen consumption reduces backup power run time, a test that minimises hydrogen consumption would be particularly advantageous.

Existing fuel cell testing and modelling methods were reviewed, and the applicability to backup power based fuel cell systems was considered. The main testing methods currently utilized are VI curve evaluation, Electrochemical Impedance Spectroscopy, and current interrupt/pulse techniques. The primary focus of testing was found to be aimed at fundamental study of the fuel cell, such as isolating the magnitude of the individual loss mechanisms. Almost all of the testing methods reviewed are performed on the fuel cell in an active state, and substantial electronic testing equipment is generally required.

Review of literature showed an emphasis for active behaviour PEMFC Modelling. Steady state modelling is most commonly achieved using a semi-empirical model, fitted to VI data of a functioning fuel cell. To capture the dynamic properties of an active fuel cell, an equivalent circuit model is used. Although a stack VI curve, (containing VI curves of each cell) can be used to determine individual cell properties by fitting the data to a model, testing and modelling dynamic behaviour using an ECM is restricted to single cell analysis using current techniques.

The construction and operating characteristics of double layer capacitors (DLC), and DLC testing and modelling methods were reviewed. A DLC was shown to be physically similar to a PEM fuel cell. Certain testing and modelling techniques for DLCs and fuel cells are the same, such as electrochemical impedance spectroscopy and equivalent circuit modelling. The testing and modelling of a DLC is primarily aimed at defining the electrical characteristics such as the capacitance (as a function of test frequency or applied voltage), and resistance (including leakage current through the cell).

In summary, fuel cell testing and modelling methods currently used are not particularly suited for an application setting such as telecommunications back up power. Thus, the PSDB test and associated passive ECM were proposed and developed in this thesis.

9.3 PSDB TEST DEVELOPMENT AND EXPERIMENTAL METHOD & ANALYSIS

The PSDB test method is conducted while the fuel cell is in a non-functioning, passive state, with no hydrogen present in the cell. The fuel cell is essentially charged and discharged during the test process using a simple test circuit consisting of a small DC voltage supply, two switches and two resistors. The test protocol is implemented across the electrical terminals of a stack, and the voltage response of each cell is measured and recorded.

The PSDB test results were analysed using an equivalent circuit model, derived by considering the physical properties of a PEM fuel cell in a passive state. The circuit parameters of the ECM were attributed to fuel cell physical properties. Hence, the circuit parameter values can be used to indicate the physical state of the fuel cell. A method to determine the ECM parameter values was also developed. An iterative numerical technique was used that enabling the ECM parameter values of numerous cells to be determined using the results of a single stack test. The equivalent circuit model, and method for determining the ECM parameter values, provides the necessary tool for assessing the condition of a fuel cell stack.

An experimental test system was developed, and the passive and active properties of three different fuel cells was evaluated. A direct correlation between passive and active testing results was demonstrated. Specifically, the rate of voltage decay after a charge period of the PSDB test, was found to correlate with the voltage performance of the cells when active. The PSDB test and circuit model analysis was successfully used to identify which cells experienced a change in their hydration state. Considering the physical properties attributed to the circuit model parameters, the values changed in a manner expected with an increase in hydration. Using the measured change in the circuit model parameters, the active performance of the affected cells was successfully predicted to increase. In summary, a PSDB test implemented across a fuel cell stack, together with a circuit model analysis of the results, has been used to successfully predict a change in the active performance of individual cells within the stack. In summary, the experimental test system was successfully used to implement the PSDB test, with the measured

voltage response being used to determine the capacitive and resistive parameter values of the passive ECM, leading to a successful prediction of the active performance.

9.4 ACCOMPLISHMENTS

The main outcome of this research was the development of the PSDB test, a novel testing and analysis technique, designed for backup-power based PEM fuel cell systems. There are a number of unique features of the PSDB test method and circuit model analysis that distinguishes it from the prior art. Specifically, novel features are;

- The test is carried out while the fuel cell is in a passive state
- ECM of a Passive FC developed
- Only a single test implemented on the entire stack is used to acquire the individual properties of each cell in the stack
- A method of determining model parameter values for many individual cells from the results of a single stack test was developed
- The test method is simple, and requires minimal equipment

These features of the test method are particularly suited for backup power applications.

The testing method originality, coupled with the usefulness of the test for backup power based fuel cell systems was further confirmed by the application, and successful examination of an international patent application (see Appendix I). The patent was filed by Eaton Corporation, New Zealand, a global leader in DC backup power systems for telecommunications.

9.5 FUTURE WORK

The novelty of the PSDB test method opens many avenues for future research, not only in relation to application based testing, but also on a more fundamental level. Future development and refinement of the PSDB test have been alluded to in the description of the method and results analysis. These ideas are further explained, together with future work in the area of fundamental study.

Chapter 8 demonstrated how prior established baseline data, i.e. ECM parameter values and active performance data, was used in predicting the change in fuel cell performance. Specifically, the increased performance of certain cells was predicted from the change in circuit model parameter values due to a change in the hydration state. This analysis could be extended, such that the magnitude of the observed change in ECM parameter values is related to a specific performance change. This analysis could be quantified, such that a specific performance change could be predicted from the change in ECM parameter values. A functional relationship between the ECM parameter values, hydration and active performance, could be established with a set of controlled experiments. Other physical properties of the fuel cell could be altered, and the same comparative analysis could be conducted. For instance, the fuel cell may be purposely poisoned with CO or Sulphur compounds, and the resulting change in circuit model parameters could be observed, together with the change in the stack functionality. The way in which additional physical factors effect the circuit model values, and how this relates to the active performance of the stack, will clearly add to the value of the PSDB test.

Variations of the passive testing process, and optimization of the fitting method are definite areas of future investigations. Throughout this thesis, a consistent passive testing sequence was used, consisting of a charge, open circuit, discharge and open circuit. Clearly, the particular protocol is not limited to this sequence only, and additional periods of interaction with the test circuit may be included. A different testing sequence may aid in identifying ECM parameter values with greater accuracy. This may be particularly true of circuit element R_c, representing electrical resistance between the cells, which is assumed to be very small (thus ignored) in the results presented. The iterative fitting method used to determine the ECM parameter values could also be optimized. Although Matlab Simulink provided a simple and flexible tool for acquiring the ECM model response, the software was computationally expensive. A mathematical model could be directly computed and solved for a fuel cell stack and testing conditions imposed. In summary, there is a wide scope of alternative passive testing sequences, and potential optimization of the fitting method.

Interpretation of the passive test results was limited by the lack of fuel cell stack construction and material composition information. For example, the observed difference between passive test results of various Avista cartridges was attributed to age differences. Newer cartridges (identified by their higher serial numbers) are physically different, due to ongoing R & D to improve cell performance. However, the specific physical differences between new and old cartridges were unknown due to proprietary considerations of manufacture. Thus, the difference

in passive test results among various cartridges could not be attributed to any specific physical property of the fuel cell. With detailed information on stack and cell construction, specific features of the passive test response may be attributed to physical aspects of the cell, providing greater insight to the passive test results.

A potential area for future research is passive testing and equivalent circuit modelling of a PEM fuel cell, aimed at fundamental study, rather than an application driven approach. For example, a number of individual cells that differ in a single physical property (such as catalysis loading) could be passively tested and analysed with the ECM. Implementing the passive test in this fashion may provide a means to directly link the circuit parameter values with cell properties. Thus far, the circuit model parameters, although indicative of cell condition, have not been quantitatively linked to physical properties of the fuel cell. For example, even though resistor R_b is associated with the ionic resistance of the membrane, which decreased with humidification as expected, the value obtained is not a direct measure of the ionic resistance when the fuel cell is in operation. Likewise, specific capacitance values cannot be linked to the real surface area of a cell. Implementing the passive test method on a single cell, under controlled conditions, would allow the results of the passive test method and circuit model analysis, to be compared with cell properties measured using other testing techniques.

APPENDIX A: PUBLICATIONS, REVIEWS AND PATENTS

A number of works have been published as result of the fuel cell research conducted. A full list of the published papers is provided below. Two papers that detailed the research most comprehensively, are reproduced, together with the peer review assessments of these papers. Lastly, the front page of patent is reproduced, detailing the filing dates, classifications, etc.

Journal Publications

Shannon C Page, Adnan H. Anbuky, Susan P Krumdieck, Jack Brouwer,; "Test Method and Equivalent Circuit Modeling of a PEM Fuel Cell in a Passive State" IEEE Transactions on Energy Conversion, Vol. 22, pp. 764–773, Sep. 2007
Award: Runner up in the 2006 Department of Mechanical Engineering Best Paper Competition

Krumdieck S, Page S, Round S, "Solid oxide fuel cell architecture and system design for secure power on an unstable grid", Journal of Power Sources, Vol. 125, pp. 189-198, Jan. 2004

Conference Publications

S. C. Page, S. P. Krumdieck, A. Anbuky, "Testing Procedure for Passive Fuel Cell State of Health", Australasian Universities Power Engineering Conference, University of Queensland, Brisbane, Australia, 26 – 29 September 2004
Award: Student presentation Prize
Award: Student Travel Prize (based on paper content)

S. C. Page, S. P. Krumdieck, A. Anbuky; "Condition Assessment Monitoring (CAM) Test for PEM Back-up Power Systems" Fuel Cell Seminar (San Antonio, Texas November 2004)

S. C. Page, A. Anbuky S. P. Krumdieck, “Framework Model of a Proton Membrane Exchange Fuel Cell (PEMFC) System” Australasian Universities Power Engineering Conference, Christchurch, New Zealand, September 2003

S. C. Page, A. Anbuky, S. P. Krumdieck Modular “Organization for PEMFC System Simulation Model”, Fuel Cell Seminar 2003 (Miami, Florida November 2003)

Krumdieck, S. and S. Page, “SOFC Architecture and System Design for Secure Power, in Proceedings of the Fuel Cell Seminar” (Palm Springs, California November 2002).

Patents

Page, Shannon Charles; Krumdieck, Susan Pran; Al-Anbuky, Adnan; “Method of testing an electrochemical device” WO/2005/093447, PCT NZ/05/00053, March 2005

Brown, Michael Asher; Krumdieck, Susan Pran; Abrahamson, John Curnow; Owen John; Page, Shannon Charles; *Method for regeneration of metal hydrides and hydrogen storage systems*; New Zealand Provisional Patent #526352, December 2003

Test Method and Equivalent Circuit Modeling of a PEM Fuel Cell in a Passive State

Shannon C. Page, Adnan H. Anbuky, Susan P. Krumdieck, and Jack Brouwer

***Abstract*— A novel test protocol is proposed for fuel cells that are in a non-functioning, or passive, state. Standard fuel cell test methods are reviewed, along with the equivalent circuit models (ECM) used to represent functioning, or active, fuel cells. Standard active tests focus on single cells, while the passive test is shown to be applicable to testing multiple cells. The passive test measures electrical characteristics of the fuel cell in the absence of electrochemical reactions. A simple ECM is developed to describe the cell behavior under the passive test conditions. Circuit model parameters of many series-connected cells can be acquired using the results of a single stack test. PEM fuel cells from three manufacturers were tested, ranging in system power from 12 – 500W. Test results for each PEMFC exhibited similar behavior that is well predicted by the ECM. A strong similarity between a passive fuel cell and a double layer capacitor (DLC) is discussed.**

***Index Terms*— Capacitors, Circuit modeling, Electrochemical devices, Fuel cells, Testing**

I. Introduction

FUEL cells have undergone significant development in the last 15 years, spurred in part by their unique energy conversion characteristics, including high efficiency and minimal environmental impact at the point of use. Fuel cell technology is in pre-commercialization development, with increasing interest in manufacturing and application issues.

A Proton Exchange Membrane (PEM) fuel cell employs a hydrated polymer membrane as the electrolyte, which conducts hydrogen ions (H^+), but not electric current. The electrodes consist of activated carbon, with a finely dispersed catalyst (typically platinum) at the electrode-electrolyte interface. Many different designs for individual cells and stacks have been developed, manufactured and then integrated into power systems with generation capacity from 10W to 100kW. Testing methods to monitor material properties and cell condition are needed for reliability of fuel cells in target applications such as back-up power.

This paper presents a new testing technique that is versatile, simple, can be implemented on an entire stack, and through numerical analysis indicates properties of individual fuel cells. The passive test technique probes the electrical properties of the fuel cell in the absence of electrochemical reactions, a strategy not previously reported.

Section II of this paper reviews existing testing methods, describing the particular fuel cell properties measured. The results of these test methods are often interpreted with the aid of equivalent circuit models (ECM), thus Section III reviews the range of models employed. Section IV illustrates the physical similarity between a PEM fuel cell and a double layer capacitor (DLC). The experimental systems, including three distinct fuel cell designs, used to evaluate the new test method are described in Section V. The passive test method itself, experimental results and qualitative analysis are given in Section VI. Section VII details the proposed ECM, and describes the technique employed for acquiring the circuit model parameters. Section VIII demonstrates how the testing method and circuit model analysis is used to find the properties of each cell in a stack using the results from a single test. Finally, concluding remarks are presented in Section IX.

II. Review of Common Fuel Cell Testing Techniques

Fuel cell testing methods are derived from general electrochemistry techniques. Material properties can be tested *ex situ*, as in [1] where the ionic resistance of the polymer membrane is measured. [2] used a cyclic voltammetry test method to investigate various PEM catalysts in a half-cell configuration. A range of testing approaches have been used for full fuel cells, stack assemblies and working PEMFC systems. The main testing techniques are reviewed below, including VI curve evaluation, electrochemical impedance spectroscopy (EIS), and current pulse/interrupt methods.

A. VI Evaluation

The most common method of testing a PEM fuel cell is to obtain a steady state voltage versus current (VI) curve of an operating cell or stack. The VI curve is generally obtained by holding the fuel cell operating conditions constant (such as the temperature, gas stoichiometry, humidity etc.) and measuring the steady state voltage versus a set of current values. The VI curve can be characterised by either mechanistic (as in [3], [4]) or empirical (as in [5], [6]) model equations, resulting in a mathematical description of fuel cell performance. Analysis of the VI curves and resulting model equations allows the magnitude of the three main loss mechanisms to be inferred, as they influence the VI curve at different current values. Losses caused by the charge-transfer processes at the electrode-electrolyte interface (often referred to as activation loss) results in a relatively steep decline of the VI curve at low currents. Membrane ionic resistance, together with electronic resistance of the electrodes and current-collectors, results in a linear decrease of voltage with increasing current at nominal operating currents. At high currents, a rapid decay in the VI curve is observed, due to a reactant/product reaching the limiting rate at which it can be transported to/from the reaction sites. This loss is generally referred to as diffusion or mass-transport loss.

Different loss mechanisms dominate different current ranges, but each still affects the performance at all operating points. The VI curve provides the net performance of an active stack under a certain set of steady state operating conditions. In order to identify the losses more clearly, and to assess the impact of operating conditions, a family of VI curves are often obtained, with the fuel cell being held at different operating conditions for each curve. Thus, VI curve evaluation is conducted in a lab environment, where accurate control over test conditions can be maintained.

B. Electrochemical Impedance Spectroscopy (EIS)

Electrochemical Impedance Spectroscopy (EIS) or AC impedance testing is commonly employed for determining fuel cell properties. The technique consists of imposing a low amplitude sinusoidal voltage (or current) onto the fuel cell while it is operating at a specific level of current production (a certain point on the VI curve). The impedance is calculated by measuring the phase and amplitude of the current (or voltage) response at that condition. A frequency sweep is used (typically 10mHz to 100kHz) in order to obtain a full impedance spectrum (i.e., map the entire range of dynamic response characteristics). Usually, a functioning fuel cell is tested, in which case the AC perturbation is superimposed onto a DC load that can be changed to map the performance over the entire operating regime of the fuel cell.

EIS is accepted to be superior to steady state VI curve evaluation for separating out and identifying the different loss mechanisms of a fuel cell, due to the association of certain loss mechanisms with particular frequency ranges [7]. For instance, at very high frequencies, the impedance is due to ohmic losses, predominantly the membrane ionic resistance. At intermediate frequencies, charge transfer resistance coupled with the double layer capacitance, also contributes to the impedance. Finally, at low frequencies, diffusion/mass-transport losses add to the measured fuel cell impedance [8], [9].

Despite the different loss mechanisms contributing to the impedance at different frequency limits, it is not always clear what specific features of the impedance spectrum relate to which physical, chemical or electrochemical processes and features of the fuel cell. Multiple tests can be conducted in order to relate fuel cell processes and properties more clearly to features of the impedance spectra. In these cases the fuel cell can be held at a different current density (as in [10], [11]) or other operating variable can be changed for each impedance test. Whereas this approach may provide more insight into the physical, chemical or electrochemical features of the fuel cell that contribute to the impedance spectra, insight is not guaranteed and the testing process may become arduous and difficult to interpret. In addition, EIS is limited to a single cell, and requires substantial electronic equipment. Most would agree that this technique is limited to laboratory testing only.

C. Current Interrupt/Pulse Methods

Current interrupt or current pulse methods have been proposed as a simpler technique (compared with EIS) for obtaining fuel cell properties. These methods involve subjecting a functioning fuel cell to a step change in current, and measuring the resulting voltage transient. A variation on this method involves subjecting a functioning fuel cell to a short duration current pulse [12], [13]. The main properties that can be obtained using this method are the ohmic resistance, calculated from the instantaneous change in potential, and charge transfer loss, obtained from the gradual change in potential to a steady state value [14], [15]. Longer voltage transients have been attributed to diffusion losses when, for example, a molten carbonate fuel cell was subjected to a current interrupt test [16]. As with EIS, current pulse/interrupt testing is implemented on a single cell only. In addition, current interrupt/pulse methods are limited to finding only certain features of fuel cell operation related to ohmic and activation losses.

D. Activation Loss Analysis

PEMFC testing has been reported with the specific aim of isolating and clearly identifying the magnitude of certain loss mechanisms. . A common strategy is to conduct multiple tests with the fuel cell at different operating conditions. Isolating the activation loss associated with hydrogen and oxygen half-cell reactions at the cathode or anode is particularly challenging. For other electrochemical devices, such as batteries, a reference electrode is inserted in the electrolyte to isolate the losses occurring at each electrode. However, this is not practical for a PEM fuel cell.

Wagner *et al*. [10], [11] conducted EIS with a symmetrical gas arrangement at open circuit. Two spectra were obtained, one with H_2 at both electrodes, and the other with O_2 at both electrodes. The loss associated with the anode and cathode was inferred from the H_2/H_2 and O_2/O_2 impedance spectra respectively. Andreaus *et al*. [9], [13] isolated losses at the anode by conducting EIS while operating the cell as a hydrogen pump, reducing H_2 at one electrode and oxidising H^+

This work was supported by the Foundation of Research Science and Technology, through the Technology in Industry Fellowship, contract number IESL0101.

S. C. Page is with the Department of Mechanical Engineering, University of Canterbury, Christchurch, New Zealand (e-mail: scp24@student.canterbury.ac.nz)

A. H. Anbuky is with the Electrical & Electronic Engineering Department, Auckland University of Technology, Auckland, New Zealand (e-mail: adnan.anbuky@aut.ac.nz)

S. P. Krumdieck is with the Department of Mechanical Engineering, University of Canterbury, Christchurch, New Zealand (e-mail: Susan.Krumdieck@canterbury.ac.nz)

J. Brouwer is with the National Fuel Cell Research Center, University of California at Irvine, Irvine, CA 92697 USA (e-mail: Jack.Brouwer@nfcrc.uci.edu)

at the other, with current densities of up to 500mA/cm^2. O'Hayre *et al*. [17] demonstrated a loss present at the cathode but not at the anode of their planar fuel cell, which comprised a common membrane electrode with cells externally connected in series. Lateral ionic condition of the membrane causes internal currents to flow when adjacent cells are connected in series, thus a voltage drop at open circuit is observed on each cell, except for the cell at the positive end of the stack, since no O_2 is being reduced.

III. Fuel Cell Equivalent Circuit Models (ECM)

Equivalent circuit models (ECM) are used to model fuel cell behaviour, and interpret test results in relation to cell properties. Various models have been proposed, which vary significantly in terms of complexity and form. The purpose of certain models has been to simply replicate the terminal behaviour of the fuel cell. For example, a circuit model that reproduces VI curve and voltage transient behaviour (induced by load changes) has been developed [18], [19], and a circuit that simulates the effects of inverter ripple current on a fuel cell has been proposed [20]. Other physical aspects of the fuel cell, such as changes in the gas partial pressures can also be included [21], [22]. These models are derived from net processes and thus the ECM structure and component values are not directly related to physical properties. The following review focuses on ECMs that have been derived from physical and material considerations.

A. PEM Fuel Cell Equivalent Circuit Models (ECM)

The ECM most often used to represent a fuel cell is shown in Fig. 1b, which is a basic model of any electrochemical cell [23]. R_{ionic} represents the ionic resistance of the membrane, $R_{CT,A}$ and $R_{CT,C}$ represent the charge transfer loss/resistance across the electrode-electrolyte interfaces at the anode and cathode respectively. The capacitors $C_{DL,A}$ and $C_{DL,C}$ represent the double layer capacitance present at the anode and cathode electrode-electrolyte interfaces.

Current dependent resistances $R_{CT,A}$ and $R_{CT,C}$ have been introduced to account for the non-linearity of the charge transfer resistance [17]. R_w and C_w model the diffusion/mass-transport losses, and are shown in Fig. 1d for a fuel cell [11] and Fig.1 e for a general electrochemical cell [23]. The diffusion loss or impedance, commonly referred to as the Warburg impedance, has a long time constant leading to slow voltage transients induced by load changes [16].

A simplified model shown in Fig. 1c [24], [15], is commonly referred to as the Randel's equivalent. In this circuit, the charge double layers and the activation resistances have been combined into a single resistor and capacitor respectively. A frequency dependent component ($Z(\omega)$) may be added to account for diffusion losses. This circuit has been widely used to model the essential dynamics of a fuel cell [25], [26], and for interpreting the results of current interrupt and EIS test methods [13]. A source component(s) (not shown in any of the models of Fig. 1) is sometimes included in series with the model terminals, or in series with one or both of the

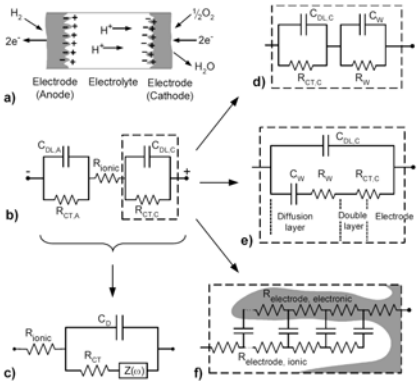

Fig. 1. A simplified schematic of a functioning fuel cell (a) shown with the common ECM (b). Modifications on the cathode side to take into account diffusion impedance for a fuel cell (d) and a general electrochemical cell (e). The classic transmission line model of a porous electrode is shown in (f). A simplified fuel cell model often used (c).

charge transfer resistances.

The classic transmission line model of a single porous electrode, shown in Fig. 1f, has been used when specific properties of the catalytic layer are investigated [8], [27]. The model consists of an electronic resistor rail connected to an ionic resistor rail through capacitors, such that ionic and electronic charges must move through a range of resistance paths to charge the double layer completely. Clearly, this model does not take into account charge transfer losses or any other active processes. Instead, the model represents the physical nature of the electrode-electrolyte interface, or catalytic layer.

B. Techniques of Acquiring Circuit Parameters

An EIS impedance spectrum is used to find the circuit parameters of an ECM in one of two ways. In both cases, the impedance as function of frequency, $Z(\omega)$, is derived for the circuit model in terms of the circuit parameters. In the first method the circuit parameter values are then found by fitting $Z(\omega)$ to the experimental impedance spectrum. This method can be used for finding the circuit parameters of a single cell regardless of circuit model complexity; however, a good fit using a complex model, does not imply a unique or physically meaningful circuit model or parameter values. Alternatively, the circuit parameter values are derived from particular regions of the spectrum, for instance, at very high frequencies the impedance of the circuit model reduces to R_{ionic}.

Voltage transients produced from current interrupt testing, can be used to calculate the circuit parameters. For instance, the sudden voltage change gives the series resistance R_{ionic}, with longer voltage transients attributed to the charge transfer resistance and double layer capacitance.

IV. Similarities with Double Layer Capacitors (DLC)

The fuel cell models reviewed thus far, along with the techniques employed for circuit parameter identification, are the same as those used for a general electrochemical cell, such as a battery or an electrolysis cell. A double layer capacitor (DLC) is another electrochemical device that is physically similar to a fuel cell, and which exhibits a similar behavior particularly when the fuel cell is in a passive/non-functioning state. The testing techniques and circuit models employed for a DLC are briefly reviewed in this section.

A. Physical Make-up of a Double Layer Capacitor

A DLC consists of two electrodes, separated by an electrolyte which contains free moving ions. When charged, a double charge layer forms at each electrode-electrolyte interface. Due to a very small charge separation between the ions in the electrolyte and the charge on the electrodes, very high capacitance values are achieved. DLCs are sometimes referred to as super capacitors or ultra capacitors; however these terms generally refer to devices in which the primary charge storage mechanism is something other than the double charge layer, such as the absorption of electrolyte species into a solid crystalline electrode [28].

Activated carbon is most commonly used for the electrodes, which is the same electrode material used in most PEM fuel cells. DLCs usually contain an organic based electrolyte, enabling higher voltages to be used before electrolyte breakdown occurs, which increases energy storage. Aqueous H_2SO_4 has also been used, and a number of DLCs employing Nafion® (a polymer membrane common in PEM fuel cells) have been developed and tested [29] – [32]. The processes in a DLC differ from a PEMFC in that only non-Faradaic processes can occur, such as the movement and accumulation of ions and electrons, whereas in a fuel cell, Faradaic processes dominate, i.e., electrochemical reactions proceed due to a charge transfer between the electrolyte and the electrode.

B. Testing and Modeling of Double Layer Capacitors

Several testing methods have been employed to characterize the electrical behavior of a DLC, which differs significantly from an ideal capacitor. EIS has been used by [33] – [36], and entails conducting an impedance sweep on the capacitor. Repeated impedance spectra are sometimes obtained, with the DLC at various levels of charge for each test. The other technique used for testing a DLC involves DC charge and/or discharge processes. This method typically involves subjecting a single DLC to a constant current charge and/or discharge, and measuring the voltage transient response [21], [37] – [42]. An important part of the test result, is the voltage transient after a charge period, where the DLC remains at open circuit.

A number of equivalent circuit models have been proposed that replicate the terminal behavior of a DLC. A multiple branched/ladder R–C circuit, as shown in Fig. 2, is commonly employed. The model has been proposed with two [41], three

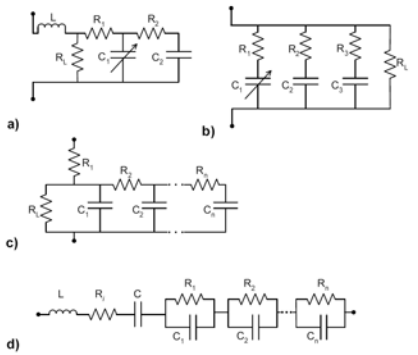

Fig. 2. Proposed Equivalent Circuit Models of Double Charge Layer Capacitors

[37], [40], or more [35] branches, depending on the time scale and accuracy required. A DLC possesses significant leakage current, for example, a DLC sold commercially (by Maxwell) loses up to 1.5% of the stored energy per day through leakage current [43]. Many DLC models have a resistor R_L across the model terminals to account for leakage current. The model shown in Fig. 2c was for highly dynamic simulations, and does not have an R_L component. The authors stated that an R_L could be added if predictions for longer times were required [33]. An inductor element is sometimes included when high frequencies are being modeled. However, as the inductor value tends to be small (in the order of nH), it is often ignored.

The capacitance of a DLC has been shown to be a function of the applied voltage [38], [40], [44]. The ECM, therefore, includes one capacitor having the form $C(V) = a + bV$ (where a and b are empirical constants) as shown in Fig. 2a and 2b. With the exception of R_L, the circuit models tend to be empirical in nature, in that no physical meaning or process is associated with the other elements of the circuit model. Although more complex DLC models have been proposed, which are based on the transmission line model of an electrode-electrolyte interface (Fig. 1f), they are not used for modeling the device.

C. Acquiring Circuit Parameter Values

Circuit parameters are typically calculated from the voltage transients produced during a charge/discharge test, requiring a number of assumptions. The R–C branches are assumed to possess distinctly different time constants. From analyzing the voltage transient, particularly just after a charge period when the cell is at open circuit, it can be assumed that the transient at a certain time is primarily due to a particular R–C branch. In addition, the initial voltage of the DLC is required to be zero, hence the initial voltage of the capacitors in the model will also be zero. For this condition to be satisfied, [28] showed that a DLC must be short-circuited for a very significant length

of time. Finally, whether EIS or DC charge/discharge testing is employed, the technique and corresponding analysis has only been reported in the literature for a single cell.

V. Experimental Testing Equipment

A. Overview of Test System

A system schematic of the test apparatus is shown in Fig. 3. A Hewlett & Packard 34970A Data Acquisition/Switch unit, containing a HP34901A 20-Channel Multiplexer module is used for voltage sensing and a HP34907A multifunction module is used for regulated voltage output. A notebook computer running Matlab is used for controlling the HP meter, and hence the test process, via an RS232 connection, with data sampled at 2Hz. Matlab is also used for data analysis and modeling.

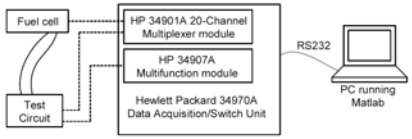

Fig. 3. Overview of experimental test system

B. Fuel Cells Tested

A low power PEM stack manufactured by MerCorp is shown in Fig. 4a, designed to operate up to 20W (~ 6.2A and 3.2V). The stack consists of six series connected cells, which have an active area of 31cm^2, and use a Nafion® based membrane electrolyte [45]. The construction of the stack is a typical bipolar design, with air and hydrogen in a counter flow arrangement. The stack is completely symmetrical, in that the electrode composition and flow field pattern are identical for the anode and cathode sides of each cell. Metal pins were clamped onto the side of each bipolar plate, allowing individual cells to be tested and monitored.

A 12W (1A and 12V) Enable fuel Cell stack is shown in Fig. 4b. The stack consisted of 23 series connected cells, each with an active area of 12cm^2. The stack is annular in design, with hydrogen introduced to the center of the stack (from both ends), and the air (through natural diffusion) entering the stack from the edges. Small clips attached to the metal separator plates of each cell allowed individual cells to be tested and monitored.

An Avista SR-12 PEM fuel cell system, which produces up to 500W (25V and 20A) was also tested (see Fig. 4c). The system contains 48 series connected cells, which are grouped into 12 removable cartridges. Each cartridge contains 4 edge current collected PEM cells, each with an active area of 50cm^2. A Nafion® based membrane electrolyte is used, and the stack design is semi passive, with air being blown across a thick gas diffusion layer. Measurements were made on individual cells by removing a cartridge from the system, and connecting to the individual cell terminals.

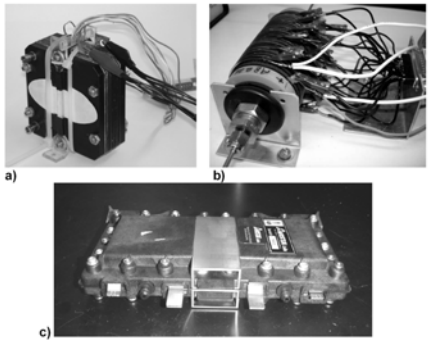

Fig. 4. Three Fuel Cells Tested, (a) MerCorp, (b) Enable and (c) a single cartridge from an Avista SR-12

VI. Test Method and Results

A. Test Protocol Employed

The test method is implemented while the fuel cell is in a passive, non-functioning state. No hydrogen is present in the stack, with air at both the anode and cathode; therefore, no electrochemical potential can form across any of the cells during the test. The electrical properties are then found using a sequence of DC electrical conditions, thereby charging and discharging the fuel cell in a capacitive sense. The simple test circuit shown in Fig. 5 is connected across a cell or a stack, and the test protocol is implemented by closing and opening the switches in the following sequence:

1. The initial voltages of the cell(s) and stack terminals are measured (S_1 and S_2 initially open)
2. The fuel cell is charged, using a constant voltage source, V_{Charge}, in series with the resistor R_{Charge}, (S_1 is closed)
3. The voltage source is disconnected, thus placing the fuel cell in an open circuit condition (S_1 is opened)
4. Charge held by the fuel cell is then dissipated through the resistor $R_{Dischage}$ (S_2 is closed)
5. The stack remains at open circuit for the remainder of the test (S_1 and S_2 opened)

The test protocol has been implemented on an individual cell from each fuel cell stack, the resulting voltage transients are shown in Fig. 6. Model results for these cells are also shown in Fig. 6 as a dashed line, and are describe in a later section.

B. Qualitative Discussion of the Test Voltage Transient

The voltage transient produced by each cell is very similar, and consists of five distinct areas that have been labelled: (1) Initial steady state, (2) Charge, (3) Decay, (4) Discharge, and (5) Self recharge. A qualitative discussion of each region is provided below.

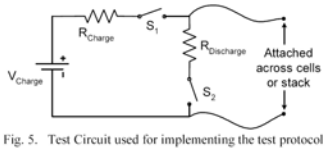

Fig. 5. Test Circuit used for implementing the test protocol

1) Initial Steady State

At the beginning of a test, it was common for a cell to possess a small "resting" potential, which is recorded during the initial test period. Initially, the resting potential was attributed to fuel cell operation days prior to the passive test. However, the resting potential was negative with respect to the polarity of the functioning cell. The results displayed in Fig. 6 only show a small resting potential; however up to 40mV has been observed with certain Avista cells. The resting potential was measured on each of the three fuel cells tested, and also on many Avista cartridges using a separate Fluke meter. Research continues to find the cause of this small, curious, and common negative resting potential.

2) Charge:

During the charge period, the cell is connected in series with a voltage source V_{Charge} and a resistor R_{Charge} (switch S_1 in the test circuit is closed). As the applied voltage is well below the level needed to decompose any water present in the membrane, the fuel cell acts primarily as a capacitor, resulting in an exponential rise in potential. In addition to electric charge accumulating on the electrodes, hydrogen ions are believed to migrate towards the negative electrode, forming a charge double layer in a similar manner to a DLC. The rise in potential deviates significantly from a pure exponential function, as the fuel cell, (like a DLC) does not behave as an ideal capacitor.

3) Decay

During the decay phase, the voltage source is disconnected (S_1 opened) and the cell remains at open circuit. The potential clearly decays for each of the fuel cells tested. There are two processes thought to be responsible for the observed decay, leakage current, and continued ion movement in the membrane.

The leakage current of a DLC is well documented and because of the physical similarity between a fuel cell and a DLC, it is postulated that leakage current also occurs in the fuel cell. The exact mechanism by which leakage current occurs is still being investigated. Direct electronic conduction across the cell may occur, either through a defect in the membrane electrode assembly (MEA) or the surrounding cell assembly. Alternatively, as oxygen is present at both electrodes, and dissolved in the water present in the membrane, it is possible that the following half-cell reactions could occur:

$$(+)\ \tfrac{1}{2}O_2 + 2H^+ + 2e^- \rightarrow H_2O \parallel H_2O \rightarrow \tfrac{1}{2}O_2 + 2H^+ + 2e^-\ (-)$$

A similar hydrogen-couple reaction could occur (as shown by [9]); however, molecular hydrogen needs to be present at the positive electrode for this to occur.

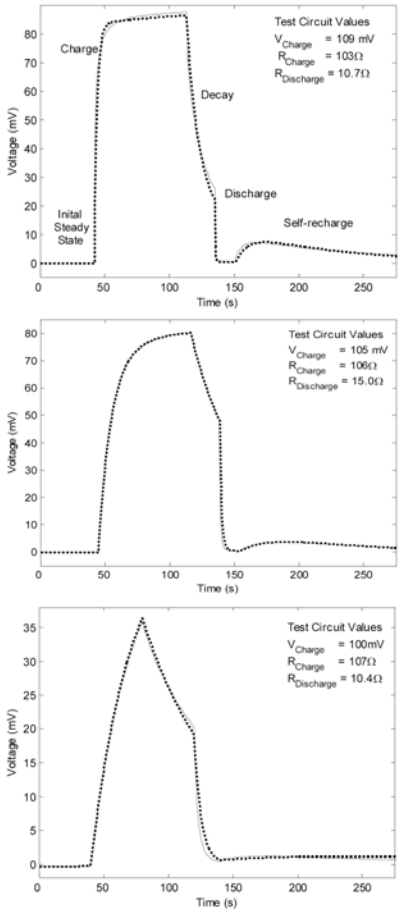

Fig. 6. Results for a single MerCorp Cell, Enable Cell, and Avista Cell, dashed line showing modelled results

The potential decay can also be attributed to the continued movement of hydrogen ions (H^+) towards the negatively charged electrode. Again, this process can be compared with phenomena known to occur in a DLC. After charging a DLC, the potential decays rapidly to a new open circuit voltage value, then continues to decay at a slow rate. Clearly, the initial fast decay in cell voltage is not due to leakage current, but instead can be attributed to continued movement of ions,

primarily at the porous electrode-electrolyte interface. Consider the transmission line model of a porous electrode-electrolyte interface (see Fig. 1f), and assume that the electronic resistance rail has negligible resistance. During a charge step, the capacitor nearest the electrolyte will then contain more charge. After the charge step has ceased, hydrogen ions will continue to penetrate further into the porous electrode, thus distributing the charge across all of the capacitors in the model, and reducing the potential across the cell. An alternative perspective, offered here for the first time, is that the membrane may possess a variable dielectric value depending on the position of the hydrogen ions within it. For instance, the closer the ions are to the negative electrode, assuming a fixed charged on the electrode, the higher the dielectric value. If a fixed charge remains on the electrodes, and the dielectric value of the membrane increases due to continued hydrogen ion movement, then the voltage across the cell (or capacitor) will decrease.

Additional experiments are required to determine the contribution of ion movement to the observed potential decay, and the various proposed leakage current mechanisms remain to be determined.

4) Discharge

During the discharge period, S_2 is closed, and the cell dissipates the accumulated charge through a resistor (with low resistance) so that nearly all of the charge is removed from the electrodes (the cell is effectively short circuited during this period). As expected, and similar to any capacitor, the potential decays rapidly in an exponential type manner during discharge.

5) Self-Recharge

The observed self-recharge is an interesting phenomenon, since despite short circuiting the cell, the potential recovers to a certain point for a period of time before decaying back toward zero. Clearly, charges are still migrating inside the cell, giving rise to this transient voltage behaviour. Potential recovery has been reported previously for DLCs, where the voltage recovers even after a short circuit period of a week or more [37].

Essentially, the processes that cause the voltage to decay after a charge step (primarily continued ion movement in the cell) are also thought to cause the self-recharge. During the discharge, almost all of the charge is dissipated off the electrodes, and the H^+ ions begin to move back toward their original (homogeneous) position in the membrane. However, the distribution of hydrogen ions will still be non-uniform for some time after the charge on the electrodes has been reduced to near zero. Therefore, H^+ ions will continue to move, and the effective dielectric value of the membrane will continue to decrease, after the short has been removed. Assuming that a small amount of charge remains on the electrodes after the short is removed, together with the fact the dielectric constant is decreasing, the potential across the cell will increase. As the rise in potential reaches a maximum then begins to decay, clearly the cell is also conducting current by some leakage mechanism, as explained in part 3. A generalized representation of this ion diffusion in the electrolyte is shown in Fig. 7. The aggregate diffusion time constant arises from electrolyte physical chemistry, boundary layer thickness, and interface details which are artifacts of materials, condition, and cell construction.

It is interesting to note the long time-constant of the self-recharge phenomenon. Long time constants are also observed during current interrupt tests of a functioning fuel cell, and are generally attributed to the rate of diffusion of chemical species.

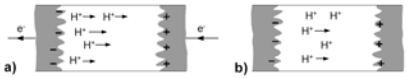

Fig. 7. Cell voltage decreases during the discharge (a) and increases immediately after the discharge ceases (b) resulting in the self-recharge region

C. Summary of Single Cell Test Results

By measuring the transient voltage response of the cell to the test protocol, features related to the cells physical makeup and operation are revealed, such as the movement of ions, and the capacitance of the cell. In order to analyze the behaviour quantitatively, an equivalent circuit model is developed, together with a method for acquiring circuit parameters.

VII. Circuit Model Analysis

The standard model of a fuel cell cannot be employed for a fuel cell in a passive state for two reasons. First, because no hydrogen is present and the applied voltage is well below 1.2V, a substantial charge transfer across the electrolyte-electrode boundary does not occur. Therefore, the resistors $R_{CT,A}$ and $R_{CT,C}$ (see Fig. 1b) would have an infinite value, representing a break in the circuit. Second, since no electrochemical reactions are occurring, there is clearly no diffusion of reactants, thus R_W C_W (see Fig. 1c), which account for diffusion effects, will not be present. Thus, the standard model would be reduced to a series circuit consisting of R_{ionic} and C, where $C = (1/C_{DL,A} + 1/C_{DL,C})^{-1}$. This circuit has been proposed previously when considering a cell composed of an ideal reversible electrode and an ideal polarizable electrode, which by definition implies no charge can be transferred across the electrode-electrolyte boundary [24]. Clearly, a series R-C circuit would not be capable of simulating the observed results of the passive test, thus a passive PEM ECM is derived to describe the observed behaviour.

A. Derived Equivalent Circuit Model (ECM)

The basic physical elements of the fuel cell in a passive state are considered in developing the ECM. The electrodes are essentially two high surface-area conductors parallel to one another, thus a capacitor C_a is placed across the terminals of the circuit model as shown in Fig. 8. For charge to be stored on the electrodes (on C_a), current must pass through each electrode with a related contact resistance. Therefore, resistor R_c is placed before capacitor C_a. The presence of the membrane has a number of effects, one of which is the presence of leakage current. Hence, resistor R_a is placed across capacitor C_a. The main effect that the membrane has on the cell is to increase the capacitance value. Therefore, capacitor C_b is placed in parallel with C_a, with the addition of resistor R_b, which is related to the ionic resistance.

The values of the circuit parameters will clearly depend upon the physical make-up of the cell, and thus may be used to indicate performance-related characteristics. For example, a larger C_a would indicate a larger surface area, a property desirable in a cell.

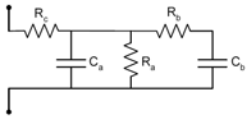

Fig. 8. Passive Fuel Cell Equivalent Circuit Model

B. Method to Acquire Circuit Parameters of a Single Cell

The circuit parameters were obtained by conducting a least squares fit of simulated data to the experimental data. PLECS V1.0.9 (from Plexim™ GmbH), which operates in the MATLAB Simulink environment, was used for simulating the equivalent circuit model response to the test protocol. An iterative algorithm scripted in MATLAB acquires the set of circuit parameters such that the least squares error between the simulated and experimental results is a minimum. The initial voltage conditions of the capacitors in the circuit model are found by fitting the initial steady state region while holding the rest of the circuit values constant. This method of finding the circuit parameters is not confined to a particular model, and can be easily extended to find the circuit parameters of multiple connected cells (in a stack), as will be shown in section VII. Using this method, the results of the single cell tests are shown in Table I, (in this case, the R_c parameter was ignored, since it was found to be small in comparison to the other circuit values).

TABLE I
Equivalent Circuit Model Parameters for Single Cell Testing

Fuel cell	Circuit Parameters			
	R_a (Ω)	R_b (Ω)	C_a (F)	C_b (F)
MerCorp Cell 2	552	1670	0.0243	0.0352
Enable Cell	309	1120	0.139	0.0320
Avista Cell	146	371	0.569	0.804

C. Circuit Model Discussion

The capacitive values (C_a and C_b) found for the Avista cell are significantly larger than for the MerCorp and Enable cells, which is to be expected considering the larger surface area of the Avista cell.

The simple 4-element ECM reproduces the electrical response of the cell relatively accurately. As with DLC's, the capacitance may be a function of the applied voltage, and this aspect could be included if it was found to be important in an application.

When modeling a two terminal circuit device with four circuit elements, the model form is not unique. There are in fact three additional circuit models, each containing two capacitors, and two resistors (but with different circuit values), that are indistinguishable at the model terminals. However, the circuit model form shown in Fig. 8 was derived from the physical attributes of a passive fuel cell. The resulting component values can be related to physical elements of the cell. For example, the cell capacitance values relate to the dynamic characteristics of the cells, while the series resistance indicates the size of internal currents, possibly identifying a shorted (failed) cell. The functional relationship of the passive fuel cell ECM values to cell conditions is the subject of on-going research.

VIII. Stack Testing and Analysis

The passive PEM test method can be used to test an entire stack, simply by attaching the test circuit across the stack terminals. Any number of cells can be tested simultaneously by monitoring the individual cell voltages. Results for a stack test conducted on the MerCorp stack are shown in Fig. 9.

The interconnected cells have dynamic inter-relationships which effectively result in each cell being subjected to a different charge/discharge pattern as reflected in the voltage responses. Similar patterns were found with the Enable and Avista stack tests. This is easily explained by series connection the passive equivalent circuit which has significantly different R_a values for each cell.

The circuit parameters for the stack can be found using the PLEC model and algorithm described above. An additional loop in the MATLAB script file was added, so that the routine determines ECM parameters for each cell. The results are shown in Table II. The circuit values found for cell 2 during the single cell test (Table I) and the stack test (Table II) are in reasonable agreement, demonstrating the validity of using a stack test to acquire properties of multiple cells.

For this stack, a range of R_a values was calculated from the test data. R_a represents the membrane leakage current. Even

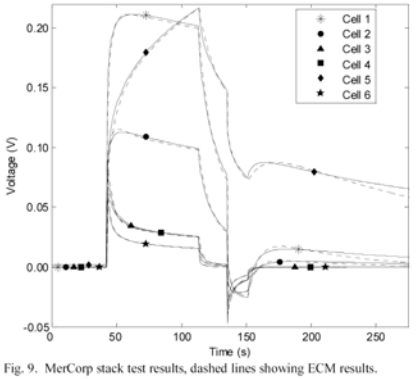

Fig. 9. MerCorp stack test results, dashed lines showing ECM results.

though in the passive test, R_a, appears to vary significantly, in an active cell, it is a minor factor. For instance, cell 6, which has smallest R_a value, would have an absolute leakage current value of 7.2mA which is significantly less than the stack (ionic) current of 6A. The very high sensitivity (large signal-to-noise ratio) of the passive test suggests that the technique could be a very robust in practice, and especially useful when knowledge of R_a variation is important.

The MerCorp Cell was in the developmental stage, and the cells performed at different voltage levels. The active cell performance was found to correlate directly with the passive test results [47]. The passive test protocol together with the property-based ECM and the numerical analysis method to derive the cell parameters represent a novel approach to PEMFC monitoring [47].

TABLE II
EQUIVALENT CIRCUIT MODEL PARAMETERS FOR PASSIVE STACK TEST

MerCorp Cell	Circuit Parameters			
	R_a (Ω)	R_b (Ω)	C_a (F)	C_b (F)
Cell 1	1000	1770	0.0150	0.0208
Cell 2	477	1108	0.0257	0.0336
Cell 3	116	1170	0.0322	0.0289
Cell 4	117	2270	0.0235	0.0158
Cell 5	2140	668	0.0278	0.0583
Cell 6	73.7	436	0.0219	0.00645

IX. SUMMARY AND CONCLUSIONS

A new testing method is introduced that examines the fuel cell while in a passive state. The test method uses a charge/discharge test protocol, which is implemented using a simple test circuit. The testing method has been conducted on individual PEM cells from three different manufacturers, all of which show a similar voltage transient response to the test. The results reveal interesting voltage transients that are not due to electrochemical processes, but to the physical nature of the cells themselves.

A passive PEMFC equivalent circuit model is proposed, and includes properties of the cell not previously considered, such as leakage current of the membrane, and a long time constant feature that is similar to a double layer capacitor due to the physical nature and response of the electrodes and membrane.

A novel method of obtaining the circuit model parameters is proposed and used to find individual cell circuit parameters from a single stack test. The method was confirmed by reasonable agreement between ECM parameters obtained from an individual cell test and a stack test.

The passive test protocol is simple, highly sensitive to some features of the cell, is implemented while the stack is in a passive state, and can measure properties of each cell with a single stack test.

X. REFERENCES

[1] S. Slade, S. A. Campbell, T. R. Ralph, F. C. Walsh, "Ionic conductivity of an extruded Nafion 1100 EW series of membranes" *J. Electrochem. Soc.*, vol. 149, pp. A1556-A1564. Dec. 2002.

[2] D. C. Papageorgopoulos, M. Keijzer, F. A. de Bruijn, "The inclusion of Mo, Nb and Ta in Pt and PtRu carbon supported 3electrocatalysts in the quest for improved CO tolerant PEMFC anodes" Electrochimica Acta, vol. 48, pp. 197-204, Nov. 2002.

[3] J. C. Amphlett, R. M. Baumert, R. F. Mann, B. A. Peppley, P. R. Roberge, T. J. Harris, "Performance Modeling of the Ballard-Mark-IV Solid Polymer Electrolyte Fuel-Cell .1. Mechanistic Model Development" *J. Electrochem. Soc.*, vol. 142, pp. 1-8, Jan. 1995.

[4] J. C. Amphlett, R. M. Baumert, R. F. Mann, B. A. Peppley, P. R. Roberge, T. J. Harris, "Performance Modeling of the Ballard-Mark-IV Solid Polymer Electrolyte Fuel-Cell .2. Empirical-Model Development", *J. Electrochem. Soc.*, vol. 142, pp. 9-15, Jan. 1995.

[5] J. Kim, S. Lee, S. Srinivasan, "Modeling of Proton Exchange Exchange with an Empirical Equation", *J. Electrochem. Soc.*, vol. 142, pp. 2670-2674, Aug. 1995.

[6] D. Chu, R. Jiang, C. Walker, "Analysis of PEM fuel cell stacks using an empirical current-voltage equation", *J. Appl. Electrochem.*, vol. 30, pp. 365-370, Mar. 2000.

[7] T. E. Springer, T. A. Zawodzinski, M. S. Wilson, S. Gottesfeld, "Characterization of polymer electrolyte fuel cells using AC impedance spectroscopy", *J. Electrochem. Soc.*, vol. 143, pp. 587-599, Feb. 1996.

[8] G. C. Li, P. G. Pickup, "Ionic conductivity of PEMFC electrodes - Effect of Nafion loading", *J. Electrochem. Soc.*, vol. 150, pp. C745-C752, Nov. 2003.

[9] B. Andreaus, A. J. McEvoy and G. G. Scherer, "Analysis of performance losses in polymer electrolyte fuel cells at high current densities by impedance spectroscopy", *Electrochimica Acta*, vol. 47, pp. 2223-2229, May. 2002.

[10] N. Wagner, W. Schnurnberger, B. Muller, M. Lang, "Electrochemical impedance spectra of solid-oxide fuel cells and polymer membrane fuel cells" *Electrochimica Acta,* vol. 43, pp. 3785-3793, Aug. 1998.

[11] N, Wagner, "Characterization of membrane electrode assemblies in polymer electrolyte fuel cells using a.c. impedance spectroscopy", *J. Appl. Electrochem.*, vol. 32, pp. 859-863, Aug. 2002.

[12] F. N. Buchi, A. Marek, G. G. Scherer, "In-Situ Membrane Resistance Measurements in Polymer Electrolyte Fuel-Cells by Fast Auxiliary Current Pulses", *J. Electrochem. Soc.*, vol. 142, pp. 1895-1901, Jun. 1995.

[13] B. Andreaus, G. G. Scherer, "Proton-conducting polymer membranes in fuel cells - humidification aspects" *Solid State Ionics*, vol. 168, pp. 311-320, Mar. 2004.

[14] J. R. J. Larminie, **"**Current interrupt techniques for circuit modelling" in *Proc 1994 IEE Colloquium on Electrochemical Measurement,* pp. 12/1 -12/6.

[15] J. Larminie, A. Dicks, "Fuel cell system explained" second edition, West Sussex, John Wiley & Sons Ltd, 2003, pp. 63-66, 62

[16] C. G. Lee, N. Nakano, T. Nishina, I. Uchida, S. Kuroe, "Characterization of a 100 cm(2) class molten carbonate fuel cell with current interruption" *J. Electrochem. Soc.,* vol. 145, pp. 2747-2751, Aug. 1998.

[17] R. O'Hayre, T. Fabian, S. J. Lee, F. B. Prinz, "Lateral ionic conduction in planar array fuel cells", *J. Electrochem. Soc.*, vol. 150, pp. A430-A438, Apr. 2003.

[18] S. Yuvarajan, D. Yu, "Characteristics and modeling of PEM fuel cells" in *Proc. of the 2004 International Symposium Circuits and Systems,* vol. 5, pp. V880-V883.

[19] D. Yu, S. Yuvarajan, "A novel circuit model for PEM fuel cells**"** in *Proc. of the 2004 Nineteenth Annual IEEE Applied Power Electronics Conference and Exposition*, vol. 1, pp. 362-366.

[20] W. Choi, P. N. Enjeti, J.W, Howze, "Development of an equivalent circuit model of a fuel cell to evaluate the effects of inverter ripple current" in *Proc. of the 2004 Nineteenth Annual IEEE Applied Power Electronics Conference and Exposition*, vol. 1, pp. 355-361

[21] C. S. Wang, M. H. Nehrir, S. R. Shaw, "Dynamic models and model validation for PEM fuel cells using electrical circuits" *IEEE Trans. on Energy Conversion*, vol. 20, pp 442-451, Jun. 2005.

[22] R. S. Gemmen, "Analysis for the effect of inverter ripple current on fuel cell operating condition" *J. Fluids Eng.*, vol. 125, pp. 576-585, May 2003.

[23] C. H. Hamann, A. Hemnett, W. Vielstich, "Electrochemistry", Wiley-VCH 1998 Verlag GmbH, Weinheim, Germany, pp 15, 240

[24] A. J. Bard, L. R. Faulkner, "Electrochemical Methods: Fundamentals and Applications": second edition, New York: John Wiley, 2001, pp 14, 376

[25] M. T. Iqbal, "Simulation of a small wind fuel cell hybrid energy system", *Renewable Energy*, vol. 28, pp. 511-522, Apr. 2003.

[26] M. T. Iqbal "Modeling and control of a wind fuel cell hybrid energy system", *Renewable Energy*, vol. 28, pp. 223-237, Feb. 2003.

[27] N. Y. Jia, R. B. Martin, Z. G. Oi, M. C. Lefebyre, P. G. Pickup, "Modification of carbon supported catalysts to improve performance in gas diffusion electrodes", *Electrochimica Acta,* vol. 46, pp. 2863- 2869, May 2001.

[28] R. A. Huggins, "Supercapacitors and electrochemical pulse sources", *Solid State Ionics*, vol. 134, pp. 179-195. Oct. 2000.

[29] F. Lufrano, P. Staiti, M. Minutoli "Evaluation of nafion based double layer capacitors by electrochemical impedance spectroscopy" *J. Power Sources*, vol. 124, pp. 314-320, Oct. 2003.

[30] F. Lufrano, P. Staiti, M. Minutoli, "Influence of Nafion content in electrodes on performance of carbon supercapacitors", *J. Electrochem. Soc.*, vol. 151, pp. A64-A68, Jan. 2004.

[31] P. Staiti, M. Minutoli and F. Lufrano "All solid electric double layer capacitors based on Nafion ionomer" *Electrochimica Acta,* vol. 47, pp. 2795-2800, Jul. 2005.

[32] P. Staiti, F. Lufrano, "Design, Fabrication, and Evaluation of a 1.5 F and 5 V Prototype of Solid-State Electrochemical Supercapacitor", *J. Electrochem. Soc.*, vol. 152, pp. A617-A621, Jan. 2005.

[33] S. Buller, E. Karden, D. Kok, R. W. De Doncker, "Modeling the dynamic behavior of supercapacitors using impedance spectroscopy", *IEEE Trans. Industry Applications,* vol. 38, pp. 1622-1626, Nov. 2002.

[34] C. Emmenegger, P. Mauron, P. Sudan, P. Wenger, V. Hermann, R. Gallay, A. Zuttel "Investigation of electrochemical double-layer (ECDL) capacitors electrodes based on carbon nanotubes and activated carbon materials" *J. Power Sources*, vol. 124 pp. 321-329, Oct 2003.

[35] R. A. Dougal, L. Gao, S. Liu "Ultracapacitor model with automatic order selection and capacity scaling for dynamic system simulation" *J. Power Sources,* vol. 126, pp. 250-257, Feb. 2004.

[36] R. M. Nelms, D. R. Cahela, B. J. Tatarchuk, "Modeling double-layer capacitor behavior using ladder circuits", *IEEE Trans. Aerospace and Electronic Systems,* vol. 39, pp. 430-438, Apr. 2003.

[37] R. Bonert, L. Zubieta, "Measurement techniques for the evaluation of double-layer power capacitors" in *Proc. Thirty-Second IEEE Industry Applications Society. Annual Meeting,* vol 2, pp. 1097-1100, Oct. 1997.

[38] L. Zubieta, R. Bonert, "Characterization of double-layer capacitors for power electronics applications", *IEEE Trans. on Industry Applications*, vol 36, pp. 199-205, Jan. 2000.

[39] L. Zubieta, R. Bonert, "Experimental 400 kW sec double-layer capacitor energy storage system", in *Proc. Thirty-Fourth IEEE Industry Applications Society. Annual Meeting,* vol. 4, pp. 2448-2453, Oct. 1999.

[40] L. Zubieta, R. Bonert, "Characterization of double-layer capacitors (DLCs) for power electronics applications", in *Proc. Thirty-Third IEEE Industry Applications Society. Annual Meeting,* vol. 2, pp. 1149-1154, Oct. 1998.

[41] H. Gualous, D. Bouquain, A. Berthon, J. M. Kauffmann, "Experimental study of supercapacitor serial resistance and capacitance variations with temperature" *J. Power Sources,* vol. 123, pp. 86-93, Sep 2003

[42] F. Belhachemi, S. Rael, B. Davat, "A physical based model of power electric double-layer supercapacitors" in *Proc. IEEE Industry Applications Conference*, vol. 5, pp. 3069-3076, Oct. 2000.

[43] Maxwell Technologies "Cell Balancing in Low Duty Cycle applications" Application Note, Available at: http://www.maxwell.com/pdf/uc/app_notes/AN-002_Cell_balancing.pdf

[44] R. L. Spyker, R. M. Nelms, "Classical equivalent circuit parameters for a double-layer capacitor" *IEEE Trans. Aerospace and Electronic Systems,* vol. 36, pp. 829-836, Jul. 2000.

[45] M. Hecht, previously of MER Corporation, Tucson, AZ, private communications, Sep. 2003

[46] S. C. Page, S. P. Krumdieck, A. Anbuky, "Testing Procedure for Passive Fuel Cell State of Health" *Australasian Universities Power Engineering Conference, University of Queensland, Australia*, Sep. 2004

[47] S. C. Page, A. Anbuky, S. P Krumdieck, "Method of testing an Electrochemical Device", PCT NZ/05/00053, Mar. 25, 2005

Shannon C. Page received the B.Sc (Honors I) in Physics from the University of Canterbury, Christchurch, New Zealand in 2000, and is currently pursing a Ph.D in mechanical engineering at the University of Canterbury.

He is currently engaged in research at Eaton Corporation, New Zealand, in conjunction with the University of Canterbury. His research interests include fuel cell technology, specifically application and integration issues, energy system modeling, and sustainable energy systems.

Adnan H. Anbuky received the degree in electrical engineering from the University of Baghdad, Baghdad, Iraq, the M.Sc. degree from the University of Salford, Salford, U.K., and the Ph.D. degree from the University of Manchester Institute of Science and Technology, Manchester, U.K., in 1969, 1971, and 1975, respectively.

From 1975 to 1991, he was with the University of Technology, Iraq, as an Academic Staff Member, becoming a Full Professor in 1987. From 1991 to 1995, he was with Yarmouk University of Jordan as Head of the Computer Engineering Group and then as the Dean of the Faculty of Engineering. From 1996 to 2004 he was with Swichtec (currently Eaton Power Quality Limited) running a research unit on DC power systems management and other interrelated standby power technologies. During 2005 he was the director of research within the Electrical & Computer Engineering of Manukau Institute of Technology, and is currently with the Electrical and Electronic Engineering Department of Auckland University of Technology as a head of department.

Susan P. Krumdieck received the BS and MS degrees in mechanical engineering from Arizona State University, Tempe, Arizona in 1986 and 1989, and the PhD in mechanical engineering from the University of Colorado at Boulder in 1999.
She started the company, Boulder Material Systems with the aid of an NSF SBIR Award to commercialize the results of her PhD research. In 2000 she took the academic position at the University of Canterbury, Christchurch, New Zealand, and is currently a Senior Lecturer.
Dr. Krumdieck is a member of the Royal Society of New Zealand, and during the PhD was a Link Foundation Energy Fellow, and ARCS Scholar, an SAE Doctoral Scholar, and the winner of the 1st place and 4th place Air&Waste Management Association Scholarships.

Jack Brouwer received the B.S. and M.S. degrees in mechanical engineering from University of California, Irvine (UCI) in 1987 and 1989, and the Ph.D. in mechanical engineering from Massachusetts Institute of Technology in 1993.

He is Adjunct Assistant Professor of Mechanical and Aerospace Engineering at UCI and the Associate Director of the National Fuel Cell Research Center (NFCRC). Prior to joining the NFCRC, Dr. Brouwer was a research faculty at the University of Utah, a Senior Engineer at Reaction Engineering International, and a Staff Scientist at Sandia National Laboratories.

Dr. Brouwer has expertise in energy systems, fuel cell technology, turbulent reacting flows, computational fluid dynamics, chemical kinetics, and electrochemical reactions with concurrent heat, mass and momentum transfer in electrochemical systems. Dr. Brouwer is leading research and development efforts on hydrogen refueling, fuel cell vehicles, hybrid fuel cell gas turbine systems, the development and application of dynamic fuel cell and hybrid fuel cell systems simulations, and the advancement of fuel processing technology. Dr. Brouwer is a regular instructor at UCI in the areas of fuel cells, thermodynamics, heat transfer, and combustion. He developed and introduced the first graduate level fuel cell course to UCI in 2001, and is a regular instructor in fuel cell short courses around the world.

IEEE PEER REVIEW

After submission of the first edition, a review was received that in which some changes to the paper were required. After the changes were made, and subsequent letters sent to the editor and reviewers, the paper was accepted without any further changes required (with the exception of minor typos). The letter written to the editor and reviews is reproduced below, in which the reviewer's options on the first edition of the paper are detailed.

Letter to the IEEE Editor

Thank you for considering our paper for publication. We have submitted a new draft of our paper that addresses the points raised by the reviewers.

In general, this paper is part of a larger work that shows the potential of using the passive test method in manufacturing and applications. We agree that this paper dose not directly address the application and particularly manufacturing issues. Although we are working on these aspects, we agree they are out of the scope of this paper and have removed reference to them as suggested by reviewers 1 and 2. Instead, the focus of the paper has been on the testing and modelling process, in the context of existing testing and modelling.

Along with the required revisions indicated by the reviewers, we addressed the length of the paper and reduced some of the narrative, making it more concise.

We look forward to your reply

Kind regards
Shannon, Adnan, Susan and Jack

Letter to the IEEE Reviewers

Dear Reviewers

Thank-you for carefully reviewing our submitted paper. We have considered the points raised, and have made corresponding changes to the paper. Below, you will find answers to the specific

points raised by reviewers 1,2, and 4. Following that, we have detailed the specific changes made to the paper, in order to make your review process easier.

Reviewer 1

General Comments and Changes:

This is an interesting and well-written paper describing the development of an electrical circuit model for PEM fuel cell and fuel cell stack in passive (non-operative) state. It is true that because of the nature (structure) of fuel cells, it is expected that they have electrical properties in the passive mode. The paper develops an equivalent circuit for the PEMFC in the passive mode and uses the least squares error criterion to estimate its equivalent circuit parameters. The wide variation of circuit parameter values, especially in the case of stack test (Table II), however, raises question about the accuracy of the model parameter estimation, although the test results and the model responses match well. Suggestions below could add to the value of the paper.

1. In the abstract and introduction of the paper, the authors claim that testing of fuel cells in the passive state could be helpful in monitoring reliability and in quality control. However, this claim is not justified. The authors therefore need to revise the introduction of the paper and justify as to how the PEMFC equivalent circuit in the passive state could be useful in testing material properties and in manufacturing, etc.

2. Related to the equivalent circuit models that predict the steady state and transient terminal characteristics of PEM fuel cells (the subject of Section III in the paper), and to the effect of ripple currents on fuel cell operating conditions, this reviewer offers the following references that the authors could refer to in their paper.

[1] C. Wang, M.H. Nehrir, and S.R. Shaw, “Dynamic Models and Model Validation for PEM Fuel Cells Using Electrical Circuits,” IEEE Transactions on Energy Conversion, Vol. 20, No. 2, pp.442-451, June 2005.

[2] R.S. Gemmen, “Analysis for the effect of inverter ripple current on fuel cell operating condition,” Transactions of the ASME - Journal of Fluids Engineering, Vol. 125, No. 3, pp.576-585, May 2003.

We have realized that the description of the test results could be represented more clearly.

Referring to the question about the wide variation of the cell parameter estimation values, we found that some cell parameter values for each cell are quite different. However, these results were highly repeatable. The MerCorp stack was an experimental stack and did not perform very well, and the operating performance of some of the cells was quite different. To clear up the distinction, we have included some information about the individual cell performance and how it relates to different aspects of the passive test, and have included a reference to our previous work which details this.

The issue raised in 1. was also raised by reviewer 2, and is addressed in the response to reviewer 2 below. Referring to the issue raised in 2, in general, many circuit models have been proposed for PEM fuel cells. Some models not only represent the fuel cell but extend the circuit model to include other physical processes, like the circuit models in the papers you recommended. This type of equivalent circuit modelling has now been included.

Reviewer 2

General Comments and Changes:

This paper presents in details a test method and an equivalent circuit model for a PEM fuel cell in a passive state. The method is conventional to a double layer capacitor where no external reactants are involved, but it is novel to a fuel cell characterization only if the performance of the fuel cell in an active state can be predicted by these passive parameters. However, the authors actually did not offer any insights on how these parameters are related to the field performance of a fuel cell, nor did they explain how to improve manufacturing quality of a fuel cell using their model. Unless these issues are addressed, there is no significance in terms of both the method and the model provided in the paper.

The paper focuses on the fundamental aspects of the test process and modelling.

In general, this paper reflects a part of a larger work in which we are investigating the applications of the test. However, as pointed out, this paper does not include the way in which the test can be used. The review of test methods and equivalent circuit models, the description of the passive test, and the results of the test on an experimental PEMFC should provide a foundation for deploying the idea.

- We have removed the references to application in manufacturing, rather than describe them in this more fundamental paper.

- We have provided additional information about the usefulness of the test in monitoring the functionality of a fuel cell by including some information linking the passive test results for each cell and the operating performance of these cells, and we have added a reference to our previous work which described this.

Reviewer 3
General Comments and Changes: This work should be published as documentation of a fine effort towards validation of equipment reliability.

Reviewer 4
General Comments and Changes: The modelling of fuel cells has become an important tool for electrical engineers. The paper describes an advance in the modelling and testing process together with analogous circuit components more familiar to the members of the PES. The length of the paper does indicate that either there should have been two papers addressing different aspects of the subject or that some of the narrative could be reduced. However, this reviewer appreciates that as Mozart said" too many notes? which ones should I take out?"

The narrative has been carefully reviewed and several instances of repeated statements were removed. The length of the paper has been reduced through further editing.

Australasian Universities Power Engineering Conference (AUPEC 2004)
26-29 September 2004, Brisbane, Australia

TESTING PROCEDURE FOR PASSIVE FUEL CELL STATE OF HEALTH

S.C. Page*, S.P. Krumdieck* and A. Anbuky**

*Department of Mechanical Engineering
University of Canterbury
Christchurch, New Zealand

**Department of Computer Science
University of Canterbury
Christchurch, New Zealand

Abstract

A promising application for Proton Exchange Membrane fuel cell technology is uninterrupted power supply (UPS) systems. The most critical aspect for UPS is reliability, which can be significantly increased and managed if information about UPS system integrity is known. A test methodology is presented to assess the condition and relative functionality of a PEM stack and/or any cell. The test comprises an electrical probing procedure that is performed while the fuel cell is in a non-active or "passive" state. The test method could be integrated into a UPS system, and will form a critical aspect of a monitoring and testing regime.

1. INTRODUCTION

Power system security is an ever present concern, with a number of industries employing Uninterruptible Power Supply (UPS) systems. Incumbent UPS systems typically employ strings of lead acid batteries and/or diesel generator sets. The recent emergence of fuel cell technology into the power industry presents another option in supplying UPS power. The most critical specification for any UPS system is reliability. In certain applications (such as electronic commerce), the system must achieve between 7 – and 8 nine's of reliability (equating to an allowable down time of 3.2 – 0.32 seconds per year).

Assurance of system reliability relies on being able to assess the condition of a backup device, and the ability of that device to perform a required task. For example, a number of testing methods have been developed to evaluate the "state of heath" and "state of charge" of a battery. These testing methods run the battery through a test load, or examine part of the battery discharge. With these test regimes integrated into a back-up power monitoring system, information regarding a potential problem or required servicing, is known before the integrity of the system is effected. This greatly increases the reliability of the system as a whole.

This paper presents a test procedure that enables the characteristics of Fuel cell to be determined, thus enabling the health or functionality to be assessed. This provides critical information regarding the capacity to which the fuel cell can produce power, thus system reliability can be increased. The testing technique and the analysis method are described, with testing results applied to a small commercial Proton Exchange Membrane (PEM) Fuel Cell.

1.1 Fuel Cell Testing and Analysis

The vast majority of existing fuel cell test methods involve testing an operating cell or stack. The most common method for testing and characterising the performance of a PEM fuel cell is to measure the steady state voltage over a current range [1, 2], thus producing a characteristic VI curve. Current pulse or interrupt methods [3], along with electrochemical impedance spectroscopy, (EIS, also referred to AC impedance testing) are also used for finding certain properties of individual fuel cells [4]. Test results using these techniques are generally correlated to discrete properties of a cell, such as the ionic resistance of the membrane or electrical conduction of the electrode layer, where as evaluation of the VI curve provides overall performance information on the fuel cell.

In order to relate test results to fuel cell properties, equivalent circuit modelling (ECM) has often been employed (particularly in the case of current pulse/interrupt or EIS). A number of circuit models have been used, which vary in the degree of complexity [5, 6]. Physical attributes of the fuel cell are often assigned to particular components in the circuit model. Thus, establishing the circuit model and model parameter values can provide information about the functionality of the fuel cell. Properties such as the ionic resistance of the membrane and electrical and ionic resistance of the electrode/electrolyte interface have been calculated using this methodology [7, 8]. The analysis reported in the literature has used the results from some form of *active* fuel cell test, that is a test performed while the fuel cell is producing power.

In a UPS application, the fuel cell is in a non-functioning, or *passive* state for the majority of the time, only becoming active when the mains power fails. A procedure is proposed to test the fuel cell while it is in this passive state. The test results and analysis from the passive stack test results, are then used to predict the operational functionally, or *health* of the fuel cell.

2. PASSIVE FUEL CELL TEST METHOD

The fuel cell is in the passive state for the duration of the test process. There is no hydrogen in the fuel cell, with the anode and cathode compartments containing air, thus no potential can be generated from electrochemical reactions. While a PEM fuel cell is in this passive state, the physical nature and the behavior of a cell is very similar to a Double-Layer Capacitor (DLC).

In both a fuel cell and a DLC, the basic construction consists of a two high surface electrodes (typically activated carbon) separated by a medium containing free moving ions (electrolyte). The electrolyte used for DLC is often organic, as higher voltages can be achieved, although, aqueous H_2SO_4 has also been employed. More recently, a DLC using Nafion (a common PEM fuel cell electrolyte) has been realized and its properties tested [9].

Exploiting the similarity between a DLC and a PEM fuel cell, a testing procedure and analysis methodology have been formulated for the fuel cell. The testing procedure conducted on the PEM fuel cell employs charging and discharging the fuel cell in a capacitive sense. As air is present at both electrodes, and the voltage used for charging is well below the level needed for electrolysis, only non-faradic processes can occur (those not involving a charge transfer between the electrolyte and electrode interface). The charging and discharging protocol is described in the following section.

3. EXPERIMENTAL TEST METHOD

The test can be implemented across any number of cells, with the voltage across each cell recorded during the test process. The testing protocol consists of charging and discharging the fuel cell in a number of discrete steps. One particular test sequence, used for the results presented in this paper, is described:

1. Initial open circuit voltage condition of the cells is monitored
2. A prescribed voltage is applied to the stack terminals (though a resistor), thus charging the cells
3. The stack is held at open circuit,
4. The stack is discharged through a very small resistor (effectively short circuiting the stack terminals)
5. The stack is held at open circuit for the reminder of the test.

The testing procedure outlined above, is achieved through a simple test circuit shown in figure 1. Switch S_1 and S_2 allow the fuel cell to be charged or discharged respectively. R_1 and R_2 are the charge and discharge resistors, which have a value of 100Ω and 4.9Ω respectively. The constant voltage source is set at values depending on how many cells are being tested. A constant voltage (V_{charge}) in the test circuit was set by the data acquisition system used.

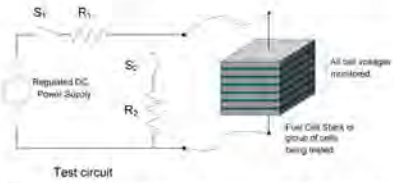

Figure 1. Test circuit used for implementing the passive fuel cell test process.

Cell voltages are recorded with an HP 34970A data acquisition/switch unit, which contains an internal digital multi-meter. The unit uses 2 interchangeable cards for measuring voltages and supplying the voltage to the test circuit. The experimental equipment is shown in figure 2. The HP unit was programmed directly in the Matlab environment, and communicated via an RS232 connection.

3.1 Signal and Data Analysis

The fuel cell characteristics reveled by the test protocol, can be most easily observed by examining the results of a single cell. The test circuit was connected to a cell in the centre of the stack (cell # 3), and the charge voltage

used was 0.05V. The voltage transient behavior of the cell is shown in figure 3.

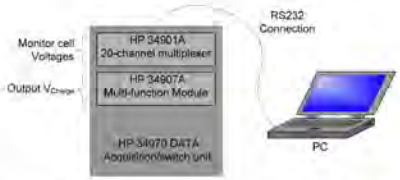

Figure 2. Data Acquisition equipment used in the testing process

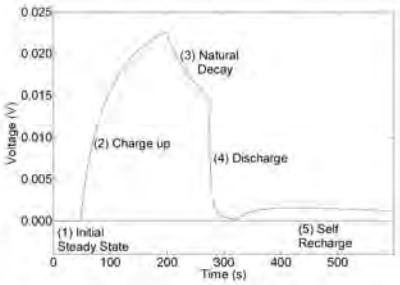

Figure 3. The cell voltage response during the test procedure.

The test sequence produces 5 distinct voltage transients in the response of the cell. The five regions have been labeled 1) Initial Steady State, 2) Charge-up 3) Natural Decay 4) Discharge and 5) Self Recharge. Most of this transient behavior would be expected from any capacitor, e.g. the exponential nature of the charge up and discharge regions. The decay in cell voltage (Natural decay region) is indicative of electron conduction through the electrolyte (a property also present in capacitors) but perhaps the most interesting phenomena is shown in the Self Recharge region. The self recharge is caused by the membrane retaining charge through an uneven distribution of H^+ ions. Even when there is no charge present on the electrodes (at the end of the discharge period) charge is still held by the membrane. This residual charge allows a charge to build back up onto the electrodes when the cell is held at open circuit. From this simple test, it is recognized that a number of fuel cell properties can be observed, such as electronic conduction of the membrane, and capacitive properties of the membrane and electrodes.

4. RESULTS AND DISCUSSION

The testing procedure was implemented on a small commercially available PEM fuel cell stack purchased from MerCorp. The stack contained 6 cells connected in series, each with an active area of 32cm^2 employing a Nafion based membrane.

The aim of the testing process is to obtain functionality information on each cell within a stack using a single test process. Therefore, the standard test involves connecting the test circuit across the stack terminals and measuring the voltage transient response on each cell. The results of this test are shown in figure 4 where the same test process as described above was conduced; however, the charge voltage was raised to 0.109V.

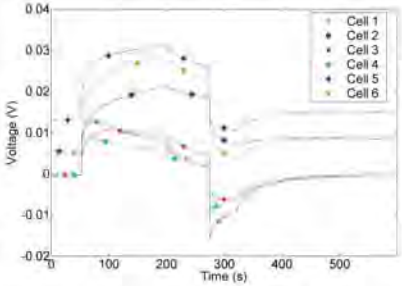

Figure 4 Passive fuel cell test method applied to a stack of 6 cells, where the solid lines are experimental data and the dashed lines are from the circuit model.

4.1 Passive Test

The results of the passive stack fuel cell test show a wide variation in cell voltage response. These differences are caused in part by different electronic properties, i.e. electronic conductance values. The different electronic properties, together with the cell interactions produce the wide ranging voltage response observed.

The varied voltage response from each cell is used for predicted the functionality of the cells. It is proposed that the different cell behaviours observed by the passive fuel cell test will correlate with the individual cell performance when the stack is active. In other words, the differential voltage response between the cells is caused by the same physical differences that cause the cells to function at different levels of health.

4.2 Correlation to Active Performance

The fuel cell was connected to a hydrogen and air supply, and a constant current load was used to obtain the steady state VI curve for the stack. Three voltage readings of each cell were taken (over a period of 6 seconds) at each current value, with the voltage readings taken in order of increasing current. The resulting VI curve of each cell is shown in figure 5.

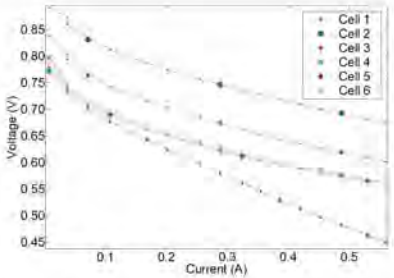

Figure 5 Performance curve for the test PEM fuel cell with constant current load.

The different levels of cell functionality (or health) are clearly demonstrated in figure 5, with cell #2 being the healthiest, and cell #1 showing the lowest level of health. To maximize the usefulness of the passive fuel cell test, a relationship between the passive and active test results must be established, so that the health level of the cells can be predicted.

Two methods have been examined for establishing this relationship, firstly, though a direct correlation between the active and passive test results, and secondly, through an equivalent circuit model analysis. The direct correlation will be briefly reviewed; however, this paper will concentrate on the equivalent Circuit modeling of the fuel cell.

4.2.1 Passive Voltage Decay Predicts Active Cell Performance

A direct correlation between certain voltage transients in the passive fuel cell test results and the active voltage of the cell has been observed. In the Natural Decay region (3), the rate of voltage decay for each cell appears to relate to the active health of that cell. Essentially, cells that have a high rate of voltage decay in the passive test will not produce a high voltage when active. This can clearly be seen by examining the behavior of cells #1 and #2, which have a rapid and slow voltage decay during the passive test, and produce a comparatively low and high voltage respectively when active. This direct correlation shows the potential of the passive fuel cell test, and that the range of voltage transients observed relate to the active functionality of the fuel cell. However, this direct correlation has yet to be confirmed on additional PEM fuel cell stacks. As a result, further analysis on the passive fuel cell test results is considered. To carry out the required analysis, an ECM has been used.

5. EQUIVALENT CIRCUIT MODEL OF THE PASSIVE FUEL CELL

Equivalent Circuit Modelling was used to analyze and model the electrical behaviour of the fuel cell. Using this methodology, an equivalent circuit model (ECM) of the fuel cell (shown in Figure 6) has been inferred from the passive test results.

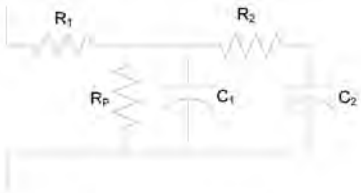

Figure 6 ECM of the passive fuel cell.

The model proposed is significantly different to existing fuel cell ECM's which have been used for active fuel cell modelling. When active fuel cell ECM's reported in the literature are reduced to model a passive cell, they are different to the model shown in Figure 6. However, the passive fuel cell model is very similar to those used for DLC's [10, 11]. In general, DLC models consist of multiple RC branches placed in series. The similarity between the model shown for a passive fuel cell and a

DLC is to be expected, considering the similarity between the two devices as described in section 2.

The objective of using the circuit model is to correlate physical properties or processes in the fuel cell with circuit components. For example, R_0 would represent the electrical resistance of the membrane, R_1 would represent any series resistance between the cells, and perhaps R_2 and C_2 are related to the capacitive and ionic condition of the membrane. Finding the values of the circuit components would indicate the physical condition of the fuel cell, which could then be used to predict the reliability of the UPS system. In any case, to utilize the model, a method to find the values of the circuit parameters is needed.

5.1 Algorithm

To obtain the circuit parameters, PLECS, a circuit simulator program that operates in the Matlab Simulink environment, was used to simulate the voltage behavior of the cells. In total, 30 circuit parameters must be found (5 circuit parameters for each of the 6 cells), using only the results from the passive stack test (figure 4). An algorithm was constructed that iterates through each circuit parameter in the model to minimize the least squares difference between the simulated and experimental results. The iterative routine also acquires the initial voltage conditions of the model capacitors. This is achieved by periodically holding the circuit parameters constant, and conducting a least squares fit on the initial steady sate region of the passive test results. Therefore, the circuit parameters can be found regardless of the initial state of the fuel cell.

Using a least squares fit algorithm to acquire the circuit parameters has some advantages over methods presently used. The circuit parameters of a DLC are generally found by conducting a constant current charge of the capacitor. With the capacitor at an initial state of 0V, the voltage transients have been used to calculate the circuit model parameters [12]. The circuit components of a fuel cell are found in a similar fashion when current pulse or interrupt techniques are used, however, fitting experimental results to modelled data has been used when EIS is employed [4]. All of these methods have been employed on a single cell only. Utilizing the least squares fit algorithm, all cell parameters can be found from a single test, the resulting parameter values are shown in table 1.

Using the circuit values in table 1, the circuit model predicts the behaviour of the passive fuel cell test response with a high degree of agreement, as shown in figure 4. However, this agreement should be treated with some caution. As a fitting algorithm was used, the agreement between the experimental and modelled data is expected. It is possible that other (similar) circuit models may predict the behaviour of the fuel cell. A degree of confidence can be placed in the model when the R_1 values for each cell are examined. In the steady state region, cells #6 #5 and #2 show a comparatively high voltage. This voltage is created from the previous day's active operation of the stack, coupled with a high electronic resistance of these three cells (so that the voltage does not completely dissipate). From inspection of table 1, high resistance values are given for these three cells.

	R_0	R_1	C_1	R_2	C_2
Cell 1	13.2	112	0.199	22.1	0.224
Cell 2	6.46	1780	0.636	284	0.373
Cell 3	8.09	165	0.537	310	0.199
Cell 4	10.9	78.2	0.501	77.3	0.227
Cell 5	13.6	2140	0.425	236	0.591
Cell 6	13.7	1720	0.360	353	0.334

Table 1 Circuit Model Values derived from passive fuel cell stack test

Additional analysis and interpretation of the circuit model is continuing, particularly with respect to the physical interpretation of the circuit components. However, just the simple example of the prediction of cell electrical conduction (which adversely affects the health of the cell) illustrates the potential of this analysis method.

6. CONCLUSION

A new methodology for testing a PEM fuel cell has been presented. The test method focuses on the fuel cell in a passive state, and draws on the similarities with Double Layer Capacitors for the modelling and analysis.

A direct correlation between the passive fuel cell results and the functioning of the fuel cell has been observed, which demonstrates the usefulness of passive testing for health prediction. While a direct correlation between passive and active test results could be used for health prediction of the fuel cell, the analysis method focused on, has used an equivalent circuit model.

The structure of the ECM is closer to that of a DLC as opposed to existing fuel cell models. This is to be expected due to the similarity in the physical construction and electrical conditions imposed while the fuel cell is in a passive state. An algorithm for acquiring the model parameters and initial conditions has been developed. The algorithm can acquire the parameters and initial conditions for many cells in a stack from the results of a single stack test. Further investigations of the results and relation of the circuit parameters to physical properties within the stack are currently being undertaken to determine the state of health of a fuel cell in a UPS system.

7. REFERENCES

[1] Kim, J., Lee S.M., Srinivasan, S., "Modeling of Proton Exchange Exchange with an Empirical Equation", Journal of the Electrochemical Society, Vol 142 (8), August 1995, pp 2670-2674

[2] Chu D., Jiang R., Walker C., "Analysis of PEM fuel cell stacks using an empirical current-voltage equation" Journal of Applied Electrochemistry Vol 30 (3), March 2000, pp 365-370

[3] Larminie, J.R.J, "Current interrupt techniques for circuit modeling" Electrochemical Measurement, IEE Colloquium on, 1994 pp 12/1 -12/6

[4] Wagner, N., "Characterization of membrane electrode assemblies in polymer electrolyte fuel cells using a.c. impedance spectroscopy", Journal of Applied Electrochemistry, Vol 32 (8), August 2002, pp 859-863

[5] O'Hayre, R., Fabian, T., Lee, S.J., Prinz, F.B., "Lateral ionic conduction in planar array fuel cells", Journal of the Electrochemical Society, Vol 150 (4), April 2003, pp A430-A438

[6] Li, G.C., Pickup, P.G., "Ionic conductivity of PEMFC electrodes - Effect of Nafion loading", Journal of the Electrochemical Society, Vol 150 (11), November 2003, pp C745-C752

[7] Saab, A.P., Garzon, F.H., Zawodzinski, T.A., "Determination of ionic and electronic resistivities in carbon/polyelectrolyte fuel-cell composite electrodes", Journal of the Electrochemical Society, Vol 149 (12), December 2002, pp A1541-A1546

[8] Wagner N., Schnurnberger W., Muller B., Lang M., "Electrochemical impedance spectra of solid-oxide fuel cells and polymer membrane fuel cells" *E*lectrochimica Acta, Vol 43 (24), 1998, pp3785-3793

[9] Lufrano, F., Staiti, P., Minutoli, M., "Evaluation of nafion based double layer capacitors by electrochemical impedance spectroscopy", Journal of Power Sources, Vol 124 (1), October 2003, pp 314-320

[10] Gualous, H., Bouquain, D., Berthon, A., Kauffmann, J.M., "Experimental study of supercapacitor serial resistance and capacitance variations with temperature", Journal of Power Sources, Vol 123 (1), September 2003, pp 86-93

[11] Belhachemi, F., Rael, S., Davat, B., "A physical based model of power electric double-layer supercapacitors", Industry Applications Conference, Conference Record of the 2000 IEEE , Vol: 5 , 8-12 October 2000, pp 3069-3076

[12] Zubieta, L., Bonert, R.; "Characterization of double-layer capacitors (DLCs) for power electronics applications", Industry Applications Conference, Thirty-Third IAS Annual Meeting, IEEE, Vol 2, October 1998, pp 1149-1154

AUPEC PEER REVIEW

AUPEC 2004
THE UNIVERSITY OF QUEENSLAND, BRISBANE, AUSTRALIA
26-29 SEPTEMBER, 2004

REVIEW FORM FOR FULL PAPER

Paper Number: 205

Paper Title: TESTING PROCEDURE FOR PASSIVE FUEL CELL STATE OF HEALTH

Dear colleague

For the Australasian Universities Power Engineering Conference (AUPEC2004) we request that you please review the attached paper submitted to the conference.

Please complete one review form for each paper and **email** or **fax** it to the AUPEC2004 Secretariat at the address shown below. A review will not be considered complete unless all 4 sections are answered in full. (Reviewers will be kept confidential).

Section A:	*Please specify* (*electronic copy, left mouse click twice to check box*)				
Originality	☒ Excellent	☐ Good	☐ Satisfactory	☐ Unsatisfactory	☐ Poor
Contribution	☐ Excellent	☒ Good	☐ Satisfactory	☐ Unsatisfactory	☐ Poor
References	☐ Excellent	☐ Good	☒ Satisfactory	☐ Unsatisfactory	☐ Poor
Presentation Style	☐ Excellent	☒ Good	☐ Satisfactory	☐ Unsatisfactory	☐ Poor
Quality of Language	☐ Excellent	☒ Good	☐ Satisfactory	☐ Unsatisfactory	☐ Poor
Final Result	☒ Accept	☐ Accept with revision		☐ Rewrite	☐ Reject

Section B: Briefly, the contribution of the paper appears to be the following:
This paper is an interesting novel solution to fuel cell performance assessment without fuel cell operation. Development of tests as describe in this paper not only are important for assessing UPS installations but will also be essential for QC testing of fuel cells. Very interesting approach and interesting results.

Section C: Required revision:

Section D: Should the paper be considered for a journal publication:

Yes. Interesting and novel contribution.

Section E: If the first author of this paper was a student, do you believe it should be considered for the best student paper award
Yes

AUPEC'2004 Secretariat
School of Information Technology & Electrical Engineering
The University of Queensland
St Lucia, QLD 4072
Australia

Tel: +61 7 3365 3984
Fax: +61 7 3365 4999
Email: aupec04@itee.uq.edu.au
WWW: http://www.itee.uq.edu.au/~aupec04/

(12) INTERNATIONAL APPLICATION PUBLISHED UNDER THE PATENT COOPERATION TREATY (PCT)

(19) World Intellectual Property Organization
International Bureau

(43) International Publication Date
6 October 2005 (06.10.2005)

PCT

(10) International Publication Number
WO 2005/093447 A2

(51) International Patent Classification[7]: G01R 31/36, H01M 8/04, G01R 27/26

(21) International Application Number: PCT/NZ2005/000053

(22) International Filing Date: 24 March 2005 (24.03.2005)

(25) Filing Language: English

(26) Publication Language: English

(30) Priority Data:
531978 26 March 2004 (26.03.2004) NZ

(71) Applicant *(for all designated States except US)*: **EATON POWER QUALITY LIMITED** [NZ/NZ]; 39 Princess Street, Christchurch, 8004 (NZ).

(72) Inventors; and

(75) Inventors/Applicants *(for US only)*: **PAGE, Shannon Charles** [NZ/NZ]; 15 Thompsons Road, Belfast, Christchurch, 8005 (NZ). **AL-ANBUKY, Adnan** [NZ/NZ]; 23 Heath Street, Burnside, Christchurch, 8002 (NZ). **KRUMDIECK, Susan Pran** [US/NZ]; 28 Ryeland Ave, Fendalton, Christchurch, 8044 (NZ).

(74) Agent: **BALDWINS**; Baldwins Centre, Level 14, 342 Lambton Quay, Wellington, 6001 (NZ).

(81) Designated States *(unless otherwise indicated, for every kind of national protection available)*: AE, AG, AL, AM, AT, AU, AZ, BA, BB, BG, BR, BW, BY, BZ, CA, CH, CN, CO, CR, CU, CZ, DE, DK, DM, DZ, EC, EE, EG, ES, FI, GB, GD, GE, GH, GM, HR, HU, ID, IL, IN, IS, JP, KE, KG, KP, KR, KZ, LC, LK, LR, LS, LT, LU, LV, MA, MD, MG, MK, MN, MW, MX, MZ, NA, NI, NO, NZ, OM, PG, PH, PL, PT, RO, RU, SC, SD, SE, SG, SK, SL, SM, SY, TJ, TM, TN, TR, TT, TZ, UA, UG, US, UZ, VC, VN, YU, ZA, ZM, ZW.

(84) Designated States *(unless otherwise indicated, for every kind of regional protection available)*: ARIPO (BW, GH, GM, KE, LS, MW, MZ, NA, SD, SL, SZ, TZ, UG, ZM, ZW), Eurasian (AM, AZ, BY, KG, KZ, MD, RU, TJ, TM), European (AT, BE, BG, CH, CY, CZ, DE, DK, EE, ES, FI, FR, GB, GR, HU, IE, IS, IT, LT, LU, MC, NL, PL, PT, RO,

[Continued on next page]

(54) Title: METHOD OF TESTING AN ELECTROCHEMICAL DEVICE

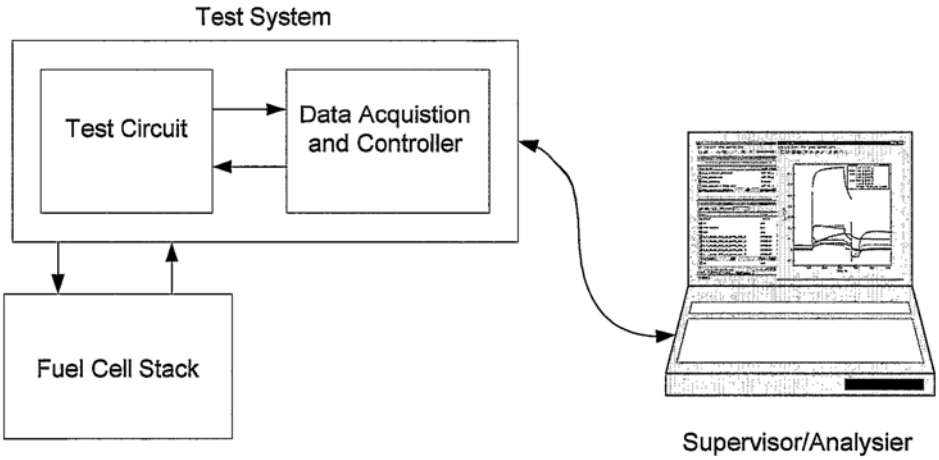

(57) Abstract: Methods and associated apparatus for testing an electrochemical device, such as a fuel cell. A first method involves charging the fuel cell during a charge period; discharging the fuel cell during a discharge period; and monitoring the response of the fuel cell during at least part of the discharge period or the open-circuit response of the fuel cell. Another method involves testing the fuel cell when the fuel cell is in a passive state in which substantially no electrochemical reactions are taking place in the fuel cell. simultaneously applying a stimulus to all of the devices, and independently monitoring the response of each of the devices to the stimulus. Further methods involve obtaining test data from a device being tested; obtaining equivalent circuit values; calculating sets of simulation data for each equivalent circuit value; comparing sets of simulation data with the test data; and selecting one of the equivalent circuit values based on the comparison. This method allows all circuit parameters of each cell in a stack to be obtained from only one quick test.

WO 2005/093447 A2

SE, SI, SK, TR), OAPI (BF, BJ, CF, CG, CI, CM, GA, GN, GQ, GW, ML, MR, NE, SN, TD, TG).

Published:

— *without international search report and to be republished upon receipt of that report*

For two-letter codes and other abbreviations, refer to the "Guidance Notes on Codes and Abbreviations" appearing at the beginning of each regular issue of the PCT Gazette.

APPENDIX B: MATLAB CODE LISTINGS

The following Appendix is divided into two sections. The program code listings involved in testing the fuel cell are presented first. The second section details the Matlab code for written for implementation of the fitting method, as described in Chapter 7.

DATA AQUESTION CODE

Numerous Matlab programs were written for testing the fuel cell, both in a passive state, and for recording the active operation. Three of these programs are listed in this section. The two smaller programs, `open.m` and `close.m`, are responsible for creating (and removing) the HP data/acquisition unit as an object in the Matlab workspace. The other program listed is `passive_test.m`, which is used for implementing the passive testing method, and recording and saving the results of the test. Additional programs written for fuel cell testing are simply variations of `passive_test.m`. For example, the scan list is altered if a different number of cells were being tested, and in the case of active testing, the part of the program which send digital signals to the HP unit (for changing a switch position) is removed.

open.m

```
global obj
obj = serial('COM1');
set(obj,'BaudRate',57600,'Parity','none','FlowControl','hardware');
fopen(obj);
```

close.m

```
fclose(obj)
delete(obj)
clear obj
```

passive_test.m

(shown in the following pages)

```
% define the file name the data is to be saved as
savefile_temp = 's_V_Avista_Stack_0388_2023_fin_9_5_temp';
savefile = 's_V_Avista_Stack_0388_2023_fin_9_5';

%%%%%%%%%% clears old results %%%%%%%%%%%%%%
FinalResults = 0;
ResultMtx = [] ;

%%%%%%%%% set up the recordings %%%%%%%%%%%%%%%%%%%%%%%%%%%%%%

% define the switch times as time intervals
time_initial = 50;
time_charge = 175;
time_decay = 60;
time_short = 30;

StartCPU = cputime;     %defines the start time of the cpu
ScanInterval = 0.1;     % time between measurements
numberScans  = 1500;    % number of time it gose throu the scan list
channelDelay = 0;       % time between the relay closing and the measurment taken


scanList = '(@104,106,107:114,115)'; % stack
control_channel = '(@301)';
fprintf(obj,'configure:voltage:DC (@104,106,107:114)'); % stack
fprintf(obj,'configure:temperature tc,k,(@115)')

switch_times = [    (time_initial)
                    (time_initial+time_charge)
                    (time_initial+time_charge+time_decay)
                    (time_initial+time_charge+time_decay+time_short) ];

% The switch list numbers correspond to
switch_list  = [   1        % switch S1 closed
                   0        % both switchs open
                   2        % switch S2 closed
                   0  ];    % both switchs open


[row_sw,col_sw] = size(switch_times); %% just need the col_sw

fprintf(obj,'Route:Scan %s\n',scanList); % sets the scan list into the HP, %s = string, \n = terminator, so scanlist is a string
fprintf(obj,'Route:Scan:Size?');        % asks the HP the number channels to be read
numberChannel = str2num(fscanf(obj));   % reads the number of channels, converts the string to a number

fprintf(obj,'Format:Reading:Time On'); % returns the time stamp with each reading
fprintf(obj,'Format:Reading:Channel On'); % returns the channel number with each reading

fprintf(obj,'Route:Channel:Delay %d,%s\n',[channelDelay scanList]); %sets the meter with the channel delay & scanlist
```

```
fprintf(obj,'Trigger:Count %d\n',numberScans);  % these three commands configure the scan interval
fprintf(obj,'Trigger:Source Timer');
fprintf(obj,'Trigger:Timer %d\n',ScanInterval);

fprintf(obj,'System:Time:Scan?'); % Whats the time HP?
FinalResults(1,1:6)= str2num(fscanf(obj)); % records the start time and writes into final resuts mtx

StartCPU = cputime;
fprintf(obj,'Initiate'); %Start the scan

% set all of the inital conditions for the test run

test = 1;
index = 0;  % used for writing the results into the matrix, increments with each results

% stay in here untill the times of the switch fliking has pasted

switch_time_pos = 1;

while switch_time_pos < (col_sw + 1);  % only col_sw positions, therfore, will exit when it has flicked the last switch
    if (cputime - StartCPU) > switch_times(1,switch_time_pos);
        fprintf(obj,'Source:Digital:Data %d,%s\n',[switch_list(1,switch_time_pos) control_channel]); % used to write the out put
        switch_time_pos = switch_time_pos + 1;
    else
    end
end % while

%%% end loop for switching the charge/discharge switches


% this section constantly reads, records and erases readings from the HP
% Meter as well as setting the load (the actulal Programe)

fprintf(obj,'Data:Points?');   % gets the number of readings stored
points = str2num(fscanf(obj)); % defines the value as points

while index < numberScans*numberChannel;

    while points < 1 % stays in this loop untill there is a value in the HP meter
        fprintf(obj,'Data:Points?');   % gets the number of readings stored
        %             pause(1);
        points = str2num(fscanf(obj)); % defines the value as points
    end
    %%%%%%%%%% now that HP has a data value, record and erase from the HP %%%%%%%%%%%%%%
    for write = 1:1:points
        fprintf(obj,'Data:Remove? 1');   % takes a data value from the memory
        ResultMtx((index + write),1:3) =  str2num(fscanf(obj));% converts, and writes it into the result MTX
        save(savefile_temp,'ResultMtx');
    end
```

```
%%%%%%%%%%%%%%%%%%%%%% save the reading %%%%%%%%%%%%%%%%%%%%%%%%%%%%%%%%

    save(savefile_temp,'ResultMtx');
    %%%%%%%%%%%%%%%%%% end of recording from the HP for now %%%%%%%%%%
    index = index + points;
    points = 0;
end

%%%%%%%%%%%%%%%%%% writes the results into the final results %%%%%%%%%%%%%
[totalresults,m] = size(ResultMtx);
ResultMtx(totalresults + numberChannel,1:3) = 0; % Adds more zeros onto the end
% incase the scan was aborted midway through the scan list.

count = 1;
for row = 2:1: ( ceil(totalresults/numberChannel) + 1 )           % Starts at the 2 row as the first is the time and date
    for column = 1:3:numberChannel*3;    % as there are three results per reading (data , time , channel)
        FinalResults(row,column:column + 2) = ResultMtx(count,1:3);
        count = count + 1;
    end
end

fprintf(obj,'System:Time:Scan?'); % Whats the time HP?
LookAtTime = str2num(fscanf(obj)) % records the start time and writes into final resuts mtx
FinalResults(1,1:6)= LookAtTime;

save(savefile,'FinalResults','ResultMtx');
```

FITTING CODE

The fitting code **`fitting_algorithm.m`** contains two separate programs. One program, labelled **`'program_plot'`**, graphs the experimental data (raw and interpolated) against the ECM model response. Marker points are also plotted, indicating the specific data values used for calculating the error. The second program, labelled **`'program_fit'`** implements the iterative fitting routine. As circuit parameter values for many stack tests were required, the fitting code, **`fitting_algorithm.m`**, was designed to determine the circuit parameter values for many stack test. The two programs **`'program_plot'`**, and **`'program_fit'`** were contained within a simple loop, defined by the counter variable **`data_fit_run.`** For each value of **`data_fit_run`** experimental data from a specific test is loaded, together with the passive test conditions. Once the circuit parameters have been found and saved, a new data set was loaded, and the fitting technique repeated. Therefore, once the **`fitting_algorithm.m`** the circuit parameter values for numerous stack tests are determined and saved.

```
warning off MATLAB:polyfit:RepeatedPointsOrRescale
warning off MATLAB:divideByZero

%% initial load of variables
load('all_2006_Dec_17.mat')

program = 'program_fit';
CicuitSim = 'Model_8_cells_6v5';
savefile_2 = 'Final_8_cells_results_3.mat';

yes_plot = 0;  %% if this is 1, then the program will plot once a solution is found

for data_fit_run =3:1:3;

    current_data_fit_run = data_fit_run;

    weight          = [  1        3          1        2         10         10        10    ];
    num_test_points = 12;          % or comparison points per section
    stack_pos       = 25;          % for plotting purposes, the mtx pos of Stack voltage
    SimTimeSet      = 1;           % SimTimeSet is the model output time interval
    dt              = SimTimeSet;  % dt is the interpolation time set
    inital_guess = [400  200    0.5  0.2    0
                    400  200    0.5  0.2    0
                    400  200    0.5  0.2    0
                    400  200    0.5  0.2    0
                    400  200    0.5  0.2    0
                    400  200    0.5  0.2    0
                    400  200    0.5  0.2    0
                    400  200    0.5  0.2    0];

    if data_fit_run == 1

        CompTimes = [ 5 45    85 222    239 283   292 314    321 350    355 400   400 500];

        savefile  = 's_V_Avista_Stack_0587_0388_fin_8_40_res_1.mat';
        TD        = s_V_Avista_Stack_0587_0388_fin_8_40;
        TD(1,:)   = [];
        TD        = [TD, TD(:,1:6)];
        TD(:,1:6) = [];

        inital_newCvalues  =  [ TD(1,1) TD(1,1)
                                TD(1,4) TD(1,4)
                                TD(1,7) TD(1,7)
                                TD(1,10) TD(1,10)
                                TD(1,13) TD(1,13)
                                TD(1,16) TD(1,16)
                                TD(1,19) TD(1,19)
                                TD(1,22) TD(1,22)];
```

```
    V_on_time_first      = 50.1275;
    V_off_time_first     = 225.3000;
    short_on_time_first  = 285.3705;
    short_off_time_first = 315.5300;

    ChargeVoltagefirst   = 0.3222;
    ChargeResistor       = 52.573;
    ShortResistor        = 10.147;

    if exist(savefile) == 0 % i.e. it dose not exist
        NewValues = inital_guess;
        newCvalues = inital_newCvalues; least_error = []; % least error is not in the algorithm at the moment
        itt_num = 0;
    else
        load(savefile) % other wise load the data and carry on
    end

elseif data_fit_run == 2

    CompTimes = [ 5 45    85 222    239 283   292 314    321 350    355 400   400 500];

    savefile  = 's_V_Avista_Stack_0587_0388_fin_8_44_res_1.mat';
    TD = s_V_Avista_Stack_0587_0388_fin_8_44;

    TD(1,:) = [];
    TD = [TD, TD(:,1:6)];
    TD(:,1:6) = [];

    inital_newCvalues= [  TD(1,1) TD(1,1)
                          TD(1,4) TD(1,4)
                          TD(1,7) TD(1,7)
                          TD(1,10) TD(1,10)
                          TD(1,13) TD(1,13)
                          TD(1,16) TD(1,16)
                          TD(1,19) TD(1,19)
                          TD(1,22) TD(1,22)];

    %% define the test circuit values and switch times, which are used in the Simulink/PLECS model
    V_on_time_first      = 50.1095;
    V_off_time_first     = 225.3145;
    short_on_time_first  = 285.5010;
    short_off_time_first = 315.5485;

    ChargeVoltagefirst   = 0.303;
    ChargeResistor       = 52.573;
    ShortResistor        = 10.147;
```

```
    if exist(savefile) == 0 % i.e. it dose not exist
              NewValues = inital_guess;
              newCvalues = inital_newCvalues; least_error = []; % least error is not in the algorithm at the moment
              itt_num = 0;
         else
              load(savefile) % other wise load the data and carry on
         end


      elseif data_fit_run == 3

         CompTimes = [ 5 45    85 222    239 283   292 314    321 350    355 400   400 500];

         savefile  = 's_V_Avista_Stack_0587_0388_fin_8_48_res_1.mat';
         TD = s_V_Avista_Stack_0587_0388_fin_8_48;

         TD(1,:) = [];
         TD = [TD, TD(:,1:6)];
         TD(:,1:6) = [];

         inital_newCvalues= [  TD(1,1) TD(1,1)
                               TD(1,4) TD(1,4)
                               TD(1,7) TD(1,7)
                               TD(1,10) TD(1,10)
                               TD(1,13) TD(1,13)
                               TD(1,16) TD(1,16)
                               TD(1,19) TD(1,19)
                               TD(1,22) TD(1,22)];

         V_on_time_first      = 50.0485;
         V_off_time_first     = 225.3940;
         short_on_time_first  = 285.5585;
         short_off_time_first = 315.6980;

         ChargeVoltagefirst   = 0.3031;
         ChargeResistor       = 52.573;
         ShortResistor        = 10.147;

         if exist(savefile) == 0 % i.e. it dose not exist
              NewValues = inital_guess;
              newCvalues = inital_newCvalues; least_error = []; % least error is not in the algorithm at the moment
              itt_num = 0;
         else
              load(savefile) % other wise load the data and carry on
         end
      else
      end
```

```
FindWhichValues = [1 2 3 4];  % which circuit vlaues are to be found by the Algorithm
[FindWhichValues_row,FindWhichValues_col] = size(FindWhichValues);
[NewValues_row,NewValues_col] = size(NewValues);  % BOTH needed for the algorithm

SteadySimTime = V_on_time_first - 1;  % just for simulating the inital steady state (for evaluating the inial cap values)

FullSimTime   = 500; % for the whole of the simullation
SSPos = round(SteadySimTime/SimTimeSet);  %% the simulation time when evaluating the inital volage on the capacitors

%%%%%%%%%% Algorithm Parameter, change these to make the algorithm faster
Total_Algo_Itt = 20;  % maximum number of time it goes through the two algorithms
itterations    = 10; % maximum number of times it goes through the parameter loop
C_itterations  = 10; % how many times it goes through the capacitor calculation

tol = 0.0001 %% the tolerance (i.e. error min when +/- of 0.01% results in a larger error)

ChangeVare   = [ 1-(tol*10^2)  1-(tol*10) 1-tol 1 1+tol 1+(tol*10) 1+(tol*10^2)]; % generates parameter values that are compared
C_spread_vec = [ 1-(tol*10^2)  1-(tol*10) 1-tol 1 1+tol 1+(tol*10) 1+(tol*10^2)]; % generates capacitor voltage values that are compared

[C_spread_row,C_spread_col] = size(C_spread_vec);  % for how many new solutions to try (C_spread_col)



switch lower(program)


    %%%%%%%%%%%%% The following program just plots the experimental data and model %%%%%%%%%%%%%%%%%%%%%%%%%%%%%%%%%%%%%%%%%%%%%%%%%%%%

    case {'program_plot'} % for two cells

        %%% interpolate part data taken not to include time header
        newdata = [];
        [row,col] = size(TD);
        end_time = FullSimTime; % final time for the interpolated data
        for cell = 1:1:col/3; % how many channels
            write_row = 0; % counter for adding in data points in the new matrix
            for new_time = 0:dt:end_time % the new interpolated times
                write_row = write_row + 1;
                %% find the closest data point
                temp_time_vect = abs(TD(:,3*cell - 1) - new_time);   % a vector with the desired time subtracted
                temp_min = min(temp_time_vect);  % finds the min value (of the absolute time)
                posmin = find( temp_min == temp_time_vect); % find the position of it
                posmin = posmin(1,1); % incase there is more that one values (doubtful)
                % now find voltage and time values either side, for
                if posmin == 1; % if the values is the first in the data set, take the next 2 values
                    time_vec = [ TD(posmin,3*cell - 1),   TD(posmin + 1,3*cell - 1),  TD(posmin + 2,3*cell - 1)];
                    V_vec =    [ TD(posmin,3*cell - 2),   TD(posmin + 1,3*cell - 2),  TD(posmin + 2,3*cell - 2)];
```

```
        elseif posmin == row; % if the values is the last in the data set, take previous 2 values
            time_vec = [ TD(posmin - 2,3*cell - 1),       TD(posmin - 1,3*cell - 1),  TD(posmin,3*cell - 1)];
            V_vec =    [ TD(posmin - 2,3*cell - 2),       TD(posmin - 1,3*cell - 2),  TD(posmin,3*cell - 2)];
        else  % otherwise, take data values either side of the point
            time_vec = [ TD(posmin - 1,3*cell - 1),   TD(posmin,3*cell - 1),      TD(posmin + 1,3*cell - 1)];
            V_vec =    [ TD(posmin - 1,3*cell - 2),   TD(posmin,3*cell - 2),      TD(posmin + 1,3*cell - 2)];
        end
        p_cof = polyfit(time_vec,V_vec,2);
        new_V = p_cof(1)*(new_time^2) + p_cof(2)*new_time + p_cof(3);
        % write it into the final matrix
        newdata(write_row,3*cell - 2) = new_V;          % new Voltage
        newdata(write_row,3*cell - 1) = new_time;       % new time
        newdata(write_row,3*cell)     = TD(2,3*cell); % channel number
    end  % new_time = 0:1:end_time % the new interpolated times
end % cell = 1:1:3; % how many channels
o_TD = TD;  % o_TD stands for old test data
TD = newdata;  % TD is now the interpolated test data
 %%% create comparison vectors   %%%%%%%%
[row,col] = size(TD);  % redefines row and col now that TD is interpolated data
comp_vec = zeros(row,1); %% comp_vec consists of ones and zeros,
comp_weights = zeros(row,1); %% comp_weights is similar but consists of the weights
for count_points = 1:1:col_comp/2
    start_time = CompTimes(2*count_points-1);
    end_time = CompTimes(2*count_points);
    step_time = round((end_time - start_time)/num_test_points);
    for goodCount = start_time:step_time:end_time
        comp_vec(goodCount,1) = 1;
        comp_weights(goodCount,1) = weight(count_points);
    end
end  %%% end create comparison vectors %%%%%%%%
%%%%%% end interpolate  %% now standard fitting test
SimTime = FullSimTime;
Ca1ini = newCvalues(1,1);     Cb1ini = newCvalues(1,2);
Ca2ini = newCvalues(2,1);     Cb2ini = newCvalues(2,2);
Ca3ini = newCvalues(3,1);     Cb3ini = newCvalues(3,2);
Ca4ini = newCvalues(4,1);     Cb4ini = newCvalues(4,2);
Ca5ini = newCvalues(5,1);     Cb5ini = newCvalues(5,2);
Ca6ini = newCvalues(6,1);     Cb6ini = newCvalues(6,2);
Ca7ini = newCvalues(7,1);     Cb7ini = newCvalues(7,2);
Ca8ini = newCvalues(8,1);     Cb8ini = newCvalues(8,2);

Ra1 = NewValues(1,1);  Rb1 = NewValues(1,2);  Ca1 = NewValues(1,3);  Cb1 = NewValues(1,4);  Rp1 = NewValues(1,5);
Ra2 = NewValues(2,1);  Rb2 = NewValues(2,2);  Ca2 = NewValues(2,3);  Cb2 = NewValues(2,4);  Rp2 = NewValues(2,5);
Ra3 = NewValues(3,1);  Rb3 = NewValues(3,2);  Ca3 = NewValues(3,3);  Cb3 = NewValues(3,4);  Rp3 = NewValues(3,5);
Ra4 = NewValues(4,1);  Rb4 = NewValues(4,2);  Ca4 = NewValues(4,3);  Cb4 = NewValues(4,4);  Rp4 = NewValues(4,5);
Ra5 = NewValues(5,1);  Rb5 = NewValues(5,2);  Ca5 = NewValues(5,3);  Cb5 = NewValues(5,4);  Rp5 = NewValues(5,5);
Ra6 = NewValues(6,1);  Rb6 = NewValues(6,2);  Ca6 = NewValues(6,3);  Cb6 = NewValues(6,4);  Rp6 = NewValues(6,5);
Ra7 = NewValues(7,1);  Rb7 = NewValues(7,2);  Ca7 = NewValues(7,3);  Cb7 = NewValues(7,4);  Rp7 = NewValues(7,5);
Ra8 = NewValues(8,1);  Rb8 = NewValues(8,2);  Ca8 = NewValues(8,3);  Cb8 = NewValues(8,4);  Rp8 = NewValues(8,5);
```

```
sim(CicuitSim)                  % after the simulation, need to get the simulated results into a mtx
[row,col] = size(TD);      % define a new data mtx
[ROW,COL] = size(FC_Cell_V1);   % size of the results, (just need the ROW)

figure(104)
%% plot the Experimental data
plot(TD(:,2),TD(:,1),TD(:,5),TD(:,4),TD(:,8),TD(:,7),TD(:,11),TD(:,10),...
    TD(:,14),TD(:,13),TD(:,17),TD(:,16),TD(:,20),TD(:,19),TD(:,23),TD(:,22));
hold on; %% plot the experimental data
plot(o_TD(:,2),o_TD(:,1),'-.',o_TD(:,5),o_TD(:,4),'-.',o_TD(:,8),o_TD(:,7),'-.',o_TD(:,11),o_TD(:,10),'-.',...
    o_TD(:,14),o_TD(:,13),'-.',o_TD(:,17),o_TD(:,16),'-.',o_TD(:,20),o_TD(:,19),'-.',o_TD(:,23),o_TD(:,22),'-.');

%% plot the simulated data
plot(time,FC_Cell_V1,':',time,FC_Cell_V2,':',time,FC_Cell_V3,':',time,FC_Cell_V4,':',...
    time,FC_Cell_V5,':',time,FC_Cell_V6,':',time,FC_Cell_V7,':',time,FC_Cell_V8,':');
legend('Cell 1','Cell 2','Cell 3','Cell 4','Cell 5','Cell 6','Cell 7','Cell 8'); xlabel('Time (s)'); ylabel('Voltage (V)');
hold off;

figure(103)  % plot the stack voltage, with comparison points.
SimResults = [ FC_Voltage ];
plot(o_TD(:,stack_pos + 1),o_TD(:,stack_pos),'black'); % plot the Experimental data
hold on
plot(time,FC_Voltage,'r'); %% plot the simulated data
plot(TD(:,stack_pos + 1),TD(:,stack_pos),'b'); %% plot the interpolated data
legend('Experimental Data','Fitted Data','Interpolated Data'); xlabel('Time (s)'); ylabel('Voltage (V)');
% now establish the comparison points,

error_val = [];
error_val_time = [];
for count_plot = 1:1:row
    if comp_vec(count_plot,1) == 1  %% then plot a point
        plot(time(count_plot),SimResults(count_plot),'.r');  % SimResults at this point are the stack voltage
        plot(TD(count_plot,stack_pos + 1),TD(count_plot,stack_pos),'.b');
        error_val = [error_val (comp_weights(count_plot)*( TD(count_plot,stack_pos) - SimResults(count_plot))^2)];
        error_val_time = [error_val_time  time(count_plot)];
    else
    end
end
hold off

figure(109)
plot(error_val_time,error_val,'.');

%%%%%%%%%%%%%%%%%%%%%% End of the plotting program %%%%%%%%%%%%%%%%%%%%%%%%%%%%%%%%%%%%%%%%%%%%%%%%%%%%%%%%%%%%%%%%%%%%%%%%
```

```
%%%%%%%%%%%%% The following program implements the fitting method %%%%%%%%%%%%%%%%%%%%%%%%%%%%%%%%%%%%%%%%%%%%%%%%%%%%%%
         case {'program_fit'}
            %%% interpolate part, data taken not to include time header %%%%%%%%%%%%%%%%%%%%%%%
            newdata = [];
            [row,col] = size(TD);
            end_time = FullSimTime; % final time for the interpolated data
            for cell = 1:1:col/3; % how many channels
                write_row = 0; % counter for adding in data points in the new matrix
                for new_time = 0:dt:end_time % the new interpolated times
                    write_row = write_row + 1;
                    %% find the closest data point
                    temp_time_vect = abs(TD(:,3*cell - 1) - new_time);   % a vector with the desired time subtracted
                    temp_min = min(temp_time_vect);  % finds the min value (of the absolute time)
                    posmin = find( temp_min == temp_time_vect); % find the position of it
                    posmin = posmin(1,1); % incase there is more that one values (doubtful)
                    % now find voltage and time values either side, for
                    if posmin == 1; % if the values is the first in the data set, take the next 2 values
                        time_vec = [ TD(posmin,3*cell - 1),     TD(posmin + 1,3*cell - 1), TD(posmin + 2,3*cell - 1)];
                        V_vec =    [ TD(posmin,3*cell - 2),     TD(posmin + 1,3*cell - 2), TD(posmin + 2,3*cell - 2)];
                    elseif posmin == row; % if the values is the last in the data set, take previous 2 values
                        time_vec = [ TD(posmin - 2,3*cell - 1), TD(posmin - 1,3*cell - 1), TD(posmin,3*cell - 1)];
                        V_vec =    [ TD(posmin - 2,3*cell - 2), TD(posmin - 1,3*cell - 2), TD(posmin,3*cell - 2)];
                    else  % otherwise, take data values either side of the point
                        time_vec = [ TD(posmin - 1,3*cell - 1), TD(posmin,3*cell - 1),     TD(posmin + 1,3*cell - 1)];
                        V_vec =    [ TD(posmin - 1,3*cell - 2), TD(posmin,3*cell - 2),     TD(posmin + 1,3*cell - 2)];
                    end
                    p_cof = polyfit(time_vec,V_vec,2);   % obtain the coefficients of 2nd order poly
                    new_V = p_cof(1)*(new_time^2) + p_cof(2)*new_time + p_cof(3); %% get the voltage values at the desired time
                    % write the values into a new matrix
                    newdata(write_row,3*cell - 2) = new_V;          % new Voltage
                    newdata(write_row,3*cell - 1) = new_time;       % new time
                    newdata(write_row,3*cell)     = TD(2,3*cell); % channel number
                end  % new_time = 0:1:end_time % the new interpolated times
            end % cell = 1:1:3; % how many channels
            o_TD = TD;
            TD = newdata;   % redefine the experimental data variable with the interpolated data set
            %%%%%% end interpolation part of the code %%%%%%%%%%%%%%%%%%%%%%%
            %%% create comparison vectors   %%%%%%%%
            [row,col] = size(TD);  % redefines row and col now that TD is interpolated data
            comp_vec = zeros(row,1); %% comp_vec consists of ones and zeros,
            comp_weights = zeros(row,1); %% comp_weights is similar but consists of the weights
            for count_points = 1:1:col_comp/2
                start_time = CompTimes(2*count_points-1);
                end_time = CompTimes(2*count_points);
                step_time = round((end_time - start_time)/num_test_points);
                for goodCount = start_time:step_time:end_time
                    comp_vec(goodCount,1) = 1;
                    comp_weights(goodCount,1) = weight(count_points);
                end
            end
```

```
SimTime = FullSimTime;
oldCvalues = newCvalues;
OldValues = NewValues;

Ca1ini = newCvalues(1,1);     Cb1ini = newCvalues(1,2);
Ca2ini = newCvalues(2,1);     Cb2ini = newCvalues(2,2);
Ca3ini = newCvalues(3,1);     Cb3ini = newCvalues(3,2);
Ca4ini = newCvalues(4,1);     Cb4ini = newCvalues(4,2);
Ca5ini = newCvalues(5,1);     Cb5ini = newCvalues(5,2);
Ca6ini = newCvalues(6,1);     Cb6ini = newCvalues(6,2);
Ca7ini = newCvalues(7,1);     Cb7ini = newCvalues(7,2);
Ca8ini = newCvalues(8,1);     Cb8ini = newCvalues(8,2);

Ra1 = NewValues(1,1);  Rb1 = NewValues(1,2);  Ca1 = NewValues(1,3);  Cb1 = NewValues(1,4);  Rp1 = NewValues(1,5);
Ra2 = NewValues(2,1);  Rb2 = NewValues(2,2);  Ca2 = NewValues(2,3);  Cb2 = NewValues(2,4);  Rp2 = NewValues(2,5);
Ra3 = NewValues(3,1);  Rb3 = NewValues(3,2);  Ca3 = NewValues(3,3);  Cb3 = NewValues(3,4);  Rp3 = NewValues(3,5);
Ra4 = NewValues(4,1);  Rb4 = NewValues(4,2);  Ca4 = NewValues(4,3);  Cb4 = NewValues(4,4);  Rp4 = NewValues(4,5);
Ra5 = NewValues(5,1);  Rb5 = NewValues(5,2);  Ca5 = NewValues(5,3);  Cb5 = NewValues(5,4);  Rp5 = NewValues(5,5);
Ra6 = NewValues(6,1);  Rb6 = NewValues(6,2);  Ca6 = NewValues(6,3);  Cb6 = NewValues(6,4);  Rp6 = NewValues(6,5);
Ra7 = NewValues(7,1);  Rb7 = NewValues(7,2);  Ca7 = NewValues(7,3);  Cb7 = NewValues(7,4);  Rp7 = NewValues(7,5);
Ra8 = NewValues(8,1);  Rb8 = NewValues(8,2);  Ca8 = NewValues(8,3);  Cb8 = NewValues(8,4);  Rp8 = NewValues(8,5);

sim(CicuitSim)                % after the simulation, need to get the simulated results into a mtx
[row,col] = size(TD);         % define a new data mtx
[ROW,COL] = size(FC_Cell_V1);   % size of the results, (just need the ROW)
SimResults = [ FC_Cell_V1, FC_Cell_V2, FC_Cell_V3, FC_Cell_V4, FC_Cell_V5, FC_Cell_V6, FC_Cell_V7, FC_Cell_V8];
[CVrow,CVcol] = size(ChangeVare);
HowGood = zeros(1,CVcol);       % takes all the errors from the different values tried
HowGoodC = HowGood;             % the same size comparison of the capacitance values
Full_exit = 0;

%%%%%% Start the fitting algorithm  %%%%%%%%%%%%
for Tot_Count = 1:1:Total_Algo_Itt;  % how many times through the whole algorithm
    for CountItt = 1:1:itterations;  % many times through the circuit variable loop

        save(savefile,'NewValues','newCvalues','inital_guess','inital_newCvalues','least_error','itt_num');
        SimTime = FullSimTime;

        NewValues % just displays the current solution
        Data_run_AND_Tot_Count_AND_CountItt = [data_fit_run, Tot_Count, CountItt] % displays the progress
        sim(CicuitSim);
        SimResults = [ FC_Cell_V1, FC_Cell_V2, FC_Cell_V3, FC_Cell_V4, FC_Cell_V5, FC_Cell_V6, FC_Cell_V7, FC_Cell_V8];

        for countCell = 1:1:NewValues_row;          % gose through each cell
            for countVarWhichOnes = 1:1:FindWhichValues_col;   % see vector at the start
                countVar = FindWhichValues(countVarWhichOnes); % this variable use to be the old one in the for loop above
```

```
            for count = 1:1:CVcol               % goes through all of the spread in values
                NewValues(countCell,countVar) = OldValues(countCell,countVar)*ChangeVare(count);
                Ra1 = NewValues(1,1);  Rb1 = NewValues(1,2);  Ca1 = NewValues(1,3);  Cb1 = NewValues(1,4); Rp1 = NewValues(1,5);
                Ra2 = NewValues(2,1);  Rb2 = NewValues(2,2);  Ca2 = NewValues(2,3);  Cb2 = NewValues(2,4); Rp2 = NewValues(2,5);
                Ra3 = NewValues(3,1);  Rb3 = NewValues(3,2);  Ca3 = NewValues(3,3);  Cb3 = NewValues(3,4); Rp3 = NewValues(3,5);
                Ra4 = NewValues(4,1);  Rb4 = NewValues(4,2);  Ca4 = NewValues(4,3);  Cb4 = NewValues(4,4); Rp4 = NewValues(4,5);
                Ra5 = NewValues(5,1);  Rb5 = NewValues(5,2);  Ca5 = NewValues(5,3);  Cb5 = NewValues(5,4); Rp5 = NewValues(5,5);
                Ra6 = NewValues(6,1);  Rb6 = NewValues(6,2);  Ca6 = NewValues(6,3);  Cb6 = NewValues(6,4); Rp6 = NewValues(6,5);
                Ra7 = NewValues(7,1);  Rb7 = NewValues(7,2);  Ca7 = NewValues(7,3);  Cb7 = NewValues(7,4); Rp7 = NewValues(7,5);
                Ra8 = NewValues(8,1);  Rb8 = NewValues(8,2);  Ca8 = NewValues(8,3);  Cb8 = NewValues(8,4); Rp8 = NewValues(8,5);
                sim(CicuitSim);
                SimResults = [ FC_Cell_V1, FC_Cell_V2, FC_Cell_V3, FC_Cell_V4, FC_Cell_V5, FC_Cell_V6, FC_Cell_V7, FC_Cell_V8];
                %%% determine how good the fit is, ie. calculates the squares error
                HowGood(count) = sum(((((TD(:,(countCell*3 - 2)) - SimResults(:, countCell)).*(comp_vec)).^2).*comp_weights));
            end  % count , (all spread of values tried)
            MinPlace = find(  HowGood == (min(HowGood)));
            MinPlace = MinPlace(1,1);
            %% redefine the circuit value based on the smallest error found
            NewValues(countCell,countVar) = OldValues(countCell,countVar)*ChangeVare(MinPlace);
            HowGood = zeros(1,CVcol);
        end  % countVar , all of the components in the cell
    end  %  countCell, of the cells in the stack
    itt_num = itt_num + 1; %% keep track of the error   %% end keep track of the error % record itt number
    if OldValues == NewValues;
        if CountItt == 1;
            Full_exit = 1;
        else
            Full_exit = 0;
        end
        break
    else
    end
    OldValues = NewValues;
    Ra1 = NewValues(1,1);  Rb1 = NewValues(1,2);  Ca1 = NewValues(1,3);  Cb1 = NewValues(1,4);  Rp1 = NewValues(1,5);
    Ra2 = NewValues(2,1);  Rb2 = NewValues(2,2);  Ca2 = NewValues(2,3);  Cb2 = NewValues(2,4);  Rp2 = NewValues(2,5);
    Ra3 = NewValues(3,1);  Rb3 = NewValues(3,2);  Ca3 = NewValues(3,3);  Cb3 = NewValues(3,4);  Rp3 = NewValues(3,5);
    Ra4 = NewValues(4,1);  Rb4 = NewValues(4,2);  Ca4 = NewValues(4,3);  Cb4 = NewValues(4,4);  Rp4 = NewValues(4,5);
    Ra5 = NewValues(5,1);  Rb5 = NewValues(5,2);  Ca5 = NewValues(5,3);  Cb5 = NewValues(5,4);  Rp5 = NewValues(5,5);
    Ra6 = NewValues(6,1);  Rb6 = NewValues(6,2);  Ca6 = NewValues(6,3);  Cb6 = NewValues(6,4);  Rp6 = NewValues(6,5);
    Ra7 = NewValues(7,1);  Rb7 = NewValues(7,2);  Ca7 = NewValues(7,3);  Cb7 = NewValues(7,4);  Rp7 = NewValues(7,5);
    Ra8 = NewValues(8,1);  Rb8 = NewValues(8,2);  Ca8 = NewValues(8,3);  Cb8 = NewValues(8,4);  Rp8 = NewValues(8,5);
end  %% iterations , max number of times it will go through the parameter algorithm
Ra1 = NewValues(1,1);  Rb1 = NewValues(1,2);  Ca1 = NewValues(1,3);  Cb1 = NewValues(1,4);  Rp1 = NewValues(1,5);
Ra2 = NewValues(2,1);  Rb2 = NewValues(2,2);  Ca2 = NewValues(2,3);  Cb2 = NewValues(2,4);  Rp2 = NewValues(2,5);
Ra3 = NewValues(3,1);  Rb3 = NewValues(3,2);  Ca3 = NewValues(3,3);  Cb3 = NewValues(3,4);  Rp3 = NewValues(3,5);
Ra4 = NewValues(4,1);  Rb4 = NewValues(4,2);  Ca4 = NewValues(4,3);  Cb4 = NewValues(4,4);  Rp4 = NewValues(4,5);
Ra5 = NewValues(5,1);  Rb5 = NewValues(5,2);  Ca5 = NewValues(5,3);  Cb5 = NewValues(5,4);  Rp5 = NewValues(5,5);
Ra6 = NewValues(6,1);  Rb6 = NewValues(6,2);  Ca6 = NewValues(6,3);  Cb6 = NewValues(6,4);  Rp6 = NewValues(6,5);
Ra7 = NewValues(7,1);  Rb7 = NewValues(7,2);  Ca7 = NewValues(7,3);  Cb7 = NewValues(7,4);  Rp7 = NewValues(7,5);
Ra8 = NewValues(8,1);  Rb8 = NewValues(8,2);  Ca8 = NewValues(8,3);  Cb8 = NewValues(8,4);  Rp8 = NewValues(8,5);
```

```
sim(CicuitSim);
SimResults = [FC_Cell_V1, FC_Cell_V2, FC_Cell_V3, FC_Cell_V4, FC_Cell_V5, FC_Cell_V6, FC_Cell_V7, FC_Cell_V8];

%%%%%%%%%%%%%%%%%%%%%%%%%%%%%%%%%%%%%%%%%%%%%%%%%%%%%%%%%%%%%%%%%%%%%%%%%%%
%%%%%%%  loop for calculating the initial conditions of the capacitors

for Count_C_itt = 1:1:C_itterations

    save(savefile,'NewValues','newCvalues','inital_guess','inital_newCvalues','least_error','itt_num');
    SimTime = SteadySimTime; %% only need to simulate the start section

    %% do a display
    Count_C_itt  % what iteration the algorithm is up to
    newCvalues   % the current initial voltage conditions of the capacitors

    Ca1ini = newCvalues(1,1);     Cb1ini = newCvalues(1,2);
    Ca2ini = newCvalues(2,1);     Cb2ini = newCvalues(2,2);
    Ca3ini = newCvalues(3,1);     Cb3ini = newCvalues(3,2);
    Ca4ini = newCvalues(4,1);     Cb4ini = newCvalues(4,2);
    Ca5ini = newCvalues(5,1);     Cb5ini = newCvalues(5,2);
    Ca6ini = newCvalues(6,1);     Cb6ini = newCvalues(6,2);
    Ca7ini = newCvalues(7,1);     Cb7ini = newCvalues(7,2);
    Ca8ini = newCvalues(8,1);     Cb8ini = newCvalues(8,2);

    sim(CicuitSim);
    SimResults = [FC_Cell_V1, FC_Cell_V2, FC_Cell_V3, FC_Cell_V4, FC_Cell_V5, FC_Cell_V6, FC_Cell_V7, FC_Cell_V8];

    [row_C_sim,col_C_sim] = size(time);  % just need the lenght for C comparison

    for C_count = 1:1:NewValues_row         % go through each cell
        for C_comp = 2:1:2                  % go through each cap component in the model, i.e. the two inner ones
            for C_try = 1:1:C_spread_col    % go through each new guess
                newCvalues(C_count,C_comp) = oldCvalues(C_count,C_comp)*C_spread_vec(1,C_try); % generate the spread
                Ca1ini = newCvalues(1,1);     Cb1ini = newCvalues(1,2);
                Ca2ini = newCvalues(2,1);     Cb2ini = newCvalues(2,2);
                Ca3ini = newCvalues(3,1);     Cb3ini = newCvalues(3,2);
                Ca4ini = newCvalues(4,1);     Cb4ini = newCvalues(4,2);
                Ca5ini = newCvalues(5,1);     Cb5ini = newCvalues(5,2);
                Ca6ini = newCvalues(6,1);     Cb6ini = newCvalues(6,2);
                Ca7ini = newCvalues(7,1);     Cb7ini = newCvalues(7,2);
                Ca8ini = newCvalues(8,1);     Cb8ini = newCvalues(8,2);
                sim(CicuitSim);
                SimResults = [FC_Cell_V1, FC_Cell_V2, FC_Cell_V3, FC_Cell_V4, FC_Cell_V5, FC_Cell_V6, FC_Cell_V7, FC_Cell_V8];
                HowGood(C_try) = sum(((((TD(1:row_C_sim,(C_count*3 - 2))...
                    - SimResults(1:row_C_sim, C_count)).*(comp_vec(1:row_C_sim))).^2).*comp_weights(1:row_C_sim)));
            end  % C_try , the spread in values
```

```
                    %picks the values that gave the smallest error one and makes that the new value
                    MinPlace = find(  HowGood == (min(HowGood)));
                    MinPlace = MinPlace(1,1);
                    newCvalues(C_count,C_comp) = oldCvalues(C_count,C_comp)*C_spread_vec(1,MinPlace);
                    HowGood = zeros(1,CVcol);
                end %% C_comp   end of going through the caps in a single cell
            end  %C_count , number of capacitor values, (cells) as there is only one V condition
            if oldCvalues == newCvalues;
                if Count_C_itt == 1;
                    Full_exit = Full_exit + 1;  %% if Full_exit = 1 at this stage, the top part exited on the first run through
                else
                    Full_exit = 0;
                end
                break
            else
            end
            oldCvalues = newCvalues;
            Ca1ini = newCvalues(1,1);     Cb1ini = newCvalues(1,2);
            Ca2ini = newCvalues(2,1);     Cb2ini = newCvalues(2,2);
            Ca3ini = newCvalues(3,1);     Cb3ini = newCvalues(3,2);
            Ca4ini = newCvalues(4,1);     Cb4ini = newCvalues(4,2);
            Ca5ini = newCvalues(5,1);     Cb5ini = newCvalues(5,2);
            Ca6ini = newCvalues(6,1);     Cb6ini = newCvalues(6,2);
            Ca7ini = newCvalues(7,1);     Cb7ini = newCvalues(7,2);
            Ca8ini = newCvalues(8,1);     Cb8ini = newCvalues(8,2);
        end  % Count_C_itt,  number of times it goes through before going back to the parameter value
        if Full_exit == 2;  %% if this condition is meet, both parts of the algorithm have converged,
            break
        else
        end
    end % Tot_Count, total exit of the algorithm
    %%% this just plots the final results (same as in the program_plot part)
    SimTime = FullSimTime;
    sim(CicuitSim);
    SimResults = [FC_Cell_V1, FC_Cell_V2, FC_Cell_V3, FC_Cell_V4, FC_Cell_V5, FC_Cell_V6, FC_Cell_V7, FC_Cell_V8];

    if yes_plot == 1;  %% once a solution has been found, it can be plotted if desired
        figure(104)
        %% plot the Experimental data
        plot(TD(:,2),TD(:,1),TD(:,5),TD(:,4),TD(:,8),TD(:,7),TD(:,11),TD(:,10),...
            TD(:,14),TD(:,13),TD(:,17),TD(:,16),TD(:,20),TD(:,19),TD(:,23),TD(:,22));
        hold on; %% plot the experimental data
        plot(o_TD(:,2),o_TD(:,1),'-.',o_TD(:,5),o_TD(:,4),'-.',o_TD(:,8),o_TD(:,7),'-.',o_TD(:,11),o_TD(:,10),...
            '-.',o_TD(:,14),o_TD(:,13),'-.',o_TD(:,17),o_TD(:,16),'-.',o_TD(:,20),o_TD(:,19),'-.',o_TD(:,23),o_TD(:,22),'-.');
        %% plot the simulated data
        plot(time,FC_Cell_V1,'.-',time,FC_Cell_V2,'.-',time,FC_Cell_V3,'.-',time,FC_Cell_V4,...
        '.-',time,FC_Cell_V5,'.-',time,FC_Cell_V6,'.-',time,FC_Cell_V7,'.-',time,FC_Cell_V8,'.-');
        legend('Cell 1','Cell 2','Cell 3','Cell 4','Cell 5','Cell 6','Cell 7','Cell 8');
        xlabel('Time (s)'); ylabel('Voltage (V)');
        hold off;
```

```
            figure(103)  % plot the stack voltage, with comparison points.
            SimResults = [ FC_Voltage ];
            plot(o_TD(:,stack_pos + 1),o_TD(:,stack_pos),'black'); % plot the Experimental data
            hold on
            plot(time,FC_Voltage,'r'); %% plot the simulated data
            plot(TD(:,stack_pos + 1),TD(:,stack_pos),'b'); %% plot the interpolated data
            legend('Experimental Data','Fitted Data','Interpolated Data'); xlabel('Time (s)'); ylabel('Voltage (V)');
            % now establish the comparison points,

            error_val = [];
            error_val_time = [];
            for count_plot = 1:1:row
                if comp_vec(count_plot,1) == 1  %% then plot a point
                    plot(time(count_plot),SimResults(count_plot),'.r');  % SimResults at this point are the stack voltage
                    plot(TD(count_plot,stack_pos + 1),TD(count_plot,stack_pos),'.b');
                    error_val = [error_val (comp_weights(count_plot)*( TD(count_plot,stack_pos) - SimResults(count_plot))^2)];
                    error_val_time = [error_val_time  time(count_plot)];
                else
                end
            end
            hold off

            figure(109)
            plot(error_val_time,error_val,'.');

        else
        end

        Big_save(1:8,1:5,data_fit_run) = NewValues;
        save(savefile_2,'Big_save','weight','ChangeVare','num_test_points','CompTimes',...
            'percent_diff','organ_Big_save','current_data_fit_run','itt_num');

        %%%%% end the fitting algorithm %%%%%%%%%%%%%%%%%%%%%%%%%%%%%%%%%%%%%%%%%%%%%%%%%%%%%%%%%%%%%%%%%%%%

    otherwise
        disp('Unknown method.')

    end  % 'program' switch
end  % data_fit_run
```